IL
NUOVO CIMENTO
ORGANO DELLA SOCIETÀ ITALIANA DI FISICA
SOTTO GLI AUSPICI DEL CONSIGLIO NAZIONALE DELLE RICERCHE

VOL. III, N. 1 *Serie decima* 1° Gennaio 1956

Velocity of the Dirac Electron.

Z. KOBA

Research Institute for Fundamental Physics, Kyoto University - Kyoto, Japan

(ricevuto il 4 Giugno 1955)

Summary. — DIRAC's simple argument concerning the velocity eigenvalues of a relativistic electron is modified, taking into account the essential role played by anti-particle states.

In his classical text-book on the principles of quantum mechanics, Dirac elucidates the velocity eigenvalues of the electron in an ingenious way, which however, seems to me somewhat oversimplified.

Having shown that a measurement of a component of the velocity of a free electron is certain to lead to the result $\pm c$, he inserts namely the following explanation [1]:

« It may be easily verified that a measurement of a component of the velocity must lead to the result $\pm c$ in a relativistic theory, simply from an elementary application of the principle of uncertainty. To measure the velocity we must measure the position at two slightly different times and then divide the change of position by the time interval. (It will not do to measure the momentum and apply a formula, as the ordinary connexion between velocity and momentum is not valid). In order that our measured velocity may approximate to the instantaneous velocity, the time interval between the two measu-

[1] P. A. M. DIRAC: *Principles of Quantum Mechanics* (Oxford, 1947), p. 261.

rements of position must be very short and hence these measurements must be very accurate. The great accuracy with which the position of the electron is known during the time-interval must give rise, according to the principle of uncertainty, to an almost complete indeterminacy in its momentum. This means that almost all values of the momentum are equally probable, so that the momentum is almost certain to be infinite. An infinite value for a component of momentum corresponds to the value $\pm c$ for the corresponding component of velocity ».

The above statement appears to me unsatisfactory at least in two points First, it is quite dubious whether the illustrated procedure really represents the measurement of a velocity component in the quantum-mechanical sense of the term, since the system after such a measurement is not necessarily in an eigenstate of the velocity operator α, while, as the author explains elsewhere in the same book ([2]), « a measurement always causes the system to jump into an eigenstate of the dynamical variable that is being measured, the eigenvalue this eigenstate belongs to being equal to the result of the measurement ».

Second, the only relativistic relation employed here is that the velocity tends to c as the momentum becomes infinite. Hence one could hardly understand why it is illegitimate to apply the same argument to the non-relativistic theory of the electron, concluding that the measurement of a velocity component of a free electron would always lead to the value $\pm\infty$ (since the non-relativistic version of that relation is evidently $v \to \infty$ as $p \to \infty$). Indeed in the Dirac theory as well as in the Schrödinger theory the measurement of the position leads usually (*) to the average value $\langle p \rangle \approx 0$ and not to infinity because the p's of both signs can appear with equal right. These considerations strongly suggest that one would hardly get at the kernel of the subject without taking into account the anti-particle states, which are characteristic of the relativistic wave equations (**). This could have been of course expected from the well-known odd property of the operator α.

A more sensible exposition along the line of Dirac's reasoning would be thus desirable, and in this note I should like to try to give one.

The velocity operator in the Dirac theory commutes with both x and p and so it can be measured, in principle, without any reference to them; it is nevertheless instructive and illuminating to take a simultaneous eigenfunction

([2]) P. A. M. Dirac: *Principles of Quantum Mechanics* (Oxford, 1947), p. 36.

(*) That is to say, « when we consider the limiting case of a symmetrical wave packet ». In general, $\langle p \rangle$ is indefinite.

(**) Dr. I. Fujiwara has pointed out that Dirac's simple argument cannot explain the velocity of the meson either, which has, in the Duffin-Kemmer formalism, the eigenvalue 0 besides c.

of x and α, because the relation between the expectation values

$$\frac{d\langle x\rangle}{dt} = c\,\langle\alpha\rangle \tag{1}$$

can then be replaced by the corresponding relation between the eigenvalues:

$$\frac{dx'}{dt} = \pm c\,. \tag{2}$$

Let us take, therefore, a simultaneous eigenfunction ψ of the operators x_3 and α_3, belonging to the eigenvalues x_3' and 1 respectively. Using the usual representation for α's and β,

$$\alpha_3 = \begin{pmatrix} 0 & \sigma_3 \\ \sigma_3 & 0 \end{pmatrix}, \qquad \sigma_3 = \begin{pmatrix} 1 & 0 \\ 0 & -1 \end{pmatrix}, \tag{3}$$

we have

$$\psi = a\psi_1 + b\psi_2\,, \tag{4}$$

a and b being arbitrary constants which satisfy the normalization condition, and

$$\psi_1 = f(x_3 - x_3')\begin{pmatrix} 1 \\ 1 \\ 1 \\ -1 \end{pmatrix}, \qquad \psi_2 = f(x_3 - x_3')\begin{pmatrix} 1 \\ -1 \\ 1 \\ 1 \end{pmatrix}. \tag{5}$$

Here $f(x_3 - x_3')$ means the normalized eigenfunction of x_3. (Roughly speaking, it is something ilke the square root of a delta function). It is easily verified that this ψ really satisfies (2) with positive sign. Thus we see that the centre (or peak) of this « wave packet » (*), which can be imagined as prepared by a simultaneous measurement of the position and the velocity (or current), travels indeed in the x_3-direction with the light velocity—at least immediately after the measurement.

We shall now examine the nature of this « wave packet » in more detail to gain an insight into the mechanism of its strange behaviour. When it is decomposed into Fourier components, it is written as

$$\psi = \int \mathrm{d}p_3' \exp\left[ip_3'(x_3 - x)\right] f(p_3') \left\{ a\begin{pmatrix} 1 \\ 1 \\ 1 \\ -1 \end{pmatrix} + b\begin{pmatrix} 1 \\ -1 \\ 1 \\ 1 \end{pmatrix} \right\}, \tag{6}$$

(*) The « wave packet » here means of course the limiting case, which resembles a δ-function.

and, since $f(x_3 - x_3')$ is something like a delta-function, $f(p_3')$ is nearly constant over the whole range of the p_3' values. On the other hand, the plane wave solutions of the Dirac equation (i.e., eigenfunctions for the momentum operator p_3 and the energy operator H) are, for positive energies,

$$(7) \qquad \begin{pmatrix} 1 \\ 1 \\ \dfrac{p_3'}{m+E} \\ \dfrac{-p_3'}{m+E} \end{pmatrix} \exp[ip_3x_3'] \quad \text{and} \quad \begin{pmatrix} 1 \\ -1 \\ \dfrac{p_3'}{m+E} \\ \dfrac{1_3'}{m+E} \end{pmatrix} \exp[ip_3'x_3].$$

Here I have put $p_1' = p_2' = 0$ for simplicity and besides taken the sum and the difference of the up-spin and down-spin solutions usually given in textbooks ([3]). It is obvious that the functions (7) tend respectively to

$$(8) \qquad \begin{pmatrix} 1 \\ 1 \\ 1 \\ -1 \end{pmatrix} \exp[ip_3'x_3] \quad \text{and} \quad \begin{pmatrix} 1 \\ -1 \\ 1 \\ 1 \end{pmatrix} \exp[ip_3'x_3],$$

as $p_3' \to +\infty$. For negative energies, on the other hand, one gets in the same way

$$(9) \qquad \begin{pmatrix} \dfrac{-p_3'}{m+|E|} \\ \dfrac{-p_3'}{m+|E|} \\ 1 \\ -1 \end{pmatrix} \exp[ip_3'x_3] \quad \text{and} \quad \begin{pmatrix} \dfrac{-p_3'}{m+|E|} \\ \dfrac{p_3'}{m+|E|} \\ 1 \\ 1 \end{pmatrix} \exp[ip_3'x_3],$$

which tend, when $p_3' \to -\infty$, to

$$(10) \qquad \begin{pmatrix} 1 \\ 1 \\ 1 \\ -1 \end{pmatrix} \exp[ip_3'x_3] \quad \text{and} \quad \begin{pmatrix} 1 \\ -1 \\ 1 \\ 1 \end{pmatrix} \exp[ip_3'x_3],$$

respectively. Notice that (8) and (10) correspond just to the eigenfunctions of α_3 with the eigenvalue $+1$.

([3]) E.g., W. HEITLER: *Quantum Theory of Radiation* (Oxford, 1953), p. 107.

Comparing (7) and (9), (8) and (10) with (6), we see at once that the wave packet (4), when expressed as a superposition of the plane wave solutions of the Dirac equation, contains both positive and negative energy components for small values of p_3', while *for positive large values of* p_3' *it consists solely of positive energy states and for negative large values of* p_3' *solely of negative energy states.* Taking into account the « donkey » properties of the negative-energy states, we realize that, though the average value of p_3 for this wave packet is nearly 0, the velocity equals $+c$, since even for negative momenta the velocity $\partial E/\partial p$ turns out positive.

It is also evident that the situation is entirely different when we turn to the Schrödinger wave packet, in which no negative energy component can ever appear. Such a non-relativistic wave packet with sharp peak in the x_3'-space (eigenfunction of x_3) would involve the Fourier components of both signs almost uniformly, so that the mean value of p_3 and hence that of r_3 would nearly vanish.

The above argument is based entirely upon the one-body interpretation of the theory. A more realistic analysis would be possible only from the standpoint of second quantization, into which, however, I shall not enter now.

* * *

I should like to express my sincere gratitude to Prof S. Tomonaga for his suggestions, to Dr. T. Takabayasi and to Dr. T. Okabayashi for their very helpful discussions and to Prof. H. Yukawa for his interest shown to this work.

RIASSUNTO (*)

Si modifica la semplice argomentazione di Dirac riguardante le autovelocità di un elettrone relativistico, tenendo conto dell'influenza essenziale esercitata dagli stati delle antiparticelle.

(*) *Traduzione a cura della Redazione.*

The Molecular Heats of Gases from the Aspects of Heat Transfer.

I. I. SHERIF

Faculty of Engineering - University of Alexandria

(ricevuto il 23 Settembre 1955)

Summary. — The molecular heats of gases have been determined by a modification of the « Hot Wire Method ». The special features of the method are that only small quantities of the gas are needed, the thermal conductivity and the accomodation coefficient can also be determined all in one single operation. Measurements have been made both at ordinary pressures, when the mean free path of the gas molecules is small compared with the dimensions of the hot wire system, and at much lower pressures, when the mean free path becomes comparable with the dimensions of the apparatus. The results obtained for the monatomic gases agree very closely with the classical value $\frac{3}{2}R$. Those for the diatomic gases approach the value $\frac{5}{2}R$ at ordinary laboratory temperatures. Values of the accomodation coefficients for each gas have also been calculated from the experimental data.

1. – Introduction.

In recent years calculations of the coefficient of thermal accomodation have been made in terms of the temperature discontinuity between a heated solid surface and the adjacent gas. Such temperature drop has been found to depend on the nature and pressure of the gas, and the experimental data on which these calculations are based is expressible in terms of the heat transfer at relatively low gas pressure, or in the more recently developed investigations associated with the heat losses from an electrically heated wire in gases at much higher pressures.

The values of the accomodation coefficients as reported by AMDUR and

co-workers [1], ROBERTS [2], MANN [3], and MANN and NEWELL [4] are very much lower on a gas-free wire than on a gas-covered wire. This is also detected in the present work where a modified form of Knudsen's equation for the free molecular conduction holds. At higher pressures, the modified Fourier's law for the temperature drop holds. The determination of the molecular heat of the gas is thus made by the elimination of the accomodation coefficient.

A detailed account of the theory was published by GREGORY and SHERIF [5] in 1951.

2. – Construction of apparatus.

In actual practice, the existance of a uniformly heated wire can be realised by means of the compensating device used by GREGORY and ARCHER [6] in their experiments on thermal conduction through gases. The system adopted in the present investigation consisted of a single pair of compensated pyrex glass tubes and platinum wires. The tubes were connected with each other, in as small a space as possible but so as to permit a good circulation round them of the water contained in the thermostat. The platinum wires were cut from a length of thermo-pure platinum wire supplied by (Johnson, Matthey and Co. Ltd.), the radius being determined by weighing. Wires of small diameters were used in order to enhance the temperature-drop effect. At the same time by using thin platinum wires the radiation correction was reduced and the accuracy of the temperature measurements increased.

The platinum wires were connected to a Callender Griffith's bridge and the temperature of the wire maintained constant by fixing the resistance of the wire and changing the current as the pressure varied.

It has been shown from theoretical considerations by GREGORY and ARCHER [6,7] that the compensated element is uniform in temperature throughout its length, provided the design of the tube system is such that the quantities

$$\cosh \sqrt{W} \cdot L_1 \qquad \text{and} \qquad \cosh \sqrt{W} \cdot L_2$$

---

[1] I. AMDUR, M. M. JONES and M. PEARLMAN: *Journ. Chem. Phys.*, **12**, 159 (1944).
[2] J. K. ROBERTS: *Proc. Roy. Soc.*, A **129**, 146 (1930); A **135**, 192 (1932); A **142**, 519 (1933).
[3] W. B. MANN: *Proc. Roy. Soc.*, A **146**, 776 (1934).
[4] W. B. MANN and W. C. NEWELL: *Proc. Roy. Soc.*, A **158**, 397 (1937).
[5] H. S. GREGORY and I. I. SHERIF: *Nature*, **168**, 1123 (1951).
[6] H. S. GREGORY and C. T. ARCHER: *Proc. Roy. Soc.*, A **110**, 91 (1926).
[7] H. S. GREGORY and C. T. ARCHER: *Phil. Mag.*, **3**, 931 (1927).

are very large compared with unity, where $2L_1$ and $2L_2$ are the lengths of the main and compensating wires and W a quantity depending on the dimensions of the system and the heat losses from the wire. Dr. B. W. PURSLOW (personal communication) gave as a criterion of compensation that the short wire (carrying the same current as the long wire) should just reach the same maximum

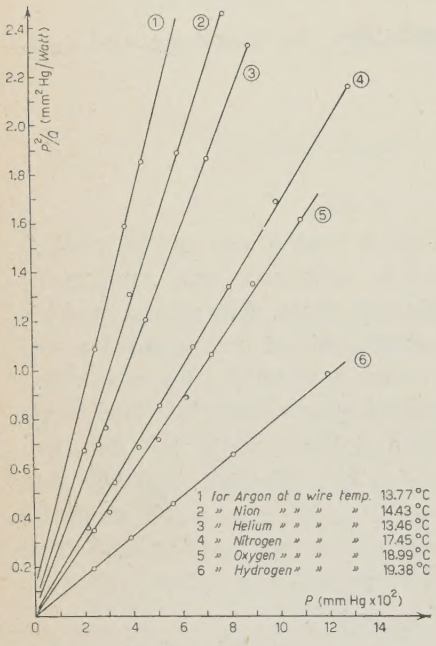

Fig. 1.

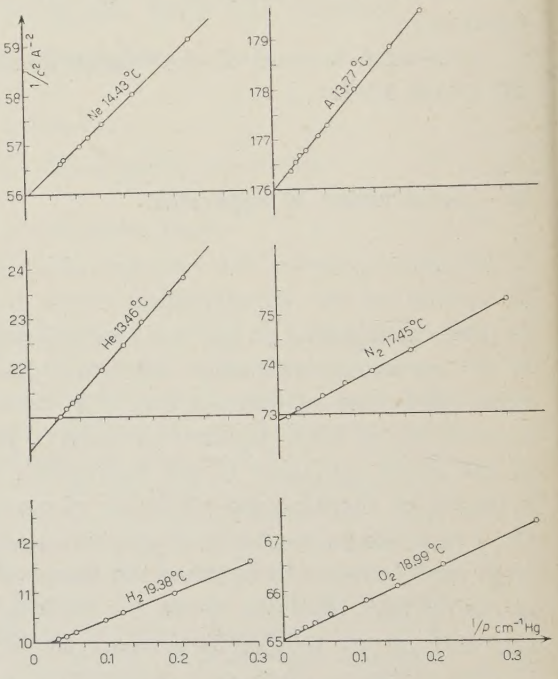

Fig. 2.

(mid-point) temperature as the long wire to within $\frac{1}{2}$ %. This gives the pressure limit for the present system in which the short wire is 5.4 cm long and a radius of about 70 μm with little variation between gases. If the limit of accuracy is taken as 2%, then for compensation the pressure limit is roughly halved.However, as illustrated in the graphs, the criterion of compensation is by no means a precise one and the region extends to much lower pressures than those calculated.

3. – Corrections and calculations.

3·1. *Radiation correction.* – The correction to be applied for the emission of heat by radiation from a wire maintained at a certain temperature to a coaxial surface maintained at a lower temperature is negligible at the tempe-

rature-drop range of pressures owing to the very small dimensions of the wires used. The only serious effect occurs when the pressure is too low where the maximum radiation losses are about 7% of the total heat loss.

The radiation correction was calculated by using a formula deduced from theoretical considerations by HELFGOTT ([8]):

$$E = \sigma T^4 (1 - e^{-\alpha T}),$$

where $\sigma = 5.72 \cdot 10^{-12}$ watt per cm^2 and $\alpha = 1.25 \cdot 10^{-4}$ for platinum.

3·2. *Wall temperature.* – The temperature T_2 of the internal wall of the tube was corrected from the temperature T_3 of the external surface by using the relation:

$$T_2 = T_3 + Q \log (r_3/r_2)/(2\pi K_g L),$$

where K_g is the thermal conductivity of the glass used at an average temperature $(T_2+T_3)/2$. Values of K_g at the appropriate temperatures were calculated in terms of the data obtained by STEPHENS ([9]).

4. – Experimental procedure.

The experimental procedure begins by determining the fixed point resistances of the wire at ice and steam temperatures. A series of small currents was passed through the bridge system, and the corresponding balance points were determined. It has been shown by GREGORY ([10,11]) that the appropriate working relation is:

$$C^2R = A + Dx,$$

where A and D are constants and x is the bridge setting corresponding to a temperature difference between the wire and the bath. Therefore if the heat loss from the wire is plotted against the balance point of the bridge, one should obtain a straight line whose intercept with the balance point axis, corresponding to zero heating effect, gives the true balance point.

After filling the apparatus with pure gas, the thermostat was set into operation and the bridge was set at a certain value which corresponds to a predetermined value of temperature not exceeding 20 °C of the wire. The current was then adjusted until balance of the bridge was obtained, the pressure of the gas being also observed. A new set of observations was then made after reducing the pressure by a suitable amount and adjusting the current passing

([8]) HELFGOTT: *Zeits. f. Phys.*, **49**, 555 (1928).
([9]) R. W. STEPHENS: *Phil. Mag.*, **14**, 897 (1932).
([10]) H. S. GREGORY and S. MARSHALL: *Proc. Roy. Soc.*, A **114**, 354 (1927).
([11]) H. S. GREGORY: *Phil. Mag.*, **22**, 257 (1936).

through the wire to balance the bridge circuit and assure constancy of temperature of this heated wire. The procedure was repeated, reducing the pressure of the gas in stages until observations were obtained over a range of pressures sufficient to meet the conditions imposed by the theoretical treatment with regard to the length of the mean free path.

Dimensions of the hot wire system:

Radius of the platinum wire = 0.00256 cm
Inner radius of the glass tube = 0.25 cm
Outer radius of the glass tube = 0.40 cm
Effective length of the wire = 15.90 cm.

5. – Observations and results.

A typical example of the observations made in the course of the work is tabulated in Table I. Table II gives the final results for the molecular heats and accomodation coefficients for all gases investigated at the temperature t of the wire. In Table I R is the resistance of the wire and C the current through it.

TABLE I. – *Argon*.

$R = 8.353\ \Omega$ $t = 13.774\ ^{o}C$ radiation $= 6.4 \cdot 10^{-5}$ W

P cm Hg	C A	P cm Hg	C A	P cm Hg	C A
37.6	0.07530	1.0	0.07184	0.0202	0.02492
30.1	0.07525	0.51	0.06871	0.0170	0.02303
18.2	0.07518	0.23	0.06245	0.012	0.01941
13.4	0.07510	0.19	0.05661	0.007	0.01486
8.9	0.07495	0.145	0.05278	0.006	0.01340
7.3	0.07486	0.080	0.04334	0.0045	0.01178
5.0	0.07463	0.049	0.03619	0.0038	0.01080
2.6	0.07390	0.0313	0.02979	0.0025	0.00873

$\alpha = 0.84$ $\beta = 1.5$ $K = 3.85 \cdot 10^{-5}$ c.g.s.

TABLE II.

Gas	H_2	N_2	O_2	He	Ne	A
$t\ ^{o}C$	19.38	17.45	18.99	13.46	14.43	13.77
βR	4.95	4.97	4.95	2.96	2.96	2.98
α	0.40	0.81	0.80	0.42	0.78	0.84

6. – Accuracy of the results.

6·1. *Accuracy of pressure measurements.* – The accuracy of the pressure measurements depends mainly on the accuracy of measuring mercury level differences in the various gauges. For the two tubed manometers an accuracy of $\pm \frac{1}{2}\%$ may justifiably be claimed by using a good cathetometer. With the Mc Leod gauges it is claimed that the measured level differences are accurate to within ± 0.05 cm at all times and the worst percentage error is 1% when the pressure is 10 μm.

6·2. *Accuracy of the electrical measurements.* – The potentiometer, measuring voltage across a standard resistance, shows four figure accuracy and the current values may be considered reliable to within $\pm 0.1\%$. The bridge was capable of measuring resistance values of the platinum wire to 0.001 ohm; for a typical system a resistance increment of 0.304 ohm produced a wire temperature 9.867 °C and for an increment of 0.304 ohm the wire temperature was 9.834 °C. Therefore for an error of 0.001 ohm in the bridge setting for an increment of 0.304, there was an error of 0.4% in the temperature calculation. However it should be stated that changes of temperature much smaller than this could be detected by the sensitive bridge network.

The resultant accuracy of the molecular heat, can now be readily estimated. Assuming a possible error of $\pm 1\%$ in the pressure measurements, $\pm 0.1\%$ in the current measurements and $\pm 0.5\%$ in the temperature measurements, the maximum percentage error in the molecular heat is 2%.

* * *

The author is very grateful to Dr. W. H. George for his generous help and advice, and to Prof. H. S. Gregory for suggesting the reserach.

RIASSUNTO (*)

Per mezzo di un modificazione del « metodo del filo caldo » si sono determinati i calori molecolari di alcuni gas. Le speciali caratteristiche del metodo permettono l'uso di solo piccole quantità di gas e di determinare con un'unica operazione la conduttività termica e il coefficiente d'accomodamento. Si sono eseguite misure sia a pressioni ordinarie alle quali il cammino libero medio delle molecole del gas è piccolo in confronto alle dimensioni del sistema a filo caldo, sia a pressioni molto inferiori alle quali il cammino libero medio è confrontabile con le dimensioni dell'apparecchio. I risultati ottenuti per i gas monoatomici sono in ottimo accordo col valore classico $\frac{3}{2}R$. Quelli per i gas biatomici si approssimano al valore $\frac{5}{2}R$ alle ordinarie temperature di laboratorio. Dai dati sperimentali si è anche calcolato per ogni gas il coefficiente di accomodamento.

(*) *Traduzione a cura della Redazione.*

Photodisintegration of Samarium.

E. Silva and J. Goldemberg

Laboratório de Física Nuclear, Faculdade de Filosofia, Ciências e Letras, Universidade de São Paulo - São Paulo, Brasil

(ricevuto il 26 Settembre 1955)

Summary. (*). — In order to study the photodisintegration of Sm induced by irradiation with X-rays, discs of pressed Sm_2O_3 were exposed to the irradiation with X-rays from the 22 MeV Betatron of the Labóratrio de Fisica Nuclear of the Uhiversity of São Paulo. In the present paper the results of the experiments are related.

(*) *Editor's care.*

Photodisintegration reaction induced in Samarium by irradiation with the X-rays of a 25 MeV synchrotron were studied before by Butement (1). In his work Butement discovered a new activity with an half-life of 8 min, due to positrons or electrons. The nucleus responsible for this activity was suggested to be ^{143}Sm, originated in the reaction $^{144}Sm(\gamma, n)^{143}Sm$, basing on a comparison between the activities of the isotopes of Samarium and their relative abundance.

In this paper work is described which besides giving the activation curve and cross-section for the correspondent (γ, n) reaction gives additional information on the decay scheme of ^{143}Sm.

X-rays from the 22 MeV Betatron of the « Laboratório de Física Nuclear » of the Universidade de S. Paulo, were used in this experiment, to irradiate discs of pressed Sm_2O_3. The mass of the samples was of the order of 6.5 g. The induced activities were measured with a Geiger counter arrangement and care was taken to obtain only the 8 min half-life activity.

Initially an accurate measurement of the half-life reported by Butement was made. A sample was irradiated at an energy below the $^{16}O(\gamma, n)^{15}O$

(1) F. D. S. Butement: *Proc. Phys. Soc.* (London), **63** A, 532 (1950).

threshold and its decay curve was measured for 5 hours. The results are shown in Fig. 1. The long lived activity present in this curve was extrapolated by means of a linear regression and subtracted. To the remaining activity was fitted a straight line which gave a corresponding half-life of 9.03 min. A test in a magnetic field indicated that the particles involved were positrons.

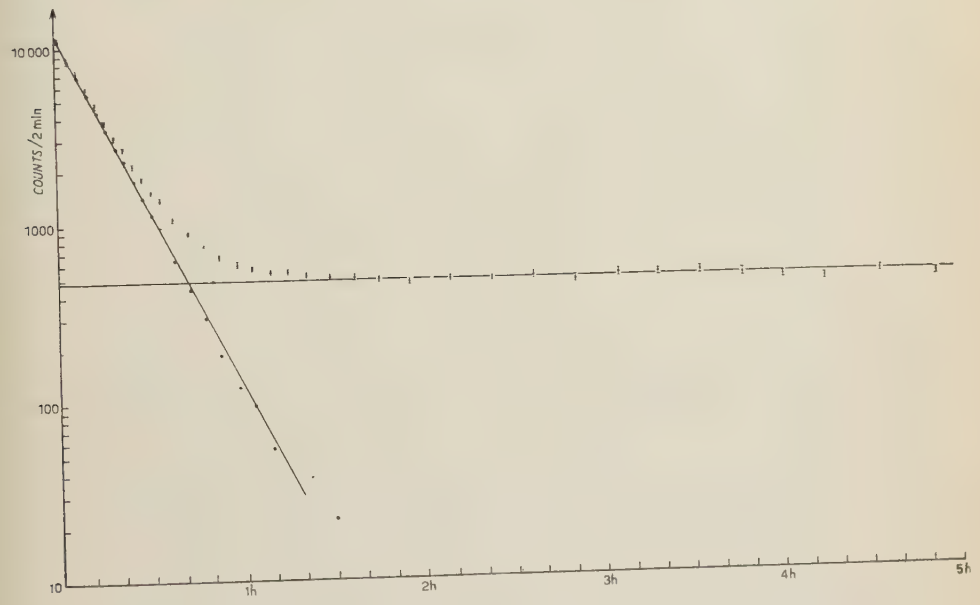

Fig. 1. – Decay curve of a Betatron irradiated Sm_2O_3 sample.

An absorption curve of the 9.03 min activity was then carefully measured and compared to an absorption curve of a standard of UX_1+UX_2 using Feather's method. The extrapolated range of the positron is 1250 mg/cm² which corresponds to an energy of 2.6 MeV.

An absorption curve was measured also using lead absorbers of thickness greater than the range of the positrons. The energy of the γ-radiation accompanying the positrons was then shown to be of the order of 500 keV, having probably its origin in positron anihilation.

An excitation function for the (γ, n) reaction leading to the 9.03 min activity was then measured. Irradiation times were of the order of 10 minutes; above the oxygen threshold a waiting time was allowed, enough to make negligible the contribution of the activity of ^{15}O; the counting time was 10 min in each case.

The absolute rate of disintegration of ^{144}Sm was determined by comparison with a copper sample irradiated and counted in the same arrangement. In

this determination we used the yield/mole/r/min given by PRICE and KERST [2]. The results obtained for ^{144}Sm are shown in Fig. 2.

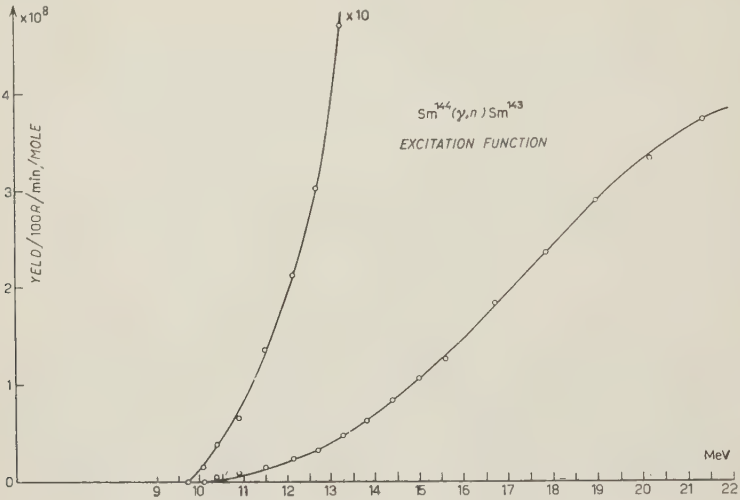

Fig. 2. – Excitation function for the reaction $^{144}Sm(\gamma, n)^{143}Sm$.

Near the threshold the energy of the Betatron was changed in small steps in order to allow an accurate determination of the threshold. This is shown in Fig. 2, which gives for the threshold the value of 9.6 MeV.

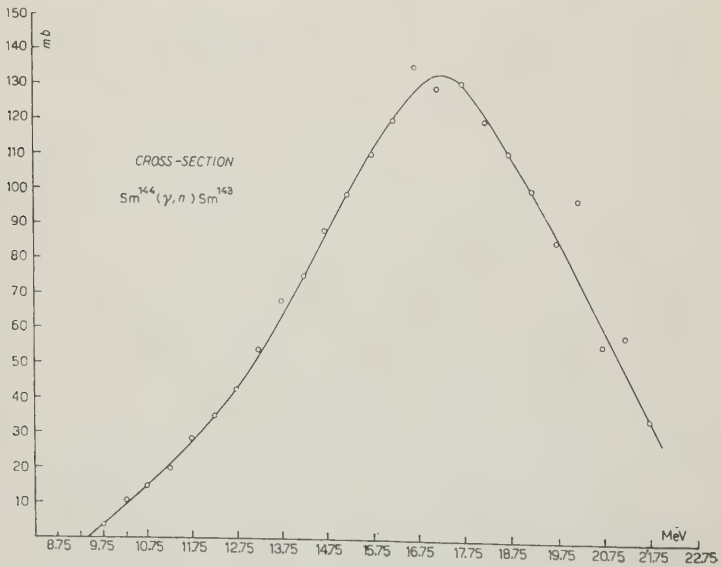

Fig. 3. Cross section for the reaction $^{144}Sm(\gamma, n)^{143}Sm$.

[2] G. PRICE and D. W. KERST: *Phys. Rev.*, **77**, 806 (1950).

The cross-section was obtained from the excitation function by the photon difference method ([3]) and is shown in Fig. 3.

The only two isotopes of Samarium that by neutron emission could result in a nucleus decaying in 9.03 minutes are ^{147}Sm (15%) and ^{144}Sm (3.1%), the other isotopes giving rise by neutron emission to other well known activities. The threshold for the reactions $^{147}Sm(\gamma, n)^{146}Sm$ and $^{144}Sm(\gamma, n)^{143}Sm$ computed from the semi-empirical mass formula are 7.08 and 9.31 MeV. Our result of 9.6 MeV supports the previous assignement of ^{144}Sm as the isotope of Samarium involved in the reaction investigated in this paper.

The yield/mole/r/min at 18 MeV according to our results is $0.24 \cdot 10^7$. Interpolating in the data of PRICE and KERST one gets for the same yield $0.93 \cdot 10^7$. Our result is then low by a factor 4. If ^{147}Sm was the isotope giving origin to the 9.03 min activity our result would be still lower by another factor of 5. This is then very unlikely to be the case.

TABLE I.

Reaction	Threshold	$E(\sigma_{max})$	σ_{max}	width	$\int \sigma dE$ (MeV barn)	
					Exp	LEVINGER BETHE
$^{144}Sm(\gamma, n)^{143}Sm$	9.6 MeV	17.25	135 mb	6.8	0.91	3.1

The discrepancy of a factor of 4 could be explained by the existence of an undetected isomeric state in ^{143}Sm to which most of transitions in the reaction $^{144}Sm(\gamma, n)^{143}Sm$ would end. It is interesting to observe that ^{143}Sm is included in one of « islands of isomerism ».

The significant data of the cross-section of Fig. 3 is in Table I.

([3]) KATZ and A. W. G. CAMERON: *Can. Jour. Phys.*, **29**, 518 (1951).

RIASSUNTO (*)

Per studiare la fotodisintegrazione del Sm indotta dall'irradiazione con raggi X. dei dischi pressati di Sm_2O_3 sono stati sottoposti ad irradiazione con raggi X prodotti dal betatrone di 22 MeV del Laboratório de Fisica Nuclear dell'Università di São Paulo. Nel presente lavoro si riferiscono i risultati dell'esperienza.

(*) *A cura della Redazione.*

IL NUOVO CIMENTO Vol. III, N. 1 1° Gennaio 1956

A Collective Model for the Nuclear Photo-Reactions.

V. de Sabbata (*) and A. Sugie (+)

Department of Mathematical Physics, University of Birmingham

(ricevuto il 2 Ottobre 1955)

Summary. — For the nuclear photo-reaction in the giant resonance region, we considered a collective model which includes both the Goldhaber-Teller and Steinwedel-Jensen type of motion. We find a coupling of these two modes through the kinetic energy. This leads us to two resonance frequencies. If we identify the higher resonance as the giant resonance, we have a better dependence on mass number A of the resonance frequency. But the absolute value of the integrated cross-section is far too small. On the other hand if we identify the lower energy level as the giant resonance, we have again a better A-dependence of the resonance frequency, and the absolute value of the integrated cross-section is of the right order of magnitude. But in this case we must increase about twice the force constants in the two models.

1. – Introduction.

The nuclear photo-reactions have been studied by several authors in two extreme types of nuclear models: the independent particle model and the collective model. It is well known that the first model has been confirmed by the shell model in the low energy region. It gives brilliant agreement with experiment for ground state spins, magnetic moments, some quadrupole moments and some low energy levels. This individual particle model presupposes that the mutual interaction between nucleons is weak compared to the common potential. On the other hand nuclear reactions at higher energy have been interpreted

(*) On leave of absence from: Istituto di Fisica, Università di Bologna, Bologna, Italy.

(+) Present address: Department of Physics, University of Tokyo, Tokyo, Japan.

with some succes by a model such as the statistical theory, which presupposes strong interaction between nucleons.

At first sight the two models contradict each other, and the strong interaction found in deuteron and in the experiments of nucleons scattering, seems to favour the strong interaction model or the collective model. But one must remember that the shell model applied always to the ground state, while the application of the collective model was for phenomena of high excitation energy. At ground state the effective interaction between two nucleons is weakened because of the Pauli principle. In fact for two nucleons inside a nucleus many scattering processes are forbidden because after scattering one or two nucleons go to the states already occupied. For high energy excitation this argument does not hold because in this case there will be many unoccupied states available. Thus the mean free path is decreased and the shell model becomes an unrealistic model.

We study here the nuclear photo-reaction at the energy of giant resonance. Since the excitation energy is relatively high (about 20 MeV) we prefer the use of the collective model. The large experimental cross-section also indicates that many nucleons participate in absorbing the photon.

2. – Peculiarity of the Model.

It is well known that the absorption of a photon by a nucleus in the region of giant resonance is principally of electric dipole nature. GOLDHABER and TELLER [1] (below abbreviated G-T) first proposed to explain the phenomenon as due to the collective motion of all the protons against all the neutrons. He used a model in which neutrons and protons are considered to be two incompressible fluids which are interpenetrable to each other. During the oscillation, the two fluids move relatively to each other as a whole so that near the surface of the nucleus these two fluids do not overlap.

With this hypothesis they found that the resonance energy changed with respect to the mass number A as $A^{-\frac{1}{6}}$. STEINWEDEL and JENSEN [2] (S-J) examined another type of collective oscillation which had also been suggested by G-T. In this model protons and neutrons are not treated as two incompressible fluids, but supposed to be compressible and longitudinal waves to occur in each fluid, but the total density and nuclear surface remain constant. With this model they found that the resonance energy changes as $A^{-\frac{1}{2}}$. The experimentally found A-dependence is about $A^{-\frac{1}{3}}$.

---

[1] M. GOLDHABER and E. TELLER: *Phys. Rev.*, 74, 1046 (1948).
[2] H. STEINWEDEL and J. H. D. JENSEN: *Zeits. f. Naturforsch.*, 5a, 343, 413 (1950).

Actually these two modes of oscillation can occur at the same time, i.e. the two fluids may move relative to each other with density changes inside them. We shall formulate this type of motion below. It will be seen that the Lagrangian of the whole system consists of three parts; the Lagrangians of the two free modes and a coupling term between them which comes from the kinetic energy in the approximation adopted below.

3. – Lagrangian of the System.

S-J wrote the Lagrangian assuming that the nuclear surface is fixed and there occurs in proton liquid and neutron liquid a density variation without changing the total density.

Then the potential energy comes from the symmetry energy, but there is no contribution from the surface region nor from the change of volume.

Write the proton and neutron density as S-J did,

$$\varrho_P = \varrho_P^0 + \eta(\boldsymbol{r}, t) ,$$

$$\varrho_N = \varrho_N^0 - \eta(\boldsymbol{r}, t) ,$$

$$\varrho_P^0 = \frac{Z}{A}\varrho_0 , \quad \varrho_N^0 = \frac{N}{A}\varrho_0 , \qquad \text{with } \frac{4}{3}\pi r_0^3 \varrho_0 = 1 ,$$

$$\varrho_P + \varrho_N = \varrho_0 = \text{const.} ,$$

then the kinetic and potential energy density become respectively,

$$\frac{M}{2}(\varrho_P \boldsymbol{v}_P^2 + \varrho_N \boldsymbol{v}_N^2) \quad \text{and} \quad K\frac{(\varrho_N - \varrho_P)^2}{\varrho_0} ,$$

where $\boldsymbol{v}_P$ and $\boldsymbol{v}_N$ are the velocities of protons and neutrons respectively. K is the coefficient of the symmetry energy in the semi-empirical mass formula. We introduce the relative velocity and the velocity potential for this:

$$\boldsymbol{v} = \boldsymbol{v}_P - \boldsymbol{v}_N = -\operatorname{grad}\varphi .$$

Since the total density is constant,

$$\varrho_P \boldsymbol{v}_P + \varrho_N \boldsymbol{v}_N = 0$$

and the continuity condition becomes

$$\frac{\partial \varrho_P}{\partial t} = \operatorname{div}(\varrho_{rel}\boldsymbol{v})$$

where

$$\varrho_{\text{red}} = \frac{\varrho_N \varrho_P}{\varrho_0} \approx \frac{NZ}{A^2} .$$

The Lagrangian of this system can be written with an undetermined multiplier, λ as

$$(1) \qquad L = \int \mathrm{d}\tau \left\{ \frac{M}{2} \varrho_{\text{red}} (\operatorname{grad} \varphi)^2 - K \frac{(\varrho_N - \varrho_P)^2}{\varrho_0} + \lambda \left[\frac{\partial \varrho_P}{\partial t} - \operatorname{div} (\varrho_{\text{red}} \operatorname{grad} \varphi) \right] \right\} .$$

From this Lagrangian the equation of motion is derived with the approximation of neglecting all terms higher than the first order in η or φ. Under the boundary condition that the radial velocity of the neutrons or protons is zero at the surface we obtain the first eigenfrequency

$$\omega \approx 60 A^{-\frac{1}{3}} .$$

Now if we allow in addition to the above motion a motion of the proton fluids as a whole in respect to the neutron fluid as a whole as in the G-T model, the Lagrangian (1) must be modified. That is, we assume that the two fluids are displaced to each other with the same density change as before in each of them. Then it is easily seen that there appears no coupling term through the potential energy. Firstly, take the potential term of S-J motion. If we denote the relative displacement of the geometrical centre of the proton fluid to the neutron fluid by $\boldsymbol{\Delta r}$, we hawe

$$\varrho_P - \varrho_N = \varrho_P^0 + \eta(\boldsymbol{r} + \boldsymbol{\Delta r}, t) - [\varrho_N^0 - \eta(\boldsymbol{r} - \boldsymbol{\Delta r}, t)] =$$
$$= \varrho_P^0 - \varrho_N^0 - 2\eta \cdot 1 r \eta' \cdot 1 r \eta' \approx 2\eta$$

and

$$\varrho_0 = \varrho_P + \varrho_N = \varrho_P^0 + \varrho_N^0 + 2 A r \eta'(\boldsymbol{r}, t) .$$

Thus the modification in the symmetry energy term is of higher order.

The same can be said for the potential energy of G-T. The G-T potential energy is proportional to the density at the surface and to the energy required to extract a proton (neutron) from the surrounding neutron (proton) liquid. If there is a S-J type density change in each liquid, as the proton density at the surface is changed from ϱ to $\varrho(1 + \varepsilon)$, the neutron density becomes $\varrho(1 - \varepsilon)$, therefore the extraction energy varies from φ to $\varphi(1 - \varepsilon)$ and the G-T potential energy is proportional to $\varrho\varphi(1 - \varepsilon^2)(\boldsymbol{\Delta r})^2$. Thus the coupling is of fourth order. Further, we should consider the change in total density. This change is already of second order as given above and, since the energy change is quadratic in the density change this effect becomes also of fourth order.

On the other hand, the relative velocity of an element of one fluid in respect to the other becomes

$$-\operatorname{grad}\varphi + \dot{\overline{\Delta \boldsymbol{r}}}\,,$$

where φ is the velocity potential when the two liquids do not move to each other as a whole. Then the Lagrangian of the whole system is

$$(2)\qquad L = \int \mathrm{d}\tau \cdot \left\{ \frac{M}{2}\varrho_{\mathrm{red}}(-\operatorname{grad}\varphi + \dot{\overline{\Delta \boldsymbol{r}}})^2 - K\frac{(\varrho_N - \varrho_P)^2}{\varrho_0} + \lambda\left[\frac{\partial \varrho_P}{\partial t} - \operatorname{div}(\varrho_{\mathrm{red}}\operatorname{grad}\varphi)\right]\right\} - \frac{k}{2}(\boldsymbol{\Delta r})^2\,,$$

where k is the coefficient in the G-T potential energy:

$$k = \frac{\pi R^2 \varrho_0 \varphi}{\varepsilon}\,.$$

The continuity condition is the same as before since

$$\operatorname{div}\varrho_{\mathrm{red}}\dot{\overline{\Delta \boldsymbol{r}}} \approx \varrho_{\mathrm{red}}\operatorname{div}\dot{\overline{\Delta \boldsymbol{r}}} = 0\,,$$

to the required order. At this point as an approximation we insert in the Lagrangian (2) the solution of S-J's form for the space part of φ and η:

$$(3)\qquad \begin{cases} \varphi = a(t) j_1(x)\cos\vartheta\,, \\ \eta = \dfrac{M\varrho_0}{8K}\dot{\varphi} \end{cases} \qquad \text{with} \quad x = \frac{r}{A_0}$$

we obtain (see Appendix I):

$$(4)\qquad L = \frac{MA}{4}\frac{R^2}{2}\{B\dot{\alpha}^2 - \omega_0^2 B\alpha^2 + \dot{\beta}^2 - \omega_1^2\beta^2 - 2D\alpha\dot{\beta}\}\,,$$

where ω_0 and ω_1 are the S-J and G-T frequencies respectively and

$$\alpha(t) = \frac{1}{RA_0\omega_0}a(t)$$

$$\beta(t) \qquad \frac{Ar}{R}\,.$$

Making the variation with respect to time $\delta\int L\mathrm{d}t = 0$, we have the fol-

lowing equation of motion

$$B\ddot{\alpha} = -B\omega_0^2\alpha - D\dot{\beta} ,$$

$$\ddot{\beta} = -\omega_1^2\beta - D\dot{\alpha} .$$

The eigenfrequencies are

$$\omega^2 = \tfrac{1}{2}[\omega_1^2 + (1+c)\omega_0^2 \pm \sqrt{(\omega_1^2 + (1+c)\omega_0^2)^2 - 4\omega_0^2\omega_1^2}], \tag{5}$$

with

$$c\omega_0^2 = \frac{D^2}{B} .$$

4. – The Gamma-Ray width Γ_γ and the Integrated Cross Section.

Now we calculate the width of the γ-ray absorption. This width can be used to predict the integrated cross-section and further, in combination with the neutron width Γ_n, to predict the maximum of the absolute value of the (γ, n) cross-section and the ratio of (γ, n) reaction to (γ, γ) scattering.

For this purpose we derive an expression for the dipole moment operator and the wave function of the ground and the excited state. The width is $\hbar$ times the transition probability and is

$$\Gamma_\gamma = \frac{4}{3}\left(\frac{\omega}{c}\right)^3 |D_{mn}|^2 . \tag{6}$$

where D_{mn} is the matrix element of the dipole moment operator. The dipole moment is the sum of that of G-T and S-J:

$$D = Ze\frac{(\Delta \boldsymbol{r})_z}{2} + e\int \eta(\boldsymbol{r})_z \, d\tau .$$

With the η of (3) the only non zero component of D is the z-component. After the integration over volume, this becomes

$$D = \frac{ZeR}{2}\beta + e\frac{A}{4}\frac{\Lambda_0}{\omega_0}\dot{\alpha}N(X) \tag{7}$$

where

$$N(X) \quad \frac{3\sin X}{X^2} \quad \frac{3\cos X}{X} \quad \sin X .$$

To calculate the eigenfunction, we apply a suitable transformation over α and β so that the cross term between them disappears from the Lagrangian.

Then it is possible to write the nuclear eigenfunction simply in terms of

linear harmonic oscillators. From the Lagrangian of (4) the following Hamiltonian is obtained:

$$H = \frac{MA}{4}\frac{R^2}{2}\left\{\frac{1}{B}p_\alpha^2 + p_\beta^2 + B\omega_0^2\alpha^2 + \omega_1^2\beta^2 + D^2\alpha^2 + 2D\alpha p_\beta\right\}; \tag{8}$$

at this point we make a canonical transformation with the generating function

$$F = \alpha\gamma\,.$$

Then, we have:

$$H = \frac{MA}{4}\frac{R^2}{2}\left\{B\Omega^2 p_\gamma^2 + \frac{1}{B}\gamma^2 + p_\beta^2 + \omega_1^2\beta^2 - 2Dp_\beta p_\gamma\right\}$$

with

$$\Omega^2 = \omega_0^2(1 + c)\,.$$

We now eliminate the cross term $-2Dp_\beta p_\gamma$. For this purpose we write the Lagrangian in terms of γ, β, $\dot\gamma$, $\dot\beta$, i.e., putting

$$\chi = \gamma/(\omega_0\sqrt{B})\,,$$

$$L = \frac{MA}{4}\frac{R^2}{2}\{\dot\chi^2 + (1 + c)\dot\beta^2 + 2\sqrt{c}\,\dot\chi\dot\beta - \omega_0^2\chi^2 - \omega_1^2\beta^2\}\,.$$

This Lagrangian can be easily diagonalized with the introduction of new coordinates ξ, η related to the old χ and β by the relation

$$\begin{cases} \chi = \sqrt{c}\omega^2\xi + \sqrt{c}\omega'^2\eta\,, \\ \beta = (\omega_0^2 - \omega^2)\xi + (\omega_0^2 - \omega'^2)\eta\,, \end{cases} \tag{9}$$

where ω and ω' are the lower and the higher frequencies of the coupled system respectively. With these new coordinates the Hamiltonian becomes

$$H = \tfrac{1}{2}m\dot\xi^2 + \tfrac{1}{2}m'\dot\eta^2 + \tfrac{1}{2}k\xi^2 + \tfrac{1}{2}k'\eta^2\,, \tag{10}$$

which is the Hamiltonian of two independent harmonic oscillators. Then we have simply for the two transitions respectively

$$\begin{cases} \Gamma_{\gamma_1} = \dfrac{4}{3}\left(\dfrac{\omega}{c}\right)^3 |D_{10}|^2 = \dfrac{4}{3}\left(\dfrac{\omega}{c}\right)^3\dfrac{1}{2}\left(\dfrac{D_1}{\alpha}\right)^2 \\ \Gamma_{\gamma_2} = \dfrac{4}{3}\left(\dfrac{\omega'}{c}\right)^3 |D_{20}|^2 = \dfrac{4}{3}\left(\dfrac{\omega'}{c}\right)^3\dfrac{1}{2}\left(\dfrac{D_2}{\beta}\right)^2\,. \end{cases} \tag{11}$$

Where D_1 and D_2 are the coefficients in the dipole moment operator and α and β are the oscillation amplitudes in the two resonances respectively (see Appendix II for their exact definitions).

The integrated cross-section is simply

$$\int_{\text{one level}} \sigma \, \mathrm{d}E = 3\pi^2 \lambda\!\!\!^{-2} \Gamma_\gamma \tag{12}$$

where $\lambda\!\!\!^{-}$ is the wave length of the incident photon divided by 2π.

The maximum value of the (γ, n) reaction is given by

$$\sigma_{\gamma \mathrm{n}}(\max) \approx 6\pi \lambda\!\!\!^{-2} \Gamma_\gamma / \Gamma_{\mathrm{n}}$$

and the ratio of $\sigma_{\gamma \mathrm{n}}$ to $\sigma_{\gamma\gamma}$ is given by $\Gamma_{\mathrm{n}}/\Gamma_\gamma$.

5. – Numerical Results and Discussion.

It can be easily seen that the higher frequency of the coupled system lies higher than ω_0 and ω_1 and the lower frequency lower than the two. If we use the original values for the constants of both S-J and G-T potentials, we find the higher level too high and the lower level too low. Considering the fact that in the S-J model the constant of the potential term had to be increased almost by a factor two to give agreement with experiment and also the ambiguous nature of the G-T constant, it will not be unreasonable to change these constants within a factor of two. Then we have two possibilities, that is, we can regard either of the two as the giant resonance level in photoreaction.

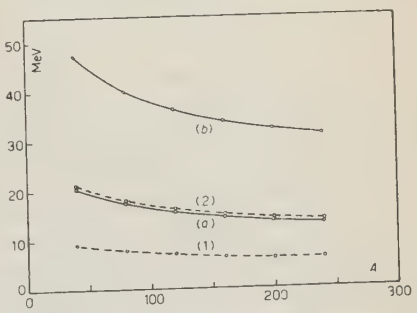

Fig. 1. The variation of the second resonance frequencies ($E_{\max}$) according to A. ----- The curve for the original S.J. and G.T. constants (written K and k respectively). . . . The curve for K' K; k' $0.5k$. The curve for K'' $0.7K$; k'' $0.5k$.

Firstly we identify the higher level as the giant resonance level by decreasing both constants (see Fig. 1). The dependence of the frequency on the mass number A is very complicated, but it is surely between $A^{-\frac{1}{3}}$ and $A^{-\frac{1}{6}}$ as it is required (see Fig. 2). In this case the lower frequency lies just in the region of the neutron threshold (see Fig. 3) so this will not appear as a peak in the (γ, n) cross-section. In the (γ, γ) scattering

cross-section there is a peak in this energy region ([3]) but this peak is accounted for by the two competitive processes. That is, as the γ-ray energy is increased the absorption of the photon increases, but as soon as the neutron threshold is passed, the excited state loses its energy more easily by neutron emission

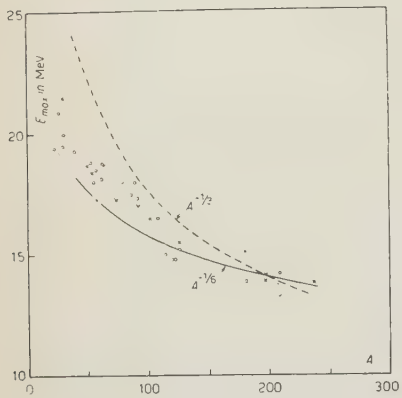

Fig. 2. – The experimental data on the giant resonance frequencies (E_{max}). ○ MONTALBETTI, KATZ, GOLDEMBERG (see ref. ([5])). × NATHANS, HALPERN (see ref. ([6])). The curves $A^{-\frac{1}{6}}$ and $A^{-\frac{1}{2}}$ are normalized at $A=211$ to 14 MeV.

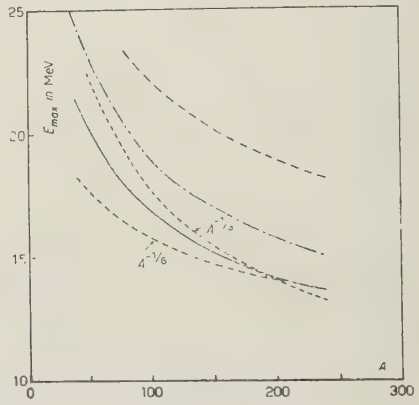

Fig. 3. – Resonance frequencies in the coupled model. (1) Lower frequency on the first interpretation. (2) Higher frequency on the first interpretation. (*a*) Lower frequency on the second interpretation. (*b*) Higher frequency on the second interpretation.

than by photon re-emission and the (γ, γ) cross-section begins to decrease. A measurement of the total nuclear photon absorption could indicate the existence of this level if there is.

As a consequence of the collective level which is orthogonal to the giant resonance level, we can say that the ratio $\sigma(\gamma, \mathrm{p})/\sigma(\gamma, \mathrm{n})$ increases compared to the statistical theory. In fact, since the energy difference of the two levels is almost the same as the nucleon binding energy, the level density in this energy region will be decreased compared to the statistical model ([4]) and hence also the emission probability for a low energy nucleon. This means that the relative probability of high energy nucleons being emitted is larger so that the Coulomb barrier will less strongly reduce the proton emission.

([3]) H. W. KOCH: *Proceedings of the 1954 Glasgow Conference on Nuclear and Meson Physics* (London and New York,) pp. 155-59.

([4]) L. I. SCHIFF: *Phys. Rev.*, **73**, 1311 (1948).

([5]) R. MONTALBETTI, L. KATZ and J. GOLDEMBERG: *Phys. Rev.*, **91**, 659 (1953).

([6]) R. NATHANS and J. HALPERN: *Phys. Rev.*, **93**, 437 (1954).

The result of the γ-ray width makes this choice very improbable. In fact Γ_γ comes out to be an order of magnitude smaller than the experimental value (see Fig. 4 and 5), The smallness of Γ_γ for the higher level is due to the fact that in this mode the two oscillations couple in an opposite way so that the net displacement of the neutrons relative to protons is very small (see Fig. 6). This is not the case for the lower level.

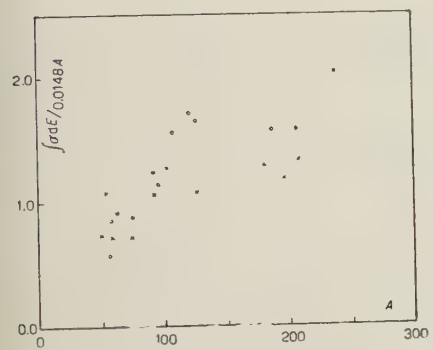

Fig. 4. – The experimental value of the ratio of the integrated cross-section to the sum rule limits $(\pi^2/2)\cdot(e^2/\hbar c)(\hbar/Mc)Mc^2A$ (as for reference see Fig. 3).

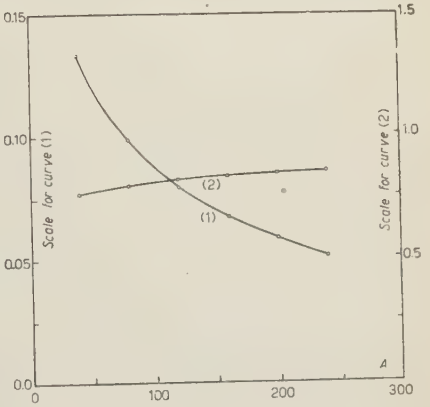

Fig. 5. – The ratio of the new integrated cross-sections to the sum rule limit $(\pi^2/2)\cdot(e^2/\hbar c)(\hbar/Mc)Mc^2A$. Curve (1): The second resonance as the giant resonance. Curve (2): The first resonance as the giant resonance.

If we identify the lower frequency as the giant resonance frequency by increasing both constants in the potential terms, we find again a good A-dependence (see Fig. 7). The higher frequency becomes so high (see Fig. 3) that for such energies the γ-ray wave-length is too small to apply the ordinary dipole approximation. In any case the width for this level is very small. The width for the lower level is of the right order of magnitude (see Fig. 4). Its A-dependence, however, is not as it should be (fig. 5).

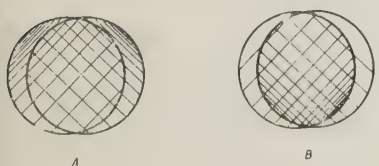

Figi 6. – Displacement of the proton sphere with regard to the neutron sphere together with the change of density inside each sphere. A: two oscillations couple in the same way, corresponding to lower frequency; B: two oscillations couple in an opposite way, corresponding to higher frequency.

It is a very undesirable thing to change the S-J constant which is the coefficient of the symmetry energy in the semiempirical mass formula and is quite well determined. The main change to be considered is that there is a further surface energy which was neglected so far. The velocity of the longitudinal wave of S-J has a zero at the surface which implies that there occurs a

change in the neutron and proton density at the surface. If the density distribution of each constituent is changed at the surface, there must be an increase in the surface energy even if the neutrons and protons do not move as a whole. The S-J approximation is that this energy change is very small compared to that due to the internal symmetry energy and the energy change due to the non-overlapping at the surface is so large that the shape of the surface is fixed. On the other hand the G-T picture is that the former energy change is so large compared to the latter that the neutron and the proton densities move as a whole without changing their shape. The inclusion of the change of the density distribution at the surface does not entail an essential change in G-T formulation except for the interpretation of the constant in the potential energy. But if one tries to combine the internal density distribution and the extra surface energy due to the change of the density distribution of each component at the surface, the problem becomes too complicated. As a matter of fact, it will be required to have a theory of the density distribution at the surface itself before studying this problem.

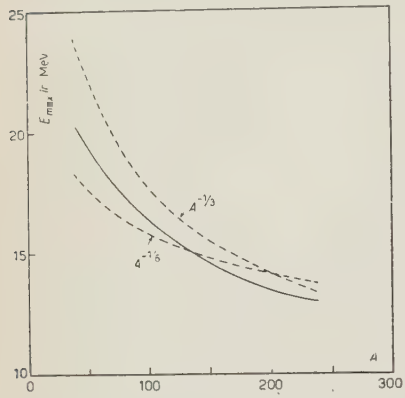

Fig. 7. – The variation of the first frequency (E_{max}) according to A. The curve for $K'''=2K$; $k'''=2k$.

6. – Conclusion.

We shall recapitulate the results obtained with this model.

I) If we identify the higher level as the giant resonance we find:

a) The A-dependence of resonance frequency becomes better than for the uncoupled model.

b) A possible explanation of the fact that the ratio $\sigma(\gamma, p)/\sigma(\gamma, n)$ is experimentally larger than the value obtained from statistical theory.

c) The absolute value of the integrated cross-section is an order of magnitude smaller than the experimental value if we take the integration over the higher resonance.

d) Γ_γ/Γ is too small if compared with the experimental ratio $\sigma_{\gamma\gamma}/\sigma_{\gamma n}$.

II) If on the other hand we identify the lower level as the giant resonance, the point a) is again good and we have the right order of magnitude for the integrated cross-section and also for the ratio Γ_γ/Γ, but we must increase the force constants about twice.

Appendix I.

Let us consider the Lagrangian (2):

$$L = \int d\tau \left\{ \frac{M}{2} \varrho_{red} (- \operatorname{grad} \varphi + \dot{\overline{\Delta r}})^2 - K \frac{(\varrho_N - \varrho_P)^2}{\varrho_0} + \lambda \left[\frac{\partial \varrho_P}{\partial t} - \operatorname{div} (\varrho_{red} \operatorname{grad} \varphi) \right] \right\} - \frac{k}{2} (\Delta r)^2 .$$

The variation of φ gives

$$\int d\tau \, \delta\varphi [- M \operatorname{div} (\varrho_{red} \operatorname{grad} \varphi) + M \operatorname{div} (\varrho_{red} \dot{\overline{\Delta r}}) - \operatorname{div} (\varrho_{red} \operatorname{grad} \lambda)]$$

and since in our approximation $\operatorname{div} (\varrho_{red} \dot{\overline{\Delta r}}) \approx 0$ we have

$$M \operatorname{div} (\varrho_{red} \operatorname{grad} \varphi) + \operatorname{div} (\varrho_{red} \operatorname{grad} \lambda) = 0,$$

that is

$$\lambda = - M\varphi ,$$

and we have

$$L = \int d\tau \left\{ \frac{M}{2} \varrho_{red} (- \operatorname{grad} \varphi + \dot{\overline{\Delta r}})^2 - K \frac{(\varrho_P - \varrho_N)^2}{\varrho_0} - M\varphi \frac{\partial \varrho_P}{\partial t} + M\varphi \operatorname{div} (\varrho_{red} \operatorname{grad} \varphi) \right\} - \frac{k}{2} (\Delta r)^2 .$$

After the partial integration of the last two terms this becomes:

$$L = \int d\tau \left\{ \frac{M}{2} \varrho_{red} (\operatorname{grad} \varphi)^2 - M \varrho_P \frac{\partial \varphi}{\partial t} - \frac{M}{2} \varrho_{red} (\dot{\overline{\Delta r}})^2 - M \varrho_{red} (\operatorname{grad} \varphi) \cdot \dot{\overline{\Delta r}} - K \frac{(\varrho_P - \varrho_N)^2}{\varrho_0} \right\} - \frac{k}{2} (\Delta r)^2 .$$

The volume integral can be easily carried out considering that

$$\varphi = a(t) j_1(x) \cos \vartheta$$

$$\eta = \frac{M \varrho_0}{8K} \dot{\varphi} \qquad \text{with} \quad x \quad \frac{r}{r_0} .$$

and

$$\varrho_{\mathrm{red}}\,(\mathrm{grad}\,\varphi)^2 \approx \varrho_0 \frac{NZ}{A^2}\,(\mathrm{grad}\,\varphi)^2$$

$$(\varrho_P \quad \varrho_N)^2 \approx 4\eta^2.$$

The result is:

$$(a) \qquad L = \frac{4\pi}{3}\frac{M\varrho_0}{2}\left\{-a^2(t)A_0\frac{NZ}{A^2} + \dot{a}^2(t)A_0^3\frac{M}{8K}\right\}F(X)$$

$$(b) \qquad + \frac{4\pi}{3}R^3\frac{M\varrho_0}{2}\frac{NZ}{A^2}\,(\dot{\overline{\Delta r}})^2 - \frac{k}{2}(\Delta r)^2 -$$

$$(c) \qquad - 2\cdot\frac{4}{3}\pi\frac{M\varrho_0}{2}\frac{NZ}{A^2}A_0^2\dot{\overline{\Delta r}}\,a(t)\,G(X)\ ,$$

with

$$k = \frac{\pi R^2\varrho_0\varphi}{\varepsilon}\ ,$$

$$F(X) = \frac{X}{2} + \frac{\sin X\cos X}{2} - \frac{\sin^2 X}{X}\ ,$$

$$G(X) = \sin X - X\cos X\ ,$$

$$X = \frac{R}{A_0} = 2.08 \quad \text{(see ref. (2))} \qquad (R = r_0A^{\frac{1}{3}}),$$

where the first part (a) is due to S-J motion, the second part (b) to G-T motion and the third (c) represents the interaction between the two motions.

Writing

$$a(t) = RA_0\omega_0\alpha(t)$$

and remembering that

$$\frac{ZN}{A^2} \approx \frac{1}{4} \quad \text{and} \quad \omega_0A_0 = \left(\frac{8K}{4M}\right)^{\frac{1}{2}}$$

we have

$$L = \frac{4}{3}\pi\frac{M\varrho_0}{8}R^3\left\{-(\omega_0A_0)^2\frac{F(X)}{X}\alpha^2(t) + A_0^2\frac{F(X)}{X}\dot{\alpha}^2(t) - \right.$$

$$\left. - 2(\omega_0A_0)\alpha(t)\dot{\overline{\Delta r}}\frac{G(X)}{X^2} + (\dot{\overline{\Delta r}})^2 - \frac{3\varphi}{MR\varepsilon}(\Delta r)^2\right\}$$

or, as $\frac{4}{3}\pi R^3\varrho_0 \quad A$,

$$L = \frac{MA}{4}\frac{R^2}{2}\left\{-\omega_0^2B\alpha^2 + B\dot{\alpha}^2 + \dot{\beta}^2 - \omega_1^2\beta^2 - D\alpha\dot{\beta}\right\},$$

with:

$$B = F(X)/X^3$$
$$D = \omega_0 G(X)/X^3$$
$$\beta = \Delta r/R$$
$$\omega_1 = \left(\frac{3\varphi}{MR\varepsilon}\right)^{\frac{1}{2}}.$$

Appendix II.

We start from the Lagrangian (4) a part from the factor $(MA/4)R^2$,

$$L = \tfrac{1}{2}\{B\dot{\alpha}^2 - \omega_0^2 B\alpha^2 + \dot{\beta}^2 - \omega_1^2\beta^2 - 2D\alpha\dot{\beta}\}.$$

Introducing the momenta

$$p_\alpha = \frac{\partial L}{\partial\dot{\alpha}} = B\dot{\alpha},$$

$$p_\beta = \frac{\partial L}{\partial\dot{\beta}} = \dot{\beta} - D\alpha,$$

we have the Hamiltonian

$$H = \frac{1}{2}\left\{\frac{p_\alpha^2}{B} + p_\beta^2 + \omega^2\alpha^2 + B\omega_0^2\alpha^2 + \omega_1^2\beta^2 + 2D\alpha p_\beta\right\}.$$

To eliminate the cross-term, we apply first a canonical transformation

$$F = \alpha\gamma,$$

$$p_\alpha = \frac{\partial F}{\partial\alpha} = \gamma,$$

$$p_\gamma = -\frac{\partial F}{\partial\gamma} = -\alpha.$$

Then

$$H = \frac{1}{2}\left\{B\Omega^2 p_\gamma^2 + \frac{\gamma^2}{B} + p_\beta^2 + \omega_1^2\beta^2 - 2Dp_\beta p_\gamma\right\},$$

with

$$\Omega^2 = \omega_0^2 \quad B^2 B \quad \omega_0^2(1 \quad c).$$

Now we express the Lagrangian in terms of γ, β, $\dot{\gamma}$, $\dot{\beta}$, where

$$\dot{\gamma} = \frac{\partial H}{\partial p_\gamma} = B\Omega^2 p_\gamma - D p_\beta ,$$

$$\dot{\beta} = \frac{\partial H}{\partial p_\beta} = p_\beta - D p_\gamma .$$

Then we obtain, writing again the factor $(MA/4)R^2$,

$$L = \frac{MA}{4}\frac{R^2}{2}\left\{\frac{1}{B\omega_0}\dot{\gamma}^2 + \left(\frac{\Omega}{\omega_0}\right)^2\dot{\beta}^2 + \frac{D}{B\omega_0^2}\dot{\gamma}\dot{\beta} - \frac{1}{B}\gamma^2 - \omega_1^2\beta^2\right\}$$

and putting

$$\chi = \frac{1}{\sqrt{B}\omega_0}\gamma ,$$

ve have simply

$$L = \frac{MA}{4}\frac{R^2}{2}\{\dot{\chi}^2 + (1+c)\dot{\beta}^2 + 2\sqrt{c}\,\dot{\chi}\dot{\beta} - \omega_0^2\chi^2 - \omega_1^2\beta^2\} .$$

At this point we diagonalize the Lagrangian. That is, we find normal coordinates ξ and η which are a linear combination of χ and β.

The equations of motion derived from the Lagrangian are

$$\begin{cases} -\ddot{\chi} - \sqrt{c}\,\ddot{\beta} - \omega_0^2\chi = 0 , \\ -(1+c)\ddot{\beta} - \sqrt{c}\,\ddot{\chi} - \omega_1^2\beta = 0 . \end{cases}$$

The secular equation is:

$$(*) \qquad \begin{vmatrix} \omega^2 - \omega_0^2 & \sqrt{c}\,\omega^2 \\ \sqrt{c}\,\omega^2 & \omega^2(1+c) - \omega_1^2 \end{vmatrix} = 0 .$$

If we call ω and ω' the roots of (*), we have the following solutions:

$$\begin{pmatrix} \sqrt{c}\,\omega^2 \\ \omega_0^2 - \omega^2 \end{pmatrix} \quad \begin{pmatrix} \sqrt{c}\,\omega'^2 \\ \omega_0^2 - \omega'^2 \end{pmatrix}$$

Then as is well known, ξ and η are given by

$$(9) \qquad \begin{cases} \chi = \sqrt{c}\,\omega^2\xi + \sqrt{c}\,\omega'^2\eta , \\ \beta = (\omega_0^2 - \omega^2)\xi + (\omega_0^2 - \omega'^2)\eta . \end{cases}$$

With these new variables, the Lagrangian becomes:

$$L = \tfrac{1}{2}(m\dot{\xi}^2 + m'\dot{\eta}^2 + k\xi^2 + k'\eta^2) ,$$

with

$$m = \frac{MA}{4} R^2\{(\omega_0^2 - \omega^2)^2 + c\omega_0^4\},$$

$$m' = \frac{MA}{4} R^2\{(\omega_0^2 - \omega'^2)^2 + c\omega_0^4\},$$

$$k = \frac{MA}{4} R^2\{\omega_1^2(\omega_0^2 - \omega^2)^2 + c\omega_0^2\omega^4\},$$

$$k' = \frac{MA}{4} R^2\{\omega_1^2(\omega_0^2 - \omega'^2)^2 + c\omega_0^2\omega'^4\},$$

where, as is easily seen $k = \omega^2 m$ and $k' = \omega'^2 m'$. We then find the eigenfunctions of the following Hamiltonian

$$H = \tfrac{1}{2}m\dot{\xi}^2 + \tfrac{1}{2}m'\dot{\eta}^2 + \tfrac{1}{2}k\xi^2 + \tfrac{1}{2}k'\eta^2 .$$

Since the variables are separable, the wave functions are $\psi_n(\xi)\psi_m(\eta)$. We are interested in the transition probabilities from the first and the second excited state to the ground state. The wave functions for the ground state, the first excited state and the second excited state are respectively

$$\psi_0(\xi)\,\psi_0(\eta) ,$$

$$\psi_1(\xi)\,\psi_0(\eta) ,$$

$$\psi_0(\xi)\,\psi_1(\eta) .$$

Writing the dipole moment in terms of ξ and η we calculate the integrals

$$D_{10} = \int \psi_1(\xi)\,\psi_0(\eta)(D_1\xi + D_2\eta)\,\psi_0(\xi)\,\psi_0(\eta)\,\mathrm{d}\xi\,\mathrm{d}\eta$$

$$D_{20} = \int \psi_0(\xi)\,\psi_1(\eta)(D_1\xi + D_2\eta)\,\psi_0(\xi)\,\psi_0(\eta)\,\mathrm{d}\xi\,\mathrm{d}\eta$$

that is, taking account of selection rules:

$$(**) \qquad \begin{cases} D_{10} = D_1 \int \psi_1(\xi)\xi\,\psi_0(\xi)\,\mathrm{d}\xi \\ D_{20} = D_2 \int \psi_1(\eta)\eta\,\psi_0(\eta)\,\mathrm{d}\eta \end{cases}$$

where

$$D_1 = \frac{eA}{4} R\{(\omega_0^2 - \omega^2) + c\omega^2\}$$

$$D_2 = \frac{eA}{4} R\{(\omega_0^2 - \omega'^2) + c\omega'^2\}$$

(see equ. (7) and (9)).

The integrals give

$$D_{10} = D_1 \frac{1}{\sqrt{2}} \frac{1}{\alpha}$$

$$D_{20} = D_2 \frac{1}{\sqrt{2}} \frac{1}{\beta}$$

with

$$\alpha^2 = \frac{\sqrt{mk}}{\hbar} = \frac{MA}{4} R^2 \{(\omega_0^2 - \omega^2)^2 + c\omega_0^4\} \frac{\omega}{\hbar},$$

$$\beta^2 = \frac{\sqrt{m'k'}}{\hbar} = \frac{MA}{4} R^2 \{(\omega_0^2 - \omega'^2)^2 + c\omega_0^4\} \frac{\omega'}{\hbar}.$$

* * *

The authors would like to express their sincere thanks for the hospitality at the Department and the valuable criticism on this work, to Professor R. E. PEIERLS.

One of them (V. DE SABBATA) is grateful to Consiglio Nazionale delle Ricerche, Roma, and the other (A. SUGIE) to the British Council for providing their scholarships.

RIASSUNTO

Nella considerazione delle reazioni foto-nucleari nella zona della risonanza gigante viene preso in esame un modello nucleare collettivo che tiene conto contemporaneamente di oscillazioni del tipo di Goldhaber-Teller (G.-T.) e del tipo di Steinwedel-Jensen (S.-J.). Si trova un termine d'accoppiamento tra i due moti che appare nell'energia cinetica. Questo conduce a una soluzione doppia per le frequenze di risonanza. Se si identifica il livello più alto con la risonanza gigante, si trova un migliore andamento della frequenza di risonanza in funzione del numero di massa A. Inoltre la presenza di un livello di risonanza più basso vicino alla soglia del processo (γ, n), potrebbe fornire una spiegazione del fatto che il rapporto $\sigma(\gamma, p)/\sigma(\gamma, n)$ è sperimentalmente assai grande. Tuttavia sia il rapporto $\Gamma_\gamma/\Gamma \simeq \sigma_{\gamma\gamma}/\sigma_{\gamma n}$ che la sezione d'urto integrata sono troppo piccoli se confrontati con l'esperienza. Se invece si identifica il livello più basso con la risonanza gigante, si ha ancora un migliore accordo con l'esperienza per quello che riguarda l'andamento della frequenza di risonanza in funzione del numero di massa. Inoltre il rapporto Γ_γ/Γ e il valore assoluto della sezione d'urto integrata sono del giusto ordine di grandezza, ma in questo caso è necessario aumentare circa del doppio le costanti delle forze di richiamo come date da G.-T. e S.-J.

Lo spettro di energia degli elettroni di decadimento dei mesoni μ in emulsione nucleare.

A. Bonetti, R. Levi Setti, M. Panetti e G. Rossi

Istituto di Scienze Fisiche dell'Università - Milano
Istituto Nazionale di Fisica Nucleare - Sezione di Milano

G. Tomasini

Istituto di Fisica dell'Università - Genova

(ricevuto il 14 Ottobre 1955)

Riassunto. — Nel presente lavoro si studia la distribuzione delle energie di 506 tracce di elettroni di decadimento di mesoni μ, ottenuta da misure di « scattering ». Le misure sono state eseguite con il metodo delle coordinate e con il metodo angolare; per il calcolo delle energie si è fatto uso della « costante di scattering » di Goldschmidt-Clermont, tenendo conto della variazione di questa con la velocità e con la lunghezza delle celle. Le varianze degli angoli medi di scattering sono state dedotte dalle teorie di Molière e di d'Espagnat. Lo spettro sperimentale, disperso dalla bremsstrahlung e dalle misure di scattering, viene confrontato con gli spettri teorici (forniti dalle teorie di Michel e di Porter e Primakoff) modificati per tener conto dei due effetti. Il metodo statistico della « massima verosimiglianza » conduce alla stima del parametro di forma ϱ introdotto da Michel, relativo nella presente esperienza ad una mescolanza di particelle positive e negative ($\varrho^{\pm}$). Si ottiene $\varrho^{\pm} = 0.57 \pm 0.14$, dove l'errore è in parte dovuto alle fluttuazioni di frequenza dello spettro sperimentale, in parte all'incertezza sulla costante di scattering. Il valore trovato risulta in buon accordo con quello ottenuto da altri sperimentatori con altre tecniche.

1. – Introduzione.

Il metodo fotografico è stato impiegato ripetutamente nello studio dello spettro energetico degli elettroni di decadimento dei mesoni μ ([1-6]). La distribuzione di energia che si ottiene con questa tecnica da misure di « scattering multiplo », differisce specialmente nella regione del punto di fine dallo spettro all'emissione degli elettroni a causa delle perdite di energia per radiazione nell'emulsione ed a causa della dispersione statistica delle misure stesse. Per ricavare perciò la forma dello spettro all'emissione è necessario ricorrere ad una distribuzione teorica e riprodurre su questa le deformazioni provocate dai fenomeni radiativi e dalla dispersione delle misure: si individua così il particolare spettro che meglio si accorda con l'esperienza.

Il risultato dipende fortemente dai valori che si adottano per i parametri caratteristici del metodo dello scattering; eventuali errori sistematici su tali valori limitano la possibilità di impiego del metodo fotografico, rispetto ad altre tecniche, per lo studio del problema in questione. Tuttavia recenti lavori teorici e sperimentali hanno migliorato la conoscenza dei parametri critici (§§ 4·2 e 6): riteniamo che questo fatto e la statistica sufficientemente ampia raccolta nel presente lavoro rendano significativa la determinazione del parametro di forma ϱ della distribuzione delle energie all'emissione.

L'esame delle deformazioni subite dallo spettro ed i metodi seguiti per il confronto con la teoria possono dare indicazioni sulle possibilità di impiego del metodo fotografico nello studio di altri spettri continui di elettroni, anche se estesi ad energie più elevate, come ad esempio quello dei secondari dei mesoni K_β.

2. – Lo spettro sperimentale.

In un lavoro precedente erano state riportate ([3]) le energie di 278 elettroni di decadimento di mesoni μ da raggi cosmici, osservati in lastre Ilford G5, di spessore fino a 1200 μm. Questa statistica è stata arricchita nella presente esperienza fino ad includere un totale di 506 eventi.

Il gruppo di tracce prese in considerazione comprende 339 eventi ottenuti in una esposizione a 2850 m e 167 in una esposizione a circa 20000 m. I cri-

([1]) J. H. Davies, W. O. Lock and H. Muirhead: *Phil. Mag.*, **40**, 1250 (1949).
([2]) H. J. Bramson, W. W. Havens: *Phys. Rev.*, **83**, 862 (1951).
([3]) R. Levi Setti e G. Tomasini: *Nuovo Cimento*, **8**, 12 (1951).
([4]) C. O'Ceallaigh: *København Meeting* (July 1951).
([5]) H. J. Bramson, A. M. Seifert e W. W. Havens: *Phys. Rev.*, **88**, 304 (1952)
([6]) C. Mabboux-Stromberg: *Ann. Phys.*, **9**, 441 (1954).

teri adottati nella scelta delle nuove tracce misurate ed i metodi impiegati nelle misure di scattering (metodo angolare e metodo delle sagitte) e nell'eliminazione della distorsione sono analoghi a quelli di cui è stato fatto uso nel gruppo precedente di misure [3]. Tuttavia l'analisi di tutto il materiale sperimentale raccolto è stata rielaborata con i seguenti criteri:

i) si è adottato il valore della « costante » di scattering e la sua variazione in funzione della lunghezza di cella e della velocità, calcolati da GOLDSCHMIDT-CLERMONT [7];

ii) si è introdotto nei risultati delle misure angolari il fattore di « smoothing » 0.934, dedotto recentemente da MOLIÈRE [8], in luogo del valore 0.96 indicato da [7];

iii) le energie dei singoli elettroni sono state corrette per la perdita di energia per ionizzazione, secondo i risultati di GOLDWASSER *et. al.* [9].

La distribuzione delle energie dei 506 elettroni è riportata in fig. 1.

Una valutazione della composizione relativa al segno delle particelle incluse nella statistica è stata compiuta in base al rapporto tra il numero di mesoni μ con e senza elettrone nelle lastre utilizzate. Dal confronto con i risultati di [10,11] abbiamo ammesso che la mescolanza di mesoni μ studiati contenga circa il 26% di particelle negative. Tuttavia, come è mostrato nel seguito (§ 5), le conclusioni dedotte dal confronto con la teoria sono assai poco sensibili al valore di questa percentuale.

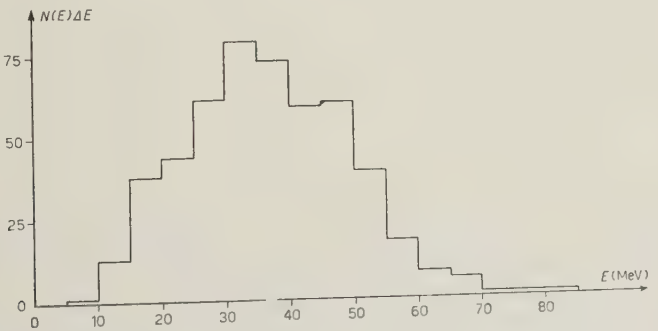

Fig. 1. – Spettro sperimentale di energia degli elettroni corretto per la perdita per ionizzazione.

(7) Y. GOLDSCHMIDT-CLERMONT: *Nuovo Cimento*, **7**, 331 (1950); Tesi (Bruxelles).
(8) G. MOLIÈRE: *Zeits. f. Naturf.*, **10** a, 177 (1955).
(9) E. L. GOLDWASSER, F. E. MILLS e A. O. HANSON: *Phys. Rev.*, **88**, 1137 (1952).
(10) W. F. FRY: *Phys. Rev.*, **79**, 893 (1950).
(11) A. BONETTI e G. TOMASINI: *Nuovo Cimento*, **8**, 693 (1951).

3. – Gli spettri teorici.

La forma dello spettro di energia degli elettroni di decadimento dei mesoni μ è stata calcolata da diversi autori postulando una disintegrazione a tre corpi $\mu^{\pm} \to e^{\pm} + \nu + \nu$ e supponendo che tra le quattro particelle interessate al processo vi sia una interazione diretta del tipo di Fermi.

3·1. *Teorie per i mesoni positivi.* – Tiomno, Wheeler e Rau [12] analizzano separatamente i cinque tipi semplici di interazione (S, V, T, A, P) della radioattività β, dando in tal modo ai risultati una forma non agevolmente confrontabile con l'esperienza.

Michel [13] adotta come densità di hamiltoniana di interazione la più generale combinazione lineare degli scalari che si possono costruire con i campi delle quattro particelle. Lo spettro di energia risulta allora espresso linearmente mediante tre funzioni K_1, K_2, K_3 quadratiche nelle costanti di accoppiamento. Siccome il termine in K_3 è trascurabile e K_1, K_2 sono legate dalla vita media del mesone μ che è nota, si può rappresentare la famiglia di curve dei possibili spettri di energia linearmente mediante un unico parametro ϱ (parametro di forma).

Il procedimento adottato a tale scopo è il seguente: dalla forma generale dello spettro si ottengono le curve relative ai tipi semplici di accoppiamento, imponendo che tutte le costanti di accoppiamento tranne una si annullino; dette P' e P'' le curve che al punto di fine presentano il massimo divario nella intensità, un generico spettro è rappresentato da $P = P' + \varrho(P'' - P')$ dove ϱ varia tra 0 e 1.

In base a queste considerazioni Michel esprime la probabilità di transizione per unità di tempo relativa ai mesoni μ^+ mediante la formula

$$P(E)\,\mathrm{d}E = \frac{12E^2}{\tau^+ W^4}\left[W - E + \frac{2}{9}\varrho(4E - 3W)\right]\mathrm{d}E\,, \tag{1}$$

dove τ^+ è la vita media del mesone μ^+. La parte dello spettro relativa alle piccole energie risulta approssimata nella (1) essendo stata trascurata la massa del positrone in confronto alla sua energia totale.

Dalla identicità dei neutrini consegue l'assenza di alcune delle forme semplici di interazione: si riconosce che anche in tal caso vale la (1) purchè sia $0 \leq \varrho \leq 0.75$. Michel [14] ha successivamente esplicitato la relazione tra il

[12] J. Tiomno, J. Wheeler e R. R. Rau: *Rev. Mod. Phys.*, **21**, 144 (1949).

[13] L. Michel: *Nature*, **163**, 959 (1949); *Proc. Phys. Soc.*, A **63**, 514 (1950); *Thèse, Université de Paris*, 1953.

[14] L. Michel: *Phys. Rev.*, **86**, 814 (1952).

parametro ϱ e le costanti di accoppiamento per neutrini distinguibili e indistinguibili. Una determinazione sperimentale di ϱ definisce pertanto in maniera univoca un legame tra le costanti di accoppiamento solo se $\varrho \neq 0.75$, nel qual caso è possibile affermare che i neutrini sono distinguibili.

Caratteristiche comuni alle curve determinate per i positroni sono:

i) l'esistenza di una energia massima $W = (m_e^2c^4 - m_\mu^2c^4)/2m_\mu c^2$ disponibile per il positrone;

ii) una intensità dello spettro in generale diversa da zero al punto di fine.

3·2. *Teorie per i mesoni positivi e negativi.* – L'estensione dei calcoli ai mesoni μ^- tenendo conto del legame tra mesone e nucleo presenta considerevoli complicazioni di carattere algebrico. Detta estensione è stata effettuata da MUTO *et al.* [15] mediante analisi separata dei tipi semplici di interazione, e da PORTER e PRIMAKOFF [16,17] in una forma di agevole confronto con la esperienza. Essi si rifanno ai risultati e al formalismo di MICHEL, combinando linearmente mediante lo stesso parametro ϱ le curve relative a due opportune forme semplici di interazione (scelte in relazione al loro comportamento al punto di fine tra quelle studiate da TIOMNO *et al.*): i calcoli vengono eseguiti soltanto per questi due casi estremi, postulando la identicità dei neutrini ($0 \leqslant \varrho \leqslant 0.75$) ed effettuando perciò la combinazione lineare in termini di $\frac{4}{3}\varrho$.

Gli spettri degli e^+ e degli e^- sono espressi rispettivamente dalle formule:

$$P(p)d\left(\frac{p}{m_e c}\right) = \frac{12}{\tau^-}(2y)^2\left[\left(1-\frac{4}{3}\varrho\right)(1-2y)+\frac{2}{3}\varrho\left(1-\frac{2}{3}2y\right)\right]\mathrm{d}(2y) \qquad \text{per } y \leqslant \frac{1}{2}, \tag{2}$$

$$P(p)d\left(\frac{p}{m_e c}\right) = \frac{12}{\tau^-}(2y)^2\left[\left(1-\frac{4}{3}\varrho\right)(1-2y)f(y)+\frac{2}{3}\varrho\left(1-\frac{2}{3}2y\right)g(y)\right]\mathrm{d}(2y) \qquad \text{per } y \leqslant 1, \tag{3}$$

e si annullano al di sopra dei limiti indicati. Nelle precedenti espressioni è $y = p/m_e c \cong E/2W$, τ^- è la vita media del mesone μ^- e $f(y)$ e $g(y)$ sono date da:

$$f(y) = \frac{1}{\pi}\left[\mathrm{tg}^{-1}\frac{1-2y}{Z\alpha} + \mathrm{tg}^{-1}\frac{1}{Z\alpha}\right] + \frac{2Z\alpha}{\pi}\frac{1-y}{1-2y}\left[1-\frac{1}{3}\frac{1-y}{y}\frac{(Z\alpha)^2}{(Z\alpha)^2+(1-2y)^2}\right],$$

---

[15] T. MUTO, M. TANIFUJI, K. INOUE e T. INOUE: *Progr. Theor. Phys.*, 8, 13 (1952).

[16] C. PORTER e H. PRIMAKOFF: *Phys. Rev.*, **83**, 849 (1951).

[17] C. PORTER e H. PRIMAKOFF: comunicazione privata.

$$g(y) = \frac{1}{\pi}\left[\mathrm{tg}^{-1}\frac{1-2y}{Z\alpha} + \mathrm{tg}^{-1}\frac{1}{Z\alpha}\right] + \\ + \frac{2Z\alpha}{\pi}\frac{1-y}{(Z\alpha)^2+(1-2y)^2}\left[1-2y-\frac{2}{3}\frac{(Z\alpha)^2(1-(3y/2))}{y(1-4(y/3))}\right].$$

Lo spettro (2) coincide con (1): ciò convalida la legittimità del procedimento che a priori avrebbe richiesto una verifica esplicita.

Le caratteristiche delle curve valide per gli e^- sono le seguenti:

i) esiste una « coda » di piccola intensità oltre il punto di fine dello spettro degli e^+;

ii) l'area racchiusa tra la curva e l'asse delle energie risulta minore che nel caso degli e^+.

L'ipotesi che una delle particelle neutre abbia massa differente da 0 è stata presa in considerazione da TIOMNO *et al.* [12] e da MUTO *et al.* [15] che nei loro lavori studiano anche il processo $\mu \to \mu_0 + e + \nu$ con diversi valori per la massa del μ_0. Conseguenze salienti di una massa finita per una delle particelle neutre sono: l'intensità dello spettro al punto di fine è nulla; detto punto di fine viene arretrato sull'asse delle energie di una quantità $(m_{\mu_0}/2m_{\mu})\cdot m_{\mu_0}c^2$ [18].

4. – Confronto tra esperienza e teoria.

Nell'effettuare il confronto tra la teoria e i dati sperimentali si sono prese in considerazione la teoria di Michel e quella di Porter e Primakoff.

In fig. 2 sono riportate le curve di Michel corrispondenti a $\varrho = 0$; 0,25; 0,50; 0.75; 1 e le curve ricavate dalle teorie di Michel e di Porter e Primakoff relative ad una mescolanza contenente il 26% di mesoni negativi, calcolate per $Z = 7$, corrispondenti a $\varrho^{\pm} = 0$; 0.25; 0.50; 0.75, dove $\varrho^{\pm}$ indica il parametro di forma delle curve mescolate.

Le curve teoriche devono essere deformate introducendovi gli effetti delle perdite radiative e della dispersione delle misure: queste cause di deformazione sono esaminate in 4·1 e 4·2 rispettivamente, e la deformazione risultante dalla loro combinazione è descritta in 4·3.

4·1. *Perdite radiative.* – La probabilità che un fascio di elettroni di energia E_0, dopo un percorso t, espresso in lunghezze di radiazione, abbia energia compresa tra E_t e $E_t - \mathrm{d}E_t$ è espressa dalla formula di « straggling » [19]:

$$(4) \qquad \pi(E_0, E_t; t)\,\mathrm{d}E_t = \frac{\mathrm{d}E_t}{E_0}(1+a)^{bt}(E_t/E_0)^{a}\frac{(\lg E_0/E_t)^{bt-1}}{(bt-1)!}$$

[18] G. E. UHLENBECK e C. S. WANG CHANG: *Phys. Rev.*, **85**, 684 (1952).
[19] B. ROSSI e K. GREISEN: *Rev. Mod. Phys.*, **13**, 240 (1941).

dove a e b sono due parametri funzioni di E_0 ([20]). Si è posto per $E_0 \leqslant 30$ MeV $a = 2/5$ e $b = 4/3$, e per $E_0 > 30$ MeV $a = 1/4$ e $b = 4/3$.

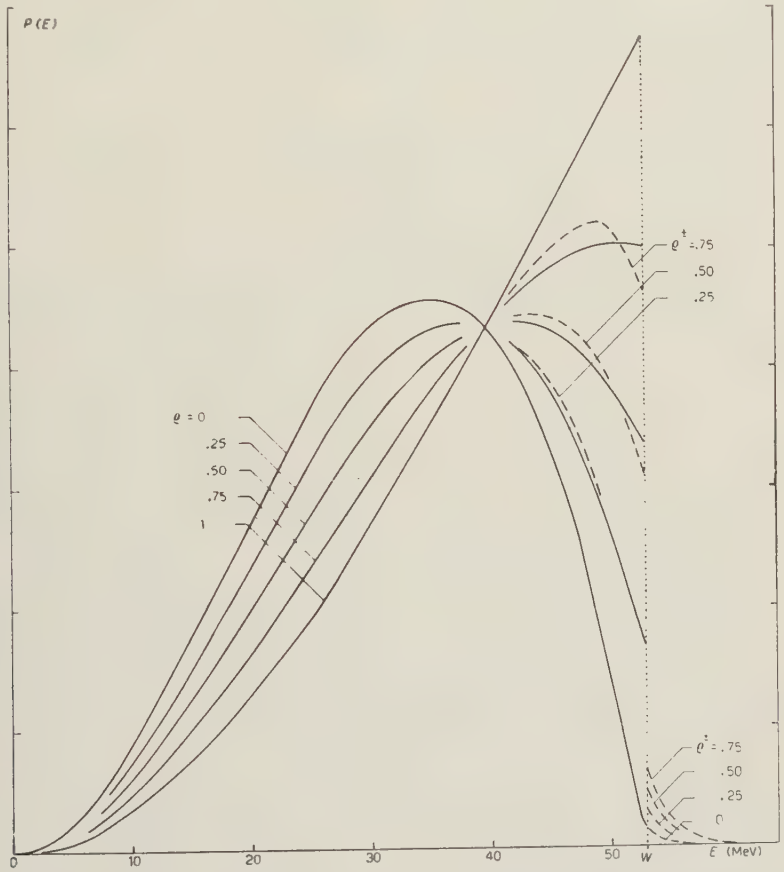

Fig. 2. – Curve di Michel (continue) e curve miste di Michel e di Porter e Primakoff (tratteggiate).

Se $P(E_0)$ è la distribuzione teorica delle energie degli elettroni la distribuzione corretta per la perdita di energia risulta

$$P^*(E, t)\mathrm{d}E = \mathrm{d}E \int_{E}^{E_{\max}} P(E_0)\,\pi(E_0, 2E - E_0; t)\,\mathrm{d}E_0\,, \tag{5}$$

([20]) L. Eyges: *Phys. Rev.*, **76**, 264 (1949).

dove si è posto che in media il valore dell'energia che si ricava dalle misure di diffusione multipla coincide con $E = (E_0 + E_t)/2$ ([21]) ed E_{max} è la massima energia della distribuzione teorica.

La espressione precedente vale per tracce di lunghezza costante t; per una distribuzione di lunghezze $L(t, E_0)$ si ha:

$$P^*(E)\,dE = dE \int_E^{E_{max}} P(E_0)\,dE_0 \int \pi(E_0, 2E - E_0, t)\, L(t, E_0)\,dt\,. \tag{6}$$

La $L(t, E_0)$ dipende dall'energia praticamente soltanto nella regione delle basse energie ($\leqslant 15$ MeV), dove un numero non facilmente determinabile di tracce può essere perduto o per non aver raggiunto la lunghezza minima richiesta, o per difficoltà di inseguimento, a causa dello scattering elevato (*). Scartando le energie inferiori a 15 MeV, si può ritenere che $L(t, E_0)$ sia indipendente da E_0 su tutto lo spettro e far uso della distribuzione sperimentale delle lunghezze data in fig. 3. Inoltre poichè nelle misure sperimentali sono state scartate le tracce con una perdita di energia superiore al 70%, nella funzione di « straggling » è stato introdotto un taglio corrispondente a tale valore.

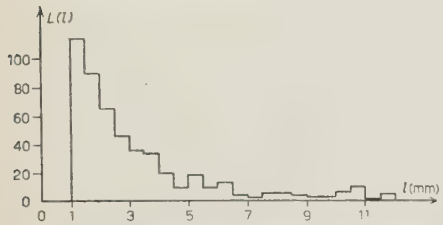

Fig. 3. – Distribuzione di lunghezza delle tracce misurate.

La (6) è stata integrata rispetto ad E_0 per via grafica, ad eccezione della regione attorno ad E, dove è stata calcolata per via analitica con una formula approssimata.

Gli spettri misti modificati per effetto della bremsstrahlung sono mostrati in fig. 4. La differenza tra questi e quelli di MICHEL, modificati in modo analogo, è sensibile soltanto nella regione prossima a W e per valori grandi di ϱ; la differenza è massima (7%) intorno a 50 MeV per $\varrho = 0.75$.

4·2. *Dispersione statistica.* – La probabilità che una particella di energia E, cui corrisponde in emulsione nucleare un angolo medio di scattering $\langle\alpha\rangle$, si presenti con un angolo medio α_{exp} compreso tra α e $\alpha + d\alpha$, è data dal-

([21]) L. JÁNOSSY: *Cosmic Radiation* (Oxford, 1950).

(*) In questa regione di energia, inoltre, il fondo di elettroni spurii è intenso, e ciò può causare ambiguità nel riconoscimento dei secondari dei mesoni μ.

'espressione:

$$\Gamma(\alpha, \langle\alpha\rangle)\,\mathrm{d}\alpha = \frac{1}{\sqrt{2\pi}\sigma}\exp\left[-(\alpha-\langle\alpha\rangle)^2/2\sigma^2\right]\mathrm{d}\alpha\,, \tag{7}$$

love σ è collegata ad $\langle\alpha\rangle$ e al numero n di celle di misura dalla relazione:

$$\sigma = \lambda\frac{\langle\alpha\rangle}{\sqrt{n}} \tag{8}$$

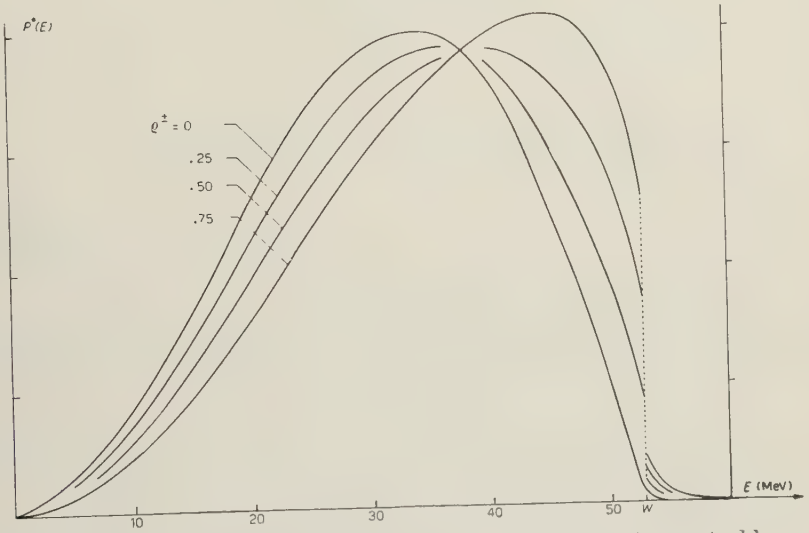

Fig. 4. – Curve di Michel modificate per effetto della bremsstrahlung.

Il coefficiente di dispersione λ è calcolato seguendo la teoria di Molière relativa ad una distribuzione non gaussiana degli angoli di scattering e la teoria di d'Espagnat ([22]) per la valutazione della dispersione, e applicando calcoli di Huybrechts ([23]) e di di Corato ([24]). Tenendo conto che nelle misure la lunghezza della cella è stata scelta in modo che il rapporto tra « noise level » ed angolo di scattering fosse inferiore al 25%, si ottengono le seguenti espressioni approssimate:

$$\sigma = 1.20\frac{\langle\alpha\rangle}{\sqrt{n}}\,, \tag{8'}$$

$$\sigma = 0.99\frac{\langle\alpha\rangle}{\sqrt{n}}\,, \tag{8''}$$

([22]) B. d'Espagnat: *Compt. Rend. Ac. Sc.*, **232**, 800 (1951).
([23]) M. Huybrechts: Tesi (Bruxelles, 1955) e comunicazione privata.
([24]) M. di Corato: comunicazione privata.

valide rispettivamente per il metodo angolare (n indica il numero di celle sovrapposte secondo GOLDSCHMIDT-CLERMONT [7]), e per il metodo delle coordinate (n indica il numero delle celle consecutive).

I valori di λ 1.20 e 0.99 corrispondono all'impiego di un taglio a 4 volte la media aritmetica senza sostituzione [22].

Per $E \gg mc^2$, come nel caso presente, si ha:

$$\langle E \rangle = K_s(\langle E \rangle)\langle x \rangle_s^{-1} \tag{9}$$

e dalle (7), (8) e (9) si ottiene

$$I'(E, \langle E \rangle)\,\mathrm{d}E = \frac{\sqrt{n}}{\sqrt{2\pi}\,\lambda} \exp\left[-\left(1 - \frac{K(E)}{K(\langle E \rangle)} \frac{\langle E \rangle}{E}\right)^2 \frac{n}{2\lambda^2}\right] \cdot \left[\frac{\mathrm{d}K(E)}{\mathrm{d}E} E - K(E)\right] \frac{\langle E \rangle \mathrm{d}E}{E^2 K(\langle E \rangle)}, \tag{10}$$

che esprime la probabilità che una particella di energia $\langle E \rangle$ appaia con energia compresa tra E ed $E+\mathrm{d}E$. Detta $N(n_i)$ la distribuzione sperimentale del

TABELLA I. – *Distribuzione del numero delle tracce $N(n_i)$ in funzione del numero di celle.*

Numero di celle	Numero di tracce		
	$E \leqslant 30$ MeV	$30 < E \leqslant 60$ MeV	60 MeV $< E$
0- 10	0	0	0
10- 20	14	36	6
20- 30	24	42	19
30- 40	16	53	12
40- 50	15	20	29
50- 60	14	29	6
60- 70	8	14	7
70- 80	12	16	4
80- 90	9	12	4
90-100	10	13	2
100-110	14	11	3
110-120	3	6	0
120-130	4	2	1
130-140	1	2	1
140-150	1	0	0
150-200	9	5	4
200-250	3	9	1
250-300	2	3	1
300-400	0	3	1

numero di tracce in funzione del numero di celle (Tab. I), la (10) diventa:

$$(11) \qquad \Gamma''(E, \langle E\rangle)\,\mathrm{d}E = \frac{1}{\sqrt{2\pi}\,\lambda}\left[\frac{\mathrm{d}K(E)}{\mathrm{d}E}\,E - K(E)\right]\frac{\langle E\rangle\,\mathrm{d}E}{E^2 K(\langle E\rangle)}\cdot$$
$$\cdot \sum_i n_i \exp\left[-\left(1 - \frac{K(E)}{K(\langle E\rangle)}\,\frac{\langle E\rangle}{E}\right)^2 \frac{n_i}{2\lambda^2}\right] N_i \Delta n_i\,.$$

4·3. *Perdite radiative e dispersione statistica.* – In base alle considerazioni precedenti la distribuzione teorica modificata per effetto di bremsstrahlung e per le fluttuazioni statistiche è data da:

$$(12) \qquad P^{**}(E)\mathrm{d}E = \mathrm{d}E \int_0^{E_{\max}} P^{*}(\langle E\rangle)\cdot \Gamma''(E, \langle E\rangle)\mathrm{d}\langle E\rangle\,.$$

La (12) è stata integrata per via grafica, tenendo conto che una parte delle tracce (322) è stata misurata col metodo angolare e una parte (170) con quello delle coordinate. La fig. 5 mostra il risultato ottenuto con le curve mescolate. La differenza tra queste e le curve deformate di Michel si mantiene inferiore al 4% anche per $\varrho = 0.75$, valore del parametro di forma per cui si verifica il massimo divario.

Nè la teoria di Michel, nè quella di Porter e Primakoff tengono conto dei fenomeni radiativi all'emissione (« innere Bremsstrahlung » o « Abstrahlung », e produzione di fotoni virtuali ([25,26])); risultati espliciti sono stati pubblicati solo per particolari tipi di accoppiamento ([26]). Per questa ragione non sono state apportate agli spettri teorici le modificazioni dovute a questi effetti.

5. – Stima del parametro $\varrho^{\pm}$.

Il parametro $\varrho^{\pm}$ si determina dal confronto tra la distribuzione sperimentale (fig. 1) e quelle teoriche modificate descritte nel § 4. Le distribuzioni sono state tagliate a 15 MeV (§ 4·1); 14 delle 506 tracce misurate sono state così eliminate.

La stima più attendibile di $\varrho^{\pm}$ è stata ottenuta per mezzo del metodo statistico della « massima verosimiglianza » ([27]). Posto:

$$\mathcal{L} = P^{**}(E_1)P^{**}(E_2)\ldots P^{**}(E_r)\,,$$

([25]) A. Lenard: *Phys. Rev.*, **90**, 968 (1953).
([26]) R. J. Finkelstein e R. E. Behrends: *Phys. Rev.*, **97**, 568 (1954).
([27]) H. Cramer: *Mathematical Methods of Statistics* (Princeton, 1946).

dove $P^{**}(E_i)$ è calcolata per ognuna delle r tracce, la stima di ϱ si ottiene rendendo massima $\mathcal{L}$, imponendo la condizione $\partial\mathcal{L}/\partial\varrho = 0$, equivalente a

$$\sum_i \frac{1}{P^{**}(E_i)} \frac{\partial P^{**}(E_i)}{\partial \varrho} = 0 \,. \tag{13}$$

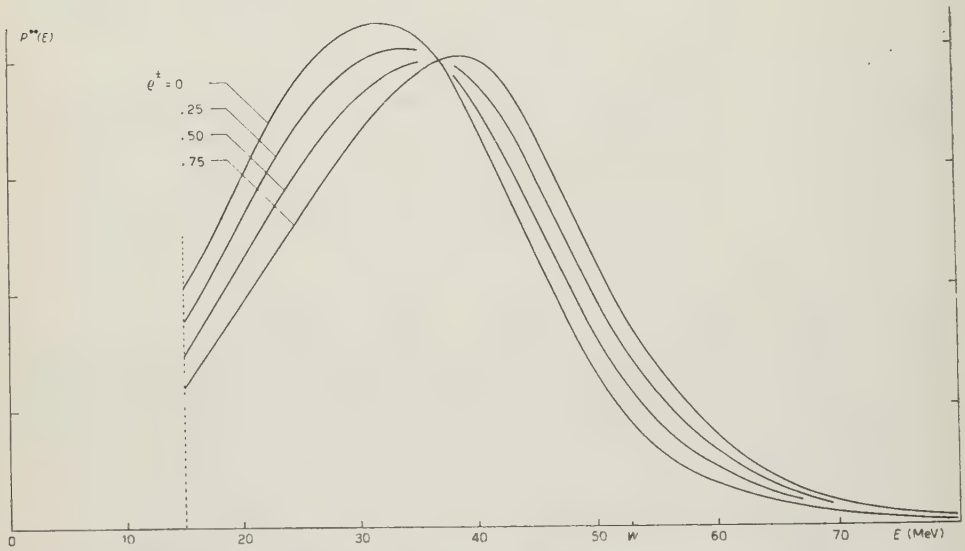

Fig. 5. – Curve miste modificate per effetto della bremsstrahlung e della dispersione statistica.

Il fatto che $\partial P^{**}(E_i)/\partial\varrho$ non dipenda da ϱ ha permesso di ricavarne i valori per via grafica dalle curve teoriche modificate. Come soluzione della (13) si trova $\varrho^{\pm} = 0.57$. La stima del parametro è poco sensibile alla percentuale di particelle negative presenti (26%). Una variazione della percentuale tra circa il 20% e il 30% non porterebbe una alterazione apprezzabile del valore di $\varrho^{\pm}$ sopra indicato. Il confronto dei dati sperimentali con le curve modificate di Michel (per particelle tutte positive) avrebbe condotto al valore $\varrho = 0.60$.

In fig. 6 è rappresentata la distribuzione sperimentale e la curva teorica deformata per $\varrho^{\pm} = 0.57$.

Si sono calcolati i momenti M_k dei primi tre ordini della distribuzione sperimentale — che vengono utilizzati per la stima della varianza su $\varrho^{\pm}$ (§ 6·1) — ed i momenti $\mathcal{M}_k(\varrho)$ degli stessi ordini per gli spettri teorici. Imponendo la condizione

$$M_i = \mathcal{M}_i(\varrho)$$

si ricava $\varrho^{\pm} = 0.58$ per il momento M_1, $\varrho^{\pm} = 0.53$ per M_2 e $\varrho^{\pm} = 0.55$ per M_3.

Allo scopo di valutare l'accordo tra esperienza e teoria è stata effettuata la prova del χ^2 per $\varrho^{\pm} = 0.57$. Per tale valore la probabilità risulta circa il 53%; nell'intorno di esso il χ^2 ha il valore minimo.

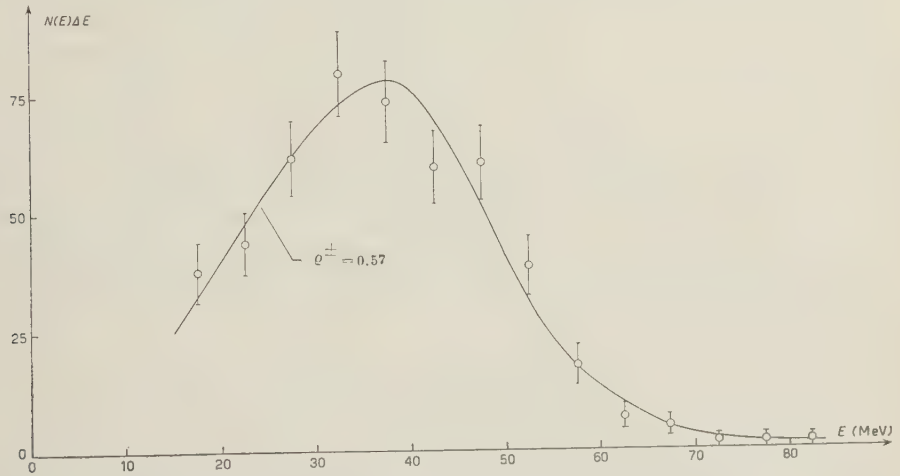

Fig. 6. – Distribuzione sperimentale e curva teorica deformata per $\varrho^{\pm} = 0.57$.

L'aver trascurato i fenomeni radiativi all'emissione, per le ragioni esposte in § 4·3, conduce ad una sottostima del parametro; l'ordine di grandezza della eventuale correzione da apportare è tuttavia piccolo (0.04 su $\varrho = 0.64$ secondo i calcoli di [28]).

6. – Stima della varianza del parametro ϱ.

La varianza del parametro ϱ può essere espressa in prima approssimazione da:

$$(\sigma_\varrho)^2_{tot} = (\sigma_\varrho)^2_{m_\mu} + (\sigma_\varrho)^2_K + (\sigma_\varrho)^2_\lambda + (\sigma_\varrho)^2_{stat} \tag{14}$$

dove m_μ è la massa del mesone μ, K e λ sono rispettivamente la « costante » di scattering e il coefficiente di dispersione (§ 3); l'ultimo termine della (14) rappresenta il contributo alla varianza di ϱ portato dalle fluttuazioni di frequenza dello spettro sperimentale.

[28] C. P. Sargent, M. Rinehart, L. M, Lederman e K. C. Rogers: *Phys. Rev.*, **99**, 885 (1955).

I contributi dei vari termini della (14) sono discussi e valutati nel seguito.

a) Ponendo $m_\mu = (206.9 \pm 0.4)\ m_e$ [29], si ottiene $(\sigma_\varrho)_{m_\mu} = 0.01$.

b) Ponendo $\eta K(E)$ in luogo di $K(E)$, essendo η un numero non molto diverso dall'unità e indipendente dall'energia, lo spettro sperimentale risulta modificato a seconda del valore di η, mentre quello teorico corretto si conserva invariato. La variazione di ϱ in funzione di η è stata ricavata attraverso i metodi della massima verosimiglianza (fig. 7, curva *a*) e dei momenti (fig. 7, curve *b*, *c* e *d*). Dall'andamento delle curve si deduce intorno al valore $\varrho = 0.60$

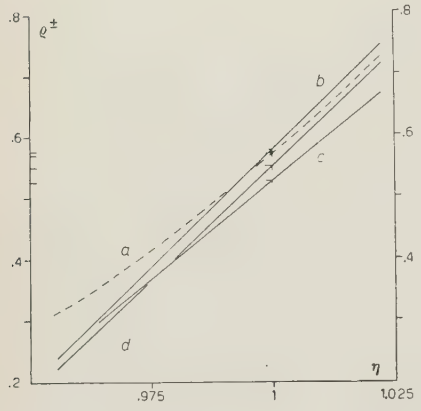

Fig. 7. – Variazione di $\varrho^\pm$ in funzione di η dedotta con il metodo della massima verosimiglianza (curva *a*) e con quello dei momenti (curve *b*, *c*, *d*).

$$\frac{(\Delta\varrho)_K}{\varrho} \cong 10\,\frac{\Delta K}{K}\,.$$

La costante di scattering adottata nel presente lavoro è quella di Goldschmidt-Clermont [7]. Per angoli tra corde, taglio a $4\langle\alpha\rangle$ senza sostituzione, e cella 100 μm e per $\beta \simeq 1$ essa assume il valore 23.3 MeV °/(100 μm)$^{\frac{1}{2}}$. Questo valore è in discreto accordo con quello calcolato da Pickup e Voyvodic [30] (23.6 MeV °/(100 μm)$^{\frac{1}{2}}$. Misure indipendenti compiute dai Gruppi di Bristol [31] e Dublino [32] mostrano che le costanti di [7] e [30] sono corrette a meno dell'1%, con una incertezza di 1.3% relativa a ciascuna delle due determinazioni sperimentali. Sembra pertanto si possa ritenere al momento attuale $\Delta K/K$ non superiore al 2%. Se si accetta questo risultato si ottiene:

$$(\sigma_\varrho)_K \cong 0.12\,.$$

c) È stata valutata la variazione di ϱ in funzione di una variazione del

[29] W. Birnbaum, F. M. Smith e W. H. Barkas: *Phys. Rev.*, **91**, 765 (1953).
[30] L. Voyvodic e E. Pickup: *Phys. Rev.*, **85**, 91 (1952).
[31] Gruppo di Bristol: comunicazione privata; G-Stack Collaboration: *Nuovo Cimento*, **2**, 1063 (1955).
[32] R. K. W. Johnston: *Rend. Congr. Intern. Pisa* (edizione poligrafata), p. 287 (1955).

coefficiente di dispersione λ, che compare nelle (8′) e (8″):

$$(\Delta\varrho)_\lambda = \left|\frac{\partial\varrho}{\partial\lambda}\right| \Delta\lambda \,.$$

Gli spettri teorici corrispondenti ad un valore $\lambda+\Delta\lambda$ permettono di ricavare, in un intorno di $\varrho^{\pm} = 0.57$, la relazione

$$\frac{(\Delta\varrho)_\lambda}{\varrho} \cong -5\,\frac{\Delta\lambda}{\lambda} \,.$$

Mancando tuttavia una verifica sperimentale dei valori di λ relativi ai metodi di misura impiegati, non è possibile valutare $(\sigma_\varrho)_\lambda$;

d) Il contributo alla varianza di ϱ dato dalle fluttuazioni statistiche è stato calcolato dal metodo dei momenti. Dalla relazione:

$$(\Delta\varrho)_{\text{stat}} = \left|\frac{\partial\varrho}{\partial\mathcal{M}_1}\right| \cdot \Delta\mathcal{M}_1 \,,$$

ponendo $\Delta\mathcal{M}_1 = \Delta M_1$, dove $\Delta M_1 = \sqrt{M_2 - M_1^2}/\sqrt{r}$, si ricava

$$(\sigma_\varrho)_{\text{stat}} \cong 0.08 \,.$$

Questo valore resta praticamente invariato includendo le fluttuazioni di frequenza causate dalla dispersione operata dalla bremsstrahlung.

In base alla (14), la varianza complessiva, escluso il contributo di $(\sigma_\varrho)_\lambda$, risulta:

$$(\sigma_\varrho)^2_{\text{tot}} = 0.0001 + 0.0144 + (?) + 0.0064 \cong 0.02 \,.$$

La stima del parametro di forma e della sua varianza portano pertanto al risultato

$$\varrho^{\pm} = 0.57 \pm 0.14 \,.$$

7. – Conclusione.

La Tab. II raccoglie i risultati più significativi di esperienze eseguite con varie tecniche. Dove possibile, si è fatta distinzione tra errore statistico ed errore totale su ϱ.

Il valore di $\varrho^{\pm}$ dedotto nella presente esperienza è in buon accordo con quello dato da BRAMSON *et al.* [5] per mesoni positivi, pure in lastre nucleari.

TABEL

Autore	Sorgente	Segno	Material di arrest
LAGARRIGUE e PEYROU [33] (1951, 1952)	r. c.	±	C, Pb e ve
HUBBARD [34] . . . . . (1952)	accel.	+	C e gas r
VILAIN e WILLIAMS [35] . . . . (1954)	»	+	antracen
SARGENT *et al.* [28] . . . . . (1955)	»	—	H
CROWE *et al.* [36] . . . . . (1955)	»	+	Li,
SAGANE *et al.* [37] . . . . . (1955)	»	+	Be, C, A
STANFORD GROUP [38] . . . . . (1955)	»	. . .	. . .
BRAMSON *et al.* [5] . . . . . (1952)	accel.	+	emulsion
Presente lavoro	r. c.	±	»

(*) Materiale sperimentale di R. B. LEIGHTON, C. D. ANDERSON e A. J. SERIFF: *Phys. Rev.*, 1432 (1949).

Non si è in grado tuttavia di giudicare quanto tale confronto sia significativo, per il fatto che questi autori non hanno preso in considerazione alcune delle cause di deformazione ed incertezza discusse nel lavoro presente.

Il confronto con i dati ricavati con altre tecniche si presta a porre in rilievo e in discussione alcune possibili conclusioni. L'insieme dei risultati, che appaiono in accordo tra loro, porta ad escludere i valori estremi $\varrho = 0$ e $\varrho = 1$ e a ritenere poco probabile, anche se non escluso, un valore superiore a 0.75; non è perciò possibile decidere, ammesso valido lo schema di decadimento $\mu^{\pm} \to e^{\pm} + \nu + \nu$ se i neutrini siano o no distinguibili. Inoltre, dati gli errori, i risultati relativi a mesoni di un solo segno non possono ritenersi contrari all'ipotesi che il parametro di forma sia identico per gli spettri di energia delle particelle positive e negative. Manca tuttavia a questo proposito una esperienza in cui si siano studiati separatamente i due spettri con il medesimo strumento di misura.

D'altra parte la concordanza tra esperienze eseguite con metodi differenti non significa che la disintegrazione del mesone μ sia descritta correttamente

---

[33] A. LAGARRIGUE e C. PEYROU: *Journ. Phys. et Rad.*, **12**, 848 (1951); *Compt. Rend. Acad. Sci.*, **233**, 478 (1951); A. LAGARRIGUE: *Compt. Rend. Acad. Sci.*, **234**, 2060 (1952).

[34] H. W. HUBBARD: *U.C.R.L.* 1623 (1952).

[35] J. H. VILAIN e R. W. WILLIAMS: *Phys. Rev.*, **94**, 1011 (1954).

[36] K. M. CROWE, R. H. HELM e G. W. TAUTFEST: *Phys. Rev.*, **99**, 872 (1955).

[37] R. SAGANE, W. F. DUDZIAK e J. VEDDER: *Phys. Rev.*, **95**, 863 (1954) e comunicazione privata (1955).

[38] STANFORD GROUP: *Proc. V Rochester Conf. on High En. Nucl. Phys.* (1955).

Tecnica di rivelazione	Numero di eventi	ϱ	Errore su ϱ	
			statistico	totale
di Wilson	150+75 (*)	~ 0.4 (**)	0.13	...
di Wilson	405	~ 0.4 (**)	0.26	...
di Wilson	280	0.50	0.10	0.13
a diffusione a pressione	415	0.64	...	0.10
m. con focalizzazione a 180°	...	0.50	0.07	0.10
metro con orbita a spirale	...	~ 0.6	...	...
metro magnet. a doppia focalizz.	...	0.5	...	...
one fotografica	286	~ 0.5 (**)	0.13	...
one fotografica	492	0.57	0.08	0.14 (***)

) Valori dedotti da ([35]) adoperando $m_\mu = (207 \pm 0.4)\, m_e$.
) Non contiene il contributo alla varianza totale dato da $(\sigma_\varrho)_\lambda$.

dallo schema accettato nella teoria di Michel ed in quella di Porter e Primakoff; infatti la risoluzione delle misure e la eventuale presenza di errori sistematici, impediscono di riconoscere con sicurezza, al momento attuale, la posizione del punto di fine dello spettro e di ricavare quindi informazioni sulla massa delle particelle neutre. Questa difficoltà è particolarmente sentita nel caso delle emulsioni nucleari.

La presente esperienza indica che, precisati i valori dei parametri caratteristici del metodo di misura, è possibile studiare con le lastre nucleari la forma di uno spettro continuo di elettroni, nella regione di energia di alcune decine di MeV. È da ritenere che questa possibilità esista anche per energie più elevate, come ad esempio quelle dei secondari dei mesoni K_β, tenendo presente tuttavia che il fenomeno della bremsstrahlung, più importante in questo caso, e l'impiego del metodo dello scattering richiederanno la definizione di criteri sperimentali più adatti alla nuova regione di energia ed eventuali modifiche nel calcolo delle deformazioni degli spettri teorici.

* * *

Esprimiamo la nostra riconoscenza ai proff. P. Caldirola, E. Pancini e G. Polvani per aver incoraggiato la presente collaborazione e la nostra gratitudine ai proff. A. Borsellino, G. Occhialini e M. Schönberg e ai dottori M. di Corato, C. Dilworth e M. Huybrechts per i preziosi consigli, critiche e discussioni.

SUMMARY

An energy spectrum of the decay electrons of μ-mesons has been obtained by scattering measurements on 506 tracks. The measurements were made by the coordinate and the angular method; the energies were calculated with the scattering constant of Goldschmidt-Clermont, allowing for variation with velocity and cell-size. The variances on the individual mean angles of scattering were deduced from the Molière-d'Espagnat theory. The experimental spectrum, blurred due to the straggling introduced by bremsstrahlung and the dispersion of the scattering measurements, is compared with the theoretical spectra (deduced from the theories of Michel and of Porter and Primakoff) modified to take into account these two effects. The statistical method of « maximum likelyhood » has been applied to the estimation of the shape parameter ϱ introduced by MICHEL, referring in the present experiment to a mixture of positive and negative particles ($\varrho^{\pm}$). The result is $\varrho^{\pm} = 0.57 \pm 0.14$, in which the error depends mainly on the uncertainty in the scattering constant and on the fluctuations of frequency of the experimental spectrum. The present value of $\varrho^{\pm}$ is close to those obtained by experimenters making use of other techniques.

IL NUOVO CIMENTO Vol. III, N. 1 1° Gennaio 1956

Photographic Methods in γ-Ray Scintillation Spectroscopy.

B. Chinaglia and F. Demichelis

Istituto di Fisica Sperimentale del Politecnico - Torino

(ricevuto il 21 Ottobre 1955)

Summary. — We deal with an experimental research on the different possibilities to get efficient photographic methods of γ-spectroscopy through scintillation crystals. The spectrum is always strongly disturbed by the Compton distribution, and the possibilities to reduce it by a fitted geometry of the crystals and an anticoincidence device, or by using a proper sized crystal, are discussed. In any case the resolving power is rather poor owing to the fluctuations in every stage of the process from the γ-ray to the recorded pulse. But strong improvements have been reached by a number of laboratories as well in the photomultipliers as in the crystals and in their mounting. This is proved by the comparison up to date spectrograms with those which it was possible to obtain only a few year ago.

1. – Introduction.

The purpose of this study is to draw attention on the actual possibilities of scintillation methods used to obtain γ-ray spectra from radioactive sources, and to present the results of our research with several of these methods.

The aim of γ spectroscopy is to obtain from these rays a spectrum which satisfies the conditions of resolution, absence of disturbances and univocal correspondence between an $h\nu$ value (energy of the γ-ray) and a line of the spectrum.

In the nuclear field this becomes quite complicated owing to:

1) the multiplicity of factors affecting the efficiency of the apparatus thus lessening the degree of resolution;

2) the number of electronic apparatuses necessary in order to record the output pulses from the photomultiplier;

3) the complexity of the interaction of γ radiation with the matter

However, within the last few years, work in this field has made very noticeable progress; in fact, today the photographic spectrum of the oscillographic pulses coming from a photomultiplier enables a ready and easy solution of qualitative problems of spectral analysis of radioactive sources.

If conveniently calibrated, the apparatus permits quick measurement of the energy of the radiations.

We have applied the scintillation device in several experiments on radioactivity [1] and these researches led us to develop several realizations in the field of the γ-rays spectroscopy.

Moreover, the photographic method can also be used in order to know the intensity of the radiation; the densitometer analysis of the exposed emulsion can give the distribution of the pulses on the film according to the usual methods of optical quantitative spectral analysis. This leads to the measurement of the intensity of the radiations, in the limits of the normal exposures.

The experimental difficulties introduced by the photographic method in this case are analogous to those of the optical spectral analysis mentioned above.

2. – Experimental methods.

The detector is a NaI(Tl) crystal placed directly on a photomultiplier which «sees» the scintillations produced in the crystal by the γ radiation.

In our research we have used Du Mont photomultipliers and cylindrical crystals of various sizes ranging between 20 mm in diameter, 13 mm in thickness and 50 mm in diameter, 50 mm in thickness.

The bigger crystals were more suitable for obtaining the spectra, for reasons that shall be explained later, thus justifying their higher cost.

The output pulses from the photomultiplier are conveniently amplified and are sent directly to a wide-band oscilloscope.

Pulses from γ-rays which lose the same amount of energy in the crystal ought to produce identical patterns.

The oscilloscope's screen is photographed with a time exposure of sufficient length with the result that pulses of the same height, adding up their photographic impression, give rise to a well defined pattern on the photographic film.

Twentyfive superposed images of successive equal patterns corresponding to the same loss of energy in the crystal, with the resolution and sweep speed of our apparatus, are sufficient to produce a quite well defined photographic impression.

---

[1] F. DEMICHELIS and R. MALVANO: *Nuovo Cimento*, **11**, 49 (1954); **12**, 358 (1954); F. DEMICHELIS: *Nuovo Cimento*, **12**, 407 (1954).

The time exposure of a spectrogram is chosen so that the emulsion may give a clear photography. For instance, the spectrograms of Fig. 1 were obtained from ≈ 100000 pulses.

a) The formation of spectrograms by means of the method indicated in a former article ([1]) proved to be of little value.

According to this method the pulse drives the vertical deflection of the electronic beam, while the horizontal deflection is driven by its derivative.

The various spectral lines appear as closed curves of different size which lie on the same side of a straight line which is tangent of all of them at the same point.

But this method has been given up both because of the lack of simmetry of the lines, and because two lines generated by two beams of γ-rays with the same intensity, but having a differing $h\nu$ energy, do not produce equal photographic impressions.

b) The following method proved preferable: the tension pulses are sent directly to the vertical deflection plates of the oscilloscope, the horizontal axis acts as the time axis, and the sweep is triggered by the same recorded γ-ray.

The simultaneous sweep of the time axis does not allow the scanning by the microphotometer of the picture of the pulses, because the pulses have leading edge much more steep than the trailing edge and their oscillographic patterns were not fit for a microphotometric scanning.

c) But we obtained pulses of equal slope for both leading and trailing edge, by means of a lumped parameter delay line.

The resulting pattern for every pulse has the shape of an error curve of Gauss, with a vertical symmetry axis passing through its top, and common to all patterns.

Furthermore, in this case the curve, near the top, is practically parallel to the time axis, and thus is traced by the electronic beam having a speed independent of its height.

Thereby a microphotometric scanning along the vertical symmetry axis produces satisfying results.

In Fig. 1 are shown some spectrograms of this type, respectively of $^{60}_{27}$Co, $^{137}_{55}$Cs, $^{226}_{88}$Ra (in equilibrium with its decay products) and $^{228}_{90}$RdTh (in equilibrium with its decay products).

In Fig. 2 is shown the scanning by means of the microphotometer upon the $^{137}_{55}$Cs spectrogram.

In these figures it is possible to see how much information is available from the spectrogram.

We must emphasize that the apparatus necessary to obtain such a spectro-

gram is quite simple, but of course it requires that both crystal and the photomultiplier can give a good resolution, and moreover the oscilloscope screen be of fine grain so as not to weaken the resolution of the apparatus.

d) Still another method can be followed; it produces a spectrogram in which the pulse pattern is formed by a series of straight lines parallel to the time axis.

Such a spectrum, which is analogous to an optical spectrum, is easily obtained in the following way.

The pulses are stretched, so that after a very short rise time, they remain at constant height for $\approx 5 \cdot 10^{-6}$ s.

On the oscillographic screen are seen straight lines whose lengths depend upon the constants of the pulse stretcher and whose heights are proportional to the γ-ray energies.

In Fig. 3 are shown some spectrograms of this type.

Since the patterns are parallel to the time axis, the sweep speed is uniform for all the pulses, and therefore for all energies.

The scanning by the microphotometer is then possible along any line perpendicular to the time axis.

e) In order to obtain the measurement of the intensity of the spectral lines without the use of a microphotometer, a neutral wedge may be used ([2]).

The wedge must be placed on the screen of the oscillograph in such a manner that isodensity lines be perpendicular to the spectral lines.

In our case there is a transmission factor, ranging from 1/5 to 1/1000 (optical density $0.7 \div 3$).

In Fig. 4 are shown spectrograms obtained by means of the method of spectral lines together with neutral wedge.

We must note however that the introduction of a lengthener of pulses requires a greater lenght of time for each pulse. If crowding occurs, it is possible for one pulse to start before the preceeding has come to end; this would result in an overlapping of pulses and consequential clouding of the spectrogram.

3. - Disturbance from Compton effect and its reduction.

From the observation of the above spectrograms it is easy to recognize the photoelectric lines and the continuous Compton distribution.

The pair production line is appreciably present only in the spectrogram of $R^{228}_{90}dTh$ due to the 2.62 MeV γ-ray of $^{208}_{82}Pb$.

([2]) D. MAEDER: *Helv. Phys. Acta*, **20**, 139 (1947); W. BERNSTEIN, R. L. CHASE and A. W. SCHARDT: *Rev. Sci. Instr.*, **24**, 437 (1953).

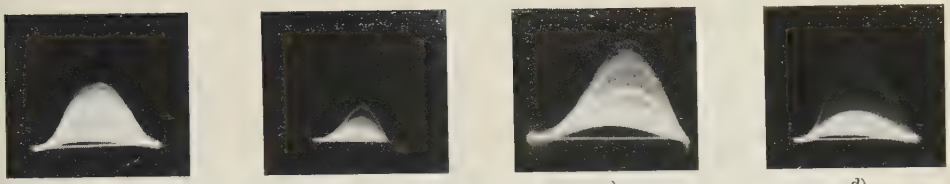

a) b) c) d)

Fig. 1. – Spectrograms of: *a)* $^{60}_{27}$Co, *b)* $^{137}_{55}$Cs, *c)* $^{226}_{88}$Ra, *d)* $^{228}_{90}$RdTh.

Fig. 2. – Microphotometric analysis of the $^{137}_{55}$Cs spectrogram of fig. 1.

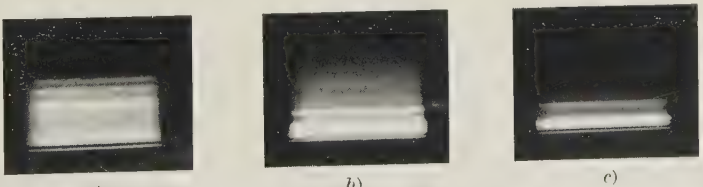

a) *b)* *c)*

Fig. 3. – Spectrograms of: *a)* $^{60}_{27}$Co, *b)* $^{226}_{88}$Ra, *c)* $^{228}_{90}$RdTh (obtained by means of a crystal 12 mm in diameter, 12 mm in thickness).

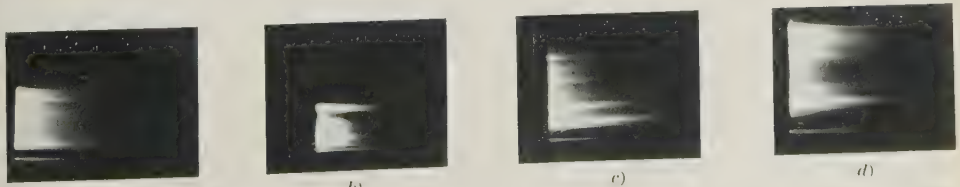

a) *b)* *c)* *d)*

Fig. 4. – Densitometer analysis of the spectrograms of: *a)* $^{60}_{27}$Co, *b)* $^{137}_{55}$Cs, *c)* $^{226}_{88}$Ra, *d)* $^{228}_{90}$RdTh, obtained by means of the neutral wedge method.

In fact the Compton continuous distribution is a strong disturbance.

The technique of reducing this Compton disturbance by means of an anti-coincidence method is not new, and has already been applied quite successfully.

This method consists in surrounding the detector crystal with another « guard » crystal which captures the radiation scattered in the former by Compton effect.

The output pulses from the second crystal are sent in anticoincidence with those from the first, so that only the photoelectric lines remain in the resulting spectrogram.

This method could be called *primary spectroscopy*, since it records only the photoelectric pulses.

We knew the work R. E. CONNALLY [3] did in γ-rays spectroscopy by means of an anticoincidence apparatus.

But when we wanted to make use of this method, it seemed to us possible to improve his apparatus in order to obtain even better results.

In fact the efficiency of this method depends simply upon the geometrical dimensions of the guard crystal: by using a crystal that would capture all the scattered γ-rays, the Compton reduction should result quite complete.

Therefore we resolved to prepare an apparatus with a crystal viewed from the central crystal with a solid angle of about 4π (see Fig. 5).

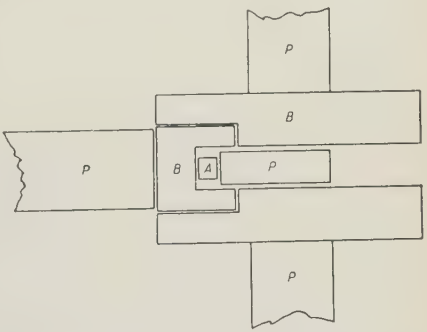

Fig. 5. – Anticoincidence γ-rays spectrometer with guard crystals viewing a solid angle near 4π. *A*) main detector; *B*) guard crystals; *P*) photomultipliers.

In the lapse of time during the actual preparation of the device, R. D. ALBERT [4] published the results of his own experiments with the anticoincidence method which were notably better than the preceeding ones.

Our own device has foreseen the use of a little photomultiplier Du Mont type K 1193; thanks to its small size, we can avoid the use of a light pipe; however, the inavailability of such a phototube up to date and the difficulty of obtaining some specially shaped scintillating crystals, have not yet allowed us to prove experimentally to what point Compton disturbance can be reduced by means of our own device.

---

[3] R. E. CONNALLY: *Rev. Sci. Instr.*, **24**, 458 (1953).
[4] R. D. ALBERT: *Rev. Sci. Instr.*, **24**, 1096 (1953).

A preliminary apparatus already in use, owing to the lack of the above phototube, is limited only to the scheme of Fig. 6.

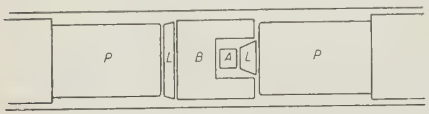

Fig. 6. – Anticoincidence γ-rays spectrometer used in this research. *A*) main detector; *B*) guard crystal; *P*) photomultipliers; *L*) plexiglass light pipes.

A is a cylindrical crystal, 12 mm in diameter and 12 mm in thickness, *B* is a hole crystal 50 mm in diameter, 50 mm in thickness, with a hole 25 mm deep and 25 mm in diameter.

In our apparatus we did not use any electronic anticoincidence circuit, as it would have been required had we used a differential analyser.

The oscilloscope alone works simply as an anticoincidence device.

As a matter of fact the pulses coming from *A* (see Fig. 6) drive vertical deflection in the usual way, while the pulses coming from *B* trigger the beam intensity till to cancel it.

Thus each time that the pulses come simultaneously from the two channels, no pattern appears upon the screen.

Some noteworthy conclusions may be drawn from this first testing of our apparatus.

In Fig. 7 is shown the expected reduction of the Compton distribution theoretically evaluated on the above geometrical dimensions of *B*, assuming *A* as a point and the energy of the incident γ-rays of 0.661 MeV.

Curve *a*) refers to rays coming from the hole side of the guard crystal, in which case the backscattered photons, corresponding to higher pulses in the scintillation spectrum, are not captured.

Curve *b*) refers to rays coming from the opposite side.

In Fig. 8 are shown the experimental spectra obtained by means of our apparatus, using the 0.661 MeV γ-rays of $^{137}_{55}$Cs, and corresponding to curves *a*) and *b*) of Fig. 7.

In applying the guard crystal technique we must pay attention to the nuclides emitting two or more γ-rays in cascade.

As a matter of fact the

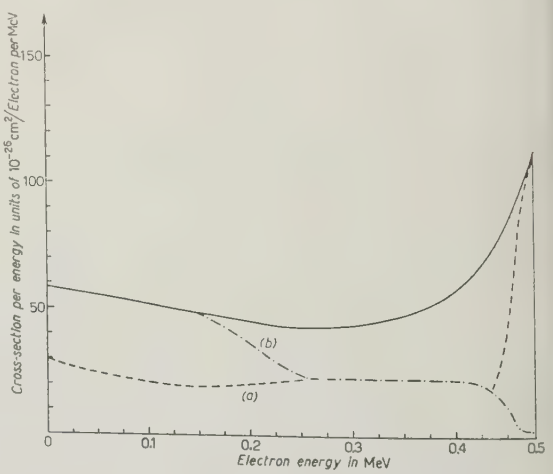

Fig. 7. – Theoric Compton recoil electrons distribution for energy of incident γ-rays of 0.661 MeV. Curve *a*) shows the reduction when γ-rays are coming from the hole side; curve *b*) when the rays are coming from the opposite side.

a) b) c) c)

Fig. 8. – *a*) Spectrogram of $^{137}_{55}$Cs. *b*) The same spectrogram obtained by means of the anticoincidence apparatus: the γ-rays come from the hole. *c*) The same spectrogram of fig. *b*: the γ-rays come from the opposite side. *d*) The same spectrogram of fig. *a*) obtained by means of the bigger crystal.

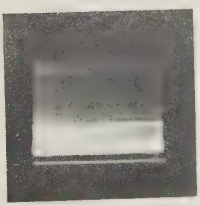

Fig. 9. – Spectrogram of $^{228}_{90}$RdTh obtained by means of the 50 mm in diameter, 50 mm in thickness crystal. Note the reduction of Compton continuum compared with the analogous spectrogram of fig. 3*c*).

intensity of the photoelectric lines of γ-rays in cascade is subject to lessening.

This is due to the fact that if one of the γ-rays is captured by photoelectric effect in A, and at the same time the other γ-ray in cascade is captured in B, the pulse generated in A is not recorded.

However this effect can be minimized by the use of a sufficiently narrow beam of γ-rays impinging on A.

It is interesting to note that the photoelectric capture in A of a photon scattered by B, does not cause the pulse recording, and therefore does not cause disturbance.

We wished also to experiment on the advantage in the ratio of the number of photoelectric to the number of Compton pulses, derived by the use of the big guard crystal as main detector ([5]).

Indeed a greater number of scattered quanta are absorbed in the crystal itself.

By the use of crystals of appropriate sizes nearly all the scattered photons lose their energy in the crystal, with an almost total reduction in the Compton distribution and an indirect photoelectric line enhancement (see Fig. 8*d*).

A spectrogram obtained by means of the bigger crystal is shown in Fig. 9. The photoelectric lines of higher energy are noticeably more intense (see also Fig. 3*d*).

The reduction of the Compton distribution is comparable witht that obtainable by the use of the same crystal as guard detector.

Though more complicated from a theoretical standpoint, the anticoincidence method is much more practical from an economical standpoint.

As regards the use of the big crystal, we must take into account its high price when used as main detector, since it must have all those properties which are necessary for a good resolution.

Poorer properties are required for a guard crystal. Since it does not require a strict uniformity, it can be made up of small crystals, not even optically worked, because an homogeneous immersion in silicone oil is sufficient.

As a low price plastic scintillator can be easily molded into any desired shape and size, we think that it can be also successfully used, but at this date we dont dispose of it.

From the very beginning of research in γ-rays scintillation spectroscopy ([6]) and through the more recent experiments up till the present day, most satisfying results have been and are still being obtained.

([5]) P. R. Bell: *Nucleonics*, **12**, 10, 15 (1954).

([6]) J. W. Coltman and F. H. Marshall: *Phys. Rev.*, **72**, 528 (1947); M. Deutsch: *Nucleonics*, **2**, 58 (1948); P. R. Bell: *Phys. Rev.*, **73**, 1405 (1948); R. Hofstadter: *Phys. Rev.*, **75**, 796 (1949); R. Hofstadter and J. A. McIntyre: *Phys. Rev.*, **78**, 617 (1950); **79**, 389 (1950).

We think that our research could have produced still more remarkable results; but too often our work was requiring particular apparatuses not easily obtainable from the firms or too expensive.

* * *

We wish to thank Prof. E. PERUCCA for his helpful interest in our study Our experimental set up was made possibe by a generous finiancial support for which we would like to express our thanks to C.N.R.

RIASSUNTO

Si prendono in esame i vari metodi fotografici di spettroscopia di raggi γ mediante cristalli scintillatori. Lo spettro è sempre perturbato dalla distribuzione dovuta all'effetto Compton. Si discute la possibilità di eliminare questo disturbo sia mediante adatta sistemazione geometrica dei cristalli ricevitori e un dispositivo ad anticoincidenze, sia utilizzando un cristallo di opportune dimensioni. La risoluzione è sempre piuttosto limitata a causa delle fluttuazioni nella catena di processi dal quanto γ incidente alla registrazione dell'impulso. Ma il progresso raggiunto da vari costruttori sia nei fotomoltiplicatori sia nei cristalli scintillatori e nel loro montaggio si rivela nei forti miglioramenti degli spettrogrammi ottenuti ora rispetto a quelli realizzati anche solo qualche anno fa.

Spurious Scattering in Nuclear Emulsions.

E. Lohrmann and M. Teucher

Physikalisches Institut der Universität - Bern (Schweiz)
Hochspannungslaboratorium Hechingen (Deutschland)

(ricevuto il 26 Ottobre 1955)

Summary. — In full agreement with the results of Biswas, Peters and Rama [1] further evidence is presented on a new form of noise in scattering measurements in nuclear emulsions, which is supposed to be produced by small dislocations in the emulsion and appears to be found in every kind of emulsion. As its mean sagitta increases about proportional to the cell length, it can be mistaken for true Coulomb scattering and affects scattering measurements at $p\beta > 2$ GeV/c very seriously. As a possible consequence the mean energy leading to a given multiplicity of shower particles seems to have been greatly underestimated. The effect could give furthermore a bias towards low mass values at mass determinations of particles of high energies by the scattering-ionization method. The ratio of third to second differences was found to be $1.45 \pm \pm 0.034$, also not far from the value 1.30 given for Coulomb scattering.

1. – Introduction.

In a recent paper Biswas, Peters and Rama [1] reported on the possibilities of scattering measurements in nuclear emulsions and their application on the charge determination of primary cosmic rays. They found that the noise in scattering measurements consists not only of the well known components of reading noise, grain noise and stage noise but of some further sources of noise. One of them is produced by differential temperature extensions of the microscope and is shown to be negligible if proper precautions are taken. The other sort of noise differs from the above mentioned ordinary noise as it increases with cell length. Therefore it can be mistaken for true Coulomb

[1] S. Biswas, B. Peters and Rama: *Proc. Ind. Acad.*, A **41**, 154 (1955).

scattering and impairs scattering measurements at high energies. PETERS *et al.* assume that this « spurious scattering » is produced by small dislocations in the emulsions and it should be found in all nuclear emulsions manufactured and developed in the usual way.

In the course of our investigations on high energy interactions we have compiled further evidence of this kind of noise in several stacks and we are going to draw some more conclusions on its influence on high energy measurements.

2. – Experimental Procedure.

Our measurements were carried out on flat tracks of particles ($\cot g\,\theta > 50$) the energy of which was known in a rough way by their interactions. We used two different stacks of stripped emulsions. The first one was flown in the Sardinia expedition 1953 and developed in Rome. The second one was flown in Texas 1955 and developed in this laboratory. All measurements were carried out on the « Koordinaten-Komparator » of E. Leitz, Wetzlar.

In order to make exact measurements of spurious scattering we had to eliminate the ordinary noise very carefully, which consists of reading noise, grain noise, stage noise and temperature noise. Following the procedure of PETERS *et al.* we determined this noise by repeated measurements on the same track at different parts of the stage. To eliminate grain noise, reading error and temperature noise the track was displaced by 50 μm for the second reading, since we used a track length of 20 μm to determine the contour of the track.

Let D_i and D'_i be the second differences of two corresponding cells, then the mean sagitta $\overline{D_n}$ of the noise is given by

$$\overline{D_n} = \frac{1}{\sqrt{2n}} \sum_i \left| D_i - D'_i \right| . \tag{1}$$

This method of noise elimination was found to be very reliable (2) and in good agreement with the interferometric measurements of stage noise (3).

Let be D_{tot} the measured sagitta, D_{cs} the sagitta due to Coulomb scattering and D_{ss} the sagitta due to spurious scattering. It is well known that under very general conditions we have regardless of the distribution of the D-values

$$\overline{D^2_{\mathrm{tot}}} = \overline{D^2_{\mathrm{cs}}} + \overline{D^2_{\mathrm{ss}}} + \overline{D^2_{\mathrm{n}}} . \tag{2}$$

(2) E. LOHRMANN: in press.

(3) F. D. HÄNNI: private communication.

It will be shown in **4** that the distribution of spurious scattering is gaussian in a good approximation; hence we have for the case of negligible Coulomb scattering

$$\overline{|D_{ss}|}^2 = \overline{|D_{tot}|}^2 - \overline{|D_n|}^2 . \tag{2a}$$

3. – Results.

We have measured 5 very long tracks which were associated with high energy interactions and had charges between 1 and 5 (Table I). Tracks 1

TABLE I.

Number of track	Atomic number	Estimated energy	$\overline{D_{ss}}$ in μm for cell length 500 μm	1 000 μm	2 000 μm	4 000 μm	Stack
1	1	700 GeV	0.19±0.03	0.37±0.05	0.76±0.11	1.43±0.29	Sard.
2	2	10 GeV/N	0.15±0.02	0.31±0.05	—	—	Sard.
3	4	10 GeV/N	0.18±0.03	0.22±0.06	—	—	Sard.
4	2	> 20 GeV/N	0.23±0.02	0.49±0.06	0.79±0.11	—	Sard.
5	2	> 5 GeV/N	0.28±0.03	0.54±0.06	—	—	Texas

and 4 produced jets with energies of 700 GeV and > 20 GeV/per nucleon respectively as estimated from their half-angles; tracks 2 and 3 were heavy primaries and α-particles resulting from fragmentations. Their energy is of the order of 10 GeV per nucleon, as can be estimated by relative scattering measurements, by the interaction which one of the α-particles produces and the angles of the fragmentation ([3]). The energy of track 5 is estimated to be > 5 GeV per nucleon by the angular distribution of the fragmentation products. At the cell lengths used we can therefore neglect the Coulomb scattering of these tracks in comparison to spurious scattering; in the case of track 5 we restricted ourselves to cell lengths ≤ 1000 μm. For the 4000 μm-cells only track 1 was used. All tracks could be shown to have negligible large-scale distortions. A correction for C-shaped distortions by subtracting from all D_{tot}-values $(1/n)\sum_i D_{i_{tot}}$ left $(1/n)\sum_i |D_{i_{tot}}|$ unaltered. We found in all cases and in all stacks approximately the same amount of spurious scattering, however with very large fluctuations. We have therefore compiled the data from all our particles in Fig. 1, which shows the mean amount of spurious scattering as a function of cell length. The limits of error given are calculated from the experimental spread of the measured noise values around

the mean value and exceed the limits given for ordinary noise by a factor of $1.5 \div 2$.

In Fig. 1 we have also drawn in the results of PETERS *et al.* [1] and of FAY [1] for comparison. All these data are in good agreement and can tentatively be represented by

$$\frac{\overline{D_{ss}}}{\mu} = 0.042 \frac{s}{100\,\mu}. \tag{3}$$

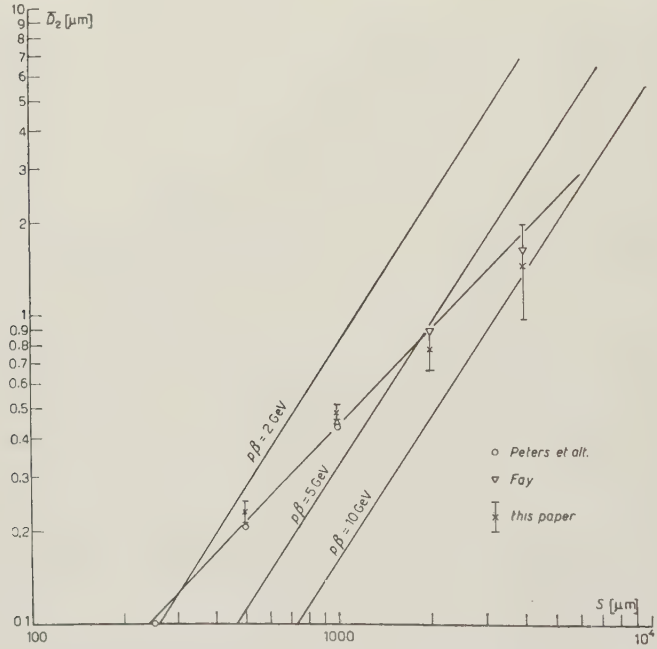

Fig. 1. – Mean sagitta of spurious scattering as function of cell length.

A possibly slower increase of spurious scattering with cell lengths for $s > 2000$ μm appears at present not to be statistically significant. In Fig. 1 we also show the true Coulomb scattering for singly charged particles of $p\beta = 2$, 5 and 10 GeV/c. One sees that even for 5 GeV reasonable scattering measurements can only be made with very long cells > 7000 μm assuming a signal to noise ratio of 2. If one has only cells of 1000 μm scattering measurements can be made up to 1.5 GeV. In view of the large fluctuations found for spurious scattering it should sometimes be possible to find smaller values of scattering. The energy calculated in these cases should only be taken as

(1) H. FAY: *Zeits. f. Naturfor.*, **10**a, 572 (1955).

a lower limit. For tracks dipping more steeply PETERS *e. al.* and FAY find even greater values for spurious scattering. The usual noise elimination by doubling the cell length using the formula of MENON *et al.* [5] or of GOTTSTEIN [6] give scattering values only slightly lower.

4. – Distribution of Second Differences.

We have plotted the distribution of 275 values of second differences measured at cell lengths between 1000 μm and 4000 μm normalized to $\overline{D_{ss}}=0.38$ μm in Fig. 2. The ratio of spurious scattering to noise was >3 in all cases. A gaussian distribution normalized to the same area and to the same $\overline{D}$ is drawn in for comparison. There seems to be a slight indication of the D-values to be more steeply distributed than the gaussian curve, but a possible deviation from a normal distribution appears to be smaller than the one found by PETERS *et al.* [1]. The value of $\langle D^2\rangle^{\frac{1}{2}}$ as calculated from the distribution is only 3% greater then $\overline{D}\sqrt{\pi/2}$, the value of $\langle D^2\rangle^{\frac{1}{2}}$ expected for a gaussian distribution. In view of these facts we think our method of noise elimination (equ. (2)) which is only valid for a normal distribution, to be correct within the present accuracy of our measurements.

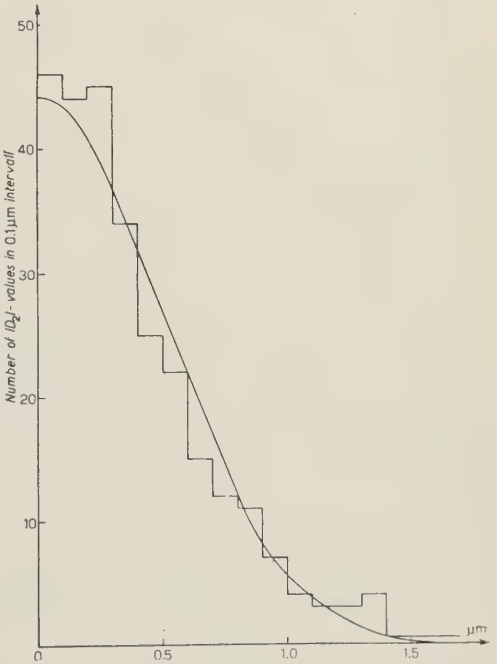

Fig. 2. – Distribution of second differences of spurious scattering.

5. – Third Differences of Spurious Scattering.

The dependence of spurious scattering on the cell length is almost the same as for true Coulomb scattering. Therefore it can hardly be distinguished from true scattering. So we tried to find a difference in the ratio between third

[5] M. G. K. MENON, C. O'CEALLAIGH and O. ROCHAT: *Phil. Mag.*, **43**, 932 (1951).
[6] K. GOTTSTEIN: *Kosmische Strahlung*; ed. W. HEISENBERG (Berlin, 1953), p. 508.

and second differences. The third differences D_3 were calculated by subtracting two succeeding second differences D_2. The ratio $q = \overline{D_3}/\overline{D_2}$ should be 1.30 for true scattering (7) and 1.825 for grain and reading noise (1). For spurious scattering we found a value of

$$q = 1.45 \pm 0.034 .$$

In account of the highly correlated nature of D_2 and D_3 the dispersion of the q-values is rather small. It can easily be shown (2) that they are normally distributed with a standard deviation

$$\delta q = \frac{1}{2\sqrt{n_{\text{eff}}}} q , \tag{4}$$

where n_{eff} is the number of cells measured in the absence of ordinary noise. If the contribution of ordinary noise cannot be neglected, the statistical weight of n measured cells should be reduced according to

$$n_{\text{eff}} = \frac{1}{(\overline{D_{\text{tot}}}/\overline{D_{ss}})^4 + (\overline{D_n}/\overline{D_{ss}})^4} n . \tag{5}$$

The distribution of the q-values found experimentally is in good agreement with the theory. The error given for the numerical value of q was calculated from the experimental spread. Even for such a low value of dispersion of q discrimination between spurious scattering and true Coulomb scattering is only possible in the case of very good statistics ($n_{\text{eff}} > 100$ cells) as the ratio of third to second differences differs only by 10%.

6. – Conclusions.

In view of the high value of spurious scattering found in all emulsions which have been examined up to now it is suggested that all scattering measurements giving $p\beta > 2$ GeV/c should be reexamined. We want to discuss only two possible consequences of errors in high-energy scattering measurements: JOHNSON (8) reports a discrepancy between the multiplicity of shower particles found in Bevatron produced stars and the multiplicity found by

(7) S. BISWAS, E. C. GEORGE, B. PETERS and M. S. SWAMY: *Suppl. Nuovo Cimento*, **12**, 369 (1954); R. H. W. JOHNSTON and C. O'CEALLAIGH: *Phil. Mag.*, **46**, 393 (1955); A. BONETTI, R. LEVI SETTI, B. LOCATELLI and G. TOMASINI. *Nuovo Cimento*, **1**, 904 (1955); M. DI CORATO, D. HIRSCHBERG and B. LOCATELLI: *Pisa Conference Report, Mimeogr. Ed.* (1955), p. 275.

(8) W. R. JOHNSTON: *Phys. Rev.*, **99**, 1049 (1955); UCRL-Report 2979 (1955).

cosmic-ray workers in the energy region between 1 and 10 GeV. It seems possible that sometimes energies are underestimated by cosmic-ray workers. This would also be in better agreement with the low multiplicities found in stars produced by secondaries of jets and of fragmentations of heavy nuclei ([3,9]).

Mass measurements of fast particles are generally made by the scattering-ionization method in nuclear emulsions. For values of $p\beta > 600$ MeV/c spurious scattering would give a bias towards too small mass values, above all because of the rather large fluctuations observed for spurious scattering.

* * *

The authors wish to thank Profs. F. G. HOUTERMANS and CH. PEYROU for their continuous interest and encouragement, Prof. B. PETERS for two stimulating discussions. One of us (E.L.) wants to express his gratitude to Prof. F. G. HOUTERMANS for the hospitality enjoyed in his Institute, to Prof. E. SCHOPPER for granting a leave of absence and the « Deutsche Forschungsgemeinschaft » for a maintenance grant.

Our participation in the Sardinia and Texas flights was made possible by the « Schweizer Nationalfonds ». We thank Dr. A. ROBERTS, ONR London, for all his trouble in the organization of the Texas flight.

([9]) D. LAL, YASH PAL and RAMA: *Suppl. Nuovo Cimento*, **12**, 347 (1954).

RIASSUNTO (*)

In perfetto accordo coi risultati di BISWAS, PETERS e RAMA ([1]), si presentano ulteriori prove di una nuova forma di disturbo di cui sono affette le misure di scattering nelle emulsioni nucleari, disturbo che si ritiene causato da piccoli spostamenti nell'emulsione e sembra trovarsi in tutti i tipi di emulsione. Dato che la sua sagitta media cresce circa proporzionalmente alla lunghezza della cella, può essere confuso con lo scattering coulombiano reale e affetta molto seriamente le misure di scattering a $p\beta < 2$ GeV/c. Una possibile conseguenza di tale errore sembra essere una notevole sottovalutazione dell'energia media producente una determinata molteplicità di particelle negli sciami. L'effetto potrebbe anche condurre a sottovalutare i valori delle masse nelle determinazioni col metodo del rapporto scattering-ionizzazione riguardante particelle di energia elevata. Il rapporto delle differenze terze alle seconde è stato trovato essere 1.45 ± 0.034, non lontano, cioè dal valore 1.30 dato per lo scattering coulombiano.

(*) *Traduzione a cura della Redazione.*

The Determination of the Scattering Potential from the Spectral Measure Function.

II. Point Eigenvalues and Proper Eigenfunctions (*).

I. Kay and H. E. Moses

Institute of Mathematical Sciences, New York University - New York

(ricevuto il 27 Ottobre 1955)

Summary. — In Part I of this paper (1) we restricted ourselves to the consideration of weight operators which led to Hamiltonians H whose spectra were identical to the spectrum of a given unperturbed Hamiltonian H_0. In this part of the paper we propose to show how one may choose weight operators which lead to Hamiltonians H having spectra different from that of H_0. To make the discussion more concrete we shall take the case where H_0 has a purely continuous spectrum extending from 0 to ∞ and where H has a spectrum which has a continuous part which coincides with the spectrum of H_0 and, in addition, has negative point eigenvalues.

1. – Introduction.

In Part I of this paper (1) we restricted ourselves to the consideration of weight operators which led to Hamiltonians H whose spectra were identical to the spectrum of a given unperturbed Hamiltonian H_0. In this part of the paper we propose to show how one may choose weight operators which lead to Hamiltonians H having spectra different from that of H_0. To make the

(*) The research reported in this article was done at the Institute of Mathematical Sciences, New York University, and has been made possible through support and sponsorship extended by Geophysics Research Directorate, Air Force Cambridge Research Center under Contract No. AF 19(122)-463.

(1) I. Kay and H. E. Moses: *Nuovo Cimento*, **2**, 917 (1955).

discussion more concrete we shall take the case where H_0 has a purely continuous spectrum extending from 0 to ∞ and where H has a spectrum which has a continuous part which coincides with the spectrum of H_0, and, in addition, has negative point eigenvalues. However, the procedure which is discussed is capable of being generalized considerably, at least in a formal fashion.

It is our objective to find operators U and U_0 such that

$$WU^* = U_0 \tag{1.1}$$

$$U_0 = U^{-1}, \tag{1.2}$$

where W is the weight operator. We wish H to be obtained from

$$H = UH_0U_0 = UH_0U^{-1}, \tag{1.3}$$

Clearly (1.3) cannot hold if H_0 and H have a different spectrum, which is the case being considered here. We shall have to define a vector space larger than Hilbert space such that the spectrum of H_0 in this larger space is the same as that of H in this space.

It will be possible to carry out the extension of the Hilbert space to the larger space in terms of the Q-representation which is the representation in which K is triangular in the sense described in Part I, i.e.,

$$\langle q|U|q'\rangle = \delta(q-q') + \varepsilon\langle q|K|q'\rangle, \tag{1.4}$$

where

$$\langle q|K|q'\rangle = 0 \qquad \text{for } q' > q. \tag{1.5}$$

Like Part I this paper has two main divisions. In the first (Sections 2 and 3) we shall characterize the weight operator assuming the operator H and its spectrum given. In the second division (Section 5) we shall show how H can be obtained from the weight operator. We shall see that in addition to prescribing the weight operator which gives the weight function of the eigenfunction of the continuous spectrum and prescribing the boundary conditions which these eigenfunctions must satisfy, we shall have to give the normalization constants and eigenvalues of the proper eigenfunctions. Furthermore, we shall have to specify a set of « eigenfunctions » of H_0 which span the vector space which must be added to the Hilbert space to assure us that the spectrum of H_0 coincides with that of H.

2. - The eigenfunctions of the unperturbed Hamiltonian and the extended vector space.

Since we shall work with a vector space larger than Hilbert space, it will be useful to introduce a projection operator which shall be denoted by $\eta(H_0)$. This operator is to have the property that

$$\eta(H_0)|\varphi\rangle = |\varphi\rangle \tag{2.1}$$

if the state $|\varphi\rangle$ is in the Hilbert space, and that

$$\eta(H_0)|\varphi\rangle = 0 \tag{2.2}$$

if $|\varphi\rangle$ is in that part of the vector space which is orthogonal to the Hilbert space.

As in Part I we shall denote the eigenstates of H_0, A_0 belonging to the eigenvalues E, a, respectively, by $|H_0, A_0; E, a\rangle$. Since we are assuming that the spectrum of H_0 is continuous and ranges from zero to ∞, we shall express the fact that the $|H_0, A_0; E, a\rangle$ for $E > 0$ are a complete set in the Hilbert space by

$$\int\int |H_0, A_0; E, a\rangle \eta(E)\, \mathrm{d}E\, \mathrm{d}a \langle H_0, A_0; E, a| = \eta(H_0)\,, \tag{2.3}$$

$\eta(E)$ being the usual Heaviside step function.

We shall extend the definition of the operator H_0 so that it has eigenvalues which correspond to the negative point eigenvalues E_i of the operator H. Toward this end we introduce « eigenfunctions » $|H_0, A_0; E, a\rangle$ which are defined for $E < 0$ in the vicinity ΔE_i of each eigenvalue E_i of H. These eigenfunctions are to span a vector space orthogonal to the Hilbert space. We shall characterize this extended space by working in the Q-representation. Every operator A defined in Hilbert space can be represented as an integral operator with the kernel $\langle q|A|q'\rangle$. If the operator A as defined in the extended space has the same form as an integral operator in the Q-representation when operating on vectors in the extended space, we shall call the operator A « a Q-extended operator ». We shall discuss Q-extended operators in more detail in Section 4.

In particular we shall take H_0 as a Q-extended operator. Hence for $E < 0$, the eigenfunctions $|H_0, A_0; E, a\rangle$ are defined by

$$\int_{q_0}^{q_1} \langle q|H_0|q'\rangle \mathrm{d}q' \langle q'|H_0, A_0; E, a\rangle = E\langle q|H_0, A_0; E, a\rangle\,, \tag{2.4}$$

for E in the vicinity ΔE_i of each point eigenvalue E_i of H. If, for example, $H_0^Q = -\mathrm{d}^2/\mathrm{d}q^2$ (where the superscript Q means that H_0 is expressed in the Q-representation) we should solve for $\langle q|H_0, A_0; E, a\rangle$ from

$$-\frac{\mathrm{d}^2}{\mathrm{d}q^2}\langle q|H_0, A_0; E, a\rangle = E\langle q|H_0, A_0; E, a\rangle .$$

Not every solution of (2.4) will be used to define an eigenfunction of H_0 in the extended space, for we shall require that $\langle q|H_0, A_0; E, a\rangle$ be quadratically integrable functions of q in the vicinity of q_0. If $q_0 = -\infty$ then a necessary condition is

$$\lim_{q\to-\infty}\langle q|H_0, A_0; E, a\rangle = 0 . \tag{2.5}$$

As we shall see in Section 6, this condition is a necessary condition for the bound states of H to be quadratically integrable functions of q.

We shall designate the function $\langle q|H_0, A_0; E, a\rangle$ which is a solution of (2.4) subject to the above condition by the ket $|H_0, A_0; E, a\rangle$. The corresponding bra $\langle H_0, A_0; E, a|$ will be used to denote the function $\langle H_0, A_0; E, a|q$ where

$$\langle H_0, A_0; E, a|q\rangle = \langle q|H_0, A_0; E, a\rangle^* \tag{2.6}$$

where the asterisk denotes complex conjugate.

Let us denote by ${}_B\langle H_0, A_0; E, a, |q\rangle^*$ another set of functions which satisfy both (2.4) and

$$\int_{q_0}^{q_l} {}_B\langle H_0, A_0; E, a|q\rangle\,\mathrm{d}q\langle q|H_0, A_0; E', a'\rangle = \delta(E-E')\delta(a, a') . \tag{2.7}$$

We also require that the eigenfunctions of H_0 belonging to the positive spectrum be orthogonal to the eigenfunctions of the extended space, i.e.,

$$\eta(-E)\eta(E')\int_{q_0}^{q_l} {}_B\langle H_0, A_0; E, a|q\rangle\,\mathrm{d}q\langle q|H_0, A_0; E', a'\rangle = 0 . \tag{2.7a}$$

$$\eta(-E)\eta(E')\int_{q_0}^{q_l} \langle H_0, A_0; E, a|q\rangle\,\mathrm{d}q\langle q|H_0, A_0; E', a'\rangle = 0 . \tag{2.7b}$$

We can write

$$\int_{q_0}^{q_l}\langle q|H_0|q'\rangle\langle q'|H_0, A_0; E, a\rangle_B = E\langle q|H_0, A_0; E, a\rangle_B , \tag{2.8}$$

where $\langle q|H_0, A_0; E, a\rangle_B$ is defined by

$$\langle q|H_0, A_0; E, a\rangle_B = {}_B\langle H_0, A_0; E, a|q\rangle^* . \tag{2.9}$$

The bra ${}_B\langle H_0, A_0; E, a|$ is used to denote ${}_B\langle H_0, A_0; E, a|q\rangle$ and the ket $|H_0, A_0; E, a\rangle_B$ is used to denote $\langle q|H_0, A_0; E, a\rangle_B$. The subscript B is used to denote the fact that ${}_B\langle H_0, A_0; E, a|$ is the « bi-orthogonal » bra to $|H_0, A_0, E, a\rangle$.

If I is the identity operator of the entire vector space, we write

$$\int_{q_0}^{q_1} |q\rangle \,\mathrm{d}q\langle q| = I , \tag{2.10}$$

$$\langle q|q'\rangle = \delta(q - q') . \tag{2.10a}$$

Then (2.7) can be written abstractly as

$$\begin{cases} {}_B\langle H_0, A_0; E, a|H_0, A_0; E', a'\rangle = \delta(E - E')\delta(a, a') , \\ \langle H_0, A_0; E, a|H_0, A_0; E', a'\rangle_B = \delta(E - E')\delta(a, a') , \quad \text{for } (E, E' < 0); \end{cases} \tag{2.11}$$

$$\eta(-E)\eta(E')\,{}_B\langle H_0, A_0; E, a|H_0, A_0; E', a'\rangle = 0 \tag{2.11a}$$

$$\eta(-E)\eta(E')\langle H_0, A_0; E, a|H_0, A_0; E', a'\rangle = 0 . \tag{2.11b}$$

We can define the projection operator $\eta(-H_0)$ by

$$\eta(-H_0) = \iint |H_0, A_0; E, a\rangle\eta(-E)\,\mathrm{d}E\,\mathrm{d}a\,{}_B\langle H_0, A_0, E, a| , \tag{2.12}$$

where the integration is carried out over the intervals ΔE_i. The extended space is defined by

$$\eta(H_0) + \eta(-H_0) = I . \tag{2.13}$$

The operator $\eta(-H_0)$ can be shown to be a projection operator which maps the Hilbert space into zero and the space added to the Hilbert space to form the full space into itself. A general vector $|\Phi\rangle$ in the full space can be written as

$$\langle q|\Phi\rangle = \iint \langle q|H_0, A_0; E, a\rangle\eta(E)\,\mathrm{d}E\,\mathrm{d}a\langle H_0, A_0; E, a|\Phi\rangle + \tag{2.14}$$

$$+ \iint \langle q|H_0, A_0; E, a\rangle\,\eta(-E)\,\mathrm{d}E\,\mathrm{d}a\,{}_B\langle H_0, A_0; E, a|\Phi\rangle ,$$

where the first integral goes over the positive E axis and the second integral goes over the intervals ΔE_i.

In (2.14) the H_0 representative of $|\Phi\rangle$ which is $\langle H_0, A_0; E, a|\Phi\rangle$ is a quadratically integrable function of E, a for $E > 0$. The function ${}_B\langle H_0, A_0; E, a|\Phi\rangle$ is an integrable function of E, a in the intervals ΔE_i for $E < 0$. The definition of ${}_B\langle H_0, A_0; E, a|\Phi\rangle$ for $E < 0$ outside the intervals ΔE_i is immeterial.

Let us now consider some properties of the projection operators $\eta(H_0)$, $\eta(-H_0)$. First of all we note

$$\text{(2.15)} \qquad \begin{cases} \eta(H_0)|H_0, A_0; E, a\rangle = \eta(E)|H_0, A_0; E, a\rangle \\ \eta(-H_0)|H_0, A_0; E, a\rangle = \eta(-E)|H_0, A_0; E, a\rangle . \end{cases}$$

The projection operator $\eta(-H_0)$ maps the Hilbert space into zero and maps that part of the vector space orthogonal to the Hilbert space into itself. By definition (2.12) and properties (2.7), (2.7a) and (2.7b)

$$\text{(2.16)} \qquad \eta(-H_0)\eta(H_0) = 0, \quad \eta^2(H_0) = \eta(H_0), \quad \eta^2(-H_0) = \eta(-H_0), \quad \eta(H_0)\eta(-H_0) = 0.$$

If T is any operator defined in the whole extended space then

$$T = T\eta(H_0) + T\eta(-H_0) ,$$

where $T\eta(H_0)$ is an operator which is zero when it operates on vectors orthogonal to the Hilbert space and where $T\eta(-H_0)$ is zero when it operates on the Hilbert space. All the operators defined in Part I may be considered to be of the form $T\eta(H_0)$ and hence most of the properties of the various operators discussed in Part I will have analogues to operators of this character appearing here. The principal purpose of the present paper is to define operators over the full space, particularly the operator U, U_-, and W, i.e., to define $U\eta(-H_0)$, etc. It will not be necessary, however, to extend $L\eta(H_0)$, $M_-(H_0)$, as will be clear from the subsequent work.

The formal Hermitian adjoint of $T\eta(H_0)$ is $\eta(H_0)T^*$. If T commutes with H_0, it can be shown formally that

$$\text{(2.17)} \qquad \eta(H_0)T^* = T^*\eta(H_0) .$$

Hence if such an operator operates on Hilbert space, its adjoint will still operate on the Hilbert space and maps vectors orthogonal to that space into zero.

If R is another operator which commutes with H_0, one can show

$$R\eta(H_0)T\eta(H_0) = RT\eta(H_0)\,. \tag{2.18}$$

Hence products of such operators R and T acting on Hilbert space can be obtained by projecting on Hilbert space the product of the operators defined on the complete space. We shall use the properties (2.17) and (2.18) often without referring to them explicitly.

3. – The eigenfunctions of the perturbed Hamiltonian and the transformation operator.

3.1. *The eigenfunctions of the continuous spectrum; the operators* $U\eta(H_0)$ $U_{\pm}\eta(H_0)$, $W\eta(H_0) = W_c$. – Let us consider the eigenfunctions $|H, A; E, a\rangle$ of $H = H_0 + \varepsilon V$. As in Part I we introduce the operator U such that

$$|H, A; E, a\rangle = U|H_0, A_0; E, a\rangle\,. \tag{3.1}$$

When $E > 0$ the eigenfunctions $|H_0, A_0; E, a\rangle$ are those which span the Hilbert space. But when $E = E_i$, where E_i is one of the point eigenvalues of H, we have

$$|H, A; E_i, a\rangle = U|H_0, A_0; E_i, a\rangle\,, \tag{3.2}$$

where $|H_0, A_0; E_i, a\rangle$ is one of the vectors added to form the extended space. In fact these elements were added in order that (3.1) should hold for all values of E in the spectrum of H.

Let us consider the continuous spectrum of H. We shall obtain expressions, for $U\eta(H_0)$, $U_{\pm}\eta(H_0)$, S, etc., analogous to those obtained in Part I where the continuous part of the spectrum which we are considering was the entire spectrum. The various expressions that are given below are obtained in an almost identical manner as those for the analogous operators of Part I. Therefore, instead of carrying out the derivations in detail, we shall indicate only the more important relationships.

For the case of the continuous spectrum, (3.1) may be written

$$\begin{aligned} |H, A; E, a\rangle &= U\eta(E)|H_0, A_0; E, a\rangle = \\ &= U\eta(H_0)|H_0, A; E, a\rangle \qquad (E > 0). \end{aligned} \tag{3.2}$$

In a manner similar to that used in Section 3 of Part I it can be shown that

$U\eta(H_0)$ satisfies the equation

$$U\eta(H_0) = L\eta(H_0) + \int \frac{P}{E - H_0} V U\eta(H_0)\delta(E - H_0)\,\mathrm{d}E, \tag{3.3}$$

where L is an arbitrary operator which commutes with H_0, and where as in Part I,

$$\delta(E - H_0) = \int |H_0, A_0; E, a\rangle\,\mathrm{d}a\langle H_0, A_0; E, a|. \tag{3.3a}$$

The integral in (3.3) is formally taken over the whole spectrum of the extended operator H_0. The factor $\eta(H_0)$ in the integral, however, in effect cuts out the negative part.

Now, as in Part I, there are two operators, $U_\pm \eta(H_0)$, which are particularly interesting and whose integral equations can be obtained by selecting $L\eta(H_0)$ properly. These operators are defined by the conditions

$$\lim_{t \to -\infty} \exp[iH_0 t] \exp[-iHt] U_- \eta(H_0)|\varphi\rangle = \eta(H_0)|\varphi\rangle, \tag{3.4}$$

$$\lim_{t \to +\infty} \exp[iH_0 t] \exp[-iHt] U_+ \eta(H_0)|\varphi\rangle = \eta(H_0)|\varphi\rangle, \tag{3.4a}$$

where $\eta(H_0)|\varphi\rangle$ is an arbitrary state in Hilbert space. As in Part I, $U_\pm \eta(H_0)$ satisfy

$$U_\pm \eta(H_0) = \eta(H_0) + \varepsilon \int \gamma_\pm(E - H_0) V U_\pm \eta(H_0)\delta(E - H_0)\,\mathrm{d}E, \tag{3.5}$$

The scattering operator S is defined by

$$\lim_{t \to +\infty} \exp[iH_0 t] \exp[-iHt] U_- \eta(H_0)|\varphi\rangle = S\eta(H_0)|\varphi\rangle, \tag{3.6}$$

where, as before, $\eta(H_0)|\varphi\rangle$ is an arbitrary state in Hilbert space. It can be shown that

$$S = \eta(H_0) - 2\pi i\varepsilon \int \delta(E - H_0) V U_- \eta(H_0)\delta(E - H_0)\,\mathrm{d}E, \tag{3.7}$$

and that its inverse is given by

$$S^{-1} = \eta(H_0) + 2\pi i\varepsilon \int \delta(E - H_0) V U_+ \eta(H_0)\delta(E - H_0)\,\mathrm{d}E. \tag{3.8}$$

From (3.7) and (3.8) it is clear that S and S^{-1} can be written

$$S = S\eta(H_0)\,, \tag{3.9}$$

$$S^{-1} = S^{-1}\eta(H_0) \tag{3.10}$$

and therefore that S and S^{-1} maps the space orthogonal to the Hilbert space into zero.

The general operator $U\eta(H_0)$ may be expressed in terms of $U_\pm\eta(H_0)$ as follows:

$$U\eta(H_0) = U_\pm\eta(H_0)M_\pm\eta(H_0), \tag{3.11}$$

where

$$M_\pm\eta(H_0) = L\eta(H_0) \pm i\varepsilon\int \delta(E - H_0)V\,U\eta(H_0)\,\delta(E - H_0)\,\mathrm{d}E\,. \tag{3.12}$$

From (3.12) it is clear that $M_\pm\eta(H_0)$ commutes with H_0. It can be shown that $M_\pm\eta(H_0)$ has an inverse in Hilbert space which commutes with H_0 and which we shall denote by $M_\pm^{-1}\eta(H_0)$:

$$M_\pm^{-1}\eta(H_0)M_\pm\eta(H_0) = M_\pm\eta(H_0)M_\pm^{-1}\eta(H_0) = \eta(H_0); \tag{3.13}$$

alternatively, noting that $M_\pm^{-1}$ commutes with H_0 and using (2.13), we can write

$$M_\pm^{-1}M_\pm\eta(H_0) = M_\pm M_\pm^{-1}\eta(H_0) = \eta(H_0). \tag{3.13a}$$

It can also be shown that

$$\eta(H_0)U_\pm^*U_\pm\eta(H_0) = \eta(H_0)\,, \tag{3.14}$$

which is a generalization of (4.21) of Part I. Equation (3.14) is essentially the normalization condition on the eigenfunctions

$$|H, A; E, a\rangle_\pm = U_\pm\eta(H_0)\,|H_0, A_0; E, a\rangle \tag{3.14a}$$

(see Part I), namely

$$\eta(E)\eta(E')\,{}_\pm\langle H, A; E, a\,|\,H, A; E', a'\rangle_\pm = \eta(E)\,\delta(E - E')\,\delta(a, a'). \tag{3.14b}$$

From (3.11) and (3.13) the correspondùng relation for U is

$$W_c\eta(H_0)U^*U\eta(H_0) = \eta(H_0) \tag{3.15}$$

where

$$W_c\eta(H_0) = M_{\pm}^{-1}\eta(H_0)M_{\pm}^{-1*}\eta(H_0) = M_{\pm}^{-1}M_{\pm}^{*-1}\eta(H_0) = \eta(H_0)W_c. \tag{3.16}$$

It is to be noted that $W_c\,\eta(H_0)$ is a positive definite operator which has an inverse in Hilbert space. Equation (3.15) expresses the orthogonality relations between the eigenfunctions of the continuous spectrum of H associated with the weight operator $W_c\eta(H_0)$.

Two expressions for S whose analogues appear in Part I are

$$S = \eta(H_0)U_+^*U_-\eta(H_0), \tag{3.17}$$

$$S = M_+\eta(H_0)M_-^{-1}\eta(H_0) = M_+M_-^{-1}\eta(H_0). \tag{3.18}$$

3·2. *The eigenfunctions of the discrete spectrum; the operator* $U\eta(-H_0)$. – Let us now consider the eigenfunctions of the discrete spectrum of H, namely $|H, A; E_i, a\rangle$. We should first note that the nature of the degeneracy operator A and its eigenvalues may be completely different for the discrete spectrum of H and for the continuous spectrum. In the case of the continuous spectrum the operator A may be chosen so that its eigenvalues are not countable (i.e., A may have a continuous spectrum). However, in the case of point eigenvalues E_i of H, the degeneracy is always countable, and in most applications is finite for a given value of E_i. Hence the operator A, when operating on that subspace of Hilbert space spanned by the eigenstates of the discrete spectrum of H, will have to be defined so as to have countable eigenvalues.

In order that the spectrum of the extended operator H_0 have the same spectrum as H, it is necessary that the degeneracy operator A_0 and its eigenvalues of additional eigenvectors $|H_0, A_0; E, a\rangle$ which are introduced for values of E in the neighborhood ΔE_i of each eigenvalue E_i of H, have the same point spectrum as the eigenvalues of A in the eigenstate $|H, A; E_i a\rangle$.

We may then write, since $E_i < 0$,

$$\begin{aligned} |H, A; E_i, a\rangle &= U|H_0, A_0; E_i, a\rangle = \\ &= U\eta(-E)|H_0, A_0; E_i, a\rangle = \\ &= U\eta(-H_0)|H_0, A_0; E_i, a\rangle . \end{aligned} \tag{3.19}$$

For each value of a and E_i the operator maps an « eigenvector » of the extended operator H_0 into an eigenvector H with the same value of a as a degeneracy label.

Generally the eigenfunctions of H corresponding to the discrete spectrum

satisfy the following orthogonality relation:

$$\langle H, A; E_i, a | H, A; E_j, b\rangle = \delta(i, j)\langle a|\omega_a^{-1}(E_i)|b\rangle , \tag{3.20}$$

where $\delta(i, j)$ is the Kronecker δ. The matrix $\langle a|\omega^{-1}(E_i)\ b$ is a positive definite Hermitian matrix in the space of eigenfunctions of the operator A corresponding to a fixed eigenvalue E_i of H. In the case where the eigenfunctions belonging to the same eigenvalue E_i but having different degeneracy labels have been made orthogonal to each other, $\langle a|\omega^{-1}(E_i)|b\rangle$ would have the

$$\langle a|\omega_a^{-1}(E_i)|b\rangle = C_{ia}\delta(a, b) .$$

The constant C_{ia} (which is always positive) is the normalization constant for the eigenfunction $|H, A; E_i, a\rangle$, that is,

$$\langle H, A; E_i, a | H, A; E_i, a\rangle = C_{ia} .$$

The operator $\langle a|\omega_a^{-1}(E_i)\ b$ has a positive-definite inverse which we denote by $\langle a|\omega_a(E_i)|b\rangle$; the latter, by definition, satisfies the relation

$$\sum_b \langle a|\omega_a(E_i)|b\rangle\langle b|\omega_a^{-1}(E_i)|c\rangle = \sum_b \langle a|\omega_a^{-1}(E_i)|b\rangle\langle b|\omega_a(E_i)c\rangle = \delta(a, c) . \tag{3.21}$$

There is one other orthogonality relation which we should note, namely the relation which expresses the orthogonality between the eigenfunctions of the discrete and continuous spectrum of H. It is

$$\eta(E)\eta(-E_i)\langle H, A; E, a | H, A; E_i, b\rangle = 0 . \tag{3.22}$$

3·3. *The completeness theorem for H; definition of H in the extended space.* – The principal difference between the results of Parts I and II arises from the fact that in the present case the Hilbert space is spanned by the eigenfunctions belonging to the discrete as well as the continuous eigenfunctions of H.

Let us consider any state $\eta(H_0)\ \varphi\rangle$ in Hilbert space. Further, let us take for the eigenfunctions of the continuous spectrum either the outgoing or incoming eigenstates $|H, A; E, a\rangle_\pm = U_\pm \eta(H_0)|H_0, A_0; E, a\rangle$. The arbitrary state $\eta(H_0)|\varphi\rangle$ can then be expanded in the following way:

$$\eta(H_0)|\varphi\rangle = \iint |H, A; E, a\rangle_\pm \eta(E)\,\mathrm{d}E\,\mathrm{d}a\ {}_\pm\langle H, A; E, a|\eta(H_0)|\varphi\rangle + \sum_i \sum_{a,b} |H, A; E_i, a\rangle\langle a|\omega_a(E_i)|b\rangle\langle H, A; E_i, b|\eta(H_0)|\varphi\rangle . \tag{3.23}$$

The coefficients of $|H, A; E, a\rangle_{\pm}$ and $|H, A; E_i, a\rangle$ in the expansion (3.23) follow from the normalization conditions (3.20) and (3.14*b*). Since $\eta(H_0)\varphi$ is an arbitrary state in Hilbert space, (3.23) is equivalent to

$$\iint |H, A; E, a\rangle_{\pm}\eta(E)\,\mathrm{d}E\,\mathrm{d}a\,{}_{\pm}\langle H, A; E, a|\eta(H_0) + \tag{3.24}$$
$$+ \sum_i \sum_{a,b} |H, A; E_i, a\rangle\langle a|\omega_a(E_i)|b\rangle\langle H, A; E_i, b|\eta(H_0) = \eta(H_0)\,.$$

It is useful to define the positive definite matrices $\langle a|\omega_a(E)|b\rangle$ in the previously described intervals ΔE_i so that for $E = E_i$ the operator $\langle a|\omega_a(E)|b\rangle$ are the matrices $\langle a|\omega_a(E_i)|b\rangle$ introduced earlier. On using (3.19), (3.14*a*) and (2.3) we have

$$U_{\pm}\eta(H_0)U^*_{\pm}\eta(H_0) + \sum_i \sum_{a,b} U\eta(-H_0)\delta(E_i - H_0)\cdot \tag{3.25}$$
$$\cdot \int |H_0, A_0; E, a\rangle\langle a|\omega_a(E)|b\rangle\,\mathrm{d}E\langle H_0, A_0; E, b|\eta(-H_0)U^*\eta(H_0) = \eta(H_0)\,,$$

where the integral is taken over each of the intervals $\Delta_i E$. Let us introduce the operator

$$W_a\eta(-H_0) = \sum_{a,b} \int |H_0, A_0; E, a\rangle\langle a|\omega_a(E)|b\rangle\,\mathrm{d}E\langle H_0, A_0; E, b|\eta(-H_0)\,. \tag{3.26}$$

It is clear that $W_a\eta(-H_0)$ is a positive definite operator in the space orthogonal to the Hilbert space and that it commutes with H_0.

On using (3.11) and (3.16), Eq. (3.25) becomes

$$UWU^*\eta(H_0) = \eta(H_0)\,, \tag{3.27}$$

where

$$W = W_c\eta(H_0) + \sum_i \delta(E_i - H_0)W_a\eta(-H_0)\,. \tag{3.28}$$

Eq. (3.28) is the weight operator for the case where point eigenvalues exist. As can be seen, the weight operator is positive definite and has an inverse in the vector space. Eq. (3.28) provides a decomposition of W into two parts: W_c, which characterizes the orthogonality relations of the continuous spectrum of H (hence the subscript c for «continuous»); and W_d which characterizes the orthogonality relations of the discrete spectrum (hence the subscript d for «discrete»).

We have not yet discussed how H is to be defined in the extended space. The extension of H can be carried out by giving the vectors which span the

extended space. Since we want the spectrum of the extended operator H to have the same spectrum as the spectrum of the extended operator H_0 and hence of the original operator H, it is seen that the eigenstates of H which span the Hilbert space must also span the extended space. It is clear that the spectrum of H is thus preserved.

The effect of the extension of the definition of H is that equation (3.27) is replaced by

$$UWU^* = I \,. \tag{3.29}$$

4. - More detailed discussion of the Q-representation and Q-extended operators.

As in Part I we shall introduce the Q-representation and require that the operators K and K_0 be triangular in terms of this representation, i.e.,

$$\begin{cases} \langle q|K|q'\rangle = 0 \,, & q' > q, \\ \langle q|K_0|q'\rangle = 0 \,, & q' > q, \end{cases} \tag{4.1}$$

where K and K_0 are given by

$$U = I + \varepsilon K \,, \qquad U_0 = WU^* = I + \varepsilon K_0 \,. \tag{4.2}$$

Generally, the Q is defined only in the Hilbert space (i.e., only $Q_{\eta}(H_0)$ is defined). Its eigenstates $|q\rangle$ satisfy the completeness relation

$$\int_{q_0}^{q_1} |q\rangle \, \mathrm{d}q \langle q|\eta(H_0) = \eta(H_0) \,, \tag{4.3}$$

where q_1 and q_0 are the upper and lower limits of the eigenvalues of Q. To extend the definition of Q into the whole vector space we write the completeness relation for the eigenfunctions $|q\rangle$ as

$$\int_{q_0}^{q_1} |q\rangle \, \mathrm{d}q \langle q| = I \,. \tag{4.4}$$

From (4.4) we have

$$\langle q|q'\rangle = \delta(q - q') = \langle q|I|q'\rangle \,. \tag{4.5}$$

. (4.4) means that any vector $|\varphi\rangle$ in the extended space has q-representa-
e namely $\langle q|\varphi\rangle$. If the state $|\varphi\rangle$ is in Hilbert space it is quadratically
egrable in the function $\langle q|\varphi\rangle$. If $\eta(-H_0)|\varphi\rangle \neq 0$, i.e., if $|\varphi\rangle$ has the com-
nent outside the Hilbert space, the functions $q\,\varphi$ are not quadratically
egrable.

As usual, every operator A defined in the extended space can be given as
integral operator with the kernel $\langle q|A|q'\rangle$, i.e., if $|\varphi\rangle$ is a state in the
tended space $\langle q|A|\varphi\rangle$ can be written as (Using (4.4))

$$\langle q|A|\varphi\rangle = \int_{q_0}^{q_1} \langle q|A|q'\rangle \,\mathrm{d}q' \langle q'|\varphi\rangle \quad . \tag{6}$$

in ordinary Hilbert space theory, the operator A is defined if the kernel
$|A|q'\rangle$ is given.

Let us consider now an operator of the form $A\eta(H_0)$. This operator oper-
es in a non-trivial way only on the Hilbert space. It maps vectors ortho-
nal to the Hilbert space into zero. The kernel $\langle q|A\eta(H_0)|q'$ is, of course,
known function of q and q'.

One might wish to extend the definition of the operator $A\eta(H_0)$ to an oper-
or A which can be applied in a non-trivial way to the whole vector space
d which can be applied in a non-trivial way to the whole vector space and
hich equals $A\eta(H_0)$ when applied to the Hilbert space. One possible way
defining the extended operator A is to define the kernel $\langle q|A|q'$ as a
nction of q and q' as being equal to the kernel $\langle q|A\eta(H_0)|q'\rangle$,

$$\langle q|A|q'\rangle = \langle q|A\eta(H_0)|q' \quad . \tag{7}$$

should be noted that Eq. (4.7) does *not* imply that $A = A\eta(H_0)$. An oper-
or A obtained from $A\eta(H_0)$ by this means vill be called a Q-extended oper-
or. In Section 2 we took H_0 to be a Q-extended operator.

The simplest example of a Q-extended operator is the identity I, which
obtained from the operator $\eta(H_0)$ because we have

$$\langle q|\eta(H_0)q'\rangle = \delta(q-q') \tag{8}$$

hen $\eta(H_0)$ acts on the Hilbert space. Furthermore,

$$\langle q|I|q'\rangle = \delta(q-q') = \langle q|\eta(H_0)|q' \quad . \tag{9}$$

We shall require that the operator U be a Q-extended operator obtained

from $U\eta(H_0)$. A consequence of this requirement is that

$$\langle q|\, K\,|q'\rangle = \langle q|\, K\eta(H_0)\,|q'\rangle\,. \tag{4.10}$$

Since every operator can be written as an integral operator with a kernel, any operator which is given in terms of the Q-representation when acting on the Hilbert space has the same form as a Q-extended operator.

It should not be thought, however, that every operator acting on the full space is a Q-extended operator. For example, the weight operator W is not a Q-extended operator, since generally

$$\langle q|\, W\eta(H_0)\,|q'\rangle = \langle q|\, W_c\eta(H_0)\,|q'\rangle$$

does *not* equal

$$\langle q|\, W\,|q'\rangle = \langle q|\, W_c\,\eta(H_0)\,|q'\rangle + \langle q|\, W_a\eta(-H_0)\,|q'\rangle\,.$$

5. – Theorems on the inverse problem. The equation for K, K_0.

We shall now present theorems analogous to those of Part I. We shall not go through the proof because the proofs of Part I are essentially the same if the Hilbert space is extended properly.

Theorem I. Let there be given a vector space spanned by the eigenfunctions of the extended operators H_0, A_0 as described above, the negative point eigenvalues of H, E_i and the degeneracy of these eigenvalues being given. Further, let us prescribe the positive definite operator

$$W = W_c\eta(H_0) + \sum_i \delta(E_i - H_0)W_a\eta(-H_0)$$

in the vector space; W commutes with H_0 and has an inverse. Then if the equations

$$U_0 = WU^* \tag{5.1}$$

$$U_0 = U^{-1} \tag{5.2}$$

can be solved for U, U_0, the operator H given by

$$H = UH_0U_0 \tag{5.3}$$

is a Hermitian operator whose eigenstates corresponding to the continuous

spectrum are

$$|H, A; E, a\rangle = U\eta(E)|H_0, A_0; E, a\rangle \qquad \text{for } 0 \leqslant E < \infty \tag{5.4}$$

and whose eigenstates corresponding to the point eigenvalues E_i with the prescribed degeneracies are

$$|H, A; E_i, a\rangle = U|H_0, A_0; E_i, a\rangle \,. \tag{5.5}$$

The eigenstates of H will satisfy the completeness relation

$$\int\int\int |H, A; E, a\rangle \,\mathrm{d}a\langle a|\omega_c(E)|b\rangle\eta(E)\,\mathrm{d}E\,\mathrm{d}b\langle H, A; E, b| + \tag{5.6}$$

$$+ \sum_i \sum_{a,b} |H, A; E_i, a\rangle\langle a|\omega_a(E_i)|b\rangle\langle H, A; E_i, b| = I \,,$$

where

$$\langle a|\omega_c(E)|b\rangle\eta(E)$$

and

$$\langle a|\omega_a(E)|b\rangle\eta(-E)$$

are defined by

$$\langle H_0, A_0; E, a|W_c\eta(H_0)|H_0, A_0; E', b\rangle = \delta(E - E')\langle a|\omega_c(E)|b\rangle\eta(E) \,, \tag{5.7}$$

$$_B\langle H_0, A_0; E, a|W_a\eta(-H_0)|H_0, A_0; E', b\rangle_B = \delta(E - E')\langle a|\omega_a(E)|b\rangle\eta(-E). \tag{5.8}$$

Furthermore, the eigenfunctions will satisfy the normalization conditions

$$\int\langle a|\omega_c(E)|b\rangle\,\mathrm{d}b\langle H, A; E, b|H, A; F, c\rangle = \delta(E - F)\delta(a, c) \,, \tag{5.9}$$

$$\langle H, A; E, b|H, A; E_i, c\rangle = 0 \,, \qquad (E > 0), \tag{5.10}$$

$$\sum_i \langle a|\omega_a(E_i)|b\rangle\langle H, A; E_i, b|H, A; E_j, c\rangle = \delta(i, j)\delta(a, c) \,. \tag{5.11}$$

The condition that W be a positive definite operator which commutes with H_0 and which has an inverse is equivalent to requiring the same properties of $W_c\eta(H_0)$ and $W_a\eta(-H_0)$ in the Hilbert space and the vector space orthogonal to the Hilbert space respectively.

Theorem II. If we write $U = I + \varepsilon K$, $U_0 = I + \varepsilon K_0$ and require K, K_0 to be triangular in the Q-representation then $U_0 = WU^*$ has a unique

solution for U, U_0 if W satisfies conditions analogous to those required in Part I.

Theorem III. It can be shown that if the extension of the Hilbert space is carried out properly then $U_0 = U^{-1}$.

We shall now write the generalized Gelfand-Levitan equation for K. From (5.1) we have

$$UW = U_0^* . \tag{5.12}$$

Let us write

$$\begin{cases} U = I + \varepsilon K \\ U_0 = I + \varepsilon K_0 \\ W = \eta(H_0) + \varepsilon\Omega . \end{cases} \tag{5.13}$$

Then (5.12) becomes

$$\eta(H_0) + \varepsilon\Omega + \varepsilon K\eta(H_0) + \varepsilon^2 K\Omega = I + \varepsilon K_0^* \tag{5.14}$$

or in terms of the Q-representation

$$\langle q|\eta(H_0)|q'\rangle + \varepsilon\langle q|\Omega|q'\rangle + \varepsilon\langle q|K\eta(H_0)|q'\rangle + \tag{5.15}$$

$$+ \varepsilon^2\langle q|K\Omega|q'\rangle = \delta(q-q') + \varepsilon\langle q|K_0^*|q'\rangle .$$

Now

$$\langle q|\eta(H_0)|q'\rangle = \delta(q-q') \tag{5.16}$$

when $\eta(H_0)$ acts on Hilbert space; otherwise

$$\langle q|\eta(H_0)|q'\rangle = 0 .$$

Hence

$$\langle q|\eta(H_0)|q'\rangle \equiv 0 \qquad (q > q'). \tag{5.17}$$

From the triangularity condition (4.1) on K_0

$$\langle q|K_0^*|q'\rangle = 0 \qquad (q > q'). \tag{5.18}$$

We now use the fact that K is a Q-extended operator and write

$$\langle q|K\eta(H_0)q'\rangle = \langle q|K|q'\rangle . \tag{5.19}$$

Hence, finally we obtain our equation for K, namely

$$\langle q|K|q'\rangle = -\langle q|\Omega|q'\rangle - \varepsilon\int_{q_0}^{q}\langle q|K|q''\rangle\,\mathrm{d}q''\langle q''|\Omega|q'\rangle\,, \qquad (q>q'), \tag{5.20}$$

which is the same equation for $\langle q|K|q'\rangle$ as obtained in Part I.

6. – Conditions on the eigenfunctions $|H_0, A_0; E_i, a\rangle$.

The condition that $|H, A; E_i, a\rangle$ be in Hilbert space and hence that the q-representative $\langle q|H, A; E_i, a\rangle$ be a quadratically integrable function of q leads to a condition on $\langle q|H_0, A_0; E_i, a\rangle$ if we assume K as triangular in the Q-representation. We can write

$$\langle q|H, A; E_i, a\rangle = \langle q|H_0, A_0; E_i, a\rangle - \varepsilon\int_{q_0}^{q}\langle q|K|q'\rangle\,\mathrm{d}q'\langle q'|H_0, A_0; E_i, a\rangle\,. \tag{6.1}$$

Now since the second term approaches zero as q approaches q_0, we see that the quadratic integrability of $\langle q|H, A; E, a\rangle$ implies that $\langle q|H_0, A_0; E_i, a\rangle$ be a quadratically integrable function of q in the neighborhood of $q = q_0$:

It appears, in fact, that a sufficient condition on the extension of the Hilbert space to guarantee the validity of the three theorems of Section 5 is the condition that $\langle q|H_0, A_0; E_i, a\rangle$ satisfy

$$\int_{q_0}^{q_a}\langle H_0, A_0; E_i, a|q'\rangle\,\mathrm{d}q'\langle q'|H_0; A_0; E_i, a\rangle < \infty \qquad \text{for } q < q_1\,. \tag{6.2}$$

That is, the added eigenfunctions $\langle q|H_0, A_0; E_i, a\rangle$ are «essentially» in Hilbert space if one replaces these functions by zero in the vicinity of $q = q_1$. The functions $\langle q|H_0, A_0; E_i, a\rangle$ will have to be singular at $q = q_1$ in order that these eigenfunctions span a space bigger than Hilbert space. Then the q-representative $\langle q|\varphi\rangle$ of any state $|\varphi\rangle$ as a function of q is quadratically integrable

$$\int_{q_0}^{q_a}\langle\varphi|q\rangle\,\mathrm{d}q\langle q|\varphi\rangle < \infty \qquad \text{for } q < q_1\,. \tag{6.3}$$

Those states $|\varphi\rangle$ which are in Hilbert space are, of course, quadratically integ-

rable in $q_0 \leqslant q \leqslant q_1$ be definition:

$$\int_{q_0}^{q_1} \langle \varphi | q \rangle \, dq \langle q | \varphi \rangle < \infty . \tag{6.4}$$

States which are not in Hilbert space will have representatives $\langle q|\varphi\rangle$ which have singularities for $q = q_1$ which are so severe that the square $\langle q|\varphi\rangle$ does not exist:

$$\int_{q_0}^{q_1} \langle \varphi | q \rangle \, dq \langle q | \varphi \rangle = \infty . \tag{6.5}$$

Under the conditions of these extension of the Hilbert space, one can say that the Hilbert space is « dense » in the vector space; that is, every state in the vector space $\langle q|\varphi\rangle$ can be considered as being approximated by an element of Hilbert space for $q < q_1$.

The vector space of Ref. [2] has essentially this property.

---

[2] I. KAY: *On the determination of a linear system from the reflection coefficient*; EM-74, *Institute of Mathematical Sciences, Division of Electromagnetic Research, New York University*.

RIASSUNTO (*)

Nella Parte I di questo lavoro ci siamo limitati alla considerazione di operatori di ponderazione che conducono ad Hamiltoniane H i cui spettri sono identici allo spettro di una data Hamiltoniana imperturbata H_0. In questa parte del lavoro ci proponiamo di mostrare come si possano scegliere degli operatori di ponderazione che conducano ad Hamiltoniane H dotate di spettri differenti di quelli di H_0. Per rendere la discussione più concreta tratteremo il caso in cui H_0 ha spettro puramente continuo estendentesi da 0 a ∞ e in cui H ha uno spettro dotato di una parte continua coincidente con lo spettro di H_0 e, inoltre, ha autovalori discreti negativi.

(*) *Traduzione a cura della Redazione.*

The Masses of Positive K-Particles.

H. H. Heckman, F. M. Smith and W. H. Barkas

Radiation Laboratory, University of California - Berkeley, California

(ricevuto il 28 Ottobre 1955)

Summary. — Our program of measuring meson masses has been extended to the positive τ, $K_{\mu 2}$, $K_{\pi 2}$, $K_{\mu 3}$, and τ'-particles. With the Bevatron as a source, and employing a modification of the Kerth-Stork quadrupole lens and analyzing-magnet arrangement, we have obtained a mass resolution of 1.6% for an individual particle. Using the stopping behavior or the grain density of the secondary for K-particle classification, and the multiple scattering as a check, we obtained practically pure samples of the above types of K-mesons for analysis. The particles were compared directly with protons of the same momentum, and also with the τ-meson, the mass of which is known accurately. Relative to the mean τ mass of 966 m_e we obtain the following results, all in electron mass units: τ (966$\pm$3.1), $K_{\mu 2}$ (962.5$\pm$3.2), $K_{\pi 2}$ (972.2$\pm$4.7), $K_{\mu 3}$ (951.2$\pm$10.6), τ' (951.1$\pm$10.9). These are all consistent with a single K mass of 966. The results are independent of the range-momentum relation; however, the intercomparison of the masses measured relative to the τ-meson and relative to the proton check closely, indicating that there are no large systematic errors and that the shape of the range-momentum relation must be nearly correct.

The meson-mass measurement program [1] that was started some years ago now has been extended to several types of K-mesons. Although a number of important parts of the new work remain to be completed, particularly studies of the energy-momentum balance in the various decay schemes, the

[1] W. H. Barkas, W. Birnbaum and F. M. Smith: *The Mass-Ratio Method Applied to the Measurement of* τ-*Meson Masses and the Energy Balance in Pion Decay*, in *University of California Radiation Laboratory Report* No. UCRL-3147 (1955); and F. M. Smith, W. Birnbaum and W. H. Barkas: *Phys. Rev.*, **91**, 765 (1953).

current interest in the K-mesons mass(es), and the conflicting results that have been obtained [2], prompt us to make this preliminary report.

After experimenting with other geometries, we developed our apparatus from the basic design of KERTH and STORK [3]. With this arrangement the particles from a Bevatron target pass first through a strong-focusing lens and then through an analyzing magnetic field before detection in a stack of emulsion. Unfortunately, a window through which the particles must pass in emerging from the vacum, chamber, and several feet of air path, each cause considerable multiple scattering of the beam and reduce the efficiency and momentum resolution of the strong-focusing lens. To improve the momentum selection obtained with the original apparatus we redefined the particle orbits by introducing a 6-inch lead collimator containing a 0.25-inch vertical slit preceding the analyzing magnet. The stretched-wire technique was used to check the rather critical line-up of the collimator. Also, to reduce the multiple scattering and energy loss of the particles while traversing the analyzing magnet, the air in the path between the collimator and detector was replaced by helium. The result of these various improvements was to substantially better the momentum resolution. The effect of the momentum interval on the mass resolution was reduced so as to become comparable to the effect of the inherent straggling of ranges.

In this work the rectified particle track length R was measured for each identified particle. The ranges were determined by measuring the length of each segment of track that could be considered straight and adding the lengths together. Since the edge of the emulsion is distorted in processing, provision was made for correctly determining its original location. The surface of the stack upon which the particles are incident nearly normally was milled flat and sharp V-shaped grooves were cut in the side of the stack. Before processing, a 1 mm rectangular grid was contact-printed on each pellicle in a position determined to within less than 20 μm by the machined features of the pellicle. After processing, the grid constituted a coordinate frame, not only for the location of events but also to define the edge. Use was also made of the fact that in addition to pions, K-particles, and protons, there are deuterons, tritons, ^{3}He, and ^{4}He particles as abundant constituents of the beam. Since all the particle orbits entering the emulsion stack at the same point have the same magnetic rigidity, the depths to which the various particles penetrate give precise information on the edge correction.

---

[2] For example, T. F. HOANG, L. JAUNEAU, G. KAYAS, A. ORKIN-LECOURTOIS, L. LEPRINCE-RINGUET, D. MORELLET, G. TARIEL and J. TREMBLEY, *Suppl. Nuovo Cimento*, **12**, 242 (1954); R. ARMENTEROS, B. GREGORY, A. HENDEL, A. LAGARRIGUE, L. LEPRINCE-RINGUET, F. MULLER and CH. PEYROU: *Nuovo Cimento*, **1**, 915 (1955).

[3] R. W. BIRGE, R. P. HADDOCK, L. T. KERTH, J. R. PETERSON, J. SANDWEISS, D. H. STORK and M. N. WHITEHEAD: *Phys. Rev.*, **99**, 329 (1955).

In order to avoid bias in the selection of K-particles for measurement, the emulsion was scanned along a band where the τ-meson was expected to have a residual range of about 1.5 cm. Each non-minimum track found within 10° of the expected direction of the K-particle tracks was followed until it stopped, or was identified as a proton.

The behavior of the secondary particles into which they decay provided the basis of classification of the K-particles; it had been assumed from the beginning that mass measurements would be meaningful only for mesons identified as to type. The development of the emulsion was remarkably uniform, and it was found that if 400 grains were counted in tracks dipping less than 15° a separation of better than 90 % could be effected between the $K_{\mu 2}$-mesons (1.05 × min) and the $K_{\pi 2}$-mesons (1.21 × min). These types, along with the τ-mesons, constitute the bulk of the particles found. All secondaries ionizing more intensely than those of the $K_{\pi 2}$ were followed until they stopped or left the stack. The τ' has one positive pion of low energy (< 53.9 MeV) as a secondary. The $K_{\mu 3}$ is recognized by the presence of a muon secondary, the energy of which is lower than that of the secondary from the $K_{\mu 2}$. In this way four $K_{\mu 3}$ and four τ'-particles were identified.

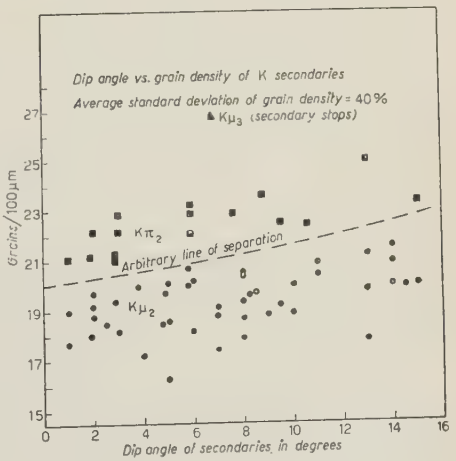

Fig. 1. – Grain densities of secondaries as a function of dip angle δ. Events below the arbitrary line of separation are classified as $K_{\mu 2}$'s, those above as $K_{\pi 2}$'s. The secondary with the exceptionally high grain count stopped in the emulsion stack and was identified as a muon from the decay of a $K_{\mu 3}$-particle.

In Fig. 1 is shown the grain densities (actually « blob » densities) of the secondaries plotted as a function of the dip angle δ. It is noteworthy that the observed grain density does not vary strictly in proportion to sec δ, presumably partly because of an influence of the random background grains. The separation achieved by the grain counting is perhaps even slightly better than expected. No bias was detected in the method of recording the data and the multiple scattering of 20 particles classified by grain density as $K_{\mu 2}$ secondaries confirmed this classification.

The multiple-scattering work was carried out both to insure the purity of the sample of $K_{\mu 2}$-mesons and to look for K_{e3} particles, since the electron

secondary cannot be distinguished from the $K_{\mu 2}$ secondary by grain count alone. The criteria used to select a secondary for a multiple-scattering measurement were that it have a dip angle δ less than 10° and be at least one centimeter from the edge of the emulsion. In order that the noise correction to the observed scattering be small, a cell of sufficient length to insure a signal-to-noise ratio of at least 4 to 1 is required. In these measurements, a 300 μm cell length met this condition. With this cell length and a velocity of 0.91 c (the velocity of the $K_{\mu 2}$ secondary) the scattering factor K_{cc} [4] is 25.5 MeV deg. After the second differences were measured by the Fowler technique, the procedure used to eliminate large single-scattering events was to discard all measurements that exceed four times the resultant mean. About 65 cells vere used to estimate the $p\beta c$ of each secondary. The mean of the secondary differences then has a standard deviation of about 10 %. With this precision, electron secondaries of $p\beta c < 150$ MeV could easily be detected. While the secondary from the $K_{\pi 2}$-meson ($p\beta c = 169.6$ MeV) could not be so readily identified, the probability would be 0.65 of resolving it from the μ-meson distribution if even one such event were present in the sample that was multiply scattered. Of the 20 secondaries measured, all were consistent with being muons from the decay of the $K_{\mu 2}$-meson. The mean $p\beta c$ of all events was 214.0 ± 3.4 MeV, which agrees well with the calculated value of 214.8 MeV, assuming the $K_{\mu 2}$ mass to be 966 m_e. This measurement tends to confirm the correctness of the scattering factor. We have also concluded from these results that the fraction of K_{e3}'s among the $K_{\mu 2}$'s is probably less than 5 %. In addition the data give support to the validity of grain counting as a method to separate the $K_{\mu 2}$ and $K_{\pi 2}$ modes of decay.

By using the means described we have identified τ, τ', $K_{\mu 3}$, $K_{\pi 2}$ and $K_{\mu 2}$-mesons in the detecting emulsion. Since the proper time of flight to the stack is $\approx 1.2 \cdot 10^{-8}$ s, none of their lifetimes can be short compared to 10^{-8} s unless they themselves are decay products of a long-lived parent. In the latter event the mass being measured in this experiment is that of the parent (*). As the detection efficiencies for the particles with different types of secondaries are not equal, and yet to be determined, the relative numbers of the classified K-particles do not of course reflect the relative populations of the various K-particles that survive 10^{-8} s. The mesons were produced by bombarding a tantalum target with protons of 4.8 GeV.

The mass analysis was carried out by introducing the « Standard Range » R_0. This is the range (as deduced from the observed proton ranges using the range-

---

[4] L. Voyvodic and E. Pickup: *Phys. Rev.*, **85**, 91 (1952).

(*) This possibility was pointed out by L. W. Alvarez in connection with a decay scheme proposed by C. N. Yang.

momentum relation ([5])) that a particle of mass 966 m_e would be expected to have. It is, of course, a function of the point of entry into the stack. This range is introduced chiefly as a computational device: an error in its choice effects the final mass values only in a second approximation. For each measured range a quantity $\Delta R/R_0 = (R - R_0)/R_0$ may be calculated. Since the percentage range straggling ([6]) is almost independent of the velocity in this region and if the momentum interval is not large, the quantity $\Delta R/R_0$ for a particle of a given mass (near 966 m_e) should have a distribution that is nearly gaussian, with a standard deviation determined by the inherent range straggling and the momentum interval accepted. If the range-momentum relation is strictly correct and the true mass of the particle is 966 m_e, then the mean value of $\Delta R/R_0$ should be zero. Regardless of whether or not the range-relation is correct, the mean value of $\Delta R/R_0$ will be the same for all particles of the same mass. For τ-mesons which are known ([7,1]) to have a mass of 966.0 ± 0.6 m_e, the mean value $\langle \Delta R/R_0 \rangle$ measures the error in the range-momentum relation used as well as other systematic effects that are common to all particles. When the mean value of $\Delta R/R_0$ is not zero, we calculate the mass equivalent ΔM of this deviation by using the formula

$$\Delta M = \frac{966}{1 - q} \langle \Delta R/R_0 \rangle. \tag{1}$$

Here $q = (p/R)(\mathrm{d}R/\mathrm{d}p)$, where p is the momentum. In the velocity interval employed in this experiment $q \approx 3$. Then if the value of ΔM measured for the τ-meson is made to correspond with the mass 966, the masses of all other particles are related directly to the τ-meson.

We wish to point out that to measure a mass in an experiment such as this, the averaging of masses determined for individual particles is usually incorrect. The mass-distribution function is unsymmetrical, so that the median, mode, and mean are quite different quantities. The average obtained from a symmetrically (preferably normally) distributed function of the mass is the most useful quantity from which to derive a valid mass estimate.

For each type of K-particle classified as to mode of decay, points relating « rectified range » and position of entrance were plotted. This is illustrated by

---

([5]) W. H. Barkas and D. M. Young: *Emulsion Tables. I.* in *University of California Radiation Laboratory Report* No. UCRL-2579 (rev), 1954.

([6]) W. H. Barkas, F. M. Smith and W. Birnbaum: *Phys. Rev.*, **98**, 605 (1955).

([7]) H. H. Heckman: *Analysis of the τ-Meson Decay and Evidence for the β-Decay of a K-Meson*, in *University of California Radiation Laboratory Report* No. UCRL-3003 (1955).

Fig. 2. Superimposed on the range-vs-position data is the Standard Range curve. As described above, a systematic range correction of $+208 \pm 64$ μm was applied to all measured ranges. The apparent shrinkage of the edge of the emulsion is caused primarily by the distortion of the edge in processing. Another factor in the shrinkage may be the drying out of the edges of the emulsion stack between the times of its exposure and the mounting upon glass.

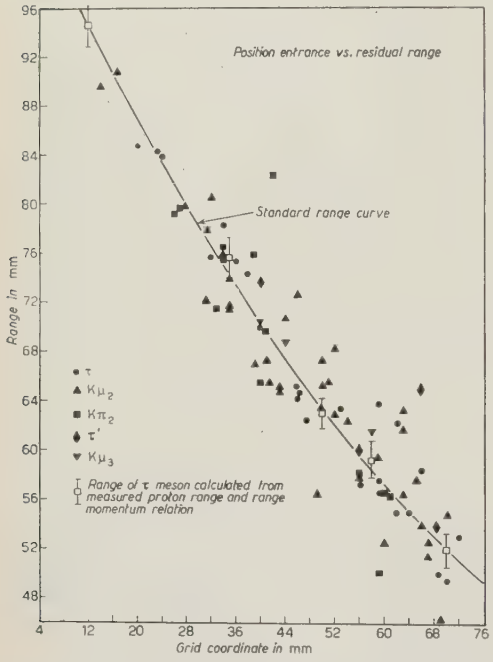

Fig. 2. – Ranges of K-mesons as a function of position of entrance along front edge of stack. The grid coordinate refers to the millimeter grid that is contact-printed on each emulsion.

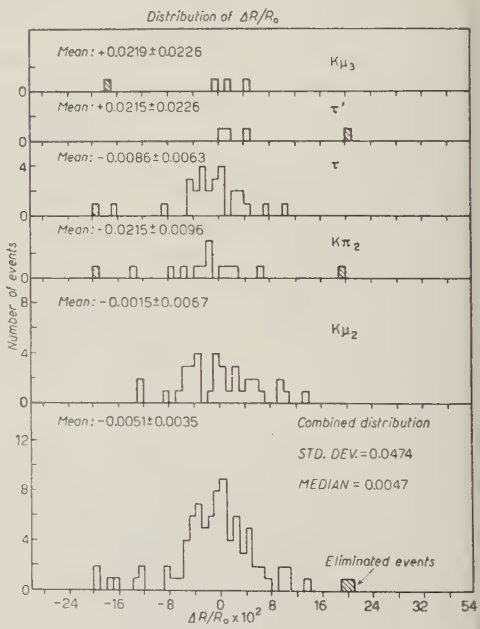

Fig. 3. – Histogram of $\Delta R/R_0$ for each type of K-particle. Every particle is shown. The five particles indicated by crosshatching were omitted in the mass calculations.

Fig. 3 shows the histograms of $(R - R_0)/R_0 = \Delta R/R_0$ for each type of K-particle. The events that are more than 2.81 standard deviations from the mean of the combined data were discarded in calculating the mean values. Of the real events, 99.5 % should then be included in the analysis. The directions of all particles were measured as they entered the stack at a point just inside the region of edge distortion. At this depth in the stack the track direction is already partially lost by multiple scattering, but of the five particles discarded because the range was anomalous, three were found to have such anomalous angles that it was unlikely that they could have come directly through the collimating slit to the stack. The resultant standard deviation

in the ranges is 4.74%. This range variance can be accounted for by assuming a 1.5% momentum resolution in addition to the 1.5% inherent range straggle of the K-particles. The observed momentum interval is about 0.5 % greater than expected when it is assumed that the particles come directly from the ¼-inch target. This increase of momentum spread is probably caused by the multiple scattering in the 0.090-inch aluminum window of the Bevatron and the 5 feet of air path traversed before entering the ¼-inch collimator. The multiple scattering would tend to make the source of particles appear diffused and not defined by the dimensions of the target. With the resolution we have

TABLE I. – *Tabulation of mass values for the* τ, τ', $K_{\pi 2}$, $K_{\mu 2}$ *and* $K_{\mu 3}$*-mesons. The probable errors of* ΔM *and the mass relative to the mean* τ *mass are the same and are listed in the last column. All masses are given in units of the electron mass.*

Type	Assumed Mode of Decay	Number	ΔM	Mass Relative to Mean τ Mass (966)	Probable Error
τ	$\pi^+ + \pi^+ + \pi^-$	27	4.2	966	3.1
$K_{\mu 2}$	$\mu^+ + \nu$	36	0.7	962.5	3.2
$K_{\pi 2}$	$\pi^+ + \pi^0$	12	10.4	972.2	4.7
τ'	$\pi^+ + \pi^0 + \pi^0$	3	— 10.3	951.5	10.9
$K_{\mu 3}$	$\mu^+ + ? + ?$	3	— 10.6	951.2	10.6
All Events	—	81	2.4	964.2	1.7
τ (Relative to Protons)	—	—	0.0	961.8	2.6

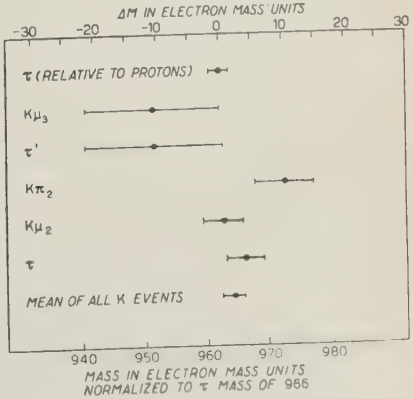

Fig. 4. Mass values for τ-, τ'-, $K_{\mu 2}$-, $K_{\pi 2}$- and $K_{\mu 3}$-mesons. ΔM is the difference in electron mass units as calculated from Eq. (1). For ΔM to be zero, the mean ranges of the particles would coincide with the expected range of a 966 m_e particle as calculated from the range of the protons and the range-momentum relation. This calculated mass point is denoted in Table I and in the above graph as τ (relative to protons). If we assign an absolute mass of 966 m_e to the τ-meson, the masses of the various K-particles are then directly related to the τ-meson.

obtained in this experiment, the probable error of a single K-mass measurement is 1.6%.

In Table I are the tabulated results of the experiment. The mass values of the K-particles with their probable errors are plotted in Fig. 4.

We agree with the amended [8] result of R. BIRGE *et al.*, who find that with their resolution the mean mass of K-particles with a near-minimum secondary is indistinguishable from the τ-meson mass. In addition we are able to make a stronger statement: namely, that with somewhat better mass resolution, each individual type of K-meson (classified by the behavior of the secondaries) remains indistinguishable from the τ-meson. All the K masses are consistent with a single value, 966 m_e. We also find that the range-momentum relation probably is not seriously in error, because, by making careful correction for systematic effects, we obtain close to the predicted range ratio for protons and τ-mesons.

Our result for the $K_{\mu 2}$-meson is not consistent with the low values found by several [9] cloud chamber groups when they deduce the $K_{\mu 2}$ mass from the range of the secondary. The results on the multiple scattering of the secondaries confirms our high mass of the $K_{\mu 2}$-mesons. We have calculated, using the formula of EGUCHI [10], the approximate energy loss in radiative decay of the $K_{\mu 2}$-particle, and find that it is insufficient to cause the discrepancy. However, it will in rare instances give rise to an event which phenomenologically is a $K_{\mu 3}$-decay.

As another part of our program of precise emulsion measurements, we are determining the range-momentum relation for magnetically analyzed pions and protons in emulsion stacks of accurately known density. It is believed that this program may be important for resolving the present inconsistencies and for further progress in the elaboration of the K-meson decay schemes.

* * *

The success of this mass measurement program was determined in a large measure by the technical competence and conscientious labor of Mrs. NANCY FREED, Miss HESTER LOWE, Mrs. ROBERTA SPEER, Mr. JOHN DYER, and

[8] R. W. BIRGE, J. R. PETERSON, D. H. STORK and M. N. WHITEHEAD: *Mass Values of the* K-*Mesons*, in *University of California Radiation Laboratory Report* No. UCRL-3083 (1955).

[9] Examples: J. BALLAM, A. L. HODSON and G. T. REYNOLDS: *Phys. Rev.*, **99**, 1038 (1955); G. T. REYNOLDS and W. A. ARON: *Phys. Rev.*, **99**, 1038 (1955); B. GREGORY, A. LAGARRIGUE, L. LEPRINCE-RINGUET, F. MULLER and CH. PEYROU: *Nuovo Cimento*, **11**, 292 (1954); H. S. BRIDGE, H. DESTAEBLER jr., B. ROSSI and B. V. SREEKANTAN: *Nuovo Cimento*, **1**, 874 (1955).

[10] T. EGUCHI: *Phys. Rev.*, **85**, 943 (1952).

Mr. JAMES GRAY, who carried out most of the scanning and measurements. We are also indebted to Mr. LEROY KERTH for information in connection with the equipment and to Dr. EDWARD LOFGREN and the operating crew of the Bevatron, both for the bombardments and for cooperation in setting up the equipment.

This work was performed under the auspices of the United States Atomic Energy Commission.

RIASSUNTO (*)

Abbiamo esteso il nostro programma di misure delle masse mesoniche alle particelle τ, $K_{\mu 2}$, $K_{\pi 2}$ $K_{\mu 3}$ e τ' positive. Col bevatrone per sorgente e impiegando una modificazione della lente a quadrupolo di Kerth-Stork e della disposizione magnetica di analisi abbiamo ottenuto per le masse una risoluzione dell'1.6% per una singola particella. Servendoci del comportamento all'arresto o della densità della traccia al secondario per la classificazione dei K e dello scattering multiplo per il controllo abbiamo ottenuto per l'analisi campioni dei suddetti tipi di particelle K praticamente puri. Le particelle furono confrontate direttamente con protoni di uguale impulso e anche col mesone τ la cui massa è nota con precisione. Rispetto alla massa del τ di 966 m_e otteniamo i seguenti risultati, tutti in unità di massa elettroniche: τ (966 $\pm$ 3.1), $K_{\mu 2}$ (962.5 $\pm$ 3.2), $K_{\pi 2}$ (972.2 $\pm$ 4.7), $K_{\mu 3}$ (951.2 $\pm$ 10.6), τ' (951.1 $\pm$ 10.9). Questi valori sono tutti compatibili con un'unica massa per il K di 966. I risultati sono indipendenti dalla relazione range impulso; non di meno il confronto delle masse misurate rispetto al mesone τ e rispetto al protone coincidono strettamente, indicando che non vi sono errori sistematici e che la forma della relazione range-impulso deve essere pressochè esatta.

(*) *Traduzione a cura della Redazione.*

Nuclear Interactions of Negative K-Mesons in Nuclear-Research Emulsion.

E. P. George, A. J. Herz, J. H. Noon and N. Solntseff

The F. B. S. Falkiner Nuclear Research and Adolph Basser Computing Laboratories. School of Physics (*), The University of Sydney - Sydney, N.S.W.

(ricevuto il 4 Novembre 1955)

Summary. — A large emulsion stack was exposed at the Bevatron to K^- mesons of life time of the order of 10^{-8} s. Fifty-two K^- particles were observed, among which 12 stopped with no visible decay or interaction, 28 ended in an evaporation star, 9 gave a fast π-meson as well as an evaporation star, 1 ejected a hyperon and a π^--meson, 1 produced the emission of what may be either a hyperdeuteron coming to rest or a Σ^+ decaying into a proton in flight, and there is 1 case of an evaporation star closely associated with a possible Λ^0-decay. Particular importance is attached to the possible hyperdeuteron as the existence of such a particle would be in contradiction to the theory of Gell-Mann as well as allowing one to estimate the strength of the nuclear interaction of the hyperon involved. The main features of the nuclear events are (i) the overall average excitation energy of the evaporation stars is about 150 MeV, (ii) π-mesons are emitted from about 17 percent of the events and most of these, if not all, are negatively charged, (iii) charged hyperons are emitted from a small fraction of the events (one in our case, accompanied by a π-meson), (iv) the mean kinetic energy of the emitted π-mesons is 40 MeV, and (v) the mean prong number of the evaporation stars associated with π-meson emission is significantly greater than the overall average. All these features can be explained qualitatively by one mechanism: the K^--particle enters into the nucleus then interacts with one nucleon in the presence of other nucleons which take up part of the available energy according to the reaction $K^- + N + \text{nucleons} \to Y + \pi + \text{nucleons} + Q$. As the primary absorption process occurs fairly near to the nuclear surface, the secondaries from this reaction each have a probability of about 50 percent of escaping without contributing to the nuclear excitation. The hyperons involved appear to be the Λ^0 and the isotopic-spin triplet Σ^+, Σ^0, Σ^-; and the observations require that the production of Λ^0's is of the order of ten times more frequent than that of any particle of the Σ group.

(*) Also supported by the Nuclear Research Foundation within the University of Sydney.

1. – Introduction.

During the last few years, many workers have observed cosmic-ray events which have been interpreted as the nuclear absorption of particles of mass about 1000 m_e, known as K-mesons. These events, while indicating some of the features of the K-meson absorption process, could not be used in an analysis of the relative frequencies of different types of events as the efficiency with which different types of events were detected was unknown.

We accordingly decided to make a systematic investigation of the processes connected with K^- absorption, using the magnetically separated beam of K^- particles from the Bevatron at the Radiation Laboratory of the University of California. The first results of this investigation, based on an analysis of fifty-two events, are reported in this paper.

Similar work has been published by the Brookhaven group who used K-particles from the Cosmotron (HORNBOSTEL and SALANT [1]) and by others working at the Bevatron (FREDEN and TICHO [2], CHUPP, GOLDHABER, GOLDHABER and WEBB [3]). Our observations are not inconsistent with the results of these workers.

In Part 2 of this paper we present those results of our investigation which are needed in the subsequent discussion of the K^- absorption process. Most experimental detail has been relegated to Part 3 which is, therefore, of little interest to non-specialists.

2. – Summary of results and discussion.

2·1. *General.* – Our emulsion stack of size $9'' \times 11'' \times 5.4$ cm was exposed to the « K^- beam » of the Bevatron. The beam contained π^- and K^--mesons of the same momentum and it entered the emulsion stack in a direction parallel to the plane of the sheets. The ratio between the numbers of π^- and K^--mesons in the beam was of the order of 10^4:1, but there was no possibility of confusion as in the range of momenta concerned (260 to 400 MeV/c) the π^--mesons were near the minimum of ionization whilst the K^--meson tracks were quite dense, having blob densities of 2 to 3 times the minimum.

The plates were scanned along a line 1 cm from the edge entered by the beam, and all tracks which had the blob density and direction expected for

(1) J. HORNBOSTEL and E. O. SALANT: *Phys. Rev.*, **98**, 218 (1955).

(2) S. C. FREDEN and H. K. TICHO: *Phys. Rev.*, **99**, 1057 (1955).

(3) W. W. CHUPP, G. GOLDHABER, S. GOLDHABER and F. H. WEBB: *Bull. Am. Phys. Soc.*, **30**, No. 5, 13 (1955).

beam K-mesons were followed to the ends of their ranges. The masses of all particles whose tracks ended within 5 mm of the expected place for beam K^- mesons were then determined, irrespective of whether there was a star at the end or not. In this way, thirty-seven K^- mesons have been found. In addition, fifteen K^--absorption events were found outside the expected region.

The events we have found can be classified roughly in the following way:

ρK events: the particle stops without giving « visible » evidence o fa nuclear interaction other than perhaps a small blob of the type sometimes seen on π^--meson endings;

σK events: the only visible tracks from the nuclear absorption of the K^--meson are those of stable fragments such as protons, α-particles etc;

σK_L events: σK events from which an L-meson is emitted;
σK_Y events: σK events from which a hyperon is emitted, and
σK_F events: σK events from which an unstable heavy fragment is emitted.

The numbers of the various types of event we have found are given in Table I. Most of the K^- endings fall within a well-defined strip which is somewhat different from the calculated one. We therefore do not believe that any significance should be attached to the fact that more than half of our σK_L events were found outside the theoretically expected region. In the case of the ρK events there is, of course, a bias favouring events in the expected region, for the masses of particles stopping outside that region where not usually determined.

TABLE I.

	ρK		σK		σK_L		σK_Y		σK_F		Total	
	no.	%	no.	%	no.	%	no.	%	no.	%	no.	%
Within 5 mm of expected position	11	29	20	54	4	11	1	3	1	3	37	100
Irrespective of position	12	23	28	54	9	17	2	4	1	2	52	100

2·2.1. *Prong-number distribution of stars at K^--meson endings.* – We now confine our attention to the tracks of evaporation particles and knock-on nucleons. The distribution in prong number of the stars (excluding recoil tracks), taking all types of events together and counting stable prongs only, is given in Fig. 1 for all events found, irrespective of position.

We can compare these distributions with prong number distributions obtained by other emulsion workers who investigated nuclear disintegrations produced by particles of known energies. In doing so we must, however, keep in mind that we are here dealing with the nuclear capture of particles which are very nearly at rest, not with nuclear interactions of fast particles, and that the fraction of events occurring in heavy nuclei may be different for the two cases. Some published data suggest also that for a given excitation energy nuclear capture of π^- mesons leads to lower average prong numbers than excitation by collision (see, for example, data given by HODGSON, MENON, MUIRHEAD and ROCHAT [4]), and discussion by LE COUTEUR [5]) and this may also be the case for K^- capture processes.

The published experimental information on low-energy stars has been summarized by HODGSON [4]. In particular, he considered stars with at least two prongs and related their mean prong number to the energy of the incident (fast) particle, so that we can use his data to estimate the average excitation energy resulting from the nucl ear capture of our K^- mesons. The average number of stable prongs for stars with more than one prong is 3, corresponding to an excitation energy of about 150 MeV.

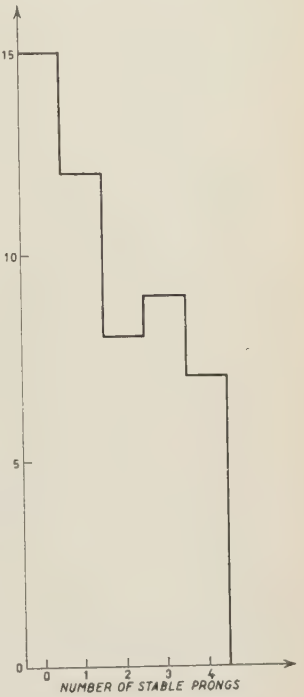

Fig. 1. – Prong-number distribution, counting stable prongs only. Recoil tracks shorter than 5 μm are omitted.

In this analysis we have to distinguish two possibilities. Firstly, we can assume that all K^- captures give rise to the same type of process. In that case it may be meaningful to estimate the mean excitation energy corresponding to the prong-number distribution of Fig. 1.

However, if we plot separately the prong-number distribution of σK_L events only (Fig. 2), we obtain a histogram that looks strikingly different from that covering all events, having a maximum for 3-prong rather than 0-prong stars. This strongly suggests that in those K^- absorptions where a charged light meson is emitted the absorption process is one which gives, on the average, higher prong numbers than in the more usual case where only evaporation particles are emitted.

---

(4) M. G. K. MENON, H. MUIRHEAD and O. ROCHAT: *Phil. Mag.*, **41**, 583 (1950); P. E. HODGSON: *Phil. Mag.*, **44**, 1113 (1953).

(5) K. J. LE COUTEUR: *Proc. Phys. Soc. Lond.*, A **65**, 718 (1952).

The number of ρK events is 29 percent of the total if only those endings are accepted which fall within 5 mm of the expected line, 23 percent, if all are admitted.

This figure is closely similar to that for π^- endings (MENON, MUIRHEAD and ROCHAT [4]), CHESTON and GOLDFARB [6]). « Blobs » of the type sometimes seen at starless π^- endings were found on two of our twelve ρK's, that

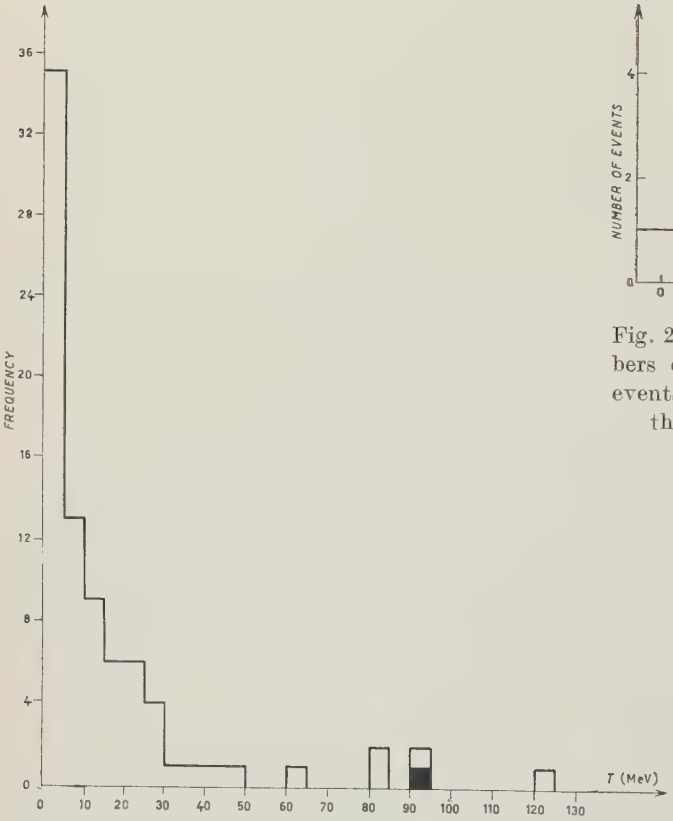

Fig. 3. – Energy distribution of stable particles.

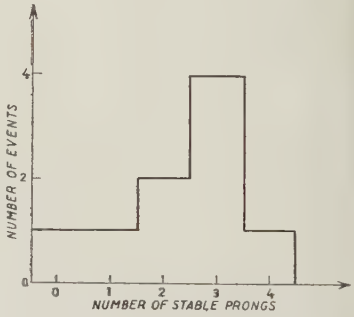

Fig. 2. – Distribution of numbers of stable prongs of σK_L events. Recoil tracks shorter than 5 μm are omitted.

is on 17 percent. This has to be compared with a frequency of 40 percent for blobs on starless π^- endings (MENON *et al.* [4]). Slow-electron tracks, presumably those of Auger electrons, were found on two of the ρK endings; one was associated with a blob, the other was not.

2·2.2. *Energy distribution of particles from* K^- *interactions.* – The distribution in kinetic energies of the stable particles from our K^--produced

[6] W. B. CHESTON and L. J. B. GOLDFARB: *Phys. Rev.*, **78**, 683 (1950).

stars is plotted in Fig. 3. In all cases, the energy was deduced from the range of the particle in the stack, assuming it to be a proton unless the appearance of the track clearly indicated a charge greater than e. All tracks of high charge were assumed to be due to α-particles. This procedure leads to an underestimate of the kinetic energies of about one third of the particles which are deuterons, tritons, α-particles and recoil fragments wrongly classed as protons. Strictly, therefore, Fig. 3 shows a distribution of lower limits to the energies of the ejected stable particles.

The filled-in square in Fig. 3 denotes the fast proton of 91 MeV ejected from event $\sigma K_L - S_8$ in which an L-meson of 16.2 MeV was also emitted. This event is further discussed in Section 2·4.3.

In Fig. 4 we give, on a more open scale, the energy distribution of the particles with energies up to 30 MeV, that is of those particles which are very likely to be evaporation fragments.

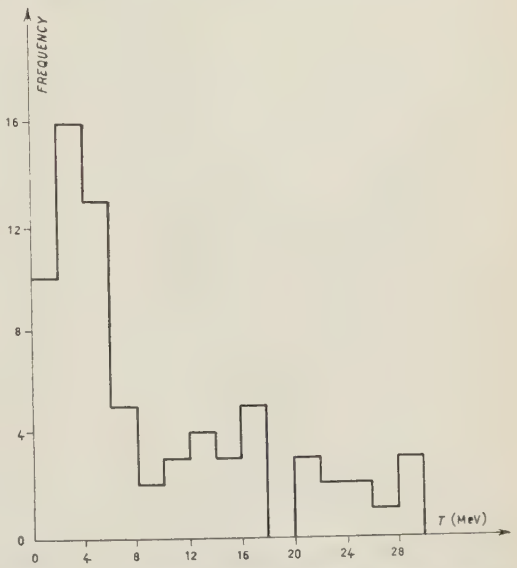

Fig. 4. – Energy distribution of evaporation tracks.

The energy distribution of the light mesons ejected from σK_L and σK_Y events is given in Fig. 5.

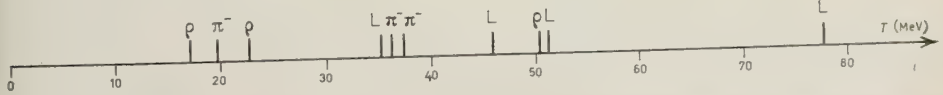

Fig. 5. – Energy distribution and classification of light mesons from σK_L and K_Y events.

2·2.3. *Identification of the* L-*mesons.* – It was possible to follow most of the ejected light mesons to the ends of their ranges. We were thus able to classify the mesons in the way shown in Fig. 5. Of the six ejected mesons which came to the ends of their ranges in the emulsion, three were certain π^- mesons, producing σ stars and three were of the ρ-meson type, showing no visible interaction or decay track. This situation is quite consistent with the assumption that all the six mesons were π^- mesons: the known probability of about 30 percent for a starless ending to a π^- track (MENON *et al.* [1]) gives a probability of 18 percent for observing three starless endings in a total of six.

We thus find that six of the light mesons ejected from our σK_L and σK_γ interactions can be classed as π^-. The remaining four, marked «L», could not be classified as their tracks could not be followed to the ends of the ranges.

2·2.4. *Emission of charged hyperons from* K^- *interactions.* – We have observed one interaction of a K^--meson at rest in which one of the ejected particles can be identified as a charged hyperon. This event (σK_γ–S_1) will now be described briefly; the remaining experimental details are given in Part 3.

A microphotograph of the event appears on Plate 1. A K^--meson (track 1) of measured mass $(1050^{+190}_{-150})\ m_e$ comes to rest and gives rise to a two-prong star consisting of a ρ-meson (presumably π^-) of 23 MeV, and a hyperon (track 2) of measured mass $(2540^{+740}_{-470})\ m_e$ and kinetic energy 38.1 MeV (assuming that it is a Σ^+ of mass 2332 m_e). The angle between the direction of ejection of the hyperon and the π^--meson is 150°.

The hyperon decays in flight into a light meson of measured mass $(262^{+55}_{-39})\ m_e$ which has a kinetic energy of (65 ± 25) MeV in the centre-of-mass system. It is classified as a π-meson, but the sign of its charge could not be determined.

K^- absorptions resulting in the simultaneous emission of a π-meson and a hyperon have been discussed by TOUSCHEK (7) and by FRIEDLANDER, FUJIMOTO, KEEFE and MENON (8)) and several examples have now been published (HORNBOSTEL and SALANT (1), CHUPP *et al.* (3)). As Σ-type hyperons have been identified amongst the particles emitted from K^- stars (G. GOLDHABER, private communication) we conclude that the event under discussion is very probably of the type

$$K^- + p + \text{nucleons} \rightarrow \Sigma^+ + \pi^- + \text{nucleons} + Q$$

with the subsequent decay

$$\Sigma^+ \rightarrow \pi^+ + n + \sim 110\ \text{MeV}\ .$$

Our observations are clearly consistent with this interpretation, but we cannot exclude the possibility that the hyperon has a negative charge. A cascade particle Σ^- of mass 2590 m_e can be ruled out as this forbidden energetically.

2·2.5. *Emission of neutral hyperons from* K^- *interactions.* – We have observed one event (Plate 2) which may show the emission of a Λ^0-particle from

(7) B. TOUSCHEK: *Suppl. Nuovo Cimento*, **12**, 281 (1954).

(8) M. W. FRIEDLANDER, Y. FUJIMOTO, D. KEEFE and M. G. K. MENOM: *Nuovo Cimento*, 2, 90 (1955).

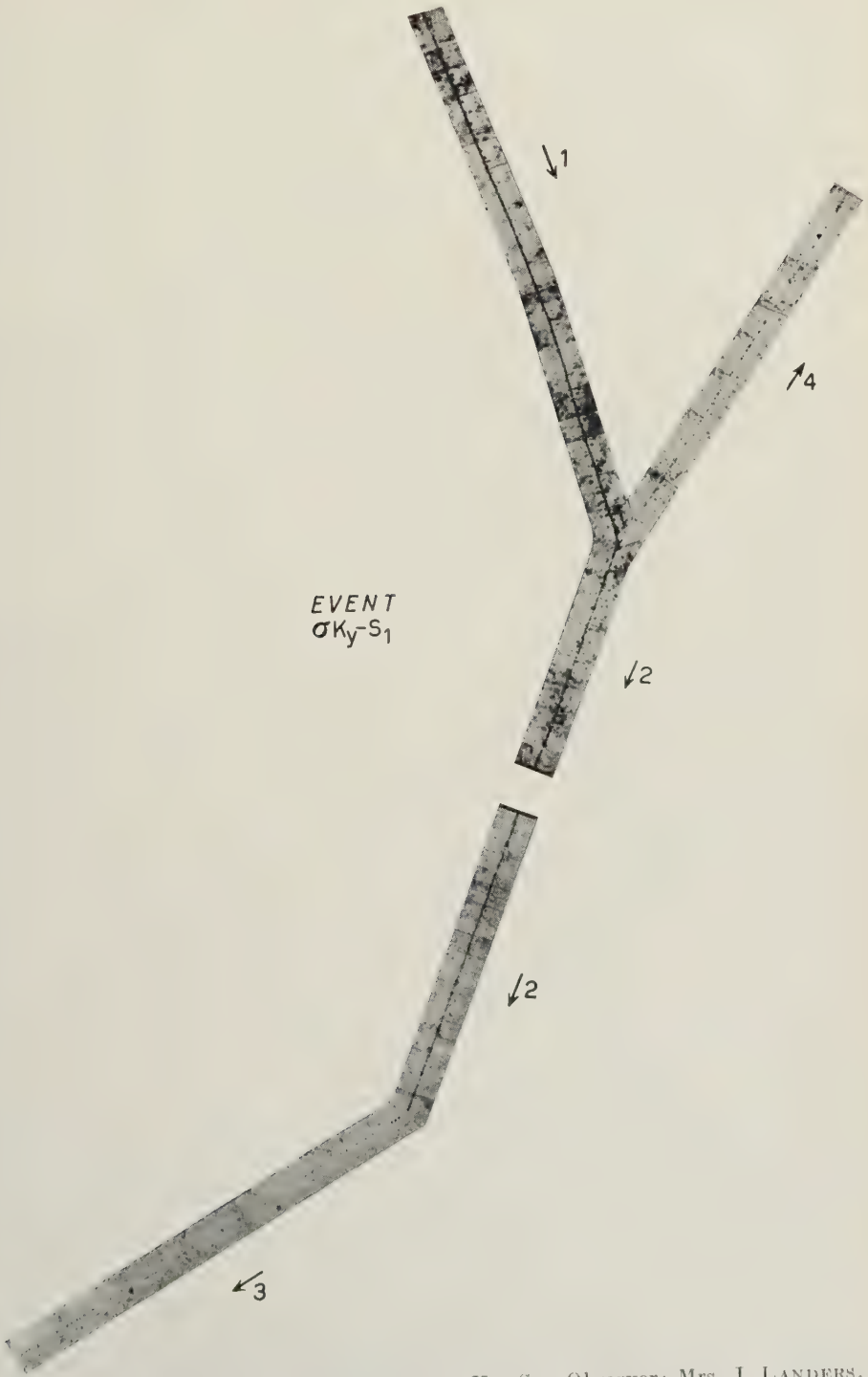

Plate 1. – Microphotograph of event σK_Y-S_1. Observer: Mrs. J. Landers.

Plate 2. – Microphotograph of event $\sigma K_Y - S_2$. Observer: A. J. Herz.

a σK star. A two-track event ($\sigma K_Y - S_2$) has its apex at a distance of 6.9 μm from the centre of a K^--produced star of type 4+0 K. One of the prongs of the V is a proton of momentum 149 MeV/c, the other has a blob density consistent with it being due to a π-meson of the expected momentum for Λ^0-decay. The V is coplanar with the assumed parent star to within the limits of error of the measurement. If this interpretation is correct, the Λ^0 was ejected with a kinetic energy of approximately 3.5 MeV.

Details of the measurements are given in Section 3·4.2.

2·2.6. *Possible emission of a hyperdeuteron.* – It is well known that unstable heavy fragments are sometimes ejected from K^--produced nuclear disintegrations (NAUGLE, FREIER and NEY (9), HORNBOSTEL and SALANT (1)). We have observed an event ($\sigma K_Y - S_2$) which can be interpreted in this way, though we cannot exclude the possibility that the ejected unstable particle is a hyperon.

In the event under discussion, a K^--meson of measured mass $(1350^{+140}_{-310})\ m_e$ comes to rest and produces a star consisting of a very short proton or α-particle track, a track with a blob density corresponding to approximately the plateau value, and a track of a singly-charged heavy fragment which comes to rest after traversing 4020 μm of emulsion and ejects a proton of 26 MeV which, in turn, comes to rest in the emulsion.

Range-scattering measurements on the track of the heavy fragment gave a mass of $(4250^{+2300}_{-1250})\ m_e = (2.3^{+1.2}_{-0.7})\ m_p$. Gap-length measurements were also made on a track length of 3 mm, using for calibration purposes the tracks of three identified protons in the same region of the emulsion; these measurements lead to a mass estimate of $(2.0 \pm 0.5)\ m_p$.

Possible interpretations of these measurements are that the fragment is a hyperdeuteron

$$^2H^* \rightarrow p + \pi^0 + n + Q$$

or, which is much less likely, a hypertriton

$$^3H^* \rightarrow p + n + n + (?\pi^0) + Q\,,$$

or that the fragment is a Σ^+ which decays in flight into a proton, thus giving the proton the energy of 26 MeV in the laboratory system.

It is very well established that the kinetic energy of the proton from the decay

$$\Sigma^+ \rightarrow p + \pi^0 + Q$$

(9) J. E. NAUGLE, P. S. FREIER and E. P. NEY: *Phys. Rev.*, **96**, 829 (1955).

is about 19 MeV (BONETTI, LEVI-SETTI, PANETTI and TOMASINI [10], BALDO, BELLIBONI, CECCARELLI, GRILLI, SECHI, VITALE and ZORN [11], FRY and SWAMI [12], FRIEDLANDER, KEEFE and MENON [13]) and using this value we can calculate what residual range the Σ^+ would have at the point of decay. This turns out to be certainly less than about 50 μm, far too little to be detectable by measurements on the track.

Our reason for stressing that this event may be a case of emission of a hyperdeuteron lies in the importance of establishing whether or not hyperdeuterons exist. The ordinary deuteron is a very loosely bound system, and it follows that any particle capable of forming a stable or metastable combination with a single nucleon must attract this nucleon through an interaction which is of the same order of magnitude as the nucleon-nucleon force or stronger. It seems well established that the binding energy of the Λ^0 hyperon in tritons and helium nuclei is considerably less than that of a neutron (LEVI SETTI [14]), and thus a hyperdeuteron would most likely represent a combination of a $\Sigma^{\pm}$ particle and a neutron.

If the existence of such a combination were confirmed, one of the major predictions of the theory of GELL-MANN [15] would be incorrect: that the Σ-type hyperon cannot be stable in the presence of nuclear matter. Even one certain case of a Σ hyperdeuteron would thus throw doubt on Gell-Mann's theory.

2·3. *Life time of* K^-*- mesons.* – From the data given by FAY, GOTTSTEIN and HAIN [16] we can calculate the total proper life time of the K^- mesons whose tracks we have followed through our stack. Taking only those parts of their lives which correspond to observed sections of track we find a total proper time of $6 \cdot 10^{-9}$ s. On the entire track lengths followed, we observed no events which could be interpreted as the decay in flight of a K-particle. Thus we may conclude that the lifetime of the K^--particles in our emulsion is likely to be longer than $6 \cdot 10^{-9}$ s.

We also note that the distance traversed by the K-particles from the target to the emulsion stack was about three metres. For K-particles of the velocity

---

(10) A. BONETTI, R. LEVI SETTI, M. PANETTI and G. TOMASINI: *Nuovo Cimento*, **10**, 1736 (1953).

(11) M. BALDO, G. BELLIBONI, M. CECCARELLI, M. GRILLI, B. SECHI, B. VITALE and G. T. ZORN: *Nuovo Cimento*, **1** 1180, (1955).

(12) W. F. FRY and M. S. SWAMI: *Phys. Rev.*, **96**, 235 (1954).

(13) M. W. FRIEDLANDER, D. KEEFE, and M. G. K., MENON, *Nuovo Cimento*, **1**, 482, (1955).

(14) R. LEVI SETTI: *Suppl. Nuovo Cimento*, **2**, 263 (1955).

(15) M. GELL-MANN: privately circulated reprint of paper read at Pisa conference, 1955.

(16) H. FAY, K. GOTTSTEIN and K. HAIN: *Suppl. Nuovo Cimento*, **11**, 234 (1955).

we are dealing with here (about 0.4 c to 0.5 c), the time of flight before entering the stack is therefore $2 \cdot 10^{-8}$ s approximately. The observed life time of the K^--particles we consider here is thus of the same order of magnitude as their time of flight from the point of production to the stack.

If there exist in the K^--beam particles of life time very much shorter than 10^{-8} s, they will be mostly lost by decay before reaching the emulsion. This would apply in particular to the 0^--particle whose life time may be of the order of 10^{-10} s (TRILLING and LEIGHTON [17]).

2·4. *Discussion.* – The more significant features of our observations of events accompanying the nuclear absorption of K^- mesons may be summarized as follows:

(i) The average nuclear excitation is low—of the order of 150 MeV—much less than the rest-mass energy of the K^- meson (493 MeV).
(ii) Charged L mesons are emitted in about 17 percent of the cases; whenever identification was possible these mesons were π-mesons, we therefore assume that all were π mesons.
(iii) Most of the emitted π mesons are negative; the charge could be determined in six out of ten cases and all were negative.
(iv) The average kinetic energy of the ejected π mesons is 40 MeV.
(v) When a charged π meson is emitted, the accompanying evaporation star seems to have, on the average, a greater number of prongs than in the case where only stable particles are emitted.
(vi) Charged hyperons are observed to be emitted from some of the interactions.
(vii) The existence of a hyperdeuteron if confirmed, contradicts one of the features of the theory of Gell-Mann.

A large number of possible elementary processes have been discussed by TOUSCHEK [17], DALLAPORTA and LANZA [18], FRIEDLANDER *et al.* [8,13] and GELL-MANN [16]. For the sake of simplicity, and in the absence of any evidence to the contrary we shall make the assumption here that all K^--particles suffer the same type of elementary absorption process. In any case, our present statistics do not allow us to consider a mixture of several processes.

From this premise we are then led to the hypothesis that the products of K^--particle absorption shall contain one hyperon and one π-meson. The events in which we do not see such particles can be understood by assuming that they are emitted as electrically neutral particles or that they are internally absorbed.

[17] G. H. TRILLING and R. B. LEIGHTON: privately circulated preprint (1954).
[18] N. DALLAPORTA and G. LANZA: *Suppl. Nuovo Cimento*, 12, 260 (1954).

The simplest reaction that can be considered is

$$\text{(1)} \qquad K^- + \text{nucleon} \to Y + \pi + Q$$

but, as has been pointed out by TOUSCHEK (7), the observed π-meson energies are too low to be consistent with this reaction as it stands (*) unless we invent a hyperon of mass $2420\,m_e$, a mass value which is inconsistent with all known experimental evidence. However, since the nucleon involved interacts strongly with nuclear matter, the neighbouring nucleons will share the available energy and momentum so that the energy of the emitted π mesons and hyperons will be reduced (this possibility has been mentioned by TOUSCHEK (7) and by FRIEDLANDER *et al.* (8,13)).

Thus, as a working hypothesis, we shall assume that reactions of type (1) are the only ones which occur. It is our purpose to see whether we can give an adequate account of our observations with this hypothesis. In more detail the reactions postulated are

$$\text{(2)} \qquad \begin{cases} K^- + p + \text{nucleons} \to \begin{cases} \Lambda^0 + \pi^0 + \text{nucleons} + Q \\ \Sigma^- + \pi^+ + \text{nucleons} + Q \\ \Sigma^0 + \pi^0 + \text{nucleons} + Q \\ \Sigma^+ + \pi^- + \text{nucleons} + Q \end{cases} \\ K^- + n + \text{nucleons} \to \begin{cases} \Lambda^0 + \pi^- + \text{nucleons} + Q \\ \Sigma^- + \pi^0 + \text{nucleons} + Q \\ \Sigma^0 + \pi^- + \text{nucleons} + Q \end{cases} \end{cases}$$

2·4.1. – *The branching ratio* Λ^0/Σ. – It is clear that the frequencies of the various types of event to be expected on the above hypothesis must depend on the relative frequencies of the reactions we have postulated. In Table II we give the frequencies of emission of various types of particle assuming several values fo the branching ratio Λ^0/Σ.

The probability that a particle from reaction (2) will emerge from the nucleus is here assumed to be 50 percent—a figure we arrive at in the following way. It can be shown that the primary absorption reaction will take place fairly near the surface of the nuclei concerned (BUTLER and BLATT (19)). A strongly-interacting particle produced in this region will have a high pro-

(*) In this reaction the kinetic energy of the π-meson is ~ 150 MeV if a Λ^0 is produced, ~ 90 MeV if the hyperon is a Σ, and the interacting particles are initially at rest. The internal motion of the nucleons would result in an energy distribution about these values. The observed π-meson energies are distributed about a mean value of 40 MeV, a value quite inconsistent with reaction (1).

(19) S. T. BUTLER and J. M. BLATT: *Nuovo Cimento*, in the press.

bability of escape if its direction of motion points outwards, while it is very likely to be absorbed if its path crosses the interior of the nucleus. This clearly leads to a probability of escape of about 50 percent. For the case of surface production of π mesons a more rigorous calculation by BUTLER [15] leads to the same result. We neglect here the possibility that the mean free path in nuclear matter of one or both types of hyperons may be large enough to give a probability of escape greater than 50 percent for these particles.

TABLE II.

Emitted particle	Observed frequency %	Calculated frequency (%) for Λ^0/Σ =			
		1	3	10	20
π^-	10 to 20	23	24	25	25
π^+	0 to 6	4.2	2	0.8	0.4
π^0	—	23	24	25	25
$\Sigma^\pm$	2 to 4	15	7	3	1.4
Σ^0	—	10	5	2	1
Λ^0	—	25	38	45	48

The probability of the simultaneous emission of a Σ^- and a π^- will depend on the directional correlation between the initial directions of flight of these particles, and on the size of the nucleus concerned. Even on our present crude picture, however, it seems unlikely that the observed frequency of these events is consistent with a Λ^0/Σ ratio much in excess of 10. On the other hand, our observations do not favour a ratio much less than that.

Table II also shows that the calculated frequency of emission of π^- mesons is insensitive to the Λ^0/Σ ratio and of the observed order of magnitude.

2·4.2. *The frequency of* ρK *events.* – If we accept a value of the Λ^0/Σ ratio of the order of 10, the reactions which dominate our statistical picture are

$$\text{(3}a\text{)} \qquad K^- + p + \text{nucleons} \rightarrow \Lambda^0 + \pi^0 + \text{nucleons} + Q$$

$$\text{(3}b\text{)} \qquad K^- + n + \text{nucleons} \rightarrow \Lambda^0 + \pi^- + \text{nucleons} + Q\,.$$

In reaction (3*a*), a ρK event will be very probable if both the Λ^0 and the π^0 escape, and in both reactions (3*a*) and (3*b*) a fraction of the cases where the π-meson (average energy 40 MeV) is captured but the Λ^0 is not will lead to ρK events. If as a rough guess, we take this fraction to be 15 percent,

and if we assume that all hyperon captures give rise to visible stars, and that Λ^0 and π^0 will both escape in about 25 percent of the cases of reaction (3*a*), we find an expected frequency of ρK events of 16 percent. This is of the right order of magnitude; in view of the many assumptions made the disagreement with our observed figure of 29 percent does not seem to be very disturbing.

2·4.3. *Magnitude of nuclear excitation following* K^-*-meson capture.* – A further feature of K^- captures which is consistent with our model is the rather low average level of nuclear excitation resulting from K^- absorption. When the rest masses of the π-meson and the hyperon have been taken into account, the sum of the kinetic energies of the secondary particles from reactions (2) is about 175 MeV. Approximately one-half of this energy will escape, so that the average nuclear excitation due to the kinetic energy of the reaction products will be about 90 MeV. If, in addition, the π-meson is captured we have to add to this the excitation energy due to the π-meson rest mass, that is about 80 MeV (Le Couteur ([6])), giving a total of 170 MeV.

It is reasonable to suppose that there is a directional correlation between the directions of emission of the hyperon and the π meson, such that the capture of both these particles is a rare event. The absence of large evaporation stars among our sample of fifty-two is not, therefore, surprising.

Finally we have to consider those cases in which the π meson is emitted, while the hyperon is absorbed. An interesting example of this type of event may be σK_L–S_s where a fast proton of 91 MeV is emitted. This proton could have been produced in the initial reaction, showing that high-energy nucleons are produced there, but it may also be a result of the decay of a bound hyperon in the nucleus.

Because of directional correlations, absorption of the hyperon into the nucleus will probably occur in the majority of K^- absorptions from which a π meson is emitted. Initially, the nucleus will be excited by collisions of the reactions products, gaining an energy of about 90 MeV which is then dissipated in an evaporation process lasting about 10^{-20} s. As the excitation is fairly low, the majority of the evaporated particles will be neutrons, so that we are left with a residual nucleus which is deficient in neutrons. The hyperon will be bound in this residual nucleus and we thus have a system similar to a hyperfragment which is unstable and decays with a life time of the order of 10^{-10} s. In most cases the residual nucleus will be appreciably heavier than ^{4}He, so that the decay is very probably non-mesonic (Levi Setti ([14])). The decay of the bound hyperon will then give a second-stage evaporation star corresponding to an excitation of the residual nucleus of 175 MeV. The average number of charged prongs in the second-stage stars will be rather greater than is usually the case for stars corresponding to this excitation energy as

we are here starting with a nucleus which is neutron-deficient. In an evaporation process, the ratio between the number of protons and neutrons emitted is closely controlled by the neutron excess and tends to keep the neutron excess at a value which gives the greatest stability to the nucleus (LE COUTEUR ([20])); thus if we start with a neutron-deficient nucleus there will be more charged prongs for a given excitation energy than in the case of a normal stable nucleus.

We can thus say qualitatively that the high average prong number of σK_L events can be understood as resulting from the nuclear absorption of the hyperon in the majority of these events.

2·4.4. *Summary of the discussion.* – Summarizing we can say that the reactions (2) are adequate to explain the main features of the observations, provided that events in which Λ^0 particles are produced occur of the order of ten times more frequently than events in which Σ particles are produced.

We must emphasize, however, that we cannot, at present, exclude the possibility that other types of reaction make a significant contribution to K^--capture events. What we have shown is that it is unnecessary to invoke reactions other than those we have considered to explain our observations.

3. – Experimental details.

3·1. *Exposure.* – Our emulsion stack consisted of ninety sheets of 600 μm Ilford G5 emulsion. During the exposure the sheets were placed in direct contact with one another (i.e. not separated by tissue paper) and the stack was firmly clamped between two $\frac{3}{4}$-inch bakelite plates. The emulsion sheets were shuffled before and after the exposure to ensure that only tracks produced on the day of the exposure could be traced through the stack.

The method of exposure was similar to that described by BIRGE, HADDOCK, KERTH, PETERSON, SANDWEISS, STORK and WHITEHEAD ([21]) and their equipment was used for momentum selection and focusing of the K^--particles.

To facilitate the tracing of tracks from one sheet to the next, a millimetre grid was printed onto the emulsion-glass interface of each emulsion sheet by the method of BARKAS and HECKMANN ([22]). The presence of this grid turned the tracing of all but awkwardly situated minimum-ionization tracks into an operation which could easily be carried out by our scanners.

([20]) K. J. LE COUTEUR: *Proc. Phys. Soc. Lond.*, A **63**, 259 (1950).

([21]) R. W. BIRGE, R. P. HADDOCK, L. R. KERTH, L. R. PETERSON, J. SANDWEISS D. H. STORK and M. N. WHITEHEAD: *Phys. Rev.*, **99**, 329 (1955).

([22]) W. H. BARKAS and H. HECKMANN: private communication (1955).

3·2. *Processing.* – The plates were processed in batches of twelve, using the Bristol-type amidol-bisulphite developer (DAVIES [23]) with a warm stage of 30 minutes at 22 °C. This gave an average blob density for tracks of minimum to plateau ionization of about 20 blobs per 100 μm.

3·3. *Scattering measurements.* – Scattering measurements on the tracks of particles coming to rest in the emulsion were made according to the constant-sagitta range-scattering scheme of BISWAS, GEORGE and PETERS [24]. The mean sagitta, corrected for noise, and the noise level were estimated using the expressions given by D'ESPAGNAT [25]. Corrections for dip were made where necessary.

In the estimation of the errors in our range-scattering results we have followed the approach of BISWAS *et al.* [26]. Rearranging their expressions we find that the statistical standard deviation $\sigma(\bar{D}_s)$ in the mean sagitta (corrected for noise), $\bar{D}_s$, is given by

$$\sigma(\bar{D}_s) = \frac{0\cdot 76}{\sqrt{N}}\left(1 + \frac{2n^2}{\bar{D}_s^2} + \frac{2n^4}{\bar{D}_s^4}\right)^{\frac{1}{2}}\bar{D}_s$$

where n is the mean sagitta due to noise, and N is the number of second differences actually used in the calculation of $\bar{D}_s$.

The errors given with our mass values obtained from range-scattering measurements are thus based on the estimated standard deviations in the mean sagittae.

In some cases, where range-scattering methods gave an ambiguous or doubtful result, or where fast particles were concerned, we have also made grain-density-scattering measurements on the fast portion of the track. Corrections for noise were again made using d'Espagnat's [25] formulae, and the masses of the particles were estimated using empirical curves by GEORGE [26], except where otherwise stated. The Molière scattering constant (with cut-off) was used (GOTTSTEIN, MENON, MULVEY, O'CEALLAIGH and ROCHAT [27]).

It is clear from the results given in Table III that the width of our mass distribution for K^- particles is considerably greater than what would be expected from the errors given. As a matter of prudence one should, therefore, double the error in Table III, though, it may well be that the spread is due to a real spread in the mass values. Our statistics are, as yet, insufficient to allow us to come to a decision on this question.

---

[23] J. H. DAVIES: private communication (1955).

[24] S. BISWAS, E. C. GEORGE and B. PETERS: *Proc. Ind. Acad. Sci.*, A **38**, 418 (1953).

[25] B. D.ESPAGNAT, *Journ. Phys. et Rad.*, **13**, 74 (1952).

[26] E. P. GEORGE: private communication (1955)

[27] K. GOTTSTEIN, M. G. K. MENON, J. H. MULVEY, C. O'CEALLAIGH and O. ROCHAT: *Phil. Mag.*, **42**, 708 (1951).

TABLE III.

PRIMARY		NUCLEAR EVENT		
		Star particles		Remarks
K Particle	Mass in m_e	Identity	Kinetic Energy (MeV)	
$\rho K - S_1$	1230^{+360}_{-260}			
$\rho K - S_2$	800^{+170}_{-140}			
$\rho K - S_3$	1250^{+260}_{-230}			
$\rho K - k_4$	970^{+210}_{-150}			Slow electron at ending
$\rho K - S_5$	1140^{+210}_{-180}			
$\rho K - S_6$	1360^{+270}_{-210}			Blob and slow electron at ending
$\rho K - S_7$	1117^{+680}_{-350}			
$\rho K - S_8$	1130^{+240}_{-200}			
$\rho K - S_9$	1300^{+230}_{-170}			1 blob at ending
$\rho K - S_{10}$	1040^{+480}_{-280}			
$\rho K - S_{11}$	1200^{+350}_{-220}			
$\rho K - S_{12}$	927^{+620}_{-330}			
$\sigma K - S_1$	800^{+290}_{-190}	1. recoil 2. recoil 3. P	27.5	
$\sigma K - S_2$	1230^{+470}_{-280}	1. recoil 2. P	120	
$\sigma K - S_3$	1270^{+330}_{-270}	1. P	18	
$\sigma K - S_4$	870^{+110}_{-100}	1. P	1	
$\sigma K - S_5$	1360^{+490}_{-230}	1. P	12.8	
$\sigma K - S_6$	1150^{+220}_{-170}	1. P	7.0	

TABLE III. - (*Continued*)

PRIMARY		NUCLEAR EVENT		Remarks
		Star particles		
K Particle	Mass in m_e	Identity	Kinetic Energy (MeV)	
$\sigma K - S_7$	810^{+140}_{-110}	1.P	36	
$\sigma K - S_8$	870^{+140}_{-120}	1.P	2.5	
$\sigma K - S_9$	1460^{+380}_{-310}	1.P	21.6	
$\sigma K - S_{10}$	1200^{+600}_{-330}	1.recoil 2.P	 5.6	Slow (Auger) electron
$\sigma K - S_{11}$	1050^{+450}_{-270}	1.recoil 2.P	 16.2	
$\sigma K - S_{12}$	1050^{+250}_{-160}	1.P 2.P	2.1 2.3	Possible electron pair starts $\sim 2\ \mu m$ from this event.
$\sigma K - S_{13}$	1330^{+270}_{-200}	1.P 2.α	6.3 4.7	
$\sigma K - S_{14}$	938^{+250}_{-160}	1.P 2.P	1.6 1	
$\sigma K - S_{15}$	1460^{+380}_{-300}	1.α 2.α	5 3	
$\sigma K - S_{16}$	1460^{+340}_{-240}	1.P 2.P	11.2 3.9	
$\sigma K - S_{17}$	1260^{+330}_{-250}	1.P 2.P 3.α	1.4 0.6 3.4	
$\sigma K - S_{18}$	1260^{+260}_{-190}	1.P 2.P 3.P	2.2 > 80 84	
$\sigma K - S_{19}$	690^{+370}_{-210}	1.P 2.P 3.P	1.6 4 50	

TABLE III. - (*Continued*)

PRIMARY		NUCLEAR EVENT		
		Star particles		Remarks
K Particle	Mass in m_e	Identity	KineticEnergy (MeV)	
$\sigma K - S_{20}$	860^{+270}_{-200}	1.P	28.4	
		2.P	15.6	
		3.P	3.6	
$\sigma K - S_{21}$	1460^{+410}_{-290}	1.P	25	
		2.P	2	
		3.P	23	
		4.P	2.1	
$\sigma K - S_{22}$	1300^{+380}_{-320}	1.P	0.9	
		2.α	65	
		3.P	2.6	
		4.P	34	
$\sigma K - S_{23}$	1150^{+270}_{-210}	1.P	3.1	
		2.P	3.0	
		3.P	13.5	
		4.P	90.5	
$\sigma K - S_{24}$	1040^{+260}_{-180}	1.P	3.7	
		2.recoil		
		3.P	14.8	
		4.P	44.5	
$\sigma K - S_{25}$	1130^{+370}_{-230}	1.recoil		
		2.α	10	
		3.P	24	
		4.P	30	
		5.P	13.6	
$\sigma K - S_{26}$	800^{+260}_{-190}	1.P	22	
$\sigma K - S_{27}$	1240^{+290}_{-220}	1.P	10	
		2.P	7.2	
		3.recoil		
$\sigma K - S_{28}$	1350^{+450}_{-320}	1.P	5.4	
		2.P	4.3	
		3.P	16.7	
		4.P	4.6	

TABLE III. - (*Continued*)

PRIMARY		NUCLEAR EVENT		Remarks
		Star particles		
K Particle	Mass in m_e	Identity	Kinetic Energy MeV	
$\sigma K_L - S_1$	810^{+340}_{-220}	1.P 2.L	21.2 46 ± 1	Meson leaves stack very near to end of its range after traversing 32 mm of emulsion.
$\sigma K_L - S_2$	$1\,110^{+380}_{-240}$	1.P 2.P 3.L	4.8 6.1 $\sim$ 51 (if π)	L-meson identified by scattering-blob density method.
$\sigma K_L - S_3$	$1\,110^{+510}_{-290}$	1.L	78	L-meson, identified by scattering-blob density method. Could not be traced.
$\sigma K_L - S_4$	950^{+300}_{-160}	1.P 2.P 3.P 4.π^- (σ)	17 3.5 13.3 20	
$\sigma K_L - S_5$	950^{+570}_{-210}	+1.P 2.P 3.P 4.π^- (σ)	1.8 25 14.5 36.7	
$\sigma K_L - S_6$	970^{+330}_{-205}	1.recoil 2.α 3.P 4.L(ρ)	 18 11.1 50.6 (if π)	Mass of L-meson from range - scattering is $(335^{+105}_{-65})\,m_e$. It ends in the emulsion without visible decay or interaction; it is therefore classed as a π^--meson.
$\sigma K_L - S_7$	$1\,870^{+410}_{-340}$	1.P 2.P 3.P 4$\delta\pi^-$ (η)	2.7 4.1 5.0 37.8	

TABLE III. - (*Continued*)

PRIMARY		NUCLEAR EVENT		
		Star particles		Remarks
K Particle	Mass in m_e	Identity	Kinetic Energy (MeV)	
$\sigma K_L - S_8$	880^{+250}_{-140}	1.P 2.P 3.P 4.P 5.L(ρ)	91 4.7 5.1 1.9 16.2 (if π)	Light meson comes to rest without visible decay or interaction, it is therefore classed as a τ^- meson
$\sigma K_L - S_9$	930^{+280}_{-210}	1.P 2.P 3.P 4.recoil 4.recoil 6.L	6.7 5.4 10.1 ~ 36	L-meson identified from scattering-blob density measurements. It could not be followed to the end.
$\sigma K_Y \; S_1$	$1\,050^{+130}_{-120}$	1.Y Mass $2\,540^{+740}_{-470}$) 2.L (ρ)	38.1 (if Σ^+) 23 (if π^-)	See sections 2·2.4 and 3·4.1 for details.
$\sigma K_Y - S_2$	950^{+220}_{-160}	1.P 2.P 3.P 4.P 5.1 Λ^0	28.3 5.4 1.3 5.3 3.5	See sections 2·2.5 and 3·4.2 for details.

The identification of our ρK events was based entirely on scattering measurements, We believe that this identification is reliable because the experimental mass distribution of the particles giving ρK events was closely similar to that of all other K^--particles, and because the proton background was low: there were only about twelve proton tracks for each of the ρK events.

3·4. *Measurements on events of special interest.*

3·4.1. *Event* σK_Y-S_1. – This event is shown in Plate 1.

Range-scattering measurements on track 1 gave a mass of $(1050^{+180}_{-150})\,m_e$. Particle 2 traversed 1310 μm of emulsion before decaying in flight into particle 3. The remaining measurements on this event are summarized in Table IV. The angle between particles 2 + 3 1.5 48°.

TABLE IV. – *Measurements* on σK_Y-S_1.

Particle	β	$\bar{\alpha}_{100^\circ}$	$p\beta$ (MeV/c)	Mass
2	0.25	0.31 ± 0.07	$80.4^{+23.3}_{-13.9}$	$2\,540^{+740}_{-470}$
3	0.79	0.17 ± 0.03	135^{+28}_{-20}	262^{+55}_{-39}
4	meson (π^-) coming to rest. K.E. 23 MeV.			

The velocity β was measured by comparing the grain density with that of protons of known range and that of beam π mesons.

Assuming that particle 2 is a Σ^+ of mass 2332 m_e, and that particle 3 is a π^+ we find from the values of β that the kinetic energy of the hyperon was 38.1 MeV, and that of the π^+ meson 85 MeV in the laboratory system. Transformation to the centre-of-mass system gives the c.o.m. energy of the π^+ as (65 ± 25) MeV.

3·4.2. *Possible emission of a* Λ^0 *particle.* – A microphotograph of the event $\sigma K_Y - S_2$ is shown in Plate 2. Unfortunately, the geometry of the event was unfavourable to precise measurements as the track of the faster of the two prongs of the V, (*b*), had a dip angle of nearly 63° and could not be traced to its end owing to very bad distortion (a bubble) in one of the emulsion sheets. Thus all that can be said about this track is that its blob density is approximatey twice the plateau value.

The more heavily ionizing of the two particles, (*a*), was traced to the end of its range and was identified by inspection to be a proton. Its range and momentum are 724 μm and 149 MeV/c respectively.

The geometry of the event was determined independently by two of us, and our final result is that the centre of the primary σK star is not more than 1 μm away from the plane of the V, and that the distance between the centre and the apex of the V is 6.9 μm.

With the geometry known, we calculated the expected blob density of the light track, assuming that the V event was indeed the decay of a Λ^0 particle of mass 2182 m_e with the decay scheme

$$\Lambda^0 \rightarrow p + \pi^- + Q \,.$$

The expected blob density for the light track turned out to be twice the minimum value; it is therefore consistent with the experimental one.

From the dynamics of the decay, the kinetic energy of the Λ^0 particle was found to be 3.5 MeV.

3·4.3. *Table of events.* – In Table III we give details of all the events on which this paper is based. The errors in the masses are based on the estimated standard deviations of the mean sagittae; they should be doubled to fit the experimental distribution (see Section 3·3).

All tracks shorter than 5 μm have been classed as « recoils ».

4. – Conclusions.

From the examination of the nuclear events produced by 52 K^- particles of life time of the order of 10^{-8} s or more we conclude that all the events can be satisfactorily explained if we assume the basic interaction process to be

$$K^- + N + \text{nucleons} \rightarrow Y + \pi + \text{nucleons} + Q ,$$

where N is the nucleon on which the K^--particle is annihilated and the surrounding nucleons take up part of the available energy. As the mean energy of the π mesons is only 40 MeV, our observations are definitely inconsistent with a process in which the surrounding nucleons do not take a share of the energy.

The hyperons involved are most likely the Λ^0 and the isootpic-spin triplet Σ^0, Σ^+, Σ^-. We have observed one $\Sigma^\pm$ and a possible case of a Λ^0 emitted from K^- interactions.

The evaporation stars which accompany the nuclear absorption of K^--particles show that the nuclear excitation is low: about 150 MeV or so on the average. This we explain as due to the fact that the primary absorption reaction takes place fairly near to the nuclear surface, and that about 50 percent of the secondaries can thus escape without further interaction. We do not require a mixture of strongly-interacting and weakly-interacting particles to explain our data.

As we have observed only one definite case of the emission of a Σ hyperon (and a possible one, the « hyperdeuteron ») we conclude that the frequency of production of Λ^0 particles must be of the order of ten times greater than that of the Σ-particles.

The possible case of a hyperdeuteron has drawn our attention to the fact that the existence of such a particle, if confirmed, would be contrary to the theory of Gell-Mann ([16]), and that it would allow an estimation of the strength of the nuclear interaction of the hyperon involved.

* * *

A very large number of friends, colleagues and authorities have helped us in the work of getting the emulsion stack manufactured, exposed, processed and finally sent to Sydney. We should like to thank them all: Mr. C. WALLER and his staff at Ilford Limited, Professor E. O. LAWRENCE for permission to work at the Bevatron, Dr. E. J. LOFGREN and the Bevatron operating crews for making the K particles, the BARKAS, GOLDHABER and RICHMAN groups for much help and advice during the exposure, and Professor L. LEPRINCE-RINGUET and the members of his research team at the École Polytechnique in Paris in whose laboratory the stack was processed.

Our team of scanners in Sydney has helped greatly in all stages of the work and we very much appreciate their willingness and enthusiasm. They are Miss P. AYLMORE, Miss D. BARKER, Miss A. CASTLE, Mrs. M. CHARTRES, Mrs. M. DOCHERTY, Mrs. J. LANDERS, Miss S. O'REILLY and Mrs. E. THOW. We are grateful also to Miss B. BARNES for her help with the scattering measurements.

We have benefited greatly from many stimulating and useful discussions with Professor H. MESSEL, Dr. J. M. BLATT, Dr. S. T. BUTLER and Mr. D. A. TIDMAN. We should like to thank Professor MESSEL also for arranging the excellent facilities and financial support for this work.

The work was supported by the Nuclear Research Foundation within the University of Sydney and by the Research Committee of the University of Sydney who also provided a Research Studentship and a Research Fellowship for two of us.

RIASSUNTO (*)

Un grosso pacco di emulsioni è stato esposto al Bevatrone al fascio di mesoni K^- di vita media dell'ordine di 10^{-8} s. Furono osservate 52 particelle K^-, di cui 12 si arrestarono senza decadimento o interazione apparente. 28 terminarono in una stella di evaporazione, 9 dettero un mesone π veloce oltre a una stella di evaporazione, 1 emise un iperone e un mesone π^-, 1 produsse l'emissione di una particella che può essere interpretata sia come un iperdeutone che successivamente si arresta, sia un Σ^+ che si disentegra in volo in un protone, e si ha inoltre un caso di una stella di evaporazione strttamente associata a un possibile decadimento Λ^0. Si dà particolare importanza al possibile iperdeutone in quando l'esistenza di una tale particella sarebbe in contraddizione con la teoria di GELL-MANN e permetterebbe altresì di stimare l'energia

(*) *Traduzione a cura della Redazione.*

dell'interazione nucleare dell'iperone coinvolto. Le caratteristiche principali degli eventi nucleari sono: (i) l'energia d'eccitazione totale delle stelle di evaporazione è di circa 150 MeV, (ii) i mesoni π sono emessi in circa il 17% degli eventi e la maggior parte, se non tutti, sono cariche negativamente, (iii) gli iperoni carichi sono emessi da una piccola frazione degli eventi (uno nel nostro caso, accompagnato da un mesone π). (iv) l'energia cinetica media dei mesoni π emessi è 40 MeV e (v) il numero medio di rami delle stelle di evaporazione associate all'emissione di mesoni π supera in modo significante la media generale. Tutte queste caratteristiche si possono spiegare qualitativamente col seguente meccanismo: la particella K^- raggiunge la sua prima orbita, poi interagisce con un nucleone in presenza di altri nucleoni che assorbono parte dell'energia disponibile secondo la reazione $K^- + N + \text{nucleoni} \rightarrow Y + \pi + \text{nucleoni} + Q$. Dato che il processo primario di assorbimento avviene assai vicino alla superficie del nucleo, ciascuno dei secondari di questa reazione ha una probabilità di circa il 50% di sfuggire senza contribuire all'eccitazione nucleare. Gli iperoni coinvolti si dimostrano essere Λ^0 e il tripletto di spin isotopico Σ^+, Σ^0, Σ^-; e le osservazioni richiedono che la produzione di Λ^0 abbia una frequenza d'ordine 10 volte maggiore di qualsiasi particella del gruppo Σ.

IL NUOVO CIMENTO Vol. III, N. 1 1° Gennaio 1956

Cosmic Ray Showers of Wide Extent.

G. R. MACLEOD (*)

Cavendish Laboratory - Cambridge, England

(ricevuto il 4 Novembre 1955)

Summary. — Extensive air showers have been observed at sea level, using a maximum counter tray separation of 1200 m, by a method allowing a direct determination of the angular distribution of the shower axes to be made; it is found to be proportional to $(\cos\theta)^{6.5\pm0.5}$. Comparison of the decoherence rates of the showers with nucleon cascade theory predictions, shows that the angular dependence of the nucleon collision cross section which determines the lateral spread of the shower, is very sharply peaked in the forward direction. The shower rates are compatible with the known rates of electron-photon cascades at sea level, if each of these is considered to be associated with a penetrating cascade of much larger spread and lower particle density. The penetrating cascade carries about 1/5-th of the total shower energy, and contains about 1/10-th of the total number of particles in the shower at sea level.

1. – Introduction.

It is now believed that the generating process of an extensive air shower is a mixed meson-nucleon cascade, initiated by a high energy proton or heavier particle and that the electron cascade is a secondary phenomenon, produced through the agency of π^0-meson decay (GREISEN *et al.* [1], GREGORY and TINLOT [2], MILONE [3], KASNITZ and SITTE [4], SITTE [5]). A theoretical attempt has been made to produce a cascade theory for nucleons (MESSEL [6]),

(*) Now at CERN, S.T.S. Division, Geneva, Switzerland.

(1) K. GREISEN, W. D. WALKER and S. P. WALKER: *Phys. Rev.*, **80**, 535 (1950).
(2) B. P. GREGORY and J. H. TINLOT: *Phys. Rev.*, **81**, 675 (1951).
(3) C. MILONE: *Phys. Rev.*, **87**, 680 (1952).
(4) H. L. KASNITZ and K. SITTE: *Phys. Rev.*, **94**, 977 (1954).
(5) K. SITTE, D. S. STIERWALT and I. L. KOFSKY: *Phys. Rev.*, **94**, 988 (1954).
(6) H. MESSEL: *Progr. Cosmic Ray Phys.*, **2** (1954).

and it is shown that the spread of such cascades is a sensitive function of the angular dependence of the differential nucleon-nucleon collision cross-section.

The present experiment set out to determine whether the coincidence rate of Geiger counters at large separation (of hundreds of meters) is much greater than the rate at which electron-photon cascades (of tens of meters radius) are recorded at sea level. Such an effect may be expected if, in the nuclear interactions produced by cosmic ray primaries of comparatively low energy (less than 10^{11} eV, say), a fairly wide spread in the angular distribution of the secondary products exists. The soft cascade produced by such a primary would be much attenuated by the atmosphere, and at sea level the event would appear as a wide shower (of hundreds of meters diameter) and extremely low particle density. An experimental method was devised to make a direct measurement of the angular distribution of the shower axes.

2. – Outline of the experiment.

We have used two counter trays at sea level, one at the « local site », L, and one at the « distant site », D, where $LD = d$ km. All pulses from the tray at D are transmitted by radio to L; each pulse from the tray at L starts a timing mechanism which is stopped by the next pulse received from D. In this way a number of time delays are measured, and these are sorted into appropriate channels by a « delay sorter ». Each channel will record delays at the rate

$$C_r = (r_1 \cdot r_2 \cdot t)$$

due to the random counting rates of the two trays (r_1 and r_2 per second). t is the channel width.

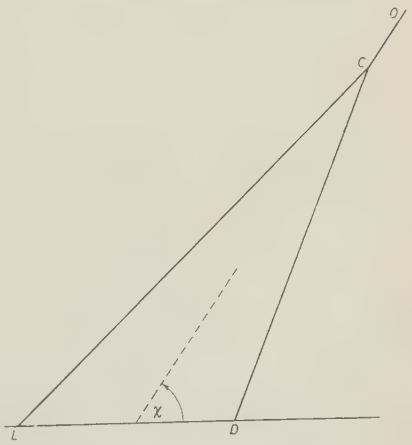

Fig. 1.

Consider a primary cosmic ray particle moving along OC (Fig. 1) inclined at θ to the vertical; at C, a height h in the atmosphere, a nuclear interaction occurs, producing two highly relativistic secondaries which continue without further interaction to strike the counter trays at L and D. For such an event the delay recorded by the apparatus will be

$$\tau = d(1 - \cos \chi)/c, \tag{1}$$

for $h \gg d$, where c is the velocity of light.

The delay times which can be caused by air showers range between 0 and $2d/c$. If the delay sorter is constructed to measure delay times up to a

maximum of $4d/c$, then a continuous measurement of C_r may be made in the channels between $2d/c$ and $4d/c$. This value of C_r can then be subtracted from the rates recorded in the channels between 0 and $2d/c$ to give the counting rate R in these channels due solely to shower events.

It may be shown that the counting rate in the n-th channel is related to the angular distribution of the shower axes about the vertical by expression of the form

$$R(\chi_n, \chi_{n+1}:q) = 2j_0 \int_0^{\pi/2} \cos^q \varphi \cdot \int_{\chi_n}^{\chi_{n+1}} \sin^{q+1}\chi \cdot \mathrm{d}\varphi \cdot \mathrm{d}\chi \,, \tag{2}$$

where χ_n, χ_{n+1} are the inclinations of shower axes corresponding to the boundaries of the n-th channel, φ is the projected angle of inclination of the shower axis on a plane perpendicular to LD, and where the angular distribution of the shower axes about the vertical is assumed to be of the form $j_0 \cdot \cos^q \theta$.

3. – Description of apparatus.

3·1. *Counter trays.* – These had a sensitive area of 1 m² and were made up of twenty-five counters, each of length 2 m and internal diameter 2 cm. The counters were very simply constructed with a polished duralumin tube as cathode; a 0.006 cm diameter « Motung » wire anode was tensioned between 2 glass end seals, which were « Araldited » into the cathode tube. A filling of 6 cm argon and 1 cm alcohol gave a lifetime of 10^8 to 10^9 counts, with plateaux of 100 to 200 V. A separate input valve for each counter was employed, and after mixing, the signal was fed to a 75db amplifier of 0.05 μs rise time. Fast electrical quenching was used, and the overall delay time of each tray was less than 0.2 μs. The normal counting rate per tray was 420 per second.

3·2. *The Radio channel.* – A 3 cm klystron of 0.1 W output was reflector-modulated by a 1.0 μs pulse. Transmitting and receiving paraboloids of 18-inches diameter were used with wave-guide feed. A wave-guide mixer and crystal detector fed a 60 db I.F. amplifier of 20 MHz bandwith (JEWITT (7)); this was followed by a 40 db video amplifier, and an A.F.C. device was employed. The overall rise time of the channel was 0.08 μs and the electronic delay 0.4 μs.

3·3. *The Delay sorter,* – The counter tray pulses were used to gate a free-running oscillator-controlled pulse generator, the L pulse opening the gate and the D pulse closing it. A fast scaling circuit counted the number of pulses

(7) H. S. JEWITT: *Wireless World*, **60**, 86 (1954).

passed, and high-speed mechanical relays, in combination with a 4 > 4 diode grid, selected the appropriate message register. Sixteen channels were provided, whose widths could be varied between 2 and 0.2 μs; these widths were stable and equal to better than 0.5%. A single channel accepted counts up to a maximum of 10 per second.

3·4. *The small shower sets.* – Two simple shower sets were used at the local site. Each set comprised three single geiger counters in coincidence, placed in a straight line, at seven meters separation. The so-called *A* set had counters of 224 cm² and the *B* set 46 cm². The mean particle density of « *A* showers » was taken to be 40 per m² and of « *B* showers » 220 per m². « *A* + *B* showers » which fired both sets would in general have rather higher densities.

3·5. *The checking routine.* – The channel totals of the delay sorter were photographed hourly, together with a clock, and ratemeters which monitored the various counter trays. A daily checking routine using meter and oscilloscope was developed for the delay sorter. This device was also checked every 100 hours by applying a χ^2 test to the channel totals ($\sim 10^4$ counts) obtained after running the device for twenty-four hours with two independent random input pulse trains.

4. – Experimental measurements.

Measurements were made at separations of 350, 600 and 1200 m, corresponding to channel widths of 0.3, 0.5 and 1.0 μs respectively. At each separation a two-fold measurement was made, using one counter tray at the local and distant sites; a three-fold measurement was made using two trays 7 m apart at the local site, and one tray at the distant site. In some cases two runs were made in each arrangement, using different counter tray areas. In any one measurement, the counter trays all had equal areas.

Table I gives the various results obtained. Column 1 identifies each measurement, column 2 lists the coincidence arrangement used: column 3 shows *S*, the counter tray areas; column 4 presents the duration of the run *T*, whilst the separation of the counter trays is given in column 5. The channel totals per hour, corrected for background rate, are given in column 6; all errors are standard deviations.

The use of a free-running oscillator to generate the timing pulses in the delay sorter means that there is an indeterminateness of one channel width as to the channel which will record a given delay. This indeterminateness has to be taken into account in determining the expected distribution of counts

TABLE I.

	Coinc.	S m²	T h	d m	channel totals 1	2	3	4	5	6	7	8	9	C_r h^{-1}	R h^{-1}
a	2f	0.88	269	1200	No channel significantly different from zero									544 ±2	—
b	3f	0.60	636	1200	—	0.01	0.03	0.06	0.06	0.07	—	0.05	0.01	0.32 ±0.01	0.28 ±0.05
								all	±0.02						
c	3f	1.00	574	1200	—	0.05	0.06	0.13	0.13	0.11	0.06	0.07	0.04	0.83 ±0.02	0.65 ±0.11
								all	±0.04						
d	2f	1.00	147	600	0.3	2.8	4.8	5.6	7.8	4.5	4.0	3.7	—	382.4 ±0.8	33.5 ±4.3
								all	±1.5						
e	3f	1.00	171	600	0.01	0.05	0.23	0.41	0.82	0.62	0.21	0.03	0.01	0.47 ±0.03	2.66 ±0.24
								all	±0.07						
f	2f	0.72	347	350	0.3	1.3	5.0	7.4	12.3	10.2	7.1	2.6	0.6	109.4 ±0.3	46.1 ±1.7
								all	±0.5						
g	2f	1.00	230	350	—	4.0	6.0	11.5	17.1	16.7	12.1	5.4	2.7	204.2 ±0.3	72.4 ±2.1
								all	±0.5						
h	3f	1.00	31	350	0.15	0.25	1.30	1.65	3.25	2.37	1.92	0.40	—	0.29 ±0.13	10.6 ±0.7
								all	±0.30						

in the channels from equations of the form of (2). It is found that the distribution of counts due to shower events, which should be contained in the first eight channels according to geometrical considerations, is « smeared » into nine channels by this indeterminateness. In column 7 is given the background counting rate C_r in each channel, and column 8 shows the total shower rate per hour.

TABLE II.

Measurement	A-showers rate h^{-1}	B-showers, number recorded	$A + B$ showers, number recorded
d	0.07 ±0.02	2	2
e	0.06 ±0.02	1	1
g (*)	0.14 ±0.04	1	1
h	0.13 ±0.07		
c	0.012 ±0.005	2	1

(*) Small shower sets are in operation for only 97 hours of this measurement.

Table II shows the number of showers, using the nomenclature of sec. 3·4, which triggered both the large separation trays and the small shower set. The numbers of such showers are no more than one would expect from the small proportion of all the showers triggering the large separation trays which fall with their axes sufficiently close to the local site to give the large particle densities necessary to trigger the small shower set.

5. – Discussion of results.

5·1. *Total Shower Rates.* – The theoretical expression for the two-fold coincidence rate of two counter trays of area s and separation d is:

$$R(2:d) = \int_{\psi=0}^{2\pi} \int_{r=0}^{\infty} \int_{N=0}^{\infty} r(1 - \exp[-sx_1])(1 - \exp[-sx_2]) \cdot f(N)\,\mathrm{d}N \cdot \mathrm{d}r \cdot \mathrm{d}\psi\,, \tag{3}$$

where r, ψ, are the coordinates of the shower axis referred to an origin mid-way between the counters; x is the particle density given by $x = N \cdot S(r)$ at a point r from the axis of a shower of structure function S and total number of particles N.

We have made an approximate evaluation of this integral, and the corresponding one for the three-fold rate $R(3:d)$. For the structure function we have taken

$$S(r) \sim \exp[-\alpha r]\,,$$

with $\alpha = 0.76$ and $\alpha = 6.44\ \mathrm{km}^{-1}$. These are the radial distribution functions calculated by MESSEL and GREEN [8] for nucleons at sea level with energies U greater than 3 GeV. The first corresponds to the assumption of a quasi-isotropic angular dependence, in the C-system, of the nucleon-nucleon collision cross-section; the second to an angular dependence of the form $\exp[-144U(1 - \cos\delta)]$ in the laboratory system where δ is the scattering angle.

For $f(N)\,\mathrm{d}N$ we used the results of SINGER [9], who measured the number distribution of electron-photon cascades at sea level. The simplifying assumption was made that, for all showers at sea level, a constant ratio ε exists between the number of particles in the soft cascade and the total number in the shower.

Table III compares the calculated and observed values of the coincidence rates. The values for $\alpha = 6.44$ are in fair agreement, whilst those for $\alpha = 0.76$ are in striking disagreement. The form of the theoretical decoherence curve

---

[8] H. MESSEL and H. S. GREEN: *Phys. Rev.*, **87**, 738 (1952).
[9] S. F. SINGER: *Phys. Rev.*, **81**, 579 (1951).

TABLE III.

	2 fold coincidences h^{-1}			3 fold coincidences h^{-1}		
d m	350	600	1 200	350	600	1 200
R calculated ($\alpha = 0.76$)	18	17	15	1.7	1.7	1.7
R observed	72	33	1	10.6	2.7	0.6
R calculated ($\alpha = 6.44$)	51	24	0.6	7	2.3	0.4

was found to be insensitive to the value of ε, but the absolute values gave best agreement for $\varepsilon = 0.9$. This agrees with the Russian workers (see report of WATAGHIN [10]), who found that the penetrating cascade contained about 10 % of the total number of particles in the shower at 3 860 m.

The coincidence rates at large separations were not higher than the rates of electron-photon cascades lead one to expect, if each soft cascade is associated with a wider and less dense penetrating cascade. The observed and theoretical rates agree only if one assumes that the nucleon collision cross-section does not have as wide an angular distribution as predicted by most field theories. If the coincidences at these separations are due largely to μ mesons (EIDUS *et* al. [11]), then the actual form of the angular dependence of the cross sections will be more steeply peaked than that proposed by MESSEL and GREEN [8].

5·2. *Distribution of shower axes.* – Comparison of the distribution of counts in the channels of the delay sorter and the distribution calculated from expressions of the form of equation (2) shows that the experimental results are satisfactorily accounted for if $q = 6.5 \pm 0.5$ (st. devn.) It is not possible to discriminate more finely the value of q, as it is the counts in the channels at the wings of the distribution which change most as q changes; it is in just these channels that the statistical errors are greatest.

5·3. *Shower energies.* – An estimate of the lower limit of shower energy may be made assuming that all showers causing the three-fold coincidences must present particle densities 1 per m^2 at the two counter sites, and that all the penetrating particles in the shower have energies of 3 GeV. Using this approximation the energies corresponding to tray separations of 350, 600 and 1 200 m respectively are 1.1, 2.0 and $7.5 \cdot 10^{16}$ eV. The fractional energy carried in the penetrating cascade is at least 0.13, 0.15 and 0.29 in these cases.

---

[10] G. WATAGHIN: *Suppl. Nuovo Cimento*, **10**, 489 (1953).

[11] L. K. EIDUS, N. M. BLINOVA, V. G. VIDENSKII and L. D. SUDOROV: *Dok. Akad. Nauk*, **74**, 477 (1950).

The increase of this fraction with total energy may be expected if we remember that the ratio at production of charged to neutral π-mesons is 2:1 (CARLSON *et al.* [12]). The increased meson production in higher energy showers will favour the transference of more energy to the penetrating component. A plot of the coincidence rate against energy gives a line of slope -1.7 ± 0.2 as the best fit, though in view of the uncertainty in the energy determination this value cannot be taken to exclude the possibility, favoured by some authors, that the primary spectrum exponent is as high as -1.1.

Comparison of measurements at a given separation with different counter areas, and of two- and three-fold coincidence arrangements, gives the mean particle densities averaged over all showers as 0.17 ± 0.02 and 0.09 ± 0.01 particles per square meter for counter tray separations of 350 and 600 m respectively.

* * *

The author wishes to thank his supervisors, Prof. O. R. FRISCH and Mr. T. GOLD for their interest and encouragement over the course of this work; Mr. R. B. TATTERSALL for the building and maintenance of the radio channel, for help in constructional work and for many useful discussions; Messers LAMB and DAVIES for making the Geiger counters; Decca Navigation Ltd. for the supply of an engineered design of the I.F. amplifier; the Master and Fellows of Christ's College, Cambridge, for a research scholarship, and the D.S.I.R. for a maintenance grant.

---

(12) A. G. CARLSON, J. E. HOOPER and D. T. KING: *Phil. Mag.*, **41**, 701 (1950).

RIASSUNTO (*)

Si sono osservati al livello del mare gli sciami estesi dell'aria per mezzo di una separazione massima dei telescopi di contatori di 1200 m con un metodo che permette la determinazione diretta della distribuzione angolare degli assi degli sciami, che si trova essere proporzionale a $(\cos \theta)^{6.5 \pm 0.5}$. Il confronto delle deviazioni degli sciami dalle predizioni della teoria della cascata nucleonica, mostra che la dipendenza angolare della sezione d'urto per collisione nucleare che determina l'allargamento laterale dello sciame ha un pronunciato picco in avanti. Le proporzioni degli sciami sono compatibili con le proporzioni note delle cascate elettroni-fotoniche al livello del mare se ognuna di queste si considera associata con una cascata penetrante di molto maggior dispersione laterale e minor densità di particelle. La cascata penetrante trasporta circa 1/5 dell'energia totale dello sciame e contiene circa 1/10 del numero totale di particelle presenti nello sciame al livello del mare.

(* *Traduzione a cura della Redazione.*

IL NUOVO CIMENTO Vol. III, N. 1 1° Gennaio 1956

On a Bilocal Interpretation of Isotopic Spin.

J. Rayski

Institute of Theoretical Physics, Nicolas Copernicus University - Toruń, Poland

(ricevuto il 5 Novembre 1955)

Summary. — The systematization of elementary particles by Gell-Mann and the author are complementary. Arguments against the existence of an isotopic spin space are given. The isotopic spin seems to be explicable within the framework of the bilocal field theory without necessity of increasing the number of dimensions of the physical space.

Recently the problem of systematization of elementary particles was attacked from two different viewpoints. One of the two competing views represented by Pais [1], Gell-Mann [2], d'Espagnat and Prentki [3], and others is (mainly) a systematization with respect to the group of transformations in an isotopic spin space (iso-space). The other, represented by the present author [4], is a systematization (mainly) with respect to the group of transformations in the ordinary space.

Both modes of approach have undeniable advantages: the former (especially the Gell-Mann model) is particularly useful for a systematization of particles from the point of view of their interactions and coupling constants. The latter arose from the ideas of bilocalizability and reciprocity leading to a generalization of the field theory and accounts, in a very natural way, of the existence of families of elementary particles with a spectrum of masses and spins. The comparison of the predicted mass spectra with the present experimental data seems promising.

---

(1) A. Pais: *Physica*, **19**, 869 (1953).

(2) M. Gell-Mann: *Phys. Rev.*, **92**, 833 (1953).

(3) B. d'Espagnat and J. Prentki: *CERN publication* 55-11 (1955).

(4) J. Rayski: *Nuovo Cimento*, **10**, 1729 (1953); **2**, 255 (1955); *Acta Phys. Pol.*, **14**, 107 (1955); *Bull. Acad. Pol. Sc.*, 3, 255 (1955).

We notice a remarkable coincidence when comparing the two systematizations. Namely, the particles which in our formalism are described by the first (second) order field equations or mass eigen-equations, in the Gell-Mann model are characterized by half-integer (integer) iso-spin respectively. Thus, in spite of apparently heterogeneous points of view, the two systematizations seem to be complementary, and their interrelations have to be clarified.

Both schemes introduce additional degrees of freedom so that the field quantity becomes $\psi(x, \omega)$ in a representation. However, this analogy is superficial since in Pais theory ω denotes a manifold of points in a new space called iso-space (being completely disconnected from the ordinary space) whereas in the bilocal field theory ω (or r_μ) denotes variables of internal structure of the particle in the ordinary space.

In the bilocal field theory the variables ω (or r_μ) transform simultaneously with the variables x_μ under a Lorentz transformation so that the additional degrees of freedom contribute to the ordinary spin instead of iso-spin.

The arguments in favour of increasing the number of dimensions of physical space with the aim of taking account of the iso-spin are based on an apparent analogy between the iso-spin and the ordinary spin. (i) Both are connected with representations of the unimodular group. (ii) There exists a homomorphism between the Lorentz group and the unimodular group. (iii) The Lorentz group is a group of transformations of coordinates in the physical space (Minkowski's world). By analogy it was inferred that there must exist also a group of transformations of coordinates of points forming another space (iso-space) homomorphic with that unimodular group which is connected with the iso-spin. Both spaces may be combined in the sense of a cartesian product to form a space with an increased number of dimensions.

This analogy seems to go too far. Objections of a methodological as well as aesthetic nature may be raised against the idea of introducing an iso-space on equal footing with the ordinary space. First of all, if such a space really exists, why does it not reveal itself in experiment more directly but only via isotopic spin? Secondly, it would be a very ugly space since several fundamental Laws of Physics cannot be covariant under rotations in the isospace. E.g. electromagnetic interactions privilege a direction in this space. In view of such anisotropy I think that the notion of iso-space should be abandoned altogether. The above mentioned analogy reminds of the old endeavour of promoting the analogy between electromagnetism and mechanics whereby the notion of iso-space plays a similar role (of a naïve model) as the old conception of ether in the last century. What we really need, in order to do justice to the notion of iso-spin, is (no more and no less but) a new unimodular group disconnected from the group of Lorentz transformations. We have not to bother about a hypothetic space and a group of transformations (in it) homomorphic with this new unimodular group. It will be shown that the bilocal

field theory disposes of a unimodular group and therefore it may be expected to include also automatically the notion of isotopic spin.

In the bilocal field theory the field quantities are functions of the position and displacement operators–fourvectors $x_\mu\, d_\mu \cdot \boldsymbol{x}$ and d_4 are real, x_4 and $\boldsymbol{d}$ are imaginary operators. If expressed in natural units $c = l = 1$, they form a non-commutative algebra, i.e. may be added, multiplied by complex numbers and by each other. The multiplication is associative but not commutative. Their commutators are

$$[x_\mu, d_\nu] = \delta_{\mu\nu}\,, \qquad [x_\mu, x_\nu] = [d_\mu, d_\nu] = 0\,. \tag{1}$$

Let us consider the group of linear homogeneous transformations of the eight operators x_μ, d_ν. This group contains two important sub-groups commuting with each other. One of the two groups is the group of (simultaneous) transformations

$$x'_\mu = a_{\mu\nu} x_\nu\,, \qquad d'_\mu = a_{\mu\nu} d_\nu\,, \tag{2}$$

where $a_{\mu\nu}$ are matrix elements of the homogeneous Lorentz transformations. The other is a sub-group of the group of canonical transformations preserving the fourvector character of the operators x_μ and d_μ

$$x'_\mu = \alpha x_\mu + \beta d_\mu\,, \qquad d'_\mu = \gamma x_\mu + \delta d_\mu\,, \tag{3}$$

where the coefficients α, β, γ, δ are independent of the parameters of the Lorentz group. The transformation (3) is called canonical if it preserves the commutation relations (1). It is easily seen that a sufficient and necessary condition for (3) to be canonical is

$$\begin{vmatrix} \alpha & \beta \\ \gamma & \delta \end{vmatrix} = 1\,. \tag{4}$$

It should be noticed that neither the transformation matrix needs to be unitary nor its elements to be real. The group of transformations (3), (4) is nothing else but the unimodular group.

The basic relations of the bilocal theory may be written in the form

$$[[\psi, d_\mu], d_\mu] = M^2\psi\,, \qquad [[\psi, x_\mu], x_\mu] = M^2\psi\,, \tag{5'}$$

$$[[\psi, d_\mu], x_\mu] = 0\,, \tag{5''}$$

where M^2 is the square of the mass operator. The commutators are covariant

concepts with respect to canonical transformations (being quantum Poisson brackets). On the other hand, the mass operator involves anticommutators and therefore is not a covariant concept. Hovewer, by specializing the field quantities to be eigensolutions $\psi^{(n)}$ of the mass operator to the eigenvalues M_n, i.e. if working in the rest mass representation, we may replace M^2 by the number M_n^2 so that (5) becomes a covariant set of relations to be satisfied by $\psi^{(n)}$. Denoting $x_\mu = {}_1u_\mu$, $d_\mu = {}_2u_\mu$ the set (5) may be written in the concise form

$$[[\psi^{(n)}, {}_iu_\mu], {}_ku_\mu] = \delta_{ik} M_n^2 \psi^{(n)} , \tag{6}$$

with

$$[{}_iu_\mu, {}_ku_\nu] = \gamma_{ik}\delta_{\mu\nu} , \tag{7}$$

where γ_{ik} is the fundamental metric spinor

$$\gamma = \begin{pmatrix} 0 & 1 \\ -1 & 0 \end{pmatrix} . \tag{8}$$

The set (6) preserves its form with respect to the complex orthogonal group (which is a subgroup of the unimodular group) but may be easily generalized for the whole unimodular group by generalizing δ_{ik} to Δ_{ik} where the last quantity means a symmetric spinor which may be reduced to δ_{ik} by a suitable unimodular transformation.

The field quantity $\psi^{(n)}({}_1u_\mu, {}_2u_\nu)$ should be also a covariant concept with respect to the transformations (3), (4), i.e. should transform according to a representation of the unimodular group. In other words $\psi^{(n)}$ should be a spinor.

As the two groups of transformations (2) and (3) commute and possess only one common element: the unity, we may consider their direct product. It seems natural to assume that the bilocal field quantities $\psi^{(n)}$ form a basis in the vector space of an irreducible representation of the group product. In this way $\psi^{(n)}$ becomes a spinor in a twofold sense. Its transformation character with respect to the Lorentz group be indicated by the index α while that with respect to the unimodular group (3), (4) by the index ϱ. In order to avoid confusion we may put the index ϱ to the left

$${}_\varrho\psi_\alpha^{(n)}({}_1u_\mu, {}_2u_\nu) . \tag{9}$$

It is tempting and suggestive to connect the index ϱ with the physical notion of isotopic spin. Assuming this interpretation the name « canonical spin » would be more suitable than « isotopic spin ». Since the corresponding unimodular group appears here as primary, it is useless to refer to any iso-space

(whose group of transformations be homomorphic with the group (3), (4)) The notion of isospace seems to be futile.

In the absence of the notion of isospace, no compulsory reasons exist for demanding a covariance of all Laws of Physics with respect to our unimodular group of transformations, Indeed, the requirements of covariance have been necessary only in those cases where we have to account for the isotropic character of a space. Nevertheless, such a covariance would be welcomed since it means a higher degree of symmetry (of a physical law). Thus, some physical laws (e.g. those connected with strong interactions) may be covariant, while some others (weak interactions) do not need to be covariant. Such a situation is quite admissible from our point of view whereas it would seem strange if we believed in an actual existence of an isospace.

All elementary particles known at present find their place in a systematization according to spin, parity, and iso-spin. At the present moment the question is no more why there are so many particle sorts but why some of the theoretical possibilities are not confirmed by experiments. E.g. we do not know why a scalar particle with iso-spin equal to unity has never been observed.

RIASSUNTO (*)

Le sistemazioni delle particelle elementari data da Gell-Mann e dall'autore sono complementari. Si dànno argomenti contrari all'esistenza di uno spazio dello spin isotopico. Lo spin isotopico sembra potersi interpretare nel quadro della teoria dei campi bilocali senza necessità di aumentare il numero delle dimensioni dello spazio fisico.

(*) *Traduzione a cura della Redazione.*

IL NUOVO CIMENTO Vol. III, N. 1 1° Gennaio 1956

Heavy Unstable Particles Produced in the High Energy Pion Beam of the Berkeley Bevatron (*).

M. Schein, D. M. Haskin and R. G. Glasser (+)

Department of Physics, University of Chicago - Chicago, Illinois

(ricevuto il 5 Novembre 1955)

Summary. — Stacks of 600 μm pellicles were exposed to the 4.6 and 3.0 GeV pion beam of the Berkeley Bevatron. A number of heavy unstable particles and hyperfragments were obtained. The ratio of the frequency of occurrence of K^+ and K^--mesons has been found to be approximately unity in contrast to the large positive excess in the proton beam. As a possible explanation, it is suggested that the K^--meson is produced in conjunction with a K^+-meson according to the following reaction: $\pi^- + p \to K^+ + K^- + N$. Two hyperfragment decays of hydrogen have been fo nd in which the π^--meson stops. One of the hyperfragments was identified as a ${}^4_1H^*$ produced by a Σ^--hyperon; the other one is a ${}^3_1H^*$ produced directly by the high energy pion. The range of all the charged particles was accurately determined which yielded a reliable value of the binding energy. The value of the binding energy (B.E.) for ${}^3_1H^*$ was found to be 1.2 ± 0.6 and for ${}^4_1H^*$ B.E.$(\Lambda^0) = 3.3 \pm 1$. The mean free path for nuclear collisions was determined for 5.7 GeV protons and 3 GeV π^--mesons. The results yielded for protons 37.6 ± 5.3 cm and for π^--mesons 35.5 ± 5.0 cm. Both mean free paths are longer than the geometrical mean free path for nuclear collisions in the emulsion, which is 25 cm.

1. – Introduction.

Two 10 cm × 15 cm × 15 cm stacks of Ilford G-5 emulsion were exposed to the high energy π^--meson beam of the Berkeley Bevatron. In the first exposure the average energy was 4.6 GeV and in the second one, 3 GeV. For a nu nber of

(*) Supported in part by a joint program of the U. S. Office of Naval Research and the U. S. Atomic Energy Commission.

(+) Now at the Naval Research Laboratory, Washington, D. C.

reasons, we were interested to expose plates to the highest energy pions available in machines at the present time. First of all, the center of mass energy is higher in the pion beam than in any other beam available in machines. Calculations show that in order to create a proton anti-proton pair, one needs an energy around 2.6 GeV in the pion beam. It can then be expected that at energies around 4 GeV some of the anti-protons going backward with reasonably high energy in the center of mass system, will be emitted with a sufficiently low energy so that they can be detected in photographic plates. In particular, one can expect that some of these anti-protons have a sufficiently low energy to undergo an annihilation process before being destroyed by nuclear collisions. We hope to be able to detect one day annihilation processes of this kind since it is of great interest to know the mechanisms by which anti-protons do annihilate. Another possible way to obtain evidence for anti-protons in photographic emulsions consists of the observation of low energy anti-hyperons. It is presumed that these hyperons are produced from pre-existing anti-protons at sufficiently high energies in the pion beam. A computation shows that one can expect anti-Λ^0 and anti-Σ hyperons to occur at pion energies above 3 GeV. It should be particularly revealing to observe anti-Σ hyperons of relatively slow velocity which should decay in 50% of the cases according to the following scheme:

$$\Sigma^- \rightarrow p^- + \pi^0 + Q \,. \tag{1}$$

The Σ^- should emit in such a process a rather low energy anti-proton of short range which would then annihilate in the plate and hence should easily be recognized.

Our immediate purpose for exposing plates in the high energy π^--beam was to study the production of hyperons, K-mesons, and hyperfragments. This should be possible since in practically all the events in which heavy unstable particles do occur, they are produced inside the stack by the impact of π^--mesons upon nuclei. Naturally considerable statistics will be needed before one can draw definite conclusions about the elementary act in which these particles are created. We just started to scan a few pellicles of the stack and hence can give only very preliminary results. One of the encouraging aspects of this research is that we were able to trace back almost every single unstable heavy particle to its origin. Hence we have confidence that our method will work. Some of the preliminary results can be summarized as follows: In the stack exposed to the pion beams we have found so far K^+ and K^- mesons and hyperfragments. Two of the K^+-mesons are complete decays of τ-mesons in which the sign could definitely be established as positive. It is also interesting to mention that the π^--meson in one of the τ-decays has the unusually high energy of $E_{\pi^-} = 48$ MeV.

2. – Production of K-Mesons.

Probably the most intersting result of this investigation is the fact that the ratio of the K^- to the K^+-mesons has been found to be close to one. Since it is easier to recognize a K^--star than the decay of a K^+-meson into a singly charged particle of minimum ionization, it is quite possible that some of the K^+ events were missed. We have made a careful study of the efficiency of detection of stopping particles decaying into tracks of minimum ionization. This was done by studying μ-e-decays in various parts of the emulsion. According to the most pessimistic estimate, we could not have missed more than 40% of the minimum tracks. It is then clear that the detected ratio between positive and negative K-mesons stopping in the stack could be at the most 2:1. This result would have to be compared with the spectacular ratio of 100:1 found in the proton beam at Brookhaven and at Berkeley. It would be very hard to visualize a mechanism by which the K^+-mesons would have a completely different energy spectrum in the pion beam than that observed in the proton beam. The number of stopping K^+-mesons is therefore assumed to be of the same order of magnitude in the two beams. Accordingly, we must find a different explanation for the very spectacular difference in the ratio of K^+ to K^- in the proton and pion beams. One possibility is that K^--mesons are produced by a reaction which requires a higher center of mass energy that that of K^+-mesons. This high center of mass energy is provided in the pion beam of the Bevatron. Hence, we should like to propose that K^--mesons are predominantly produced by the following fundamental reaction:

$$\pi^- + p \rightarrow K^+ + K^- + N \,. \tag{2}$$

In contrast K^+-mesons can easily be produced in association with hyperons. Reaction (2) is of great interest since it represents the first process in which K-mesons are not produced in conjunction with hyperons. According to the Gell-Mann–Pais scheme [1], the K^--meson has a strangeness of -1 and the K^+-meson the strangeness of $+1$. Hence reaction (2) preserves strangeness. It has the further interesting consequence that the K^--meson is not necessarily identical with the K^+-meson since its strangeness quantum number must be different in reaction (2). Only further studies will show whether nuclear interactions induced by K^--mesons are indeed different from those of K^+-mesons.

It was of interest to trace back the K^+ and K^--mesons to the original star in which they occurred. In most cases the K-mesons are emitted from rather

[1] M. Gell-Mann and A. Pais: *Proceedings of the International Conference, Glasgow* (London, 1954)

large π^--stars of from 6 to 12 prongs. Not all the prongs have been traced and identified so far. However, in one case a very interesting event was observed in which a 3 GeV π^--meson undergoes a nuclear collision and as a result two visible prongs appear. One of the prongs is definitely a slow K^+-meson decaying into a minimum track. The other track is at minimum ionization and is deviated by a few degrees from the original direction of the pion. The preliminary analysis of this event shows that a reasonable explanation can be found by assuming pair production of K^+ and K^- according to reaction (2). In this particular case the K^+ is slow and hence it is emitted backward in the center of mass system whereas the K^- is fast and is moving in the forward direction. It will be of great interest to locate additional cases of events of this kind which should throw direct light on the mechanism of pair production of K-mesons by pions.

3. – Hyperfragment Decays.

A number of hyperfragments have been located in plates exposed to the π^--beam. We shall give here the description of two cases in which the binding energy can be determined reliably. One of the hyperfragments is a ${}^4_1H$ resulting from the capture of a Σ^--hyperon and the other one is a ${}^3_1H$. Fig. 1 shows the event in which the ${}^4_1H$ hyperfragment was produced. A nine prong star initiated by a 3.0 GeV π^- contains a 12620 μm long track (Σ) which ends in a three prong capture star (1, 2 and 3). One prong (3) of the secondary star is a 255 μm long, singly charged track which comes to rest in the emulsion, decaying into a co-linear 8 μm saturated track (*a*) and a π^--meson (*b*) which forms a ρ-ending after passing through 21 pellicles, with a range of 36170 μm. Table I lists the experimental data for the individual tracks of the event.

TABLE I.

Track	Identity	Range (μm)	Energy (MeV)	Momentum (MeV/c)
	Σ^-	12 620	63	
1	α	80	12.3	
2	p	7	.6	
3	${}^4_1H$	255	11.0	
a	${}^4_2He$	8	2.4	134
b	π^-	36 170	51	130

In order to identify track Σ, an integral gap vs. range measurement was carried out, and compared with that of identified protons and π-mesons. This is

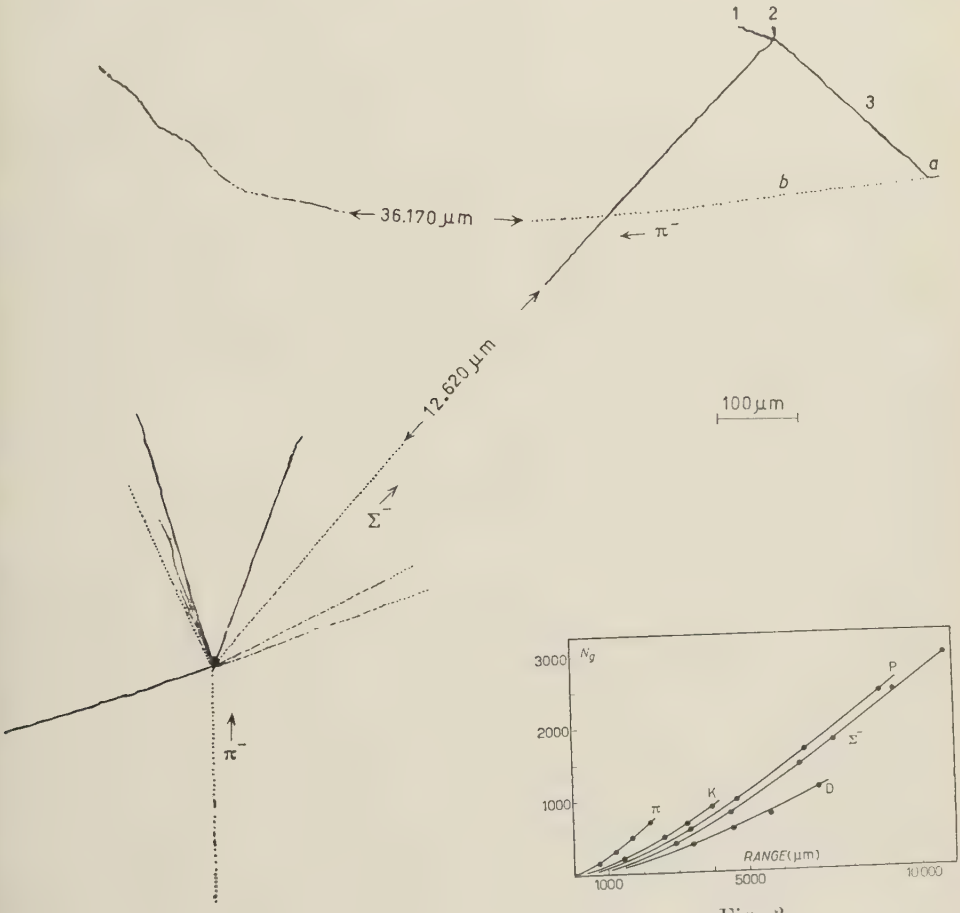

Fig. 1.

Fig. 2.

shown in Fig. 2. A K^--meson found in the same stack is plotted also for comparison. It is seen that the mass of particle Σ must lie between that of the proton and that of the deuteron. In addition, a grain-density vs. range measurement of track Σ at 12 000 μm residual range and on a π-meson track for comparison, gives for the former a mass of 2270 ± 250. electron masses This is in good agreement with the mass of the Σ-hyperon.

Since track 3 undergoes mesonic decay, it must be a hyperfragment containing a Λ^0-hyperon. It is then assumed that the capture of the Σ takes place in a heavy nucleus, according to the process:

$$\Sigma^- + p \rightarrow n + \Lambda^0 + Q\,, \tag{3}$$

which is in accordance with the Gell-Mann-Pais scheme. Q is the mass excess of the Σ^- over the Λ^0, equal to 78 MeV. Considering this process first as an elementary interaction between particles at rest, we calculate that the neutron in this reaction is emitted with an energy of 42 MeV. In the star under consideration, the Λ^0 definitely appears bound to a fragment, which will be shown to be ${}^4_1\mathrm{H}$; in addition, there are two other visible tracks, which are most probably an α-particle and a proton. (See Table I). To balance the residual momentum of the visible prongs, 280 MeV/c, the emission of a neutron must be postulated. A π^0-meson could not be assumed because it would have to have an excessively high energy. A neutron of this momentum corresponds to an energy of 41 MeV. This checks surprisingly well with the energy of the neutron as calculated above for the elementary interaction, implying that the emitted neutron did not appreciably penetrate the nucleus. The process also implies that the Λ^0 strongly interacts with nuclear matter, since its energy in the fragment is considerably reduced.

It is of interest to compare the total kinetic energy output of the Σ-star with the Q-value of reaction (3). The energy of the visible tracks plus the neutron totals 65 MeV; which is consistent with the Q-value, taking the difference to represent binding energy.

Fragment (3), emerging from the Σ^--star, has the appearance of a singly charged track coming to rest in the emulsion. Since it decays co-linearly into a π^- and a visible recoil nucleus, an accurate measurement of the energy release was possible. As seen in Table I, this energy release is 53.4 MeV, which is considerably in excess of the Q-value for the decay of a free Λ^0. This rules out the possibility that the recoil nucleus is ${}^3_2\mathrm{He}$. The large energy difference must arise from the large binding energy of the last protons in ${}^4_2\mathrm{He}$. The process accordingly should be represented as

$$(4)\qquad \begin{cases} {}^4_1\mathrm{H}^* \rightarrow {}^4_2\mathrm{He} + \pi^- + Q & (Q = 53.4\ \mathrm{MeV}) \\ \Lambda^0\ (\mathrm{bound}) \rightarrow \mathrm{p} + \pi^- + 36.9\ \mathrm{MeV} \\ \mathrm{p} + {}^3_1\mathrm{H} \rightarrow {}^4_2\mathrm{He} + 19.8\ \mathrm{MeV}\,. \end{cases}$$

Since the fragment decays into visible tracks only, the energy release may be readily calculated, from which a good value can be obtained for the binding energy of the Λ^0. The result yields the binding energy of the Λ^0 in the fragment

$$\mathrm{B.E.}\ (\Lambda^0) = 36.9 + 19.8 - 53.4$$

$$\mathrm{B.E.}\ (\Lambda^0) = 3.3 \pm 1\ \mathrm{MeV}$$

The meaning of the numbers appearing here is made clear by reference to

the reactions in (4). This value may be compared with the binding energy of the second neutron in ${}^{3}_{1}\mathrm{H}$ which is 6.3 MeV.

The event we have described is of interest for the following reasons:

(1) It is a case of Σ^- capture in which the emergence of a Λ^0 can be detected because it is bound in an unstable fragment.

(2) The fragment decays into two co-linear tracks, furnishing a reliable value for the binding energy of the Λ^0 in the fragment.

The second hyperfragment is produced in a 3 GeV π^--star of the type $10+2\pi$ and is shown in Fig. 3. Track 1 is emitted at an angle of 140° with respect to the incident pion and has a range of 152 μm. From the number of gaps along the track and the complete lack of δ-rays, track 1 has definitely the appearance of unit charge. A comparison of the track with nearby ending protons bears out this conclusion. The scattering at the end of track 1 is typical of a particle coming to rest. Three secondary tracks emerge from the point of disintegration. Track *a* has been identified by grain density and scattering as a π-meson. After passing through six pellicles with a total range of 11 100 μm track *a* comes to rest and forms a two prong capture star, identifying it as a π^--meson. Tracks *b* and *c* are compatible with the tracks of protons, as will be shown later. The experimental data is summarized in Table II.

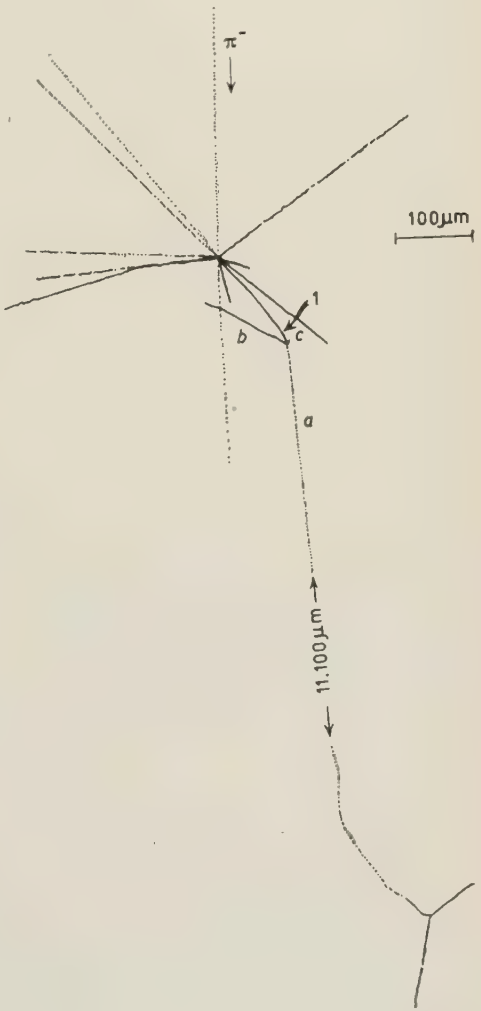

Fig. 3.

The total energy release in the disintegration, on the basis of the above assumptions, is somewhat less than the Q-value for the decay of the Λ^0. The event does not represent the decay of ${}^{4}_{1}\mathrm{H}$, since in that case the expected energy release is about 50 MeV as shown before. The possibility that either track *b* or *c* is a deuteron and the decay is according

TABLE II. – *Summary of experimental and computed data for the mesonic decay of a tritium hyperfragment.*

		Identity	Range (μm)	Energy (MeV)	Component of momentum (MeV/c)		
					x	y	z
Event 1	1	$^3_1$H*	152	7			
	a	π^-	11 100	24.5	— 36.4	— 63.0	61.0
	b	p	157	4.8	— 32.8	77.2	19.4
	c	p	3	.3	10.6	0	— 17.0

to the scheme

$$^3_1\mathrm{H}^* \rightarrow \mathrm{p} + \mathrm{d} + \pi^-$$

can be ruled out, since the event is clearly not co-planar, implying the emission of a neutral particle. The process therefore is

$$^3_1\mathrm{H}^* \rightarrow \mathrm{p} + \mathrm{p} + \mathrm{N} - \pi^- + Q\,.$$

From the Q of the reaction, the binding of the Λ^0 can be determined. The energies of *a*, *b*, and *c* have been evaluated from the range-energy relation of Barkas and are tabulated in Table II. From the momenta and directions of *a*, *b*, and *c* the residual momentum is determined to be 86.4 MeV/c. This momentum implies that a neutron of 4.0 MeV is needed to balance the momentum of the system. The Q of the reaction is then the sum of energies of the individual particles plus the binding energy of the deuteron, 2.27 MeV. This yields a Q-value of 35.7 MeV (see Table II). The binding energy of the Λ^0 is then

$$\mathrm{B.E.}(\Lambda^0) = Q(\Lambda^0) - Q = 36.9 - 35.7 = 1.2 \pm 0.6.$$

It is of definite interest to see that in cases where the π^--meson stops, the binding energy of hydrogen hyperfragments can be reliably estimated. The results obtained are in good agreement with results of other laboratories presented at the Conference. We are considering only cases in which the hyperfragments have been definitely identified and the π^--meson stopped. This is very satisfactory because it shows that the binding energy of the Λ^0 particle in tritium and in $^4_1$H is unique. It is then of great interest to try a theoretical calculation of the magnitude of the forces which act upon the Λ^0 particle in

these nuclei. The experimental results definitely indicate that the binding energy of ${}^3H_1$ is smaller by a factor of two than that of ${}^1_1H$. A difference of this kind in the binding energy has been anticipated by F. Duimio, who presented his tentative calculations at the Pisa Conference.

4. – The Nuclear Mean Free Path of 5.7 GeV Protons and 3.0 GeV π^--Mesons.

Stars produced by 5.7 GeV protons and 3.0 GeV π^--mesons from the Berkeley Bevatron have been found by the method of following along tracks in Ilford G-5 emulsion. The average prong number for the proton stars is 10.7 and for the pion stars 9.5. The maximum prong numbers observed are 30 and 20 respectively. The average number of visible shower tracks is 2.1 for the proton initiated stars, and 0.9 for the π^- initiated stars. The maximum number of shower tracks found amounted to 6 and 4 respectively. Among the proton events there are 3 cases where a pion is ejected into the backward hemisphere. No case of a similar kind has been found in the pion beam. From 50 events in each beam, the mean free path is found to be 37.6 ± 5.3 cm for protons and 35.5 ± 5.0 cm for π^--mesons. This should be compared with the geometrical mean free path for nuclear collisions in the emulsion, which is 25 cm. The relatively large difference has interesting theoretical implications.

* * *

We wish to thank Professors E. O. Lawrence and E. J. Lofgren for their excellent cooperation in making possible the Bevatron exposures. We also wish to thank Professor N. Dallaporta of Padua for his private communication concerning hyperfragment decays. It is a pleasure to acknowledge the valuable assistance of Dr. Theodore Bowen and Robert E. Cavanaugh.

RIASSUNTO (*)

Pacchi di pellicole di 600 μm sono stati esposti a fasci di protoni di 4.6 e 3.0 GeV del Bevatrone di Berkeley. Si sono ottenuti un certo numero di particelle instabili pesanti e di iperframmenti. Il rapporto della frequenza di produzione di mesoni K^+ e K^- è risultato circa 1 in contrasto col grande eccesso positivo nel fascio protonico.

(*) *Traduzione a cura della Redazione.*

Come possibile spiegazione del fenomeno si pensa che il mesone K^- sia prodotto in unione con un mesone K^+ secondo la reazione $\pi^- + p \rightarrow K^+ K^- + N$. Si sono trovati due iperframmenti da decadimento dell'idrogeno in cui si arresta il mesone π^-. Uno degli iperframmenti è stato identificato con un ${}^4_1H^*$ prodotto da un iperone Σ^-; l'altro è un ${}^3_1H^*$ prodotto direttamente dal pione di grande energia. Il percorso di tutte le particelle cariche è stato accuratamente determinato, ottenendo un valore attendibile dell'energia di legame. Il valore dell'energia di legame (B.E.) per il ${}^3_1H^*$ risulta essere 1.2 ± 0.6 e per il ${}^4_1H^*$ B.E.$(\Lambda^0) = 3.3 \pm 1$. Il cammino libero medio per le collisioni nucleari è stato determinato per protoni di 5.7 GeV e per mesoni π^- di 3 GeV. Si ottenne per i protoni 37.6 ± 5.3 cm e per i mesoni π^- 35.5 ± 5.0 cm. I due cammini liberi medi sono maggiori del cammino libero medio geometrico per collisioni nucleari in emulsione che è di 25 cm.

On Cosmic Rays Jets.

G. Bertolino

Istituto di Fisica dell'Università - Torino

(ricevuto il 9 Novembre 1955)

Summary. — We have studied 59 jets found in the scanning of nuclear plates exposed to cosmic radiation during the Sardinia Expedition of 1952 and 1953 and measured in the Turin and Padua Sections of the National Institute of Nuclear Physics. Studying the angular distribution of jet-tracks, a substantial and abrupt increase of the angle has been noted at the last tracks, which increase can be considered as due to secondary phenomena after the primary collision. The primary energy and anelasticity coefficient of jets has been calculated, excluding the tracks considered as due to secondary phenomena: the jets can consequently be divided in two classes having as mean value for the anelasticity coefficients 0.52 and 0.18, respectively. The incongruency arising from the fact that in previous works values of the anelasticity coefficient greater that 1 have been calculated has been eliminated.

In a previous work [1] anelasticity coefficients have been studied for jets found in the scanning of nuclear plates exposed to cosmic radiation at an height of about 29000 m during the Sardinia expedition of 1952-53. The results are studied again in this work, adding to the measurements previously discussed the measurements effected on 30 jets which have been found in plates exposed to quite similar conditions and scanned at the Padua Section of the National Institute of Nuclear Physics.

---

[1] G. Bertolino and D. Pescetti: *Nuovo Cimento*, **12**, 630 (1954).

The method followed for the study of the energy of the jets is based ([2,6]) on a simple intrinsic property of the Lorentz transformation and on the following hypotheses ([1]):

1) The distribution of momentum of the jet is assumed to be simmetrical in the center of mass (C.M.) system with respect to the line of flight of the colliding particles and to the plane perpendicular to said line. This hypothesis is correct in the nucleon-nucleon collision.

2) The velocities $c\beta_\pi$ of mesons produced in the C.M. system are of the same order of the velocities $c\beta_0$ of the center of mass of the system, which hypothesis is satisfied if both the velocity of the center of mass and the velocities of mesons approach the velocity of light.

The calculation of the anelasticity coefficient ([1,5]) is based on the calculation of the mean energy for each meson emitted. Said mean energy is correlated to the angle ϑ_L, i. e. to the angle formed by the most peripheric track of the jet with the jet axis. By using this formula « ad litteram » the values of the anelasticity coefficient referred in Fig. 2 of the cited work ([1]) have been found. It is noted in this figure that some anelasticity coefficients have values greater than 1. The same results appear in Fig. 2 of the work of T. H. Hoang indicated under ([5]). Similar results are found if the same formula is applied to the jets of the Padua measurements: the anelasticity coefficient for some jets, also in this case, is greater than 1.

Considering this result from a merely energetic point of view, a value of an anelasticity coefficient greater than 1 is meaningless. Consequently, the anelasticity coefficients greater than 1 had been considered as anomalous values due to some systematic error in the method of calculation.

A quite particular distribution has been observed in many of the jets having a calculated anelasticity coefficient greater than 1. It has been noted, arranging the tracks of the jets in an ordered sequence according to the value of the angle formed by the track with the jet axis, that this angle increases abruptly and substantially at the last tracks. Considering a jet formed with n tracks, it is not infrequent that the angle ϑ_n, corresponding to the n-th track is almost double than the angle ϑ_{n-2} corresponding to the $(n-2)$-th track.

([2]) C. C. Dilworth, S. J. Goldsack, T. F. Hoang and L. Scarsi: *Compt. Rend.*, **236**, 1551 (1953).

([3]) C. C. Dilworth, S. J. Goldasck, T. F. Hoang and L. Scarsi: *Nuovo Cimento*, **11**, 1260 (1953).

([4]) T. F. Hoang: *Journ. de Phys.*, **14**, 395 (1953).

([5]) T. F. Hoang: *Journ. de Phys.*, **15**, 337 (1954).

([6]) C. Castagnoli, G. Cortini, C. Franzinetti, A. Manfredini and D. Moreno: *Nuovo Cimento*, **10**, 1939 (1953).

The above distribution, more particularly for jets having a value of ϑ_n greater, for instance, than $45 \div 50°$, leads to a calculated value for the anelasticity coefficient greater than 1. Table I reads the angular values for a typical angular distribution of this type for a jet measured at Turin and a jet measured at Padua, respectively. The values calculated for the anelasticity coefficient of these jets, using as value for ϑ_L the value of ϑ_n corresponding to the n-th track, are $K = 1.2$ and $K = 1.6$ respectively.

The particular angular distribution referred above, with reference, for instance, to the data of Table I, has some consequence in the calculation of

TABLE I.

Turin Jet No. 3		Padua Jet No. 42	
9+2 P		10+3 P	
Track	Angle	Track	Angle
1	2° 20′	1	2° 45′
2	4° 50′	2	4° 20′
3	5° 10′	3	5° 35′
4	10° 40′	4	10° 5′
5	12° 30′	5	15° 40′
6	12° 30′	6	20° 30′
7	30° 40′	7	25° 15′
8	59° 40′	8	38° 5′
9	70° 5′	9	78° 15′
		10	80° 0′
$K = 1.2$		$K = 1.6$	

the jet energy. This calculation has been effected by applying the formula referred to in the cited work (1)

$$\frac{1}{\gamma_c^2} = \operatorname{tg} \vartheta_f \cdot \operatorname{tg} \vartheta_{1-f}$$

taking as a value for γ_c the mean value of the different $(\gamma_c)_f$ calculated introducing in the above formula the values measured for angles ϑ_f and ϑ_{1-f} in all possible combinations. Were the angular distribution of the tracks isotropic, the values for the above products would be equal; obviously, however, the observed values for the track angles are subjected to fluctuations. The root mean square value of the differences between the mean value of the products of the tangents used for calculating γ_c and the value of single products of said tangents can be taken as an index showing the limits within which the hypothesis, on the ground of which the calculations are effected, are satisfied, in the jet studied. As an illustrative example, considering the two jets

referred in Table I, we note that, taking all the tracks of said jets, that is 9 and 10 tracks respectively, the root mean square value of the difference referred above is 31% and 47% respectively; on the contrary, considering only the first seven or eight tracks, respectively, of the above jets, the values of said root mean square of the differences decrease to 13% and 14% respectively.

The phenomena which can interfere and complicate the angular distribution observed in the jet can be summarized as follows:

1) The hypothesis that the velocity of mesons produced in the C.M. frame is equal to the velocity of the C.M. itself in the laboratory frame corresponds substantially to the hypothesis that the velocity of all mesons produced is the same. It is obvious however to think that the mesons emitted will have a velocity distribution, and consequently, more particularly for velocities $\beta \simeq 1$, the energies and momenta for the different mesons can differ by considerable amounts.

2) The colliding nucleons, after the primary collision, can collide against a further nucleon of the target nucleus or other nucleus. These secondary collisions produce in the C.M. frame an enlargement of the beam of particles forming the jet.

3) The mesons produced in the nucleon-nucleon collision, can produce, by collision with other nucleons in the target nucleus, the emission of secondary mesons. The energy of said secondary mesons is obviously lower than the energy of the primary mesons.

The above mentioned phenomena have, as a common consequence, the enlargement of the jet with respect to the jet produced in the nucleon-nucleon collision. More particularly, also the phenomena indicated under 1) — mesons produced with lower velocity than the mean velocity of mesons emitted — contributes with the other phenomena to produce an enlargement of the jet, for the scattering effect, to which the meson is subjected by other particles in the emulsion, increases lowering the velocity of the meson.

By the above reasons it can be inferred that, in the jets of the type referred to in Table I, the nucleon-nucleon collision is accompanied by other phenomena. The more enlarged tracks in the jet are probably due to said secondary phenomena, such as scattering phenomena of primary mesons emitted against the nucleons or secondary production of further shower particles.

These remarks can obviously be considered in the calculation of K. The introduction of angle ϑ_L, corresponding to the utmost track of the jet, in the calculation of K has a meaning in the case of a nucleon-nucleon collision without any secondary phenomenon, but is meaningless if the track considered has been subjected to a scattering or is due to a particle the energy of which was, after the primary collision, lower than the mean energy of mesons emitted.

The calculation of the anelasticity coefficient must consequently be effected, introducing in the formula not the value of ϑ_n corresponding to the utmost track, but the angle corresponding to the utmost track which has not been probably subjected to secondary phenomena, after the primary nucleon-nucleon collision. It is introduced here the concept of « primary jet » or « reduced jet », that is a jet in which not all the relativistic tracks in the jet are considered, but eventually only the tracks in the central part of the jet, in the case of reasonable opportunity of excluding tracks which have been subjected to secondary phenomena, after the primary collision.

The selection of the tracks which must be excluded in the passage from the jet as measured—which will be hereinafter indicated as « normal jet »—and the reduced or primary jet can seem arbitrary; the study of the angular distribution of the tracks of the normal jet considerably reduces the arbitrariety. As a normal rule, used with some elasticity, the more peripheral tracks of the jet have been excluded, beginning from the track forming with the jet axis an angle equal at least to 1.5 times the angle formed by the next previous track. In the practice, no more than two tracks in a jet are normally excluded; in eight jets only, three tracks have been excluded, while in nineteen jets no track has been excluded.

Table II reads the number of the excluded tracks and the angles formed by said tracks with the jet axis, compared with the values of the angles formed by the tracks of the reduced jet with the jet axis. Reference P indicates that the event has been measured at Padùa and reference T indicates that the event has been measured at Turin.

TABLE II.

Number of normal jets	T 27	P 32	Total 59
Number of normal jets with no track excluded	T 13	P 6	Total 19
Number of normal jets with tracks excluded	T 14	P 26	Total 40
Total number of tracks of 59 jets	T (180+25)	P (261+41)	Total (441+66)
Total number of tracks excluded	T 25	P 41	Total 66
Mean angle of the tracks of the primary jets	(40+19) for 441 tracks		$14^\circ\ 13'$
Number of the tracks in 40 primary jets with tracks excluded	T 91	P 213	Total 304
Mean angle of 304 tracks of 40 primary jets with tracks excluded			$13^\circ\ 18'$
Mean angle of 66 tracks excluded			$60^\circ\ 11'$
Angle ϑ_L (mean value) formed by the utmost track considered in 40 reduced jets			$27^\circ\ 4'$

Experimental results.

The experimental results referred below relate to primary or reduced jets.

1) *Total energy and number of tracks.* – In Fig. 1 the energy γ_c of the jet is indicated on the x-axis and the number of the particle of the corresponding jet is indicated on the y-axis.

The subdivision introduced in a previous work [1] corresponds to zone A and zone B of the diagram.

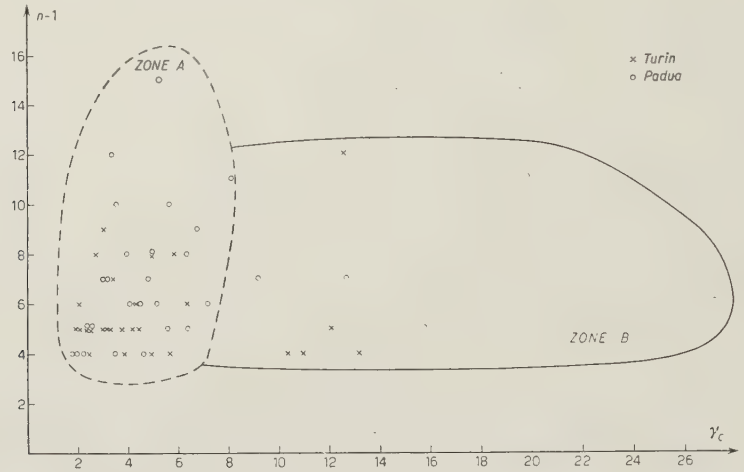

Fig. 1.

2) *Anelasticity coefficient.* – The anelasticity coefficient K has been calculated introducing in the formula

$$K = \frac{1.5 n_{\pm} \gamma_c \sin \vartheta_L}{2\mu(\gamma_c - 1)}$$

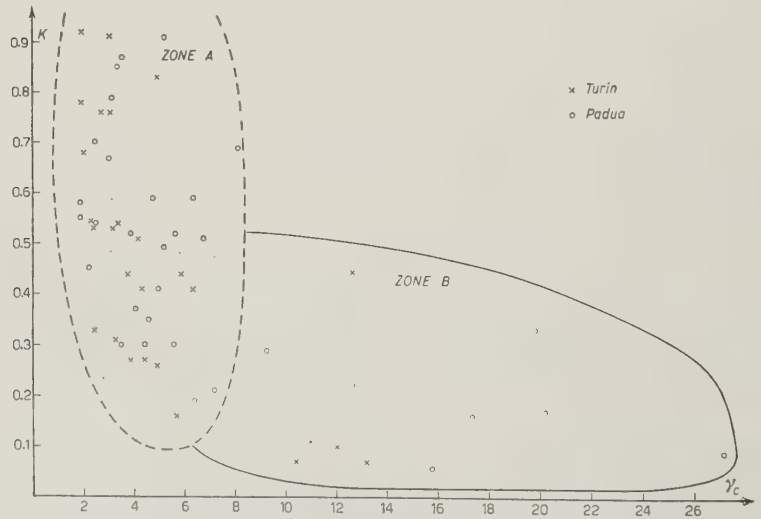

Fig. 2.

as value of ϑ_L, the angle formed by the utmost track in the reduced jet. Correspondingly $n_{\pm}$ is the number of tracks in the primary jet, less 1, considering the track of angle ϑ_L as the last track of the jet.

The hypotheses on which the above formula is calculated are referred in work (1).

The values of the anelasticity coefficient (y-axis) correlated to the jet energy (x-axis) are referred in Fig. 2.

The diagrams shows:

a) values of anelasticity coefficient greater than 1 no longer appear;

b) the diagram can be divided in two zones corresponding to the previous zone A and zone B of work (1).

The value of anelasticity coefficient calculated as mean value, introducing the root mean square of the differences, is:

for all jets:	59 jets	$K = 0.46 \pm 0.21$
for zone A:	47 jets	$K = 0.52 \pm 0.21$
for zone B:	12 jets	$K = 0.18 \pm 0.12$

From this results and considering also Fig. 3, it might be inferred that the jets of zone B, for which the primary energy is greater than for the jets of zone A, have a lower anelasticity coefficient.

Fig. 3 shows a diagram of the distribution of the values of anelasticity coefficients. The x-axis is divided in ten equal parts corresponding to ten intervals of the anelasticity coefficient; the number of jets having values comprised in the intervals of the x-axis are plotted on the y-axis.

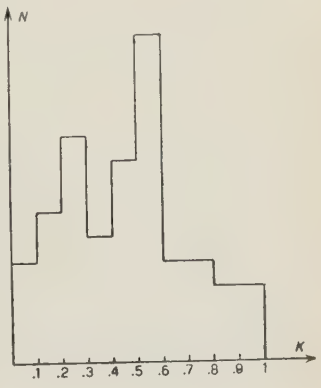

Fig. 3.

3) *Energy absorbed in meson production in the jets.* – Fig. 4 plots on the y-axis the number of mesons of the reduced jet and on the x-axis the value

$$K(\gamma_c - 1) = \tfrac{1}{2}\Delta E\,,$$

where ΔE is the most probable value of the energy absorbed by mesons in the jet production.

Fig. 5 plots on the y-axis the number of mesons produced less 1, and on the x-axis the mean value of ΔE of the corresponding jets. The points, with the exception of the point corresponding to the value of $(n - 1) = 11$, representative of two jets, are arranged in a satisfactory manner along a straight line, the equation of which has been calculated by the method of minimum

squares. In view of the fact that the different experimental points in Fig. 5 are representative of different numbers of tracks, the coefficients of the straight line have been calculated introducing a weight factor calculated in the following way:

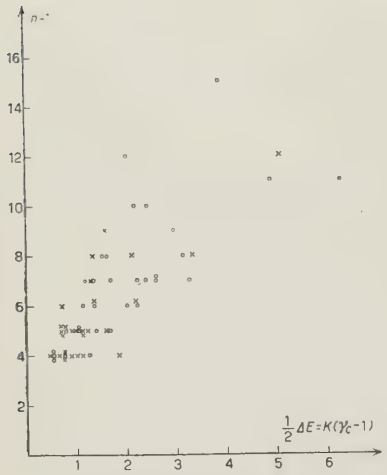

Fig. 4.

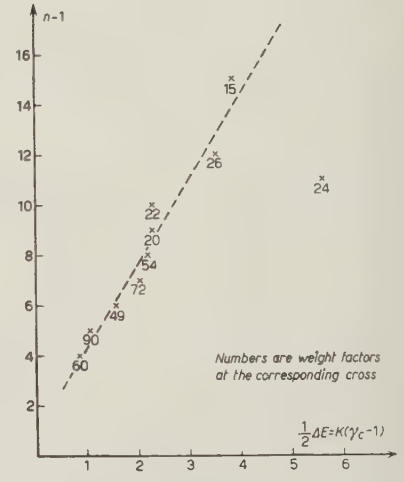

Fig. 5.

a) the weight factor of the experimental point increases proportionally with the number of jets from which said point is calculated;

b) the weight factor of the experimental point increases with the number of tracks in the corresponding primary jet. It is pointed out here that the calculation of energy has been effected starting from the mean value of the products of the tangents of corresponding angles, and consequently the value calculated for the energy of the jet is more probable on increase of the number of the jet particles.

The weight factor p for the different points of the diagram has been taken, in view of the above considerations, equal to

$$p = nN ,$$

wherein n is the number of the tracks in the jet and N is the number of the jets having n tracks. The factor p is, in other words, equal to the number of tracks corresponding to each of the considered points.

The coefficients of the straight line, correlating the number $(n - 1)$ of mesons emitted and the half total energy for said mesons, have been calculated imposing that the expression

$$\sum_i p_i (y - y_i)^2$$

be a minimum. In the above expression y is the ordinate of the straight line, y_i the value of the corresponding experimental point and p_i the weight factor corresponding to said point. The equation of the straight line is

$$(n-1) = 3.33K(\gamma_c - 1) + 0.975 .$$

The energy for each meson emitted in the reduced jets, calculated on a total number of 441 tracks, is 473 ± 58 MeV, wherein 58 is the root mean square value of the difference between the mean value calculated for the energy of the mesons and the energy of each meson ([1,4,5]).

This result is in good agreement with the experimental results of previous works ([1,4]). The result also agrees with the theoretical results found by WATAGHIN in a work ([8]) of 1941. In this work, considering the most probable distribution of momenta and energy, in an high energy nucleon-nucleon collision, for the mesons emitted, it is inferred that, in the case of nearly isotropic angular distribution, the most probable energy for each meson produced is $\sim 3\mu c^2$. Assuming 274 for the mass of the π-meson, the value of the energy corresponding to $3\mu c^2$ is 420 MeV in good agreement with the above experimental result.

4) *Angular distribution.* – The angular distribution of the tracks in the C.M. frame has been studied by the known methods ([6,1]) of transforming the angles in the laboratory frame in the angles in the C.M. frame, drawing afterwards a diagram in which the solid angle in the C.M. system of the two colliding nucleons is divided in ten equal parts. The formula for the transformation from the laboratory frame to the C.M. frame is as follows:

$$\operatorname{tg} \frac{\vartheta'}{2} = \gamma \operatorname{tg} \vartheta ,$$

which formula is approximated within the same limits of the hypotheses on which the previous study of jets is based.

In the diagram of the angular distribution indicated in Figs. 6 and 7, jets are considered both with charged and neutral primary. The distinction followed in the previous work ([1]) of the jets with charged primary and jets with neutral primary has not been effected here, for the merely contingent reason, that the events added in this work with respect to the previous works are all events with charged primary. This does not mean that events with neutral primary have not been found in the scanning, but merely that the measurements have been effected only on events having a charged primary.

([7]) A. ENGLER, U. HABER-SCHAIM and W. WINKLER: *Nuovo Cimento*, **12**, 931 (1954)
([8]) G. WATAGHIN: *Symposium sôbre raios cosmicos, Rio de Janeiro*, 1941, p. 129

The diagram of Fig. 6 relates to the angular distribution for the reduced jets. It might be inferred from this diagram that the distribution of mesons emitted is not isotropic in the C.M. frame, but nearly shaped with a maximum

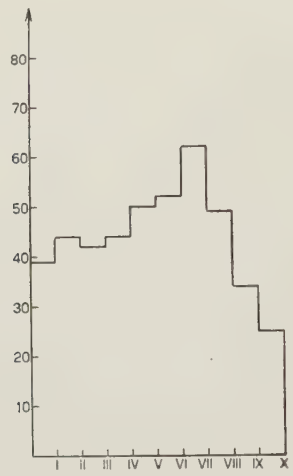

Fig. 6.

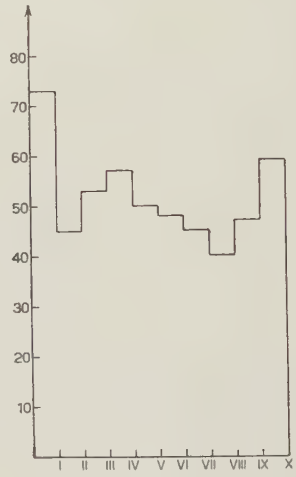

Fig. 7.

in the meridian zone with respect to the line of flight of the colliding nucleons. The number of events considered (441 tracks, 59 jets) is however too small for supporting this conclusion; the angular distribution can be considered isotropic within the limits of statistical fluctuations.

The angular distribution for the jets has been calculated also for normal jets, considering all the relativistic tracks forming with the incident primary, or with the jet axis in the case of a neutral primary, an angle smaller than 90° in the laboratory frame. The value of the energy introduced in the calculation, for the transformation of angular values from the laboratory frame to the C.M. frame, is obviously lower than in the case of the corresponding reduced jet. The resulting angular distribution is plotted in the diagram of Fig. 7.

From the comparison of Fig. 6 and Fig. 7, two maximums are noted in Fig. 7 at the utmost tenths of the solid angle. The explanation of these maximun can be easily given.

The increase in the number of tracks at the last tenth of the solid angle in Fig. 7 is due to the tracks which have not been considered in the reduced jets, because their angles with the axis of the jet were abnormally great with respect to the angles of the other tracks of the jet. In the transformation from the laboratory frame to the CM. frame, these tracks fall in the last tenth of the solid angle corresponding to a value of $\mathrm{tg}\,\vartheta'/2$ between $+3.00$ and $+\infty$.

Referring to the maximum at the first tenth of the solid angle, it is noted

hat the energy calculated for the jet appears in the formula for the transormation from the laboratory frame to the C.M. frame. Considering that, s previously observed, in the passage from the reduced jet to the normal et the value calculated for the energy increases, it can be easily inferred that ll the tracks that in the diagram relating to the reduced jet fall in the first enth of the solid angle, will fall also in the first tenth of the solid angle in he diagram relating to normal jets. Moreover, also some of the tracks that n the diagram for reduced jets fall in the second tenth of the solid angle will fall, due to the reduction in the energy value, in the first tenth of the diagram for normal jets. This explains the reason for which the number of tracks in the first tenth of the solid angle of the diagram of normal jets is greater than in the diagram for reduced jets.

* * *

I am indebted to Prof. G. WATAGHIN for his interest in this work and to Prof. G. LOVERA for his constant interest and useful discussion.

I would thank Prof. A. ROSTAGNI and Prof. N. DALLAPORTA for their kindness, by which I could use the data of the events found in the scanning of nuclear plates at the Padua Institute, and Prof. M. MERLIN for his work in development of the plates and in measurement of the jets.

RIASSUNTO

Si sono studiati 59 getti trovati nelle lastre nucleari nelle spedizioni di Cagliari del 1952 e 1953 e misurati in parte a Torino ed in parte a Padova. Studiando la distribuzione angolare delle tracce dei getti si è notato un allargamento nei getti in corrispondenza alle tracce estreme, allargamento che è stato attribuito a fenomeni secondari dopo la collisione primaria. Si è calcolato l'energia primaria ed il coefficiente di anelasticità dei getti, escludendo le tracce più allargate, considerate dovute a fenomeni secondari: i getti vengono in questo modo a dividersi in due categorie con valori medi del coefficiente di anelasticità corrispondenti rispettivamente a 0.52 e 0.18, eliminando l'incongruenza, trovata in calcoli precedenti di valori del coefficente di anelasticità superiori all'unità.

β-γ Angular Correlation of $^{214}_{83}$Bi.

F. Demichelis

Istituto di Fisica Sperimentale del Politecnico - Torino

L. A. Radicati

Istituto di Fisica dell'Università - Napoli

(ricevuto il 9 Novembre 1955)

Summary. — The angular correlation between the β-transition (2.56 MeV) originating from the ground state of $^{214}_{83}$Bi and the γ-ray (0.61 MeV) to the ground state of $^{214}_{84}$Po has been measured. From the knowledge of the log *ft* values of the two β-transitions (2.56 MeV and 3.17 MeV) originating from $^{214}_{83}$Bi and the measurement of the angular correlation coefficient, the value 2- is deduced for the spin and the parity of the ground state of $^{214}_{83}$Bi.

1. – Introduction.

The experimental data about spins, parities, β-decay transition probabilities and level schemes of the very heavy nuclei are still fairly incomplete. This makes it very difficult to test the predictions of the shell model in the region where the $2g_{9/2}$, $3d_{5/2}$, ... levels begin to be occupied, i.e. for the levels occurring after the magic number 126.

A very promising source of information for this region appears to be the study of the angular correlations between β- and γ-rays. This technique, though besets by many theoretical difficulties of interpretation, has already given many useful results.

A necessary condition for its application is the forbidden character of the β-transition, allowed transitions giving rise to an isotropical correlation. We expect many forbidden β-transitions to occur for nuclei with $70 < Z < 92$, $N > 112$. Indeed in this region, according to the shell model, the protons are expected to occupy the odd parity levels $1h_{11/2}$ and $1h_{9/2}$ whereas the neutrons

ıould fill a number of levels with even parity starting from the $1i_{13/2}$, so that ıe transitions should often involve a parity change.

We want to show in this paper how the β-γ angular correlation technique llows to assigne in an almost unique way the spin and the parity to the ground tate of $^{214}_{83}$Bi. A number of different assignements have been suggested recently. n his review article on β-transitions R. W. KING (1) concludes that the spin hould be $J = 1-$. N. FEATHER (2) discussing the internal conversion coef- icients of $^{214}_{83}$Bi suggests the value $J = 3-$.

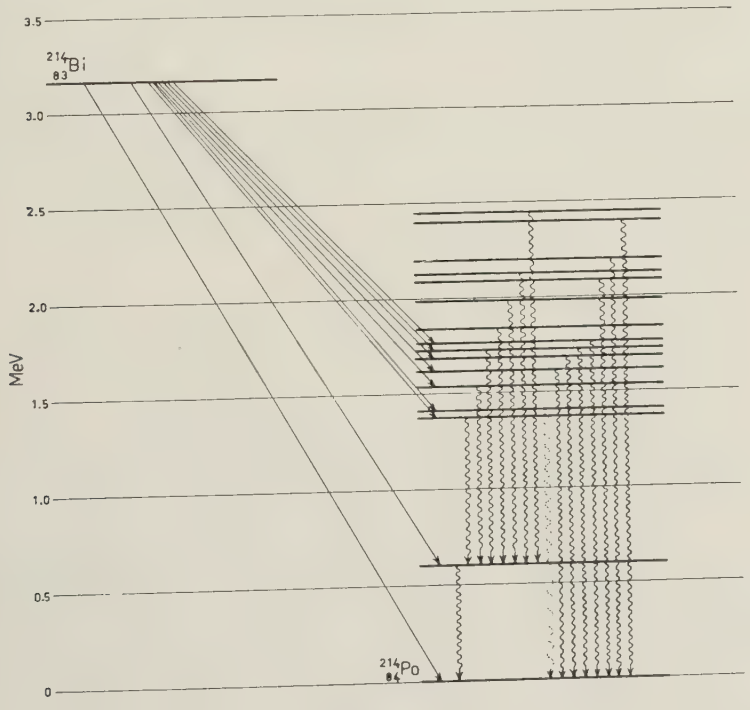

Fig. 1.

A third assignement, $J = 2-$ has been proposed by A. H. WAPSTRA (3) as a result of the analysis of the log *ft* values of the β-transitions originating from $^{214}_{83}$Bi.

$^{214}_{83}$Bi is known to decay by β^- emission to many levels of $^{214}_{84}$Po. Fig. 1

(1) R. W. KING: *Rev. Mod. Phys.*, **26**, 327 (1954).

(2) N. FEATHER: *Beta and gamma ray spectroscopy*. Edited by K. SIEGBAHN, p. 748 (Amsterdam, 1955).

(3) A. H. WAPSTRA: *Academisch Proeschrift*, (Amsterdam, 1953).

shows the level scheme of $^{214}_{84}$Po (1) and the β-transitions (5) originating from the ground state of $^{214}_{83}$Bi.

Since $^{214}_{84}$Po is an even-even nucleus its spin is assumed to be zero and the parity even.

The spin $J = 2+$ of the first excited level follows from the $E2$ (6) character of the γ-transition to the ground state.

Both the ground and the first excited state are reached by β-transitions whose log ft values (5) seem to indicate their first forbidden character. It is the purpose of the present paper to investigate the angular correlation between the 2.56 MeV β-ray to the level at 0.61 MeV of $^{214}_{84}$Po and the $E2$ γ-ray to the ground state.

We will show in section 3 that our angular correlation measurements, which are reported in section 2, can be interpreted in the more simple way by assuming that the β-transition is first forbidden and the ground state of $^{214}_{83}$Bi has $J = 2-$, in agreement with WAPSTRA's suggestion.

Finally we discuss the assignement $J = 2$ - from the point of view of the shell model theory.

1. – Experimental apparatus and results.

Fig. 2. shows the block diagram of the experimental set up.

R_1 and R_2 are the β- and γ-detectors respectively. For R_1 we use a stilbene crystal (thickness ≈ 3 mm, diameter ≈ 13 mm), for R_2 a NaI(Tl) crystal (thickness ≈ 20 mm, diameter ≈ 13 mm); for both a 6291 Du Mont photomultiplier.

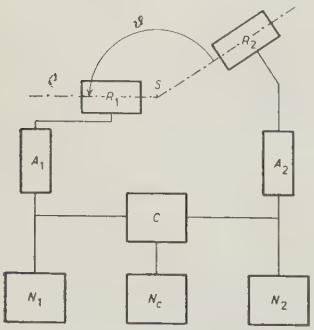

Fig. 2.

The output pulses from the photomultipliers are fed through two linear amplifiers A_1 and A_2 to the coincidence circuit C with a resolving time $\tau = 1.5 \cdot 10^{-7}$ s.

The pulses from A_1, A_2 and C are then counted by N_1, N_2, N_c respectively.

The source S is formed by a thin silver foil coated with $^{226}_{88}$Ra in equilibrium with its decay products.

An aluminium sheet (3 mm thick) placed

(1) F. DEMICHELIS and R. MALVANO: *Nuovo Cimento*, **12**, 407 (1954); R. E. ROWLAND: *Phys. Rev.*, **99**, 757 (1955).

(5) R. A. RICCI and G. TRIVERO: *Nuovo Cimento*, **2**, 745 (1955).

(6) M. MIWA and S. KAZEYAMA: *Journ. Phys. Soc. Japan*, **5**, 416 (1951); F. DEMICHELIS and R. MALVANO: *Phys. Rev.*, **93**, 526 (1954).

etween the source and the β-detector R_1 stops all the β-rays with energy less han 1.75 MeV. In the β-spectrum emitted by all the nuclei in equilibrium vith $^{226}_{88}$Ra only two β-rays are present whose end point energy is greater han the cut-off energy 1.75 MeV. They are the 2.56 and 3.17 MeV rays origi-nating from the ground state of $^{214}_{83}$Bi.

R_1 is, of course, sensitive not only to β- but also to γ-rays. It can be made ensitive only to γ-rays by placing in front of it a beryllium screen with a lensity of 1.63 g_m/cm^2 to eliminate all the β-rays.

A lead sheet (1 mm thick) is placed between the source and the γ-detector R_2 to stop all the β-rays present in the $^{226}_{88}$Ra source and to reduce the back-scattered Compton photons.

Lead shieldings were also placed on the sides of the detectors to avoid spurious coincidences due to the Compton photons scattered by the two crystals.

Let now n_t be the total coincidence rate counted by N_c without beryllium screen. n_t is given by

$$n_t = n_{\beta\gamma} + n_{\gamma\gamma} + n_s , \tag{1}$$

where: $n_{\beta\gamma}$ is the coincidence rate between the 2.56 MeV β-ray and the 0.61 MeV γ-ray.

$n_{\gamma\gamma}$ is the coincidence rate between any two γ-rays,

$n_s = 2\tau n_1 n_2$ is the accidental coincidence rate.

n_1 and n_2 are the counting rates of N_1 and N_2 respectively.

When the beryllium screen is placed in front of R_1 the total coincidence rate is

$$n_t' = n_{\gamma\gamma} + n_s' , \tag{2}$$

assuming the γ-γ coincidence rate to be unmodified by the presence of the beryllium screen. n_s' is again the accidental coincidence rate.

Combining (1) and (2) we get the β-γ coincidence rate

$$n_{\beta\gamma} = (n_t - n_s) + (n_t' - n_s') . \tag{3}$$

n_t and n_t' have been measured at $\vartheta = 90°$, 120°, 150°, 180°, ϑ being the angle between the two detectors.

For every value of ϑ a total of $\approx$ 15000 effective coincidences have been counted.

The γ-ray rate n_2 was found to be constant with ϑ within the stastitical errors.

The usual procedure (7) has been used to correct for the asymmetry of the γ-ray source, for the change with time of the detector efficiency and for the Compton scattered photons.

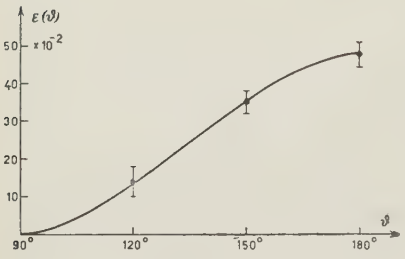

Fig. 3.

Fig. 3 shows the experimental points and their probable errors. We plot $\varepsilon(\vartheta) = (n_{e,\vartheta}/n_{e,90}) - 1 = W(\vartheta) - 1$ against ϑ, where $n_{e,\vartheta}$ and $n_{e,90}$ are the effective coincidence rates for the angles ϑ and 90° respectively.

The differential angular correlation curve has been obtained with the least square method.

3. – Discussion.

In this section we apply the theory of the β-γ angular correlation to determine the spin and the parity of $^{214}_{83}$Bi.

We shall give no detail of the theory (8) but will only quote the relevant formulae of BIEDENHARN and ROSE's paper.

From Fig. 3 we seen that the angular correlation function is of the type

$$W(\vartheta) = 1 + a \cos^2 \vartheta ,$$

where the anisotropy coefficient has the value $a = 0.47 \pm 0.03$.

Since a is different from zero it follows that the β-transition is at least first forbidden, allowed transitions giving rise to an isotropical correlation.

To find the order of forbiddeness one would need a knowledge of the spectrum shape. Lacking this information we can only rely on the value of $\log ft = 7.9$ which is of the order of magnitude one expects for first forbidden transitions (9).

That the order of forbiddeness is not higher that 1 can also be inferred from the fact that the correlation function contains no powers of $\cos \vartheta$ higher than two. Indeed according to a well known theorem (10) the maximum power ν of the $\cos \vartheta$ term must satisfy the three inequalities

$$0 \leqslant \nu \leqslant l_1$$
$$0 \leqslant \nu \leqslant J$$
$$0 \leqslant \nu \leqslant l_2$$

(7) D. T. STEVENSON and M. DEUTSCH: *Phys. Rev.*, **83**, 1202 (1951).

(8) D. L. FALKOFF and G. E. UHLENBECK: *Phys. Rev.*, **79**, 334 (1950); L. C. BIEDENHARN and M. E. ROSE: *Rev. Mod. Phys.*, **25**, 729 (1953).

(9) J. M. BLATT and V. F. WEISSKOPF: *Theoretical Nuclear Physics* (Wiley, 1952).

(10) C. N. YANG: *Phys. Rev.*, **74**, 764 (1948).

where l_1 and l_2 are the multipolarity of the β- and γ-radiations respectively, and J is the spin of the intermediate state. In our case $l_2 = 2$ and $J = 2$ therefore if also l_1 would be equal to 2 one would in general expect that the correlation function should contain a term proportional to $\cos^4 \vartheta$. We shall then base our analysis on the assumption that the transition is a first forbidden one.

The second assumption which we shall introduce is that the β-interaction contains only scalar, tensor and pseudoscalar terms. The exclusion of the vector and axialvector terms seems now well established by the empirical evidence on the shapes of first and second forbidden spectra ([11]).

It is now a straightforward matter to work out the anisotropy coefficient a for different choices of the β hamiltonian and for different spin and parity values of the initial state. This can be done by using the partial particles parameters b_ν for the β-radiation listed in Table X of BIEDENHARN and ROSE's paper. One must only note that the particles parameters are functions of the electron energy so that they must be averaged over the whole range of energies from the cut off energy $E_c = 4.43\ mc^2$, to the maximum energy $E_0 = 6.02\ mc^2$.

The partial parameters for the γ-radiation (A_ν in BIEDENHARN and ROSE's notations) are related to the functions F listed in Table I of BIEDENHARN and ROSE by formula (69a) of their paper.

The results of the calculations performed along these lines are summarized in Table I.

According to Table I only the pseudoscalar interaction is consistent with an even parity of the initial state.

TABLE I. – *Values of the anisotropy coefficient a* (*).

Interaction \ J	0	1	2	3	4	Parity of the initial state
$S \quad \lvert\int\beta\boldsymbol{r}\rvert^2$	0	0.30	— 0.25	0.08	0	odd
$T \quad \Sigma\lvert B^\beta_{ij}\rvert^2$	0	— 0.43	0.60	— 0.14	0	odd
$\lvert\int\beta\boldsymbol{\sigma}\wedge\boldsymbol{r}\rvert^2$	0	— 0.115	0.124	— 0.032	0	odd
$\lvert\int\beta\boldsymbol{\alpha}\rvert^2 + \lvert\int\beta\boldsymbol{\sigma}\wedge\boldsymbol{r}\rvert^2 + \lvert\int\beta\boldsymbol{\alpha}\rvert\,\lvert\int\beta\boldsymbol{\sigma}\wedge\boldsymbol{r}\rvert$	0	— 0.106	0.1135	— 0.031	0	odd
P	0	0.30	— 0.25	0.08	0	even

([11]) D. C. PEASLEE: *Phys. Rev.*, **91**, 1447 (1953).

(*) The notations for the interaction terms are the same as those used by BIEDENHARN and ROSE.

However the values for a predicted by the theory are in disagreement with the experimental value so that we must assume that the $^{214}_{83}$Bi has odd parity.

Another result which one gets immediately from Table I is that spins zero and four are excluded since they would give rise to an isotropic correlation. The choice is therefore restricted to $J = 1-$, $2-$, $3-$ and to the tensor and/or scalar interaction.

Clearly neither a pure scalar or tensor interaction can give a good fit of the experimental result.

We are then left with the possibility of mixing scalar and tensor terms. In this case the value of a is the sum of the contributions from the different operators plus those arising from the interference terms. The latter cannot be calculated a priori since they depend on the values of the matrix elements: a complete list of these interference terms has been given by M. MORITA ([12]).

It is however immediately evident that unless one assumes for the interference terms very high values, neither $J = 1$, nor $J = 3$ can fit the experimental value.

$J = 2$ on the other hand can give a good fit with very reasonable values of the interference terms.

The assignment $J = 2-$ to the ground state of $^{214}_{83}$Bi is consistent with the log ft value (log $ft = 7.9$) of the β-transition to the ground state of $^{214}_{84}$Po. It is indeed very plausible that this transition is also first forbidden. If this is the case one could exclude the assignment $J = 3-$ for $^{214}_{83}$Bi, since the final state has $J = 0+$. The values $J = 1$ or $J = 2$ are both consistent with the first forbidden character of the transition. Clearly a knowledge of the spectrum shape would be highly desirable to settle this point.

Finally we want to discuss briefly from the point of view of the shell model theory the assignment $J = 2-$ to the ground state of $^{214}_{83}$Bi.

$^{214}_{83}$Bi has 83 protons so that one expects the proton contribution to the total spin to be $j_p = 9/2$ (the odd proton being in the $1h_{9/2}$ orbital). The spin 9/2 of $^{209}_{83}$Bi fits indeed very well with this prediction.

Far less simple is to predict the neutron contribution to the total spin.

According to the Jensen-Mayer model one would expect that the five neutrons outside the closed shell should occupy the $2g_{9/2}$ orbital and that their spins would couple to $j_n = 9/2$.

The shell model thus predicts correctly the odd parity of $^{214}_{83}$Bi. As to the spin if one relys on NORDHEIM's ([13]) « strong-rule » one would expect that j_n and j_p couple to a total spin $J = |j_n - j_p| = 0$.

([12]) M. MORITA: *Prog. Theor. Phys.*, **10**, 363 (1953).
([13]) L. A. NORDHEIM: *Rev. Mod. Phys.*, **23**, 322 (1951).

Even assuming the general validity of Nordheim's rule and without questioning the value $j_p = 9/2$ there are at least two possible explanations for the disagreement between the value of the spin predicted by the shell model and the value which follows from our discussion.

The first would be to assume that the spins of the five neutrons do not couple to $j_n = 9/2$.

Indeed j_n can take all half integer values from 1/2 to 25/2 (with the exclusion of 23/2) and it is difficult to predict which of these values corresponds to the lowest energy.

An alternative explanation would be to assume that one of the neutrons has been raised to the $3d_{5/2}$ orbital giving a total neutron spin $j_n = 5/2$. Indeed the $3d_{5/2}$ orbital is close to the $2g_{9/2}$ and one cannot exclude that this orbital begins to be occupied before the $2g_{9/2}$ orbital has been filled.

As we mentioned in the introduction the experimental data in this region are still too scanty to test the predictions of the theory.

* * *

One of us (F.D.) is indebted to Consiglio Nazionale delle Ricerche for supporting this work; the same author wishes to thank Dr. Ing. G. Ruffino for his help in mounting and adjusting some electronic equipment.

The authors wish to thank Prof. E. Perucca for his kind interest.

RIASSUNTO

Si è proceduto alla misura della correlazione angolare differenziale tra la transizione β (energia 2.56 MeV) dallo stato fondamentale del $^{214}_{83}$Bi al primo stato eccitato del $^{214}_{84}$Po e il raggio γ (energia 0.61 MeV) dal primo stato eccitato allo stato fondamentale del $^{214}_{84}$Po. In base ai valori del log *ft* di tale transizione e del log *ft* della transizione β dallo stato fondamentale del $^{214}_{83}$Bi allo stato fondamentale del $^{214}_{84}$Po e al coefficiente di anisotropia della correlazione angolare sperimentalmente determinato si sono dedotti il valore del momento angolare e la parità dello stato fondamentale del $^{214}_{83}$Bi.

Excitation of Nuclei by Absortion of π^--Mesons - III (*).

A. Tomasini

Istituto di Fisica dell'Università - Bologna

Istituto Nazionale di Fisica Nucleare - Sezione di Padova

(ricevuto il 9 Novembre 1955)

Summary. — The results of two previous papers by Puppi *et al.* (*) are revised here. In those papers the authors examine the problem of the excitation of a medium heavy nucleus by a bound π^--meson. They assume that the pion is absorbed by a nucleon pair; the subsequent disintegration is described as a two step process: a direct emission followed from an evaporation. In the present paper the evaporation process is revised, using a more refined formula. Level densities obtained from disintegration experiments are used; it is shown that the recoil of the nucleus is not negligible in the emission of α-particles; values of level densities differentiated for α-particles and nucleons are used. The results obtained in the case of absorption by a neutron-proton pair are in good agreement with experimental data. It is concluded that the bound π^- are absorbed by neutron-proton pairs; other modes of absorption (by proton-proton pairs or by other nucleon groupings) seem to be quite improbable.

1. – Introduction.

In two previous papers Puppi *et al.* (*) have investigated the problem of the excitation of a medium heavy nucleus by the capture of π^--meson, bound in the lowest orbit of a mesic atom, and of the subsequent disintegration of the nucleus.

(*) The first two parts of this work are:
I: G. Puppi, V. de Sabbata and E. Manaresi: *Nuovo Cimento*, **9**, 726 (1952);
II: V. de Sabbata, E. Manaresi and G. Puppi: *Nuovo Cimento*, **10**, 1704 (1953): the latter referred to in the text as II.

The pion is assumed to be bound only by Coulomb forces, neglecting perturbations due to nuclear force; so it is described by a usual Schrödinger function. The potential used is the Thomson one; i.e. the charge density is assumed to be constant in the nucleus and to fall suddendly to zero at the surface; this is clearly a crude approximation and is used because of its simplicity and because we have only rough indications on the true charge distribution in the nucleus. It must be pointed out that any other model we can use gives at the surface of the nucleus a Coulomb barrier lower than the Thomson one. The authors have assumed that, because of the short range of nuclear forces, the pion is absorbed in a well defined point of the nucleus by a pairs of nucleons; clearly the relative probability of absorption of the various points of the nucleus is obtained from the wave function of the pion.

For the purpose of detailed calculations they describe the nucleus by an ideal Fermi gas; in this model the interactions between the nucleons are substituted by a potential well; because of the Pauli principle the nucleons move freely in the well, supposing the nucleus to be in the ground state. When the two fast nucleons, which absorbed the pion, cross the nuclear matter, they interact with the other nucleons: the scheme of these interactions is substantially GOLDBERGER's scheme (1). For the coherence of the model the interactions may be described in the same fashion as with free nucleons: i.e. the process is treated as a succession of two body interactions, in which cross-sections obtained in neutron-proton and proton-proton scattering are assumed to be valid. The main effect of the coexistence of the nucleons in the nucleus is due to the Pauli principle, which, by taking into account the levels occupied from the remanent nucleons, forbids some collisions. In this way the two fast nucleons give rise to two little showers of nucleons; someones of the shower nucleons, once arrived at the surface of the nucleus, escape immediately, and it is assumed that the remaning ones spread their energy on the whole nucleus.

Now we have an excited nucleus in which no one of the nucleons have sufficient energy for escaping immediately; so the subsequent disintegration is described by an evaporation.

Two cases are investigated: absorption by a neutron-proton pair, and by a proton-proton pair; the results obtained are satisfactory in the first case, whereas they disagree entirely with the experimental data in the second case. However, also in the first case, there are some discrepancies as to the percentage of the nuclei non-emitting charged particles. It would be interesting to establish whether such discrepancies are due to some wrong assmuption on the capture process, or to the crudeness of the model used to describe the disintegration.

It may be useful to find out—and this is what we aim at in this paper—

(1) M. L. GOLDBERGER: *Phys. Rev.*, **74**, 1269 (1948).

how the results are changed for the evaporation phase by using parameters different from those used in II, and by taking into account some effects neglected in II. We must take into account also that, at present, our knowledge of the matter is much wider.

2. – Experimental results.

Experiments ([2,3]) have been made to determine, with radiochemical methods, the percentage of the various residual nuclei of the disintegration. The results show remarkable errors because not all the residual nuclei are detectable, some being stable. We have very poor statistics of residual nuclei in the calculations of II (on the whole 200 nuclei in the N-P case and 144 in the P-P one) and the most reliable comparison is that in which are taken into account all the nuclei having the same atomic number. Table I shows the comparison, Z being the atomic number of the starting nucleus. The N-P case shows a better agreement but nevertheless not a good enough one.

TABLE I.

	Montecarlo method		Experimental results		
	N-P capture	P-P capture	Br ([a])	I ([b])	([c])
$Z-1$	24	6.5	34	58	42
$Z-2$	35	46	31	22	28
$Z-3$	23	28	21	11	17.5
$Z-4$	17	12	7	3	5.5
$Z-5$	1	5.5	<3	0.7	<2
$Z-6$	—	2		0.1	

([a]) Reference ([2]). ([b]) Reference ([3]). (c) Average Ag-Br (Ag interpolated).

A doubt remains as to the possibility of making a direct comparison between the experimental results and those of II. In fact the experiments have been made by absorbing completely π^- of various energies into the examined substances. The energy of the pions is 122 MeV in the experiments in Bromine, and we can calculate that $\sim 20 \div 30\,\%$ of π^- are captured before going to rest. The percentages of stars of various prongs do not change greatly according to the increasing of the energies, and consequently the total variations will not be higher than some percents. Anyhow we get a percentage of $Z-1$ nuclei a little smaller than that we would get with bound π^- only.

([2]) T. T. SUGIHARA and W. F. LIBBY: *Phys. Rev.*, **88**, 587 (1952).
([3]) L. WINSBERG: *Phys. Rev.*, **95**, 198 (1954).

Another effect we have to take into account is that of secondary reactions produced by neutrons released in the disintegrations. In the Bromine experiment the given data have been slightly corrected according to such effect; the authors, however, do not give the value of that correction. Every capture gives, as an average, $5 \div 6$ neutrons. Most of them have an energy smaller than 20 MeV and produce reactions emitting neutrons only, and creating nuclei with unchanged Z, which do not appear in the statistics. Less than one neutron per capture has energy higher than 20 MeV. Of those, fewer than $6 \div 7\%$ give secondary reactions emitting charged particles (we must remember that most of them escape without interacting); so the net effect is small. The influence of the secondary reactions is to increase the percentage of Z 1 nuclei up to a number higher than that reached only with π^- reactions. The two effects are therefore opposite and probably balance each other. On the whole, we may say that the variations they make are certainly smaller than the experimental errors.

The number of Z - 1 nuclei in the Iodine experiment is much higher than in the Bromine one, and probably this is not due only to the effect of the increase of the Coulomb barrier, but also to a different level density in the two cases. In fact it was found experimentally that the density of energy levels of the nuclei with a number of neutrons equal to a magic number plus one [4] or minus one [5], or Z magic [4] is far smaller than the average density. Perhaps such decrease happens also in nuclei with $Z = Z_{\text{magic}} \pm 1$. So at least the nuclei with $Z = 50$ and probably also those with $Z = 51$, and 49 have a level density smaller than the average one. The Iodine has $Z = 53$, and by absorbing a π^- produces a nucleus with $Z = 52$. The probability of emission being proportional to the level density of the final nucleus, in this case we shall have an emission of charged particles smaller than average. We have not tried to take into account quantitatively this effect, but we must point out that the estimate 42% assigned to nuclei with $Z - 1$ is probably an upper limit.

The charge exchange $\pi^- + \mathrm{P} \rightarrow \mathrm{N} + \pi^0$ is probably a process of production of Z - 1 nuclei. In Iodine the nucleus produced in this way would be ^{127}Te, and from the experimental results such nucleus appears to be produced in $\sim 1\%$ of the cases, and this process is therefore negligible.

Recent results of VANDERHAEGHE *et al.* [6] in photographic emulsions, give a number of stars without prongs of 35%, with no discrimination between light and heavy nuclei: in heavy nuclei the percentage will be higher than 40%.

---

[4] D. J. HUGHES, R. C. GARTH and J. G. LEVIN: *Phys. Rev.*, **91**, 1423 (1953).

[5] A. TOMASINI: *Nuovo Cimento*, **12**, 134 (1954).

[6] G. VANDERHAEGHE and M. DEMEUR: in press (see also the *Proceedings of the Pisa Conference on elementary particles*).

From experiments with residual nuclei we get a medium charge 1.7 per star (except stars without prongs); this estimate agrees with the data in emulsion of Bologna [7] (1.8) and Bruxelles [6] (1.7), whereas disagrees with the data of MENON *et al.* [8] (2.2). From the results in residual nuclei [2,3], we get a medium number ~ 5.7 of neutrons emitted per star; in II including also the neutrons in α-particles, we have 5.1 in the N-P case and 4.6 in the P-P one.

V. T. COCCONI *et al.* [9] have estimated the mean number of neutrons emitted by various elements with energy smaller than 15 MeV; by interpolation, we get ~ 4.7 for the average Ag-Br. In II we get 3,4 in the N-P case and 3,1 in the P-P one.

3. – Revision of the evaporation.

The formula used in II for the evaporation is

$$W(\varepsilon)\,\mathrm{d}\varepsilon = \text{const}\; mgT(\varepsilon)\varepsilon \exp\left[2\sqrt{a}\sqrt{E-\varepsilon-B}\right]\mathrm{d}\varepsilon\,,$$

i.e. substantially the Weisskopf formula [10]. m and g are the mass and the weight of spin states of the emitted particle; $T(\varepsilon)$ is the transmission coefficient on the surface of the nucleus; B the separation energy of the evaporated particle; the parameter a has been drawn by interpolation of the estimates found by WEISSKOPF [10]: we get $a \sim 3$ MeV^{-1} for Bromine, and ~ 6 MeV^{-1} for Silver. Recently estimates of a have been drawn from the energy spectrum of the emitted neutrons in nuclear reactions [5]; although the esperiments have been made at $14 \div 16$ MeV, we have estimates of a for excitation energies of $2 \div 3$ MeV. The estimates which can be made are 7 MeV^{-1} for Br and 9 MeV^{-1} for Ag; but as a probably decreases with the excitation energy, the estimates 6 MeV^{-1} for Br and 8 MeV^{-1} for Ag have been used here. An increase of a gives a larger probability of emission of the particles of low energy and so increases the number of neutrons and diminishes the number of charged particles.

A decrease in the probability P_α for α emission is due to the recoil of the nucleus. Considering this fact, in order to obtain the evaporation formula we say [11]: let a nucleus A, with an excitation energy E_A, emit a particle b of mass m, leaving a residual nucleus B of mass M with excitation energy E_B.

---

[7] Part II of this work.

[8] M. G. K. MENON, H. MUIRHEAD and O. ROCHAT: *Phil. Mag.*, **41**, 583 (1950).

[9] V. T. COCCONI and D. A. EDWARDS: *Phys. Rev.*, **88**, 145 (1952).

[10] I. M. BLATT and V. F. WEISSKOPF: *Theoretical Nuclear Physics* (1952).

[11] For the discussion of statistical factors see: V. WEISSKOPF: *Phys. Rev.*, **52**, 295 (1937).

If $W_c(\varepsilon)$ and $\sigma_c(\varepsilon)$ are the probability for unit time and the cross-section for the inverse process, v_r the relative velocity of b and B, ε and ε_B the energies, in the center of mass, of b and B, we have:

$$W_c(\varepsilon) = \frac{\sigma_c(\varepsilon)}{\Omega} v_r = \frac{\sigma_c(\varepsilon)}{\Omega} \sqrt{\frac{2\varepsilon}{m}} \left(1 + \frac{m}{M}\right),$$

where Ω is a volume enclosing b and B. The probability of emission for unit time and unitary interval of energy is:

$$W_b(\varepsilon)\mathrm{d}\varepsilon \cong W_c(\varepsilon) \frac{\omega_B(E_B)}{\omega_A(E_A)} \frac{\Omega g m}{2\pi^2\hbar} (2m\varepsilon)^{\frac{1}{2}}\mathrm{d}\varepsilon\,,$$

with $\omega_A(E_A)$ and $\omega_B(E_B)$ densities of levels of A and B, g weight of spin states of b. Putting

$$\omega(E) = c \exp\left[2\sqrt{aE}\right]$$

and being $E_B = E_A - \varepsilon - \varepsilon_B - B_b$, we have:

$$W_b(\varepsilon)\mathrm{d}\varepsilon \cong \text{const. } mg\sigma_c(\varepsilon)\varepsilon \exp\left[2\sqrt{a}\sqrt{E_A - \varepsilon\left(1 + \frac{m}{M}\right) - B_b}\right].$$

The effect is negligible, in heavy nuclei, for single nucleons, but it is remarkable for α-particles. For an average energy of emission we find that P_α must be multiplied for the factors shown in Table II.

TABLE II.

E_A (MeV)	30	50	100	150
Br	0.55	0.71	0.79	0.83
Ag	0.61	0.75	0.82	0.86

We get further decrease of P_α if we consider that the emission of an α-particle produces a nucleus lighter than the emission of a nucleon. As a is an increasing function of the mass number, we shall have $a_\alpha < a_N \sim a_p$ which makes a noticeable decrease of P_α [12] for great excitation energies. We can evaluate that P_α must be multiplied for the coefficients given in Table III.

TABLE III.

E_A (MeV)	30	60	100	150
Br	0.78	0.65	0.49	0.40
Ag	0.81	0.68	0.54	0.45

[12] K. J. LE COUTEUR: *Proc. Phys. Soc. London*, A **73**, 259 (1950).

4. – Results.

We have remade the calculations of the evaporation with the formulas obtained with previous considerations, by Montecarlo method, starting from the residual nuclei of the direct emission obtained in II. The Tables IV, V, VI give the results we obtained. In the P-P case the disagreement is again great. In the N-P case there is a good improvement as to the number of $Z - 1$ nuclei: the percentage of stars with various prongs are in better agreement with the experimental data; also improved is the agreement as to the number of emitted neutrons; these results would be still improved if we would use greater a.

The ratio α/P disagrees entirely. In the last years many experimental results have shown that the crude model used in the two step process is not satisfactory as regard the emission of α-particles: PAUL *et al.* ([13]) measuring the cross-section for α production with neutrons of 14 MeV, have found in the heavy nuclei values much greater than those which one could expect as a result of a true evaporation; measures by HODGSON *et al.* ([14]) of the angular distribution of α emitted in nuclear disintegrations produced by protons of various energies (from 50 to 450 MeV) show a remarkable forward-backward anisotropy. Therefore it seems that the low ratio α/P found, must not be attributed to a wrong description of the absorption of the pions, but to the crudeness of the description of the disintegration.

The average charge per star (not including stars without prongs) is 1.6 in the N-P case and 1.55 in the P-P one. The energy spectra of emitted particles are substantially the same as in II.

TABLE IV. – *Residual nuclei: statistics for atomic number, Z being the atomic number of the starting nucleus.*

	Montecarlo method		Experimental result		
	N-P capture	P-P capture	Br ([a])	I ([b])	([c])
$Z - 1$	32	7.6	34	58	42
$Z - 2$	39.5	57	31	22	28
$Z - 3$	18.5	24.9	21	11	17.5
$Z - 4$	8	8.3	7	3	5.5
$Z - 5$	1.5	2.2	< 3	0.7	< 2
$Z - 6$	1	—		0.1	

([a]) Reference ([2]). ([b]) Reference ([3]). ([c]) Average Ag-Br (Ag interpolated).

([13]) E. B. PAUL and R. L. CLARKE: *Can. Journ. Phys.*, **31**, 267 (1953).

([14]) P. E. HODGSON, M. GRILLI, M. LADU and B. VITALE: *Nuovo Cimento*, **1**, 314 (1955).

TABLE V. – *Percentage distribution in prongs, without zero prong stars.*

	Montecarlo method		Experimental results		
Number of prongs	N-P capture	P-P capture	*a*	*b*	*c*
1	63	60.9	65	66.2	50.0
2	27	33.8	23.5	27.3	33.3
3	9	4.5	10	6.1	7.4
4	1	0.8	1.5	0.2	7.4
5	—	—	0.4	—	1.9

(*a*) Part II of this work. (*b*) Reference (6). (*c*) Reference (4).

TABLE VI. – *Particles emitted in one capture.*

	Montecarlo method		Experimental results		
	N-P capture	P-P capture	*a*	*b*	*c*
α	0.085	0.09	—	—	—
P	0.92	1.25	—	—	—
α/P	0.09	0.07	0.30 ± 0.04	—	—
N (energy < 15 MeV)	3.9	3.7	—	~ 4.7	—
N (including those in α-particles	5.2	4.9	—	—	~ 5.7
d	18.4	45.5	21.4 ± 2.5		

(*a*) Reference (4). (*b*) Reference (6). (*c*) References (2,3): 5.7 is an average value.
(*d*) Particles of charge $|e|$ and energy > 30 MeV. % without zero prongs stars.

5. – Conclusions.

If we use suitable values of the densities of levels, such as those obtained in the disintegration experiments (5), if we take into account the recoil of the nucleus, and use values of *a* differentiated for α-particles and nucleons (12), we will be able to improve the agreement with the experimental results, with respect to II, as to the number of neutrons emitted, the percentages of stars of various prongs and the percentages of residual Z; on the other hand the ratio α/P is worsen. The last result may be due to a deficiency of the model used for the description of the α emission. Considering the statistical and experimental errors, the results are very good in the case of the absorption by neutron-proton pairs, whereas they remain unsatisfactory in the case of absorption by two protons.

It would be possible, by changing again the parameter a and modifying the transmission coefficient, as has been done in II, to obtain an even better agreement and to establish the maximum percentage of absorption by a proton-proton pair, compatible with experimental data. However in this case it would be necessary to revise the whole behaviour of the process, where some approximation was made which has surely modified the results (e.g. the wave function of the pion is supposed to be completely contained in the nucleus; the nucleus is described from an ideal Fermi gas with constant density, without taking into account the diminution of density near the surface). It does not seem that at present calculations refined in this way are useful, because experimental results have great errors and, as it was pointed before, the model used for the disintegration is certainly crude, at least for emission of α-particles, and perhaps of other fragments (deuterons, tritons and so on).

Anyhow from the results obtained we can conclude that absorption from a neutron-proton pair is preeminent; absorption by two protons is improbable. Absorption by groupings with a number of nucleons greater than two seems to be negligible; in fact the sharing of the rest energy of the pion on many nucleons would decrease the percentage of high energy particles, and by increasing, the energy in the evaporation, it would decrease the number of nuclei in which charged particles are not emitted.

* * *

I wish to thank Prof. PUPPI for many advices and discussions.

RIASSUNTO

Sono riveduti i risultati di due lavori precedenti di PUPPI *et al.* (*). In quei lavori gli autori esaminano il problema dell'eccitazione di un nucleo medio pesante da parte di un mesone π^- legato. Supposto che il pione sia assorbito da una coppia di nucleoni, la successiva disintegrazione viene descritta con un processo in due stadi: una emissione diretta seguita da una evaporazione. Nel presente lavoro è riveduto il processo di evaporazione, usando una formula più precisa. Vengono usate densità dei livelli ottenute da esperienze di disintegrazione; si mostra che il rinculo del nucleo non è trascurabile nella emissione di particelle α; sono usati valori delle densità dei livelli differenti per particelle α e nucleoni. I risultati ottenuti nel caso di assorbimento da una coppia neutrone-protone sono in buon accordo con i dati sperimentali. Si conclude che i π^- legati sono assorbiti da coppie neutrone-protone; altri modi di assorbimento (da coppie protone-protone o da altri gruppi di nucleoni) sembrano essere del tutto improbabili.

IL NUOVO CIMENTO Vol. III, N. 1 1° Gennaio 1956

On the Spin and Parity of the τ-Meson.

G. Costa and L. Taffara

Istituto di Fisica dell'Università - Padova
Istituto Nazionale di Fisica Nucleare - Sezione di Padova

(ricevuto il 10 Novembre 1955)

Summary. — The angular distributions of the secondaries of the τ-meson have been calculated for eight combinations of spin and parity, using the hypothesis accepted untill now about the type of interaction. Comparing these distributions with the experimental data, one finds a satisfactory agreement for the cases of even spin and odd parity, especially for the $[0, -]$ case.

1. – Introduction.

The determination of spin and parity of heavy unstable particles represents, at present, one of the main objectives for the understanding of these states of matter. In fact, it strongly influences every rigorous formulation of the interactions in which these particles are produced or absorbed. Moreover, it is very important as a criterion for deciding if the various modes of decay of those K-mesons, which have been observed, represent several particles which may be considered as intrinsecally different (i.e. with different values of spin and parity) or the different decay modes of the same particle.

Amongst the unstable particles presently known, only in the case of the τ-meson does it seem possible to obtain some information about these essential internal parameters: since the three secondaries are all charged, it is possible to determinate experimentally all the energy and angular distributions in such a three-body decay: so that, if one makes a comparison with the corresponding theoretical distributions, calculated separately for various values of spin and parity, one might decide the values of these internal parameters. For this reason the τ-meson has been occupying a privileged position amongst the unstable particles, and several works have been already devoted to the subject.

In a previous work, when the experimental techniques did not permit the determination of the sign of the charged secondaries, DALITZ [1], considering these particles as indistinguishable, analyzed the kinematics of the τ-meson decay. For this purpose, he used a bidimensional representation in which the configuration for any τ-event was given as a point on a plane surface: an eventual uniformity of the point distribution would then indicate the pseudoscalar nature of the τ-meson. He also calculated the energy spectra corresponding to several combinations of spin and parity, but the results were relatively insensitive to the variation of these parameters and the poor experimental statistics then available did not allow to draw any definite conclusions. Later, when the technique of nuclear emulsions had progressed sufficiently, it was possible to establish the signs of secondaries of the τ-mesons which were thus found to be positively charged, i.e. τ^+. DALITZ then, in a second work [2], took the sign of the charge in consideration, and obtained the result that, in this case, the energy distribution of the unlike meson was much more sensitive to variations of spin and parity than in the case when the charges were unknown; and thus it was hoped to arrive at the determination of these parameters. A similar study was made by FABRI [3]: he divided the theoretical results concerning the energy distributions of unlike mesons in a way which was more suitable for comparison with the experimental distributions obtained from the very poor statistics at that time available. In this way it was possible to exclude some combinations of spin and parity of the τ-meson.

In the above mentioned works, the energy distributions only have been explicitly calculated; moreover, the calculations have been made for the five simplest cases, i.e. $[0, -]$, $[1, +]$, $[1, -]$, $[2, +]$ and $[3, -]$. Recently, experimental results have shown a notable increase and DALITZ [4], basing his arguments on the low energy part of the spectrum of the negative secondaries, has concluded that probably the only possible cases for the τ-meson are even spin and odd parity, i.e. $[0, -]$, $[2, -]$, $[4, -]$, $[6, -]$ if one considers that low values of the spin are the most probable.

However, the energy distributions of unlike secondaries presented by AMALDI [5] at the Pisa Conference, show a very similar behaviour for these four combinations; so that, at present, experimental evidence is still not sufficiently abundant to allow us to discriminate between these four possibilities

[1] R. H. DALITZ: *Phil. Mag.*, **44**, 1068 (1953).
[2] R. H. DALITZ: *Phys. Rev.*, **94**, 1046 (1954).
[3] E. FABRI: *Nuovo Cimento*, **11**, 479 (1954).
[4] R. H. DALITZ: *Proceedings of the Fifth Rochester Conference* (1955).
[5] E. AMALDI: *Proceeding of the Pisa Conference*, in *Suppl. Nuovo Cimento* (in press) (1955).

in this way. We have thus looked to see if some other criterion would enable us to do this, and we have examined the angular distributions, which untill now have not been considered at least as far as we know. This calculation is the aim of this work.

In what follows we will first discuss the physical hypothesis on which this work is based; then the method of calculating the matrix elements and the distributions of the secondaries; and finally we will discuss the conclusions that one can draw concerning the spin and the parity of the τ-meson, taking into account the results relative to the energy distributions and making use of the latest experimental data.

2. – Evaluation of the matrix element.

As in the preceeding works, the calculation of the decay probability of the τ-meson in a given energetic and angular configuration, was made to a first approximation, by means of the well known formula:

$$w = \frac{2\pi}{\hbar} |H|^2 \varrho, \tag{1}$$

where H represents the matrix element and ϱ the statistical weight of the considered configuration. We will briefly describe the way in which these quantities have been calculated. As in the works already cited, we indicate with p the relative momentum of the two positive π-mesons, with p' the momentum of the unlike meson relative to the center of mass system of the two like ones and with ϑ the angle between p and p'. Clearly a knowledge of these three parameters (interconnected by energy and momentum conservation theorems), allows us to determine the configuration of the secondaries of a given event.

The general expression of the matrix element, as a function of these three variables, was given by DALITZ and FABRI and, in the form used by FABRI, is:

$$F(p, \vartheta) = \sum_j \Big| \sum_{ll'} c_{ll'}(p) s^{(l,l')}_{J,0,j} \left\{ (2l+1)(2l'+1) \frac{(l'-|j|)!}{(l'+|j|)!} \right\}^{\frac{1}{2}} P^{|j|}_{l'}(\cos\vartheta) \Big|^2 \tag{2}$$

In (2) l, l' denote the angular momenta of the secondaries, J the spin of the τ-meson; j its orientation in space (i.e. its component in the direction l) and $s^{(l,l')}_{J,0,j}$ are the Clebsch-Gordon coefficients.

The coefficients $c_{l,l'}(p)$ represent the transition probabilities between the initial and final states of the decay process and are expressed in the form:

$$c_{l,l'}(p) = a \int \mathrm{d}\boldsymbol{r}\,\mathrm{d}\boldsymbol{r}' f_{l,l'}(r, r') j_l(pr) j_{l'}(p'r') \,. \tag{3}$$

In (3) are contained the radial part of the eigenfunction of the final state and the function $f_{l,l'}(r, r')$ which contains the eigenfunction of initial state and the Hamiltonian of interaction, which are, at present, unknown. The summation in (2) is made over those pair of values l, l' permitted by the conservation theorems of angular momentum and parity.

The expression (2) is exact, but it is obvious that, owing to the unknown elements of the $c_{l,l'}$ coefficients, we can only make an evaluation in a approximate way.

DALITZ and FABRI have fully discussed this approximation and its meaning; we give here a short summary:

a) The function $f_{l,l'}(r, r')$ which contains the initial eigenfunction and the interaction between π- and τ-meson, is considered to be dependent only on the relative distance of the pions and rapidly decreasing as this distance increases (it is practically equal to zero at distance larger than the λ of the τ-meson). This is, at present, the most natural hypothesis one can make.

Moreover, one supposes that this function does not depend in a sensitive way on l and l': this, perhaps, is the most critical point of the hypothesis. If the interaction should prove to be strongly dependent on the values of the final angular momentum, then probably all the conclusions obtained in the preceeding and in the present work would have to be corrected.

b) The Coulomb interaction between the particles considered in the reaction is ignored. We justify this hypothesis by means of the following considerations: the energy of two charged pions, at a distance equal to the range of the nuclear forces (i.e. in a region in which these forces are comparable with the Coulomb interaction) is of the order of one MeV. For this reason, the corrections will only influence a small part of the spectra and it will be probably sufficient to consider that the number of negative pions with energy less than $5 \div 10$ MeV is a little greater than that calculated without the Coulomb interaction. However, as some important arguments for the deduction of spin and parity are based on the behaviour of the energy spectra of secondaries in the region of low energy, it might be advisable to consider this part in a little more detail.

c) Finally, a purely mathematical semplification consists in approximating the Bessel functions of (3) with the first term of their series expansion. This is justifyable because $p \cdot r$ and $p' \cdot r'$ are respectively much smaller than l and l'.

Using these approximations one obtains for the expression for the coefficient $c_{l,l'}$:

$$(4) \qquad c_{l,l'}(p) = A \cdot \frac{\chi_{l+l'}}{(l+l'+1)!!} \left(\frac{m}{M}\right)^{l+l'} \frac{(l-1)!!}{(2l+1)!!} \frac{(l'-1)!!}{(2l'-1)!!} \left(\frac{p}{m}\right)^{l} \cdot \left(\frac{p'}{m}\right)^{l'}$$

It is clear that, the Q-value of the τ-meson decay being small, the terms (p/m) result also small, so that the coefficients are strongly decreasing with the increase of $l+l'$. The values of these pairs are then limited to those reported in Table I:

TABLE I. – *Pairs* (l, l') *with minimum* $l+l'$.

$[J, P]$	(l, l')
$[0, -]$	$(0, 0)$
$[1, +]$	$(0, 1)$
$[1, -]$	$(2, 2)$
$[2, +]$	$(2, 1)$
$[2, -]$	$(0, 2)$; $(2, 0)$
$[3, -]$	$(2, 2)$
$[4, -]$	$(0, 4)$; $(2, 2)$; $(4, 0)$
$[6, -]$	$(0, 6)$; $(2, 4)$; $(4, 2)$; $(6, 0)$

As one can see, in five cases (i.e. those already studied by different authors) the summation over l and l' which appears in (2) reduces to one term only: the calculation of the coefficients $c_{l,l'}$ therefore becomes useless. In the other cases, for which we have to consider more terms in the summation, one cannot avoid introducing these coefficients and therefore these cases are the most sensitive to the preceeding hypotheses.

In Table II we give the matrix elements which we have used to obtain the different distributions, combining those already calculated with the three cases considered by us in the present work.

TABLE II.

Spin	Matrix elements
$[0, -]$	1
$[1, +]$	p'^2
$[1, -]$	$p^4 p'^4 \sin^2\vartheta \cos^2\vartheta$
$[2, +]$	$p^4 p'^2 \sin^2\vartheta$
$[2, -]$	$p^4 + p'^4 + p^2 p'^2(3\cos^2\vartheta - 1)$
$[3, -]$	$p^4 p'^4 \sin^2\vartheta(5 + 3\cos^2\vartheta)$
$[4, -]$	$p^8 + p'^8 + 3.012(p^6 p'^2 + p^2 p'^6)(3\cos^2\vartheta - 1) +$ $+ p^4 p'^4(9.317\cos^4\vartheta - 4.098\cos^2\vartheta + 5.853)$
$[6, -]$	$p^{12} + p'^{12} + 5.125(p^{10} p'^2 + p^2 p'^{10})(3\cos^2\vartheta - 1) +$ $+ (p^8 p'^4 + p^4 p'^8)(44.835\cos^4\vartheta - 28.794\cos^2\vartheta + 16.455) +$ $+ p^6 p'^6(28.875\cos^6\vartheta - 39.375\cos^4\vartheta + 13.125\cos^2\vartheta - 0.625)$

3. – Distributions of the secondaries.

For the calculation of the statistical weights which appear in (1), we have used the representation of DALITZ (also used by FABRI) which consists in identifying each τ-event with a point in an equilateral triangle; the distances from the sides being proportional to the kinetic energies of the three secondaries.

Assuming a system of cartesian coordinates (x, y) with the origin in the center of the triangle and the x-axis in the direction of one of its perpendiculars (as one can see in Fig. 1), we obtain for the three kinetic energies which are expressed, for simplicity, in unities $Q/3$:

$$\begin{cases} E_1 = 1 - \frac{1}{2}(x + \sqrt{3}y) \\ E_2 = 1 - \frac{1}{2}(x - \sqrt{3}y) \\ E_3 = 1 + x\,. \end{cases} \tag{5}$$

The statistical weight of each configuration then is directly proportional to the area $dx \cdot dy$ around the point P.

a) Since our aim is to calculate the angular distributions of the secondaries, we have determined the locus of the points which represent τ-events with the same angle between the two π^+, by considering E_3 as the energy of the π^- and using the theorems of conservation of momentum and energy. One sees that the loci relative to 0° and 180°, as limiting cases, are coincident with the curve which bounds the region of triangle corresponding to events compatible with the theorems of conservation. This is a circle in the classical approximation and a curve of the third degree in the relativistic approximation; for the intermediate angle one obtains respectively

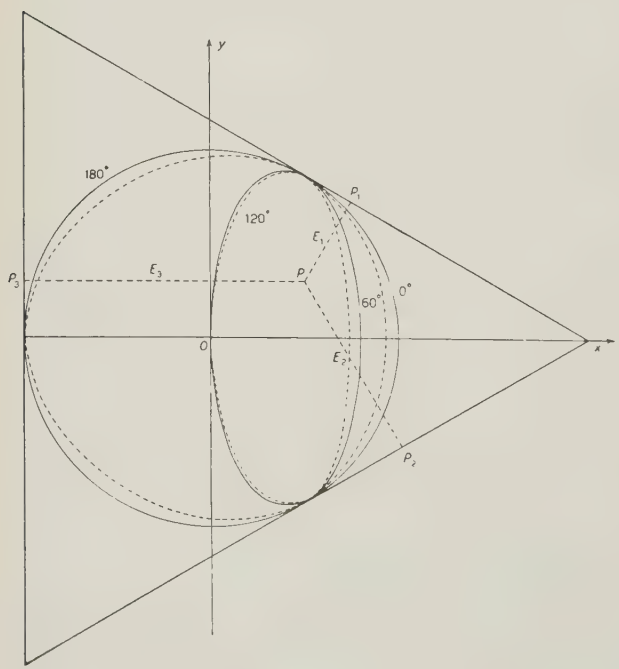

Fig. 1.

ellipses and curves of the fourth degree. The curves are represented in Fig. 1: with full and dotted lines respectively for classical and relativistic cases.

We have only determined the loci corresponding to angles 0°, 60°, 120° and 180° in order to divide the whole of the permitted region into three parts. By integrating the matrix elements given in Table I over the areas of these three regions for each of the cases considered, we obtained the relative probabilities that the angle between the two positive pions has a value respectively between 0° and 60°, 60° and 120°, 120° and 180°.

TABLE III. – *Distributions of the angles between the like mesons.*

Spin and parity	0° ÷ 60°	60° ÷ 120°	120° ÷ 180°
[0, —]	0.073	0.358	0.569
[1, +]	0.134	0.501	0.365
[1, —]	0.012	0.355	0.633
[2, +]	0.004	0.280	0.716
[2, —]	0.104	0.315	0.581
[3, —]	0.008	0.424	0.568
[4, —]	0.108	0.279	0.613
[6, —]	0.121	0.253	0.626
experimental data	0.081 ± 0.031	0.333 ± 0.062	0.586 ± 0.082

TABLE IV. – *Distributions of the angles between the unlike and one of the likeme sons.*

Spin and parity	0° ÷ 60°	60° ÷ 120°	120° ÷ 180°
[0, —]	0.073	0,358	0,569
[1, +]	0.043	0.286	0.671
[1, —]	0.069	0.396	0.535
[2, +]	0.030	0.504	0.466
[2, —]	0.104	0.315	0.581
[3, —]	0.080	0.652	0.268
[4, —]	0.144	0.281	0.575
[6, —]	0.169	0.271	0.560
experimental data	0.055 ± 0.016	0.330 ± 0.041	0.615 ± 0.055

b) On interchanging E_3 with E_1 or E_2, the same curves already determined now represent the locus of the point corresponding to τ-events with the same angle between the π^- and one of the π^+. In this way it is possible to repeat the preceeding calculation and to obtain the probabilities that the angle between π^- and π^+ lies in one of the three angular intervals.

c) Adding the first distribution to twice the value of the second we obtain the probability that any angle falls in one of the three regions.

TABLE V. – *Distribution of the angles between any two mesons.*

Spin and parity	$0^\circ \div 60^\circ$	$60^\circ \div 120^\circ$	$120^\circ \div 180^\circ$
[0, −]	0.073	0.358	0.569
[1, +]	0.073	0.358	0.569
[1, −]	0.052	0.382	0.566
[2, +]	0.021	0.430	0.549
[2, −]	0.104	0.315	0.581
[3, −]	0.056	0.576	0.368
[4, −]	0.116	0.280	0.604
[6, −]	0.137	0.259	0.604
experimental data	0.063 ± 0.013	0.366 ± 0.032	0.571 ± 0.039

We have made the calculations classically; in this way the treatment is completely analytical: this is justified by the fact that the kinetic energy of secondaries is always less than 50 MeV. A numerical evaluation of the relativistic formular shows that the correction we should apply to the value obtained in the classical approximation never exceeds 10%.

In the Tables III, IV and V we have collected the numerical results obtained for the angular distributions *a*), *b*) and *c*) corresponding to the eight possibilities of spin and parity considered. The last row of each table shows the experimental data obtained from 123 τ-events for 97 of which the π^-'s were identified ([6]).

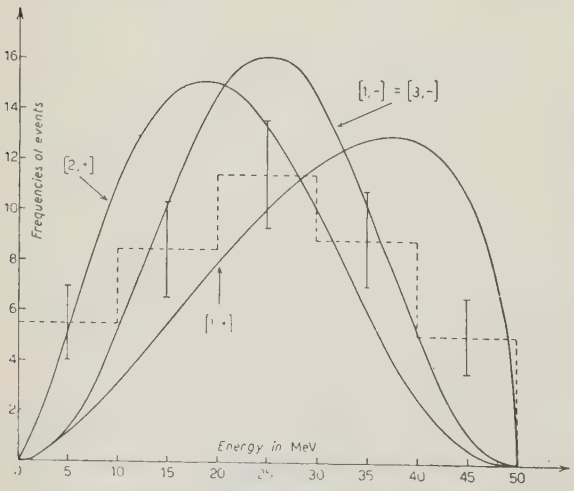

Fig. 2.

4. – Conclusion.

In order to discuss in the most complete way the conclusions which nowadays it is possible to deduce about the spin and parity of the τ-meson, we have also taken into account those results for energetic distributions

([6]) One can find the main part of the experimental data we have used in AMALDI's report of the Pisa Conference: we have considered also some events found recently by the Padua group.

obtained by different authors. In Fig. 2 and 3 are represented the energetic distributions of the π^- for seven different cases, as calculated by DALITZ. In Table VI we also give the data relative to the energy distributions grouped together in the same way as in the work by FABRI, completing them with the three new cases considered by us.

These distributions consist in dividing the number of the negative secondaries in three parts depending on whether their energy is less, intermediate or larger than that of the two positive ones.

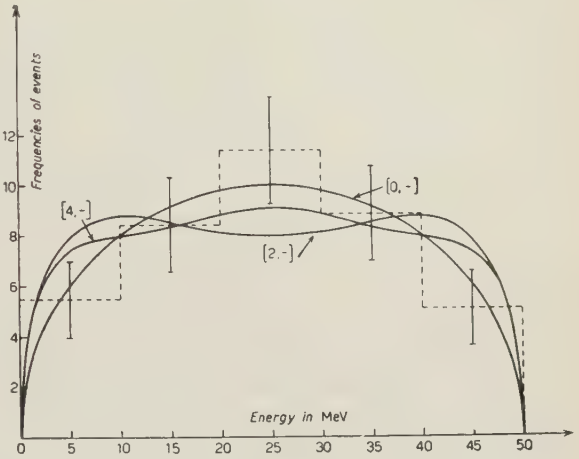

Fig. 3.

From an examination of the different results obtained and of the experimental data, we arrive at the following conclusions, in the limits of the hypotheses already discussed.

TABLE VI. – *Energetic distributions of the negative secondaries according to Fabri's rule.*

Spin and parity	*a*	*b*	*c*
[0, —]	0.333	0,334	0,333
[1, +]	0.425	0,334	0.241
[1, —]	0.196	0.608	0.196
[2, +]	0.241	0.334	0.425
[2, —]	0.333	0.334	0.333
[3, —]	0.294	0.412	0.294
[4, —]	0.293	0.414	0.293
[6, —]	0,271	0.458	0.271
experimental data	0.340 ± 0.059	0.330 ± 0.058	0.330 ± 0.058

Let us first examine the distributions calculated by FABRI: we see that with the present experimental data, we can definitely reject some cases such

as [1, —], and also consider as very improbable the cases [1, +], [2, +] [6, —]. The displacement of [3, —] and [4, —] is only just outside the errors, while [0, —] and [2, —], which conform much more closely to the experimental distributions, are completely indistinguishable from each other.

The detailed energetic distributions of the negative prongs, as one can see in Fig. 2 and 3, allow a higher degree of discrimination because they make the [3, —] case much more improbable, while, at the present stage, they allow one to conclude very little about the other cases [0, —], [2, —], [4, —], notwithstanding a slight tendency in favour of [0, —].

The angular distributions calculated by us offer a further criterion of judgement, because they completely confirm and render rather more evident the rejection of some cases (e.g. [3, —], [1, +], [2, +]), while in the cases which are the most controversial and the most difficult to distinguish, they offer further evidence in favour of [0, —] with respect to [2, —] and [4, —]. Obviously, the strong similarity of all the spectra in these last three cases makes it still necessary to increase the experimental statistics before one can reach a definitive conclusion. Despite this, the fact that the different criteria adopted give concordant results in favour of [0, —] makes us think that this last case is the most probable solution of the problem.

It is important, however, that, unless one assumes very large values of the spin, for which the calculation has not yet been made, and which a priori do not seem very plausible, in the picture of our present ideas, all the cases [0, —] [2,—] [4, —], amongst which the possible choice of the definitive solution seems to be confined, are incompatible with a decay into two pions only. Therefore, whatever may be the final choice amongst these cases, we would be led to the conclusion that under no circumstances the particles that suffer decay in the τ- and χ-mode may be the same particle.

* * *

We are greatly indebted to Prof. DALLAPORTA for useful discussions and advices.

Note added in proof.

This work was just submitted for publication, when we received the results of an analysis of 54 τ-events, produced in a large emulsion stack by the K-meson beam from the Berkeley Bevatron (B. T. FELD, A. C. ODIAN, D. M. RITSON and A. WATTEMBERG, M.I.T.). The energy spectrum of the secondaries of these events is in good agreement with the theoretical distribution calculated by DALITZ of the [1+] case. We have plotted the angular distributions of the same events in order to compare them with

the calculated distributions of tables III, IV and V; the result is:

Table	0°—60°	60°—120°	120°—180°
III	0.133 + 0.054	0.511 + 0.107	0.356 + 0.088
IV	0.056 + 0.025	0.270 + 0.055	0.674 + 0.087
V	0.082 + 0.025	0.351 + 0.051	0.567 + 0.065

which shows also a very good agreement with the [1+] distributions.

RIASSUNTO

Sono state calcolate, sulla base delle ipotesi finora accettate sul tipo di interazione, le distribuzioni angolari dei secondari del mesone τ, per otto combinazioni dello spin e della parità. Un confronto di queste distribuzioni con i dati sperimentali mostra un accordo soddisfacente per i casi di spin pari e di parità negativa, soprattutto per il caso [0, —].

An Anomalous V^0 Event.

M. Deutschmann

Max-Planck-Institut für Physik - Göttingen

M. Cresti, W. D. B. Greening, L. Guerriero, A. Loria and G. Zago

Istituto di Fisica dell'Università - Padova
Istituto Nazionale di Fisica Nucleare - Sezione di Padova

(ricevuto il 19 Novembre 1955)

Summary. — An even has been observed in a multiplate cloud chamber and has the typical aspect of an anomalous V^0 decay: it is compalible with the decay scheme $\tau^0 \to \pi^+ + \pi^- + \pi^0 + 80$ MeV.

In a multiplate cloud chamber we have observed a two-prong event, the two ionizing particles of which are of rather low energy and are stopped within the illuminated zone of the chamber. It has the typical aspect of an anomalous V^0 decay, and since these decays have so far only been found in magnetic chambers ([1,2,3]), we have thought it worth while to give a brief description of the event.

As can be seen from Figs. 1 and 2, the apex of the fork lies in the gas between the fourth and fifth plates (all plates are of Pb, 1 cm thick), the distance of the apex from the lower surface of the fourth plate being 2 ± 0.3 mm. From the clearly visible change of ionization of the two particles we infer that both move away from the apex and stop in plates seven and eleven respectively. The ionization has been estimated and is given in Table I, together

([1]) R. W. Thompson: *Proc. Fourth Rochester Conference* (New York, 1954).

([2]) B. Rossi: *Lectures on Fundamental Particles*, Varenna, 1954, *Suppl. Nuovo Cimento*, **1**, 163 (1955).

([3]) R. W. Tompson: *Progress in Cosmic Ray Physics*, J. G. Wilson ed. vol. 3 (Amsterdam, in press).

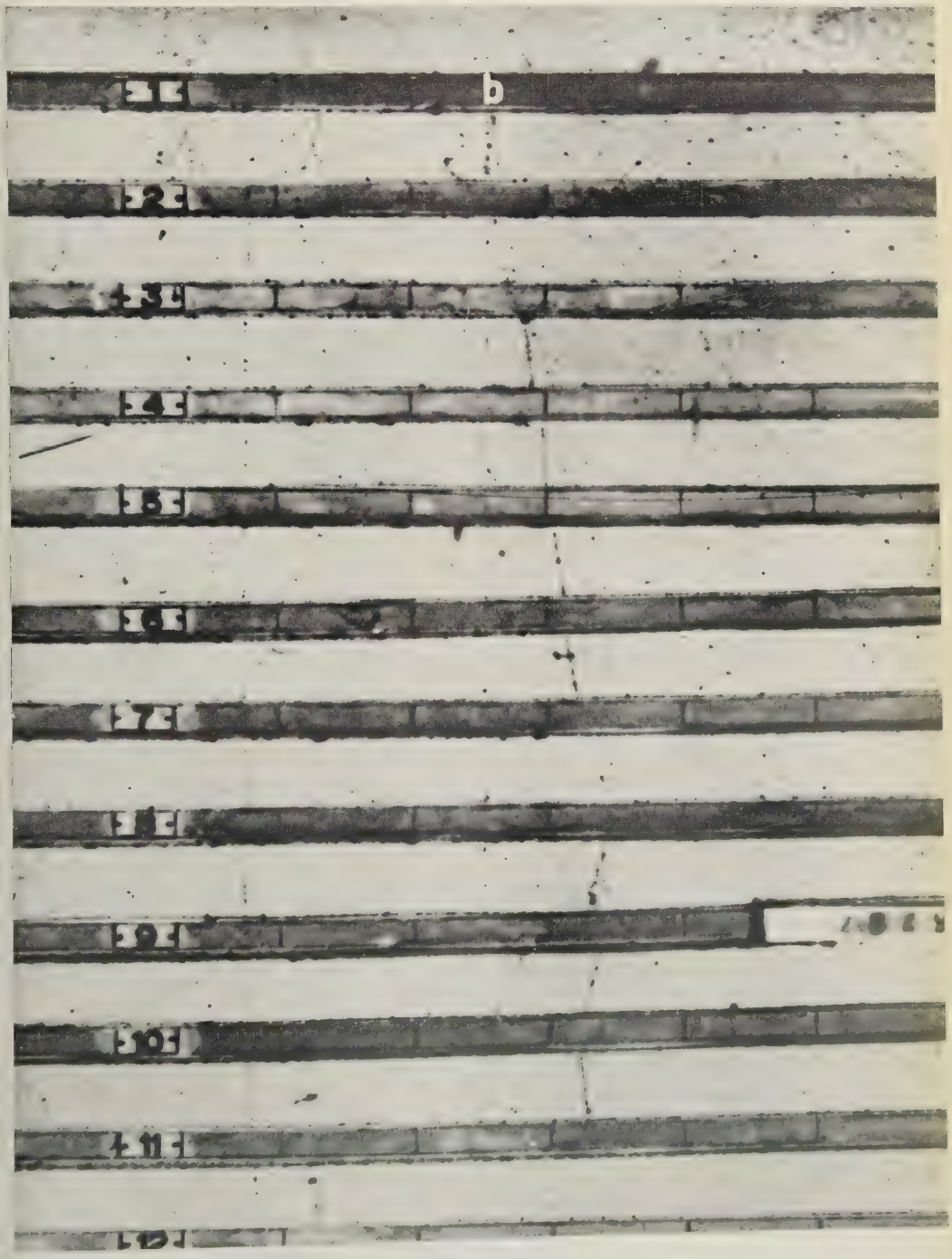

Fig. 1.

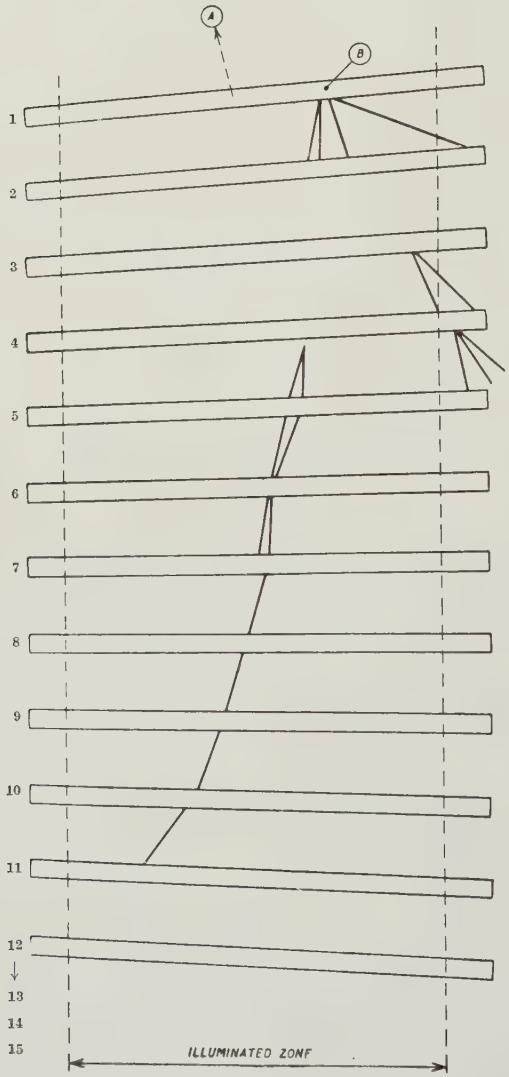

Fig. 2. – Side view of the event.

with the expected values for particles of different masses. One sees that both particles are most likely L-mesons, an assumption which is also favoured by the measured scattering in the plates. For $\pi^{\pm}$-mesons the observed ranges (taking into account the ionization in the last part of the track) lead to the momenta (1): $p_1c = 154 \pm 7$ MeV (left) and $p_2c = 234 \pm 6$ MeV (right). The angle between the tracks is $\gamma_{1,2} = 22.3^{\circ} \pm 2^{\circ}$.

TABLE I. – *Ionization of the two decay particles.*

Residual Range in cm Pb	Ionization					
	Observed		Expected			
	Particle 1	Particle 2	Proton	K-meson	L-meson	
					π	μ
6.5	—	1	2.0	1.7	1.2	1.1
5.5	—	1	2.1	1.7	1.2	1.1
4.5	—	1	2.3	1.8	1.2	1.2
3.5	—	1	2.5	2.0	1.3	1.2
2.5	1.3 ... 1.5	1	2.8	2.2	1.5	1.3
1.5	1.5 ... 2.0	1.5 ... 2.0	3.4	2.7	1.8	1.6
0.5	2.0 ... 2.5	2.0 ... 2.5	5.5	4.0	2.5	2.3

A two-body decay into π-mesons can be ruled out for the following reasons: the Q-value would be 15 ± 3 MeV, which is far too low to agree with the well-known decay scheme $\theta^0 \rightarrow \pi^+ + \pi^- + 214$ MeV; in addition there is no interaction visible (*) which, within the limits of error, is coplanar with the decay tracks and which lies on the supposed line of flight of the V^0 particle (derived from the conservation of transverse momenta of the secondaries). Thus we are led to postulate a three-body decay.

The following three body decay schemes have been suggested:

(1) $$\theta^0 \rightarrow \pi^+ + \pi^- + \gamma + 214 \text{ MeV} ;$$

(2) $$\theta^0 \rightarrow \pi^{\pm} + \mu^{\mp} + \nu + 248 \text{ MeV} ;$$

(3) $$\tau^0 \rightarrow \pi^+ + \pi^- + \pi^0 + 80 \text{ MeV} .$$

(1) W. A. ARON, B. G. HOFFMANN and F. C. WILLIAMS: *AECU Report* 663, 1951.

(*) Generally, in our chamber, the origins of the V^0-particles are easily found unless the decay occurs near the edge of the illuminated zone. In fact, of 26 normal V^0 decays observed with the same arrangement of plates, it was possible to find a coplanar origin for 23 of them. The other three decays occurred near the edge of the illuminated zone and, most probably, had their origins outside it; their supposed lines of flight crossed at most one or two plates, in contrast to the four plates available for the event being considered.

The existence of these decays has not yet been established, however the measured distribution of apparent Q-values in anomalous V^0 decays found by various workers, seems to favour the third scheme ([3]). It will therefore be interesting to see whether the present event can be described as a τ^0 decay, or if the lack of evidence for an electron cascade (to be expected from the π^0 decay photons) excludes this scheme in favour of one of the others.

From an inspection of other tracks in the chamber there are two probable origins, « A » and « B » for the V^0 particle (see Fig. 2).

Origin « A »: Tracks of three penetrating particles lead back to a common point « A » above the chamber at a distance of 98 ± 10 cm from the apex of the V^0 decay. If this is the origin we find that the angles between the line of flight of the V^0 particle and each of the ionizing particles are $\gamma_{0,1} = 32^\circ \pm 8^\circ$ and $\gamma_{0,2} = 30^\circ \pm 7^\circ$; the deviation from coplanarity (angle between the line of flight and the plane of the decay tracks) is $\delta = 28^\circ \pm 5^\circ$. Supposing the third decay particle to be a π^0-meson, one obtains from the conservation of momentum and energy a minimum Q-value of 150 ± 60 MeV. This corresponds to the situation where the plane of the decay in the centre-of-mass system lies normal to the line of flight of the V^0 particle. Any other, and more likely, orientation leads to a higher Q-value. Thus in this case we can exclude a τ^0 decay. If the neutral decay particle has zero mass the minimum Q-value is 240 ± 70 MeV which does not exclude schemes (1) or (2).

Origin « B »: In the first plate of the chamber an interaction « B » has been produced by a neutral particle which, as seen from the direction of the secondary particles, may have come from interaction « A » above the chamber. In case « B » the angles are: $\gamma_{0,1} = 8.7^\circ \pm 2.5^\circ$, $\gamma_{0,2} = 17.8^\circ \pm 1.5^\circ$ and $\delta = 7.3^\circ \pm 1.7^\circ$. Calculation shows that the event is compatible with a τ^0 decay. There are two possible directions for the π^0-meson, since it may be emitted either forwards or backwards in the centre-of-mass system. Both possibilities are considered in Table II. If the π^0 is emitted forwards it travels at a small angle with respect to the line of flight of the τ^0, and the cone which should contain at least one of its decay photons lies in the illuminated zone for a length which corresponds to the crossing of at least five plates. Since not even one electron is visible, whereas at least four are to be expected ([5]), we think that this case must be discarded. If the π^0, however, is emitted backwards, it moves towards the rear of the chamber and the resulting photons (which are of low energy) can leave the illuminated zone without crossing the plates, or else they can cross them obliquely so that the electrons would

---

([5]) P. A. BENDER: *Nuovo Cimento*, **2**, 980 (1955).

easily be missed. Thus the failure to find an electron cascade is not in conflict with an assumed τ^0 decay.

The same arguments when applied to decay scheme (1) where a γ is emitted, show that this decay can almost certainly be excluded for either origin « A » or « B ». Naturally nothing can be said about scheme (2) where the third particle is a neutrino.

TABLE II. – *Calculated data for the assumed decay of a τ^0 produced in interaction «B».*

Emission of π^0 in c.m. system	$\gamma_{0,3}$	p_{τ^0} MeV/c	p_{π^0} MeV/c	$\vartheta/2$	$N_{\min}$	φ	t_{τ^0} s
Forwards	7°	885	520	15°	5.1	63°	$2.3 \cdot 10^{-10}$
Backwards	72°	400	70	60°	1.4	50°	$5.1 \cdot 10^{-10}$

$\gamma_{0,3}$ Angle between the lines of flight of the τ^0 and the π^0 (in the laboratory system).
p_{τ^0}; p_{π^0} Momenta of the τ^0 and the π^0.
$\vartheta/2$ Half-angle of the cone which contains at least one of the photons from the π^0-decay.
$N_{\min}$ Minimum number of electron tracks (*) (in this cone) produced by a photon which has at least half the total energy of the π^0.
φ Angle between the line of flight of the τ^0 and the normal to the decay plane in the c.m. system.
t_{τ_0} Lifetime of the τ^0.

(*) Based on a track length formula E (in MeV) $= 30 \cdot t \cdot N$; where t is the thickness of the lead plates (in radiation lengths) and N is the total number of electron tracks [5].

We conclude that the present event provides evidence for an anomalous V^0 particle which decays into at least three secondaries of which two are charged L-mesons; it is compatible with the decay scheme $\tau^0 \to \pi^+ + \pi^- + \pi^0 + 80$ MeV.

* * *

We wish to thank the Società Adriatica di Elettricità for their help in connection with this work.

— — —

RIASSUNTO

È stato osservato in una camera a setti un evento che ha le caratteristiche di un decadimento V^0 anomalo. Esso può essere interpretato con lo schema $\tau^0 \to \pi^+ + \pi^- + \pi^0$ 80 MeV.

IL NUOVO CIMENTO Vol. III, N. 1 1° Gennaio 1956

Design of the Pole Faces for Circular Particle Accelerators with the Electrolytic Tank.

F. Amman

Istituto Nazionale di Fisica Nucleare, Sezione Acceleratore - Roma

L. Dadda

Istituto di Elettrotecnica Generale del Politecnico - Milano

(ricevuto il 29 Novembre 1955)

Summary. — A method is presented here for the measurement of a quantity approximately proportional to the second derivative of the electric potential in the electrolytic tank. This method is very useful for the measurement of the field index n in the gap of a circular particle accelerator.

In the design of the pole faces for a circular particle accelerator, the electrolytic tank is a very helpful way to obtain the proper pole shape without an iron model.

There are many papers on this method of field mapping (1); the main differences between the preceding methods and the one we used are:

1) We used the conjugate analogy instead of the direct analogy; in the conjugate analogy the current function in the electric current field corresponds to the magnetic potential in the magnetic field, and the electric potential corresponds to the magnetic flux function. It is possible to use the conjugate analogy only in 2-dimensional fields or in 3-dimensional fields with axial simmetry (2). We recall here that it is necessary to use the conjugate analogy

(1) G. Liebmann: *Advances in Electronics*, **2**, 101 (1950).
(2) L. Dadda: *L'Energia Elettrica*, **30**, 837 (1953).

when we have to map portions of magnetic fields where rot $H \neq 0$ (inside the coils).

2) We measured the index n, proportional to the second derivative with respect to the abscissa r of the electric potential in the current field, directly comparing in a bridge circuit two voltages proportional to the first derivative of the electric potential; previously used techniques measured the electric potential or its first derivative and obtained the second derivative graphically.

The main advantages of this method are:

1) We directly compare two voltages in a bridge circuit, therefore the shifts in the supply voltage have no influence. By using two calibrations of the probes we can reduce very much the errors due to the measuring apparatus. In effect the second derivative of the electric potential is approximately proportional to the difference between two first derivatives, which in our case have almost the same value; with such calibrations the error of this difference has the same relative value as each term of the difference; with the graphic or analytic methods, the error of the difference has the same absolute value as in each term.

2) In the direct analogy the pole piece is represented by an equipotential surface. It is difficult to define an equipotential surface in a conducting plate placed in an electrolytic solution because of the voltage drops on its surface; since the gradient is very sensitive to the precise shape of the pole, it is therefore better to use the conjugate analogy where the pole face is insulating.

3) In the conjugate analogy B_z corresponds to $\partial V/\partial r$, and $\partial B_z/\partial r$ corresponds to $\partial^2 V/\partial r^2$, a quantity which it is possible to measure with three probes alined in the r direction. In the direct analogy B_z corresponds to $\partial V/\partial z$ and $\partial B_z/\partial r$ to $\partial^2 V/\partial r\,\partial z$: to measure the mixed derivative one needs four probes and, at least, one transformer to compare the two voltages, as there are no points at the same potential.

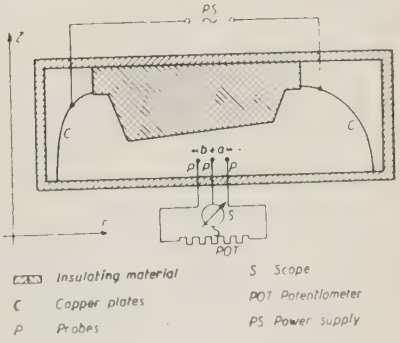

Fig. 7.

The schematic circuit we used for these measurement is sketched in Fig. 1.

The index n, defined in a magnetic field as

$$n = \frac{\delta B_z}{\delta r}\cdot\frac{r}{B_z} \tag{1}$$

is given in the conjugate analogy by

$$n = -\frac{4r}{a+b}\,\frac{V_1/V_2 - a/b}{V_1/V_2 + a/b}, \tag{2}$$

where V_1 is the voltage across the length a, and V_2 the voltage across b, a and b being the distances between the two outside probes and the inner one.

The formula (2) holds for 2-dimensional fields; in the case of 3-dimensional fields with axial simmetry, there is another term, and (2) becomes

$$n = -\frac{4r}{a+b}\,\frac{V_1/V_2 - a/b}{V_1/V_2 + a/b} + 1\,. \tag{3}$$

The obtain n we have therefore to measure three quantities: two ratios, V_1/V_2 and a/b, and the value of $a+b$.

The first ratio is measured with the probes in the model; the second ratio is measured putting the probes in a uniform field, and this is the first calibration.

The best way to measure the quantity $a+b$ is to calibrate the probes in a known current field, whose gradient is not constant; for instance the circular field, with the logarithmic potential distribution. With these two calibrations, both easy to do, the errors due to the measuring apparatus become negligible: the main cause of error we could not avoid was the unstable behaviour of the probes.

We used as probes three wires of platinum, mechanically held together, covered with platinum black and treated to eliminate occluded gases.

By this way we could not obtain a stability better than $\pm .1$ (in terms of n; this corresponds to $\pm 2.5 \cdot 10^{-5}$ of the voltage across the two external probes). However we think that an improvement is possible: we did not have the time to study deeply this side of the problem, but we found that much better results were obtainable with stainless steel, electrolytically covered with copper first, then with platinum black.

Some words about the model: we used a half model in the scale 3:1; two flux surfaces, outside the poles, are represented by two electrical equipotentials (two copper plates, covered with dag, colloidal graphite), to which is applied the supply voltage. The two flux surfaces are obtained by mapping all the field (including the coils) in a smaller scale, using the current field in a thin aluminum foil: we found this system we developed is the most convenient to map 2-dimensional fields with portions where rot $H \neq 0$: the accuracy needed in this mapping is not very high, because the gradient in the

useful region below the poles is not sensitive to the precise shape of these surfaces.

We hope in a short time to be able to print a longer paper concerning all these measurements with some of the results.

RIASSUNTO

Viene prensentato un metodo per la misura diretta, in vasca elettrolitica, di una grandezza approssimativamente proporzionale alla derivata seconda del potenziale elettrico. Questo metodo è particolarmente interessante per il rilievo dell'indice di campo n nel traferro di un acceleratore di particelle circolare.

The Rate of Extensive Showers of High Electron Density at Sea Level.

C. B. A. McCusker and B. G. Wilson (*)

Dublin Institute for Advanced Studies

(ricevuto il 2 Dicembre 1955)

Summary. — Extensive air showers of high electron density (average density ~ 700 particles/m^2) have been observed at sea level. The rates of all classes of events with respect to sidereal time are constant within the statistical errors. With respect to solar time however a variation of amplitude $\sim 20\%$ and period 12 hours has been found. This variation is out of phase with the previously observed variation of high energy local penetrating showers. Both are correlated with the oscillations of the atmosphere.

1. – Introduction.

Some time ago a variation in the rate of local penetrating showers of high energy was established (Dardis and McCusker, 1954) (1). The variation appeared to be correlated with the semi diurnal oscillation of the atmosphere (McCusker, Dardis and Wilson, 1955) (2). Since it is generally believed (Cocconi, 1950) (3) that the primaries at sea level of these showers form part of extensive air showers it was thought to be advisable to investigate other components of extensive air showers at sea level, in particular the high density electronic component. A large variation in this component had been noticed by other workers (Fornaca and Martelli, 1953) (4) and although these ob-

(*) Now with the National Research Council, Canada.

(1) J. G. Dardis and C. B. A. McCusker: *Proc. Phys. Soc.*, A **67**, 1026 (1954).

(2) C. B. A. McCusker, J. G. Dardis and B. G. Wilson: *Proc. Phys. Soc.*, A **68**, 585 (1955).

(3) G. Cocconi: *Phys. Rev.*, **79**, 1006 (1950).

(4) G. Fornaca and G. Martelli: *Proc. Bagnères Conf.*, p. 20 (1953).

servers believed the variation to be with respect to sidereal rather than solar time the rather short run of their experiment (1 200 hours) may have been misleading.

2. – Apparatus.

Accordingly a rather simple apparatus to detect these showers was constructed. Six small units (known as M-units) were made. Each consisted of three small G.M. 4 counters, each counter 15 cm² area, placed at the apices of an equilateral triangle of side 20 cm. The pulses from the three counters fed into a simple Rossi circuit. The six units were placed at six different distances from a penetrating shower set and a large unshielded tray of counters (2 500 cm² area). The distances were 0.2, 2.7, 4.2, 4.8, 7.6 and 9.3 metres from M-units to the extensive tray. When any of the M-units produced a 3-fold coincidence, or when the penetrating shower set was triggered a master pulse was produced which was fed into a hodoscope and operated a mechanical counter and a camera unit. The camera unit contained a clock. The information obtained from the hodoscope was *a*) which of the units had produced a master pulse, *b*) which of the counters in the top tray of the penetrating shower set (under 20 cm Pb) had been discharged and *c*) whether or not the large unshielded tray had been discharged. The apparatus as described was run from March 7, 1955 to October 3, 1955, a total (allowing for tests and repairs) of 4594.4 hours.

3. – Results.

The M-units were concerned in the following types of event.

a) « Local » events in which an M-unit was discharged and nothing else.

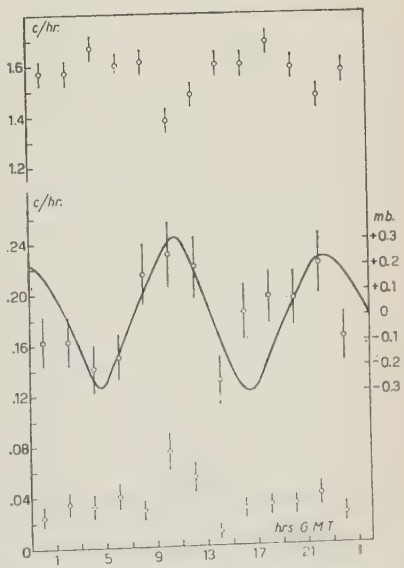

Fig. 1. – Shows at the top the rates of local penetrating showers averaged over two hourly periods beginning 23:00 to 01:00 hours G.M.T.; next the rates of « extensive » events and at the bottom the rates of « double » events. The solid curve gives the average daily pressure variation at Dublin Airport plotted as a departure from the mean value against the right hand scale.

b) « Extensive » events in which an *M*-unit and the large unshielded tray were discharged.

c) « Double » events in which two or more *M*-units were discharged. These were always also, « extensive » events.

d) Penetrating events in which one *M*-unit and the local penetrating shower set were discharged.

Table I gives for each of the hours of the solar day beginning 00:00 to 01:00 G.M.T. the numbers of each of these classes of events recorded and the number of hours. Table II gives similar information for the hours of the sidereal day. Fig. 1 shows the rates of extensive and double events averaged over 2-hourly periods of the solar day together with the rates of local penet-

TABLE I. – *The rates of the four types of event involving the M-units against solar time.*

Hour (G.M.T.)	0-1	1-2	2-3	3-4	4-5	5-6	6-7	7-8	8-9	9-10	10-11	11-12
No. of *M*-locals	25	26	25	21	20	26	19	20	23	23	19	18
No. of *M*-extensive events	28	33	32	22	34	24	35	43	39	36	41	37
No. of *M*-double events	5	7	7	5	5	7	9	8	3	6	19	10
No. of penetrating events	4	2	4	2	2	0	2	6	1	4	3	2
Hours	199.0	199.0	199.0	198.8	198.8	198.0	198.0	196.5	184.6	163.6	170.9	180.7

Hour (G.M.T.)	12-13	13-14	14-15	15-16	16-17	17-18	18-19	19-20	20-21	21-22	22-23	23-24
No. of *M*-locals	21	17	18	28	15	18	24	18	22	20	29	21
No. of *M*-extensive events	44	22	25	37	32	40	39	41	36	45	43	37
No. of *M*-double events	10	2	2	7	4	6	6	7	6	5	11	5
No. of penetrating events	5	2	1	3	4	3	3	3	3	5	3	0
Hours	186.9	181.7	179.2	184.4	190.0	195.1	197.0	197.7	198.5	199.0	199.0	199.0

rating showers under > 20 cm Pb obtained in a previous experiment. This figure also shows the average daily variation of pressure at Dublin Airport for a period of one year plotted as a departure from the mean pressure.

4. – Discussion of the Results.

a) *The Local Events.* – It will be seen from Tables I and II that the rates of local events are constant with respect to both solar and sidereal time. Since the local events will mostly consist of cascade showers generated locally in the surrounding material by single high energy electrons or photons this is

TABLE II. – *The rates of the four types of event involving the M-units against sidereal time.*

Hour (G.S.T.)	0-1	1-2	2-3	3-4	4-5	5-6	6-7	7-8	8-9	9-10	10-11	11-12
No. of local events	25	21	25	10	21	26	28	16	21	21	20	17
No. of extensive events .	31	35	34	19	27	33	35	36	36	36	40	29
No. of double events	5	7	8	5	6	4	6	4	8	10	9	6
No. of penetrating events .	3	1	1	3	1	4	2	3	2	5	3	3
No. of hours .	186.4	189.6	189.0	181.5	181.0	181.6	187.1	186.2	189.4	188.7	190.4	190.8

Hour (G.S.T.)	12-13	13-14	14-15	15-16	16-17	17-18	18-19	19-20	20-21	21-22	22-23	23-24
No. of local events	17	21	25	24	19	25	24	24	25	25	12	24
No. of extensive events .	36	36	39	44	31	43	34	32	41	39	30	49
No. of double events	2	12	5	7	5	6	5	7	10	6	7	12
No. of penetrating events .	4	5	4	2	1	6	4	0	1	5	2	2
No. of hours .	196.0	198.6	197.7	200.1	199.3	201.8	200.3	199.2	198.8	196.7	188.2	186.3

only to be expected. However it constitutes good evidence for the proper functioning of the apparatus.

b) *Sidereal Time.* – It will also be seen from Table II that, both the extensive events and the « double » extensive events appear to have a constant rate when plotted against sidereal time. This is confirmed by using a X^2 (*) test to assess the goodness of fit of a straight line through the average value to these points. The values of P obtained are, respectively 0.4 and 0.5.

c) *The « extensive » and « double » events against solar time.* – On the other hand when the « extensive » and « double » events are plotted against solar time there appears to be a variation in the rates (see Fig. 1). X^2 tests confirm that a straight line through the average values is a poor fit in both cases. The values of P obtained were 0.01 and 0.0007 respectively. An attempt was then made to fit a sine wave to the results. It was found that the rate of the extensive events could be well represented by a sine wave of 12 hour period and 19% amplitude with its maxima at 10:30 and 22:30 hours G.M.T. The probability that this could be due to a chance fluctuation was 0.0004. For the double events representation by a single sine wave was not so successful. A 12 hour wave of 28% amplitude had a probability of being due to fluctuation of 0.036. This is in accord with the appearance of the graphs.

d) *The Penetrating Events.* – This rare class of event does not show any established variation with either solar or sidereal time.

5. – Nature of the Variation.

From the above there appears to be little doubt, that at least part of the variation of the extensive events has a 12 hour period. The maxima occur between 9:00 to 11:00 and between 21:00 to 23:00 hours G.M.T. The differences of the two minima from the average of these two both exceed three standard deviations. The case of the double events is not quite so clear cut. The maximum hours are 10-11 ($.112 \pm .025$ per hour) and 22-23 ($.055 \pm .017$). The hours 4-5 and 16-17 have a rate of $.021 \pm 0.10$ each. But the minimum hours are 13-14 and 14-15. However we are here dealing with very small numbers of events with correspondingly large possible fluctuations.

6. – Discussion of the Results.

The very simple argument that prompted this experiment ran as follows: It seems likely that the flux of high energy particles at the top of the atmo-

(*) For X^2 tests the results were generally arranged in groups of 4 hours; for sine wave tests, in groups of 2 hours.

sphere which cause extensive air showers is constant with respect to solar time. Therefore the total energy flux at sea level due to these primaries is also likely to be constant with solar time. Hence if one component at sea level shows a large variation with respect to solar time some other component must show a variation out of phase with respect to the first. This last now appears to be established. The particles causing the local penetrating showers show a variation of 12 hour period with minima at 10:30 and 22:30 hours. The present paper contains evidence showing that electrons of high density show a variation with a 12 hour period with *maxima* at about the same times. When particles of the right energy and density are selected the amplitude of the variations appears to be large—possibly as big as 100% in some cases. The variations are correlated with the average daily barometric variations at sea level which themselves are due to the oscillations of the atmosphere. However it cannot yet be taken to be established that there is a very direct causal connection.

It is interesting to inquire if any previous work on extensive showers shows any trace of this effect. In fact very little work on extensive showers of such high electron densities has been published. The interesting work of FORNACA and MARTELLI has already been noted. They found a variation of showers of high electron density with an amplitude of 50 to 100% but with respect to *sidereal* time. They state that an analysis with respect to solar time gave a smaller effect. Now our experiment has run for about four times as long as the Pisa experiment and the use of six units gave a much higher rate of the very dense showers. Our results show no variation of the rates with sidereal time and the correlation of the solar variation with the already established solar variation of local penetrating showers and the atmospheric oscillation seems to be good evidence in favour of our interpretation. It seems possible that the variation obtained by the Pisa group was in fact the solar variation which an unfortunate chance fluctuation transformed into an apparent variation with sidereal time.

Some unpublished results of Dr. T. E. CRANSHAW throw some light on this. We are greatly indebted to Dr. CRANSHAW for sending us these results. His apparatus consisted of 3 G.M.4 counters spaced 5 m apart. Threefold coincidences were recorded. Thus the apparatus was similar to one of our *M*-units but with a much bigger counter separation. This apparatus ran from November 7, 1950 to November 30, 1951 at Cambridge, England. An analysis of the results shows a semi diurnal variation with respect to solar time of amplitude 26%, the probability of this being due to chance being 0.01. During this period the months of April and August showed no effect. If these two months are left out the amplitude of the semi-diurnal wave becomes 33% and the probability of a chance effect, 0.002. The maxima occurred at 00:00 and 13:00. No variation with respect to sidereal time was found. A shorter

experiment at Harwell from June 9 to December 12, 1951 gave no established effect either with solar or sidereal time. The fact that both Dublin and Cambridge experiments gave the same period; that they have similar amplitudes and that, allowing for the difference in longitude, the statistical errors and possibly the difference in the pressure waves, the maxima occurred at the same time seems good evidence in favour of this being a solar variation.

It now appears reasonably certain that there exist variations in the rates of at least two components of large air showers with respect to solar time. These variations have a twelve hour period and under suitable circumstances a large amplitude. They are correlated with the oscillations of the atmosphere. As yet, no explanation of the effects is at all satisfactory. This however may not seem surprising if one considers that the effect may well be associated with the extremely high energy nuclear interactions at the beginning of the shower. The energy here involved may be as much as a million times greater than even the energy of very rare « jets » seen in photographic plates. Moreover the interactions take place in the upper atmosphere whose behaviour is not at all well known. It seems possible that a further study of the effect may produce significant information both about these extreme energy interactions and the conditions in the upper atmosphere.

* * *

We are greatly indebted to Dr. T. E. CRANSHAW and to Professor J. G. WILSON for much helpful discussion of the results. We wish to thank Professor C. O'CEALLAIGH and Dr. F. C. ROESLER for reading the manuscript.

RIASSUNTO (*)

Sciami estesi dell'aria di elevata densità elettronica (densità media ~ 700 particelle/m^2) sono stati osservati al livello del mare. Le frequenze di tutti i tipi di evento rispetto al tempo siderale sono costanti entro gli errori statistici. Rispetto al tempo solare si è trovata tuttavia una variazione di ampiezza $\sim$ il 20% e periodo di 12 ore. Questa variazione è sfasata rispetto alla variazione degli sciami penetranti locali di alta energia precedentemente osservata. Ambedue sono correlate alle oscillazioni dell'atmosfera.

(*) *Traduzione a cura della Redazione.*

IL NUOVO CIMENTO Vol. III, N. 1 1° Gennaio 1956

A Measurement of the Direction of the Polarization Produced in the Scattering of 135 MeV Protons.

M. J. Brinkworth and B. Rose

Atomic Energy Research Establishment - Harwell, Berkshire, England

(ricevuto il 5 Dicembre 1955)

Summary. — The 135 MeV polarized proton beam, obtained from the Harwell cyclotron by scattering to the left from carbon, has been slowed down to give protons of energy less than 10 MeV, and these protons have then been scattered by helium. The ratio of the intensities scattered at the same angle to left and right of the incident beam has been measured with photographic plates. This ratio, together with a phase shift calculation of the polarization produced in proton-helium scattering, gives the direction of the polarization produced in the first scattering. The observed direction agrees with that predicted theoretically on the assumption that the spin-orbit interaction in high energy nuclear scattering is the same as in the shell model of the nucleus.

1. – Introduction.

In the nuclear scattering of an unpolarized beam of high energy protons, the scattered beam is polarized perpendicular to the scattering plane. The direction and magnitude of the polarization have been predicted theoretically on the assumption of a spin-orbit interaction (1), and it is therefore of interest to measure the direction experimentally. One such measurement has been made by Marshall and Marshall (2), with a 435 MeV polarized proton beam produced by scattering at 14° from beryllium. In the present investigation,

(1) E. Fermi: *Nuovo Cimento*, **11**, 407 (1954); B. J. Malenka: *Phys. Rev.*, **95**, 522 (1954); G. A. Snow, R. M. Sternheimer and C. N. Yang: *Phys. Rev.*, **94**, 1073 (1954); W. Heckrotte and J. V. Lepore: *Phys. Rev.*, **95**, 1109 (1954).

(2) L. Marshall and J. Marshall: *Phys. Rev.*, **98**, 1398 (1955).

a 135 MeV beam produced by scattering at 20° from carbon has been used. Preliminary results were reported at the Fifth Annual Rochester Conference on High Energy Nuclear Physics [3] and at the 1955 Spring Meeting of the Physical Society [4].

2. – Experimental procedure.

2·1. *Principle of the method.* – In a double scattering experiment, if the initial beam is unpolarized, then the intensity $I(\varphi)$ after the second scattering is given by

$$I(\varphi) \propto 1 + P_1(\theta_1)\, P_2(\theta_2) \cos\varphi \,, \tag{1}$$

where $P(\theta)$ is the polarization produced in an initially unpolarized beam on being scattered through an angle θ, and φ is the angle between the two scattering planes. Consequently if it is possible to use a second scatterer for which $P_2(\theta_2)$ is known, then measurement at the same angle θ_2 of the relative intensities at $\varphi = 0°$ and $\varphi = 180°$ will give the sign of $P_1(\theta_1)$. Now $P(\theta)$ may be calculated for the scattering by helium of low energy protons, by using the phase shifts deduced from the measured differential cross-sections. The high energy proton beam may be reduced to these energies by passing it through an absorber of low atomic number, in which the depolarization of the beam is negligible [5,6].

2·2. *Polarization in proton-helium scattering.* – Measurements have been made by various experimenters [7,8] of the differential cross-sections for the elastic scattering by helium of protons in the energy range 1 to 10 MeV, with some lack of agreement between the higher energy results. Phase shift analyses [9,8] of the earlier data have been carried out, giving results compatible with either a normal or inverted P doublet, but a polarization measurement [10]

[3] *Proceedings of the Fifth Annual Rochester Conference* (1955), p. 159.

[4] *Nature*, **175**, 1027 (1955).

[5] L. Wolfenstein: *Phys. Rev.*, **75**, 1664 (1949).

[6] E. Heiberg, U. Kruse, J. Marshall, L. Marshall and F. Solmitz: *Phys. Rev.*, **97**, 250 (1955).

[7] G. Freier, E. Lampi, W. Sleator and J. H. Williams: *Phys. Rev.*, **75**, 1345 (1949); T. M. Putnam: *Phys. Rev.*, **87**, 932 (1952); R. G. Freemantle, T. Grotdal, W. M. Gibson, R. McKeague, D. J. Prowse and J. Rotblat: *Phil. Mag.*, **45**, 1090 (1954); B. Cork and W. Hartsough: *Phys. Rev.*, **96**, 1267 (1954); J. H. Williams and S. W. Rasmussen: *Phys. Rev.*, **98**, 56 (1955).

[8] W. E. Kreger, W. Jentschke and P. G. Kruger: *Phys. Rev.*, **93**, 837 (1954).

[9] C. L. Critchfield and D. C. Dodder: *Phys. Rev.*, **76**, 602 (1949); D. C. Dodder and J. L. Gammel: *Phys. Rev.*, **88**, 520 (1952).

[10] M. Heusinkveld and G. Freier: *Phys. Rev.*, **85**, 80 (1952).

showed that the doublet is inverted. A unique set of S and P phase shifts has thus been determined, and the values used in the present calculations are given in Table I. A formula expressing the polarization in terms of these

TABLE I. – *Phase shifts in proton-helium scattering.*
The values at 3.58, 5.78 and 9.48 MeV are taken from references ([8]) and ([9]); the other values are interpolated.

Energy (lab) in MeV of incident proton	Phase shifts in degrees		
	$S_{\frac{1}{2}}$	$P_{\frac{3}{2}}$	$P_{\frac{1}{2}}$
3.58	— 35.2	105.4	20.3
4.5	— 40.5	110.7	28.3
5.78	— 47.9	112.9	38.7
7.0	— 55.0	112.1	45.5
8.0	— 61.0	110.2	49.8
8.75	— 65.6	108.1	52.1
9.48	— 70.5	105.8	53.3

phase shifts was obtained by the method of LEPORE ([11]), though with corrected coulomb dependence. This formula has also been given by WOLFENSTEIN ([5]). Fig. 1 shows the polarization calculated at centre-of-mass scattering angles 110°, 120°, 125°, 130° and 138°, for incident protons with energies between 4 and 9.5 MeV. The convention here adopted is that the polarization $\boldsymbol{P} = P(\theta)\boldsymbol{n}$, where the unit vector $\boldsymbol{n}$ is defined by $\boldsymbol{k}_{\mathrm{A}}\boldsymbol{k}' = \boldsymbol{n}k^2 \sin\theta$, and $\boldsymbol{k}$ and $\boldsymbol{k}'$ are the propagation vectors, of magnitude k, of the incident and scattered waves respectively.

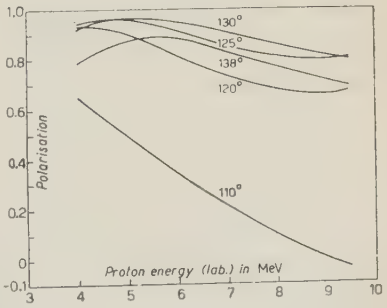

Fig. 1. – Polarization of protons elastically scattered by helium.

2·3. *Polarized proton beam.* – DICKSON, ROSE and SALTER ([12]) have described the production of a 135 MeV proton beam of approximately 68% polarization, from the Harwell synchrocyclotron, by scattering the internal beam at an angle of 20° from a carbon target. The polarized beam has an intensity of approximately 10^5 protons $\mathrm{cm}^{-2}\,\mathrm{s}^{-1}$. Nuclear emulsions were used to investigate the energy spectrum of the beam emerging from various thicknesses of aluminium absorber. With the absorber used in this work, of thick-

([11]) J. V. LEPORE: *Phys. Rev.*, **79**, 137 (1950).
([12]) J. M. DICKSON, B. ROSE and D. C. SALTER: *Proc. Phys. Soc.*, A **68**, 361 (1955).

ness 17.6 g cm^{-2}, the flux of emergent protons of energy less than 10 MeV was $5 \cdot 10^3$ protons cm^{-2} s^{-1}, which was 32 % of the total emergent flux. The spectrum had a broad peak at 7 MeV.

2·4. *Scattering camera.* – The scattering camera, illustrated in Fig. 2, contained helium at a pressure of 5 atmospheres. The front wall of the camera formed part of the absorber, and inside the camera the beam was collimated to a diameter of $\frac{3}{4}$ inch. Photographic plates were mounted to left and right

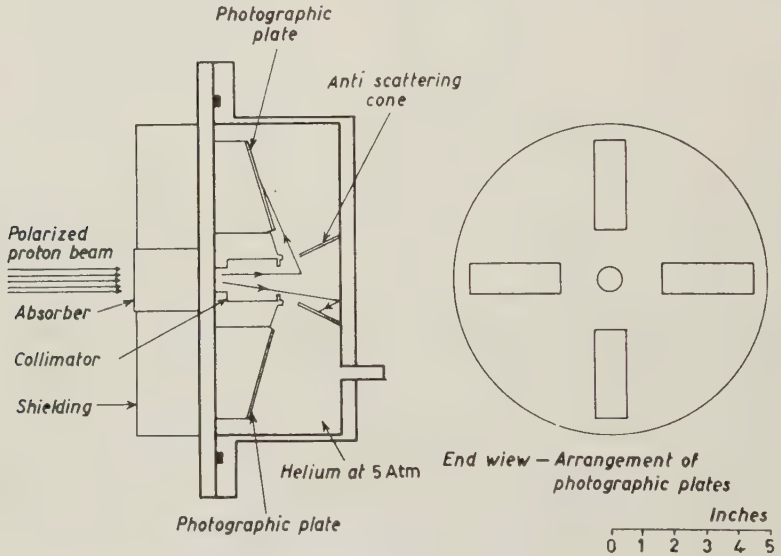

Fig. 2. – Scattering camera.

of the beam, and above and below it, at an angle such that protons scattered through 120° centre-of-mass would enter the emulsions at grazing incidence. The collimator and anti-scattering cone were so designed that no protons which had been scattered only once by the metal of the camera could enter the plates.

2·5. *Exposure.* – A preliminary exposure in the polarized proton beam, behind the concrete shielding wall 6 feet thick, showed the presence of too high a background of confusable tracks. A second exposure of 28 hours was made with about 2 tons of lead shielding close to the polarizing target inside the cyclotron tank, and with an additional thickness of 2 inches of lead and 6 inches of concrete surrounding the scattering camera. With this additional shielding, the confusable background was reduced by a factor of about three to a tolerable level.

Ilford C.2 plates of 50 μm thickness were used, and it was found unnecessary to screen the plates against the ionisation light produced by the passage

of the proton beam through the helium. It was not practicable to carry out a background run with the camera containing hydrogen of the same stopping power as the helium, as plates are fogged by hydrogen at high pressure; therefore, a background run was made with the camera evacuated. The relative exposures were recorded by means of an integrating gamma-monitor placed near the camera.

2·6. *Scanning.* – The first scattering inside the cyclotron was to the left, so that for the second scattering inside the camera the azimuthal angle φ took the values 0°, 90°, 180° and 270° for scattering in the directions left, up, right and down respectively. In scanning a plate, the acceptance criteria were that tracks should have an azimuthal angle within $\pm$ 15° of the appropriate φ value, that they should start at the surface and dip by not more than 15° in the unshrunk emulsion, that their range should be between 20 μm and 120 μm, and that from a consideration of grain density the protons should not be captured in the emulsion. These range limits corresponded to incident proton energies of 4.2 to 8.5 MeV at the minimum scattering angle, and 4.8 to 9.6 MeV at the maximum scattering angle.

2·7. *Background.* – The photographic plates were found to contain a large number of proton tracks due mainly to (n, p) events in the walls of the camera, caused by the high neutron flux in the cyclotron pit. In the scanning, in order to evaluate the proton background in the plates in each of the directions $\varphi = 0°, 90°, 180°$ and 270°, tracks were recorded satisfying the above acceptance criteria relative not only to the direction in each plate appropriate to scattering by the helium target, but also relative to the directions corresponding to each of the other three values of φ. This method of evaluating the background made the reasonable assumption that the departure of the plates from coplanarity could be neglected.

The purpose of the vacuum background run was to confirm that there was no scattering from the collimator into the plates, and also to make an independent check of the background in the plates.

3. – Results.

In order to reduce subjective errors, the plates were first scanned with wider acceptance criteria than those given above, and then each track was examined by a single observer who accepted only those satisfying the criteria of § 2·6.

The counts obtained on the left and right plates are given in Table II, the data in heavy type corresponding to tracks which could have originated in

TABLE II. – *Scanning data of helium run.*

$\varphi =$	0°	90°	180°	270°
Left	**106**	32	34	34
Right	24	22	**54**	31

the helium target. Apart from purely statistical counting errors, the main source of error in these data is due to scanning uncertainties of identification and measurement. On statistical errors alone a χ^2 test does not reveal any significant departure of the background from isotropy, and the mean background count is 30 ± 2.

The data obtained in the vacuum background run are given in Table III

TABLE III. – *Scanning data of vacuum run.*

$\varphi =$	0°	90°	180°	270°
Left	**10**	10	10	12
Right	3	11	**9**	12

They were obtained with only 32 % of the exposure and scanning required to obtain the data of Table II, but they suffice to demonstrate that the Left ($\varphi = 0°$) and Right ($\varphi = 180°$) counts of Table II could not be ascribed to scattering mainly from the collimator rather than from the helium target. The difference in the energy spectrum of protons entering the plates, due to the absence of the stopping power of the helium in the background run, could be neglected. For the same exposure and scanning conditions as in Table II, this vacuum run gives a mean background of 30 ± 4 in agreement with the value obtained in the helium run.

From Table II, the ratio of left and right scattering of protons from the helium target is found to be $L/R = (76 \pm 11)/(24 \pm 8)$. The statistical significance of this result may be assessed by noting that if x is a Poisson variate with mean m, then $x^{\frac{1}{2}}$ is distributed nearly normally with variance approximately $\frac{1}{4}$ if m is large ([13]). If the Left ($\varphi = 0°$) and Right ($\varphi = 180°$) counts of Table II be denoted by x_1 and x_2 respectively, then on the hypothesis that the true value of $L/R \leqslant 1$ the statistic $t = x_1^{\frac{1}{2}} - x_2^{\frac{1}{2}}$ is approximately normally distributed with mean $\leqslant 0$ and variance $\frac{1}{2}$. The observed value of t is 2.95, which is > 4.2 standard deviations above the mean, and the probability of a deviation, as large as or larger than this, is $\leqslant 1.5 \cdot 10^{-5}$ approximately. Thus the hypothesis that the true value of $L/R \leqslant 1$ may be rejected.

([13]) M. S. BARTLETT: *Journ. Roy. Statist. Soc. Suppl.*, **3**, 68 (1936).

The up and down plates exposed in the helium run were less extensively scanned than the left and right plates, in that for 60 % of the area scanned, tracks were accepted with a maximum dip of only 12° in the unshrunk emulsion. The counts obtained on the up and down plates, together with the data from the left and right plates conforming to the same acceptance criteria, are given in Table IV.

TABLE IV. – *Scanning data of helium run with restricted acceptance criteria.*

$\varphi =$	0°	90°	180°	270°
Left	**81**	24	24	26
Up	32	**59**	22	23
Right	17	15	**37**	22
Down	12	13	19	**58**

On statistical errors alone, this background does not appear to be isotropic, but if a reasonable allowance for scanning errors is included, for example if the variance of the background counts is increased by a factor 1.5, then here also the background does not depart significantly from isotropy. The mean background count is 21 ± 1. The ratio of left and right scattering of protons from the helium target is $L/R = (60 \pm 9)/(16 \pm 6)$, and the ratio of up and down scattering is $U/D = (38 \pm 8)/(37 \pm 8)$.

From equation (1), the polarization curves of Fig. 1, the differential cross-sections for proton-helium scattering, the energy spectrum of the incident protons, and the dependence on scattering angle of the target volume, it was calculated that according as P_1 is positive or negative the ratio L/R should be either 4.1 or 1/4.1 for the acceptance criteria of both Table II and Table IV.

This calculation of the ratio L/R assumes that only protons elastically scattered from the helium will be observed in the energy range considered. There will, in principle, be a contribution due to the inelastic scattering of protons of much higher energy (> 30 MeV). Owing to the shape of the spectrum of protons entering the scattering camera, however, the cross-sections for this process would have to be about two orders of magnitude greater than for elastic scattering at about 6 MeV in order to make any significant contribution to the observed tracks, and accordingly this effect has been ignored.

4. – Discussion.

The experimental data are in agreement with the former of the calculated L/R ratios, implying that P_1 is positive; that is, a proton beam scattered to the left, as in the Harwell cyclotron, is polarized with spin up.

The fact that the ratio U/D is approximately unity, and the fact that the mean of the up and down scattering is approximately the same as the mean of the left and right scattering, are both satisfactory checks on the experimental arrangement.

The polarized proton beam used in this experiment was produced by both elastic and inelastic scattering from the carbon target ([12]). However, its direction of polarization is the same as that due to purely elastic scattering, since it has been shown ([14]) that polarization due to inelastic scattering is in this same direction.

The observed direction of polarization is the same as that obtained by MARSHALL and MARSHALL ([2]), with different conditions for the first scattering, and with a polarization analyser depending in a different manner on the phase shifts for proton-helium scattering. This is worth noting in view of the uncertainties in these phase shifts at the higher energies. The observed direction of polarization is that predicted ([1]) on the assumption that the spin-orbit interaction operative in high energy nuclear scattering is the same as in the shell model of the nucleus.

* * *

We wish to thank Dr. C. L. OXLEY for suggesting this problem, Dr. W. G. V. ROSSER and K. W. MORTON for collaboration and advice, and Miss R. E. CLINCH for the preliminary scanning.

([14]) J. M. DICKSON and D. C. SALTER (Private communication).

RIASSUNTO (*)

Il fascio polarizzato di protoni ottenuto dal ciclotrone di Harwell per mezzo di scattering a sinistra su carbonio è stato rallentato per ottenere protoni di energia inferiore a 10 MeV e a questi protoni si fa subire uno scattering su elio. Il rapporto delle intensità diffuse sotto lo stesso angolo a destra o a sinistra del fascio incidente è stato misurato con lastre fotografiche. Tale rapporto in unione ad un calcolo in sfasamento della polarizzazione prodotta nello scattering dei protoni su elio dà la direzione della polarizzazione prodotta nel primo scattering. La direzione osservata si accorda con quella prevista dalla teoria facendo l'ipotesi che l'interazione spin-orbita nello scattering nucleare delle alte energie sia la stessa che nel modello a shell.

(*) *Traduzione a cura della Redazione.*

Experimental Measurements on Double Compton Effect.

A. Bracci, C. Coceva, L. Colli and R. Dugnani Lonati

Laboratori CISE - Milano

(ricevuto il 6 Dicembre 1955)

Summary. — The cross-section of the double Compton effect in the particular case of incident γ-rays of ~ 1 MeV energy and of scattered γ-rays making an angle of 90° throughout with each other and with the incident γ, has been experimentally measured, and the energy distribution of the scattered γ has been observed. The scattered γ-rays are detected by means of two scintillation spectrometers which use sodium iodide crystals and EMI photomultipliers working in coincidence. The pair of pulses from the photomultipliers, corresponding to γ-rays which give rise to a coincidence, are sent to a cathode-ray tube on whose screen they are photographed and then analyzed. Experimental results obtained in the present work, regarding both the cross-section value and the energy distribution, are in good agreement with the theoretical ones calculated by Mandl and Skyrme.

In this paper we describe the measurements of the cross-section of the double Compton effect, process in which one γ quantum interacts with an atomic electron giving rise to two γ quanta emitted at the same time.

Preliminary results on these measurements have been given in a previous paper [1], to which we refer for literature on the theoretical studies on this process and on preceeding experimental results.

1. – Experimental apparatus.

In our measurements we detect the γ quanta which are emitted simultaneously in a double Compton scattering process by means of two scintil-

---

[1] A. Bracci, C. Coceva, L. Colli and R. Dugnani Lonati: *Nuovo Cimento*, 1. 752 (1955).

lation spectrometers in coincidence, measuring at the same time the energy of the two γ quanta which have produced the coincidence.

The incident γ-rays are emitted from about 200 mC of ^{60}Co which emits two γ in cascade with energies of 1.17 and 1.33 MeV respectively. The incident beam is collimated with a lead screen in a solid angle of 0.004 steradian.

The scattering target is a square beryllium plate whose surface, of area 4 cm^2, is perpendicular to the incident beam. The scattered γ-rays are detected by two scintillation spectrometers using one-inch cube NaI(Tl) crystals and photomultipliers of the EMI 6262-14 dynode type. The principal symmetrical axes of the spectrometers form an angle of 90° with each other and with the direction of the incident beam and intersect each other at the center of the target. The crystals can receive scattered γ-rays at angles ranging from 80° to 100° with a solid angle of 0.07 steradian. An 8 cm thick lead sheet placed above the spectrometers diminishes the number of coincidences due to cosmic rays. Between the two crystals a layer of lead is placed, thick enough to absorb the photons which, scattered by one crystal, can be detected by the other one.

The crystals are covered by layers of magnesium oxide, aluminum and lucite, of a total weight of 120 mg/cm^2. This screening hinders the detection of electrons which, scattered in an ordinary Compton process, come out of the beryllium target and fall on the crystals: on the other hand the screening is harmless as far as the absorption of the γ-rays in the energy interval of the measurements (from 25 to 500 keV) is concerned.

The electronic circuit is formed by two chains, one with particular fast characteristics, which gives the coincidence between the pulses of the two photomultipliers; the other is a proportional chain which measures the height of the same pulses. In our experimental situation, since the events caused by the double Compton scattering are about $1/10^4$ of the events corresponding to an ordinary Compton scattering, it is necessary to use a coincidence circuit with a very short resolving time to reduce the accidental coincidences between γ-rays scattered by the target in the two crystals in two ordinary Compton scattering processes. For this reason a particular coincidence circuit has been studied, which makes it possible to reach a resolving time of the order of 10^{-8} s regardless of the heights of the triggering pulses.

This coincidence circuit makes use of two fast discriminators according to MOODY *et al.* [2] and a 6BN6 tube as a mixer according to FISHER and MARSHALL [3].

---

[2] N. E. MOODY, G. J. R. MACLUSKY and M. O. DEIGHTON: *Electronic Eng.*, **24**, 214 (1952).

[3] J. FISCHER and J. MARSHALL: *Rev. Sci. Instr.*, **23**, 417 (1952).

Since the NaI crystals have a decay constant of $2.5 \cdot 10^{-7}$ s, the coincidence circuit should work with only the first part of the rise of the pulses, which is about one tenth of the total pulse at the photomultiplier anode.

Because the coincidence circuit functions only with pulses higher than 0.2 V, the photomultipliers have to work at a rather high voltage; under these conditions the pulses at the anode are no longer proportional to the energy lost by the γ-ray in the crystals.

In our measurements we have chosen a resolving time of $3 \cdot 10^{-8}$ s; the pulse emerging from the coincidence triggers the track of a cathode ray tube.

The proportional circuit functions as follows: pulses are taken at the twelfth dynode of the photomultipliers where they are proportional to the energy. From here they are sent to the vertical plates of the oscillograph through a normal amplification circuit with a rise time of 10^{-6} s and through a pulse-shaping circuit which cuts them after $3 \cdot 10^{-6}$ s.

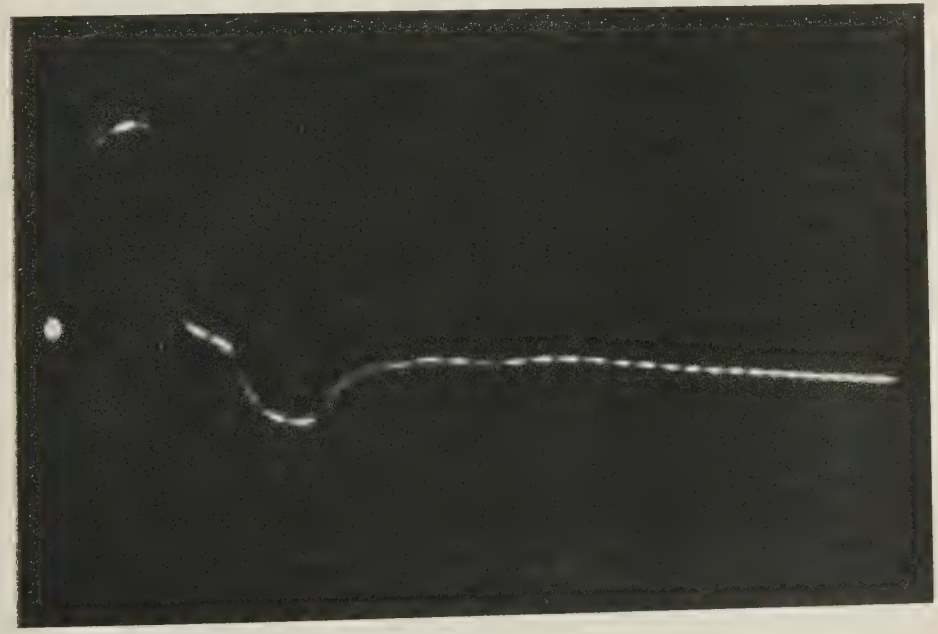

Fig. 1. – A pair of pulses as photographed on the oscillograph screen.

One of the pulses undergoes a convenient delay and in such a way that the oscillograph receives the first pulse immediately after the triggering of the track, and the second one after $6 \cdot 10^{-6}$ s. The pairs of pulses proportional to the energy lost by the coincident γ-rays in the crystasl are registered photographically. Fig. 1 shows a couple of such pulses.

2. – The method of measurement.

The number of coincidences registered per unit time, resulting from the double Compton scattering versus the energy of one of the two emitted γ-rays is given by the formula

$$n_D(k_1)\,dk_1 = 2I_0\,(d\Omega_0)\,\frac{N_{Av}}{M}\,Zs\varrho\sigma_D(k_1)(d\Omega)^2\varepsilon(k_1)\varepsilon(k_2)\,dk_1\,, \tag{1}$$

where I_0 is the number of γ emitted from the source per second, $d\Omega_0$ the solid angle subtended by the target at the source, $(N_{Av}/M)Zs\varrho$ the number of electrons in the target (N_{Av} is the Avogadro number, Z, and M the atomic number and weight respectively, s the thickness, ϱ the density). $\sigma_D(k_1)\,dk$ is the double Compton scattering cross-section in the energy interval between k_1 and $k+dk_1$ and per unit solid angle in our geometrical disposition, i.e. for scattering of the two γ-rays at 90° with the incident γ-rays and with each other, and for the incident γ energy selected by us. $d\Omega$ is the solid angle subtended by the target at the detecting crystals; $\varepsilon(k)$ is the yield of the scintillation spectrometers.

The energy k_2 of the second γ-rays scattered in a double Compton process is given by laws of conservation of energy and momentum and, in the case of scattering at 90°, is given by the formula:

$$k_2 = \frac{k_0 - k_1(1+k_0)}{1+k_0-k_1}\,. \tag{2}$$

The energy spectrum is derived from the formula:

$$\frac{n_D(k_1)}{\varepsilon(k_1)\,\varepsilon(k_2)}\,. \tag{3}$$

If we integrate the energy distribution in the energy interval determined by our experimental conditions, we get the total number of processes

$$N_D = \int_{k_{min}}^{k_{max}} \frac{n_D(k_1)}{\varepsilon(k_1)\,\varepsilon(k_2)}\,dk_1 = 2I_0(d\Omega_0)\,\frac{N_{Av}}{M}\,Zs\varrho(d\Omega)^2\int_{k_{min}}^{k_{max}}\sigma_D(k_1)\,dk_1\,. \tag{4}$$

The number of γ quanta scattered in the crystals by the target through an ordinary Compton effect at 90° is given by the formula:

$$N_s = I_0(d\Omega_0)\,\frac{N_{Av}}{M}\,Zs\varrho\sigma_e(d\Omega)\varepsilon\left(\frac{k_0}{1+k_0}\right), \tag{5}$$

where σ_e is the cross-section (per unit solid angle) of the ordinary Compton effect at 90°. From the ratio of these two expressions, we obtain the value of the double Compton scattering cross-section given by:

$$\int_{k_{\min}}^{k_{\max}} \sigma_D(k_1)\,\mathrm{d}k_1 = \frac{1}{2}\frac{N_D}{N_s}\,\varepsilon\left(\frac{k_0}{1+k_0}\right)\frac{\sigma_e}{\mathrm{d}\Omega}\,. \tag{6}$$

3. – Measurements in coincidence.

Experimental measurements have been made as follows.

In order to subtract the spurious pairs of pulses from the results, photographic registrations were taken under three different conditions:

(1) The normal conditions of measurement as previously described.

(2) A 10^{-6} s delay line is interposed between the anode of one of the photomultipliers and the coincidence circuit. By this means we eliminate « true » coincidence corresponding to the processes in which two correlated γ-rays arrive at the crystals, and we are able to measure the accidental coincidences taken under the first conditions without any variation whatsoever in either the number or the energy distribution.

(3) The beryllium target is eliminated to permit the registration of the coincidences due to cosmic rays and to any other process independent of the target.

Measurements under conditions (1) and (2) have been taken in alternate time intervals with a view to avoiding errors due to possible variations in the resolving time during the measurements, which take a few days.

The measurements have been repeated with two different targets, 1 mm and 2.5 mm thick.

Each pair of pulses has been analyzed in the following manner: from the height of the pulse the corresponding γ energy is deduced by calibrating the vertical displacement of the oscillograph beam by means of γ-rays of known energy. To do this, we used the 411 keV γ-rays of ^{198}Au and the 669 keV γ-rays of ^{137}Cs, and the X-ray line (70 keV) of ^{198}Hg. Pulses corresponding to energy less than 25 keV were not taken into account.

The two values obtained for the energy of the two pulses of the pair are respectively taken as abscissa and ordinate in a diagram in which, therefore, each point represents a coincidence. In this way three charts have been drawn as follows: (1) total counts; (2) accidental coincidences; (3) coincidences

without the target in place, due to cosmic rays and γ-rays direct from the source.

The analysis of the chart allows us, at least at the first approximation, to decide whether the points actually represent coincidences due to double

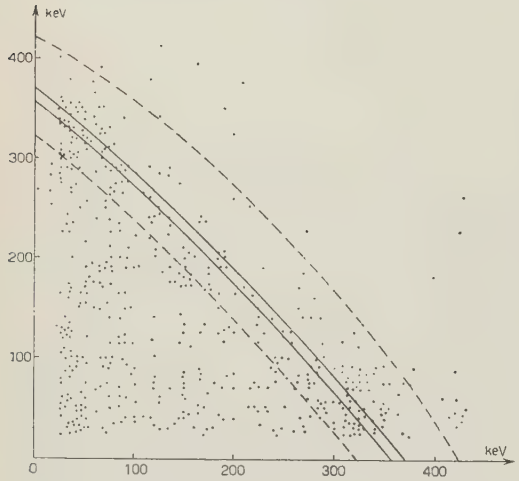

Fig. 2. – Chart showing coincidences due to double Compton effect. Each point represents a pair of γ-rays, whose energies are given by the coordinates. The solid lines trace the points corresponding to the ideal conditions of 90° scattering and photoelectric detection of the γ-rays in the crystals. The dotted lines correspond to the limiting angles under our experimental conditions, and to photoelectric detection. The target thickness is 2.5 mm.

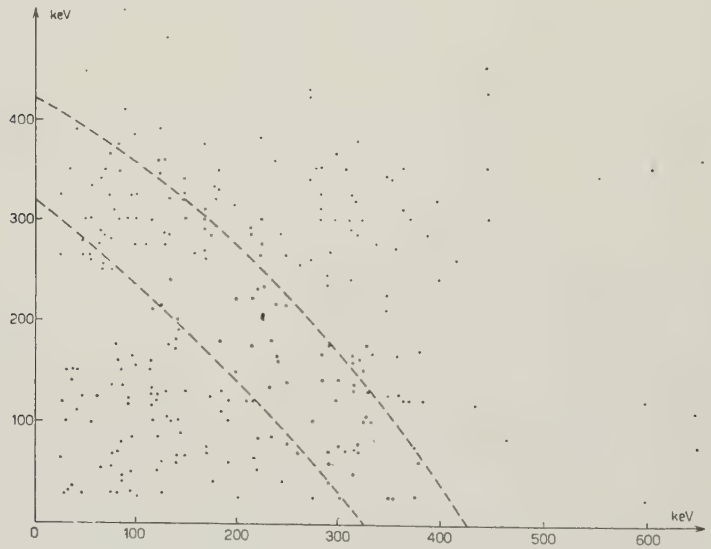

Fig. 3. – Chart showing coincidences due to accidental events. Same target as in Fig. 2.

Compton scattering and, if not, to understand in many cases to which effect they are due. Subtracting charts 2 and 4 from 1, we obtain a chart containing coincidences due to double Compton scattering. Fig. 2 shows this corrected chart. Fig. 3 shows the accidental coincidence chart.

In the charts the two solid curves represent the relation $k_1(k_2)$ in the case where the scattering is exactly at 90° as given by the formula (2) and correspond to the two values of energy of incident γ-rays 1.17 and 1.33 MeV.

The two dotted curves represent similar relations in the extreme cases of our experimental conditions where the scattering angles are smallest (upper curve) and largest (lower curve).

The points that represent coincidences due to a double Compton scattering in which both the photons have released all their energy in the crystals should be found on the chart in the area included between the dotted lines.

However, in the case where at least one of the two photons have lost only some energy in the crystal, for instance by means of a Compton scattering, they will be found in the area included between the axes and the lower dotted line.

The cosmic-ray coincidences result generally from radiations with an energy far greater than that of the γ from a double Compton scattering and correspond to a pair of pulses of which at least one is high enough to saturate the detecting system; in the chart they occupy an area covering the upper and right-hand sides, out of the area shown in the figures. Points corres-

TABLE I. – *Table showing the distribution of points in the different areas of the charts representing the measurements.*

Thickness of the target	1 mm				2.5 mm			
Duration of the measurement	1030 minutes				445 minutes			
	Experimental distribution				Experimental distribution			
	total events No. 1	accidental events No. 2	events without target No. 3	Difference	total events No. 1	accidental events No. 2	events without target No. 3	Difference
Number of events in the area above the superior curve	88	32	22	34	117	85	9	23
Number of events in the area included between the dotted curves	265	26	11	228	316	62	5	249
Number of events in the area under the inferior curve	270	55	64	151	379	98	39	242

ponding to accidental coincidences are distributed in a square area limited by parallels to the axes, corresponding to the maximum energy of the ordinary Compton scattering.

The points corresponding to the accidental and cosmic ray coincidences are subtracted from the chart of the total coincidences after the charts have been divided into squares of 50 keV sides.

In Table I we report the number of points found in the different zones of the charts and the respective duration of the measurements.

After the subtraction it can be noted that only a few points remain in the area above the upper curve, which cannot be explained by means of the double Compton effect.

The number of points under the lower curve are more than the number predicted from the ratio between Compton and photoelectric yields of the spectrometers for the energies of the γ-rays measured. This difference can be explained when one considers the photons which, scattered by the target out of the detection angle, are diffused into this angle by the lead screen or otherwise generate X-rays in the screen revealed by the crystal itself.

These photons have, however, lost energy in the second scattering and all of them fall into the zone which corresponds to low energies.

4. – Energy spectrum of photons.

To construct the energy spectrum, we take into account only the points included in the dotted lines. A histogram is constructed first projecting these points from the origin of the axes into the middle line of the strip and thereafter from this line into each of the two axes which are divided into intervals of 25 keV. The histogram is obtained as a mean value of the results found by the projection into the two axes.

To compare this spectrum with the theoretical one, it is necessary to correct it for the yield of the spectrometers and for the absorption in the target as a function of the γ energy.

The yield of NaI crystals has been deduced from the work of MAEDER, MULLER and WINTERSTEIGER [4]. These yields, calculated in the case of perpendicular incidence on the face of the crystals, have been multiplied by a factor which takes into account the angular aperture of the γ beam incident on the crystals.

The correction for absorption in the target takes into consideration the fact that the γ-rays, already scattered in a double Compton effect, can be

---

[4] D. MAEDER, R. MÜLLER and V. WINTERSTEIGER: *Helv. Phys. Acta*, **27**, 1 (1954).

rescattered in the same target and emerge from the detection angle, or otherwise loose energy, thus going into the area under the lower curve of the chart.

This correction is of the order of 25 percent.

In Table II the number of coincidences per 25 keV energy interval (in the case of the 2.5 mm target) is shown as given by the chart (first column) and after the appropriate correction (second column). The spectra obtained after having applied these corrections are shown in Fig. 4 for the two targets used. In the

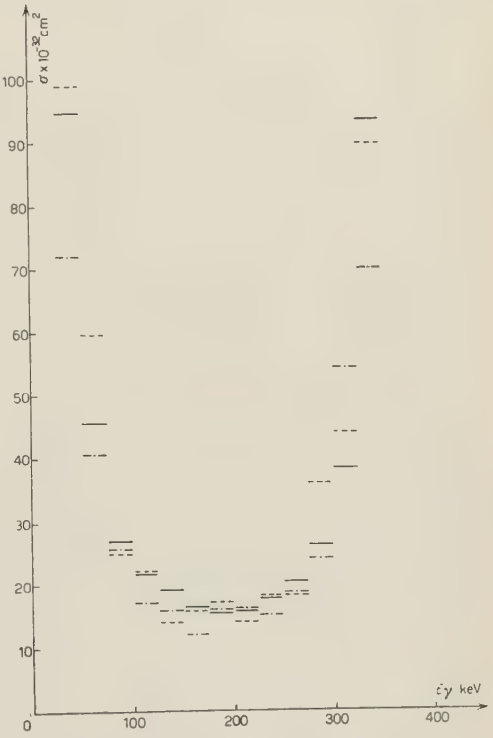

Fig. 4. – Energy spectrum of the γ-rays scattered in the double Compton effect. The ordinates give cross-section values in 10^{-32} cm². –·–·– Measurement with beryllium target 1 mm thick. – – – Measurement with beryllium target 2.5 mm thick. ——— Histogram derived from the theoretical spectrum.

TABLE II. – *Tabulated energy spectrum.*

The second column gives the number of points per 25 keV interval, as given by the experimental measurements (charts in Fig. 2). The third column gives the number of points after the appropriate corrections.

Energy interval in keV	Experimental energy spectrum	Corrected energy spectrum
25 ÷ 50	42	157
50 ÷ 75	28	95
75 ÷ 100	14	39
100 ÷ 125	13	35
125 ÷ 150	13	23
150 ÷ 175	14	25
175 ÷ 200	12	27
200 ÷ 225	9	23
225 ÷ 250	11	28
250 ÷ 275	10	28
275 ÷ 300	21	57
300 ÷ 325	24	74
325 ÷ 350	37	143

same figure the theoretical spectrum calculated from the data of MANDL and SKYRME [5] is also shown.

5. – Cross section measurements.

The cross-section, as given by formula (6), for the double Compton scattering corresponding to our experimental conditions, is obtained by integration of the spectra discussed above and by the measurement of the number of γ-rays scattered into the crystals by the target in an ordinary Compton scattering.

This latter measurement is taken observing the distribution of pulses from the twelfth dynode with a 99 channel pulse-analyzer; the peak at 360 keV which is due to γ scattered at 90° and releasing all their energy in the crystal is clearly visible as shown in Fig. 5.

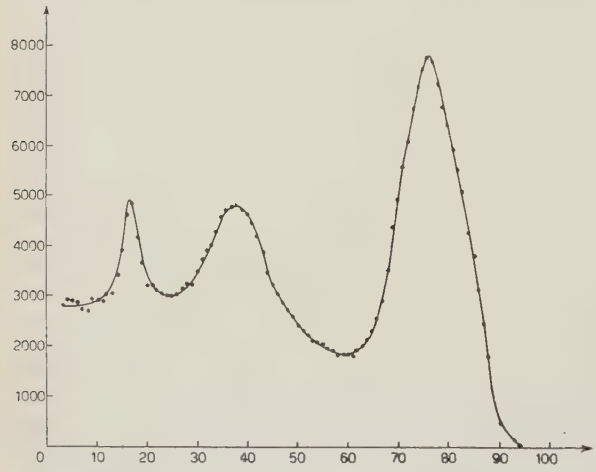

Fig. 5. – Energy spectrum of γ-rays scattered by the single Compton effect, as given by our spectrometers. The right-hand peak corresponds to the γ-rays having lost all their energy in the crystal. This energy is 360 keV. Both coordinates, γ-energy on the abscissa and number of counts on the ordinates are given in arbitrary units.

In the measurement we count only the pulses in this peak. Pulses due to source γ-rays filtered through the lead screen or scattered into the crystal by the material surrounding the exit of the collimating hole are counted independently by removing the target and are subtracted as a background. After this subtraction the number of single Compton processes is obtained by multiplying the number of pulses by the yield of the spectrometer. This enables us to calculate the absolute value of the cross-section for double Compton scattering.

For the two cases of 1 mm and 2.5 mm thickness of the beryllium target, the cross-section is finally obtained and has the following values:

$$1 \text{ mm}: \quad \sigma_D = 3.9 \cdot 10^{-30} \text{ cm}^2 \cdot \text{sterad}^{-1} ;$$

$$2.5 \text{ mm}: \quad \sigma_D = 4.7 \cdot 10^{-30} \text{ cm}^2 \cdot \text{sterad}^{-1} .$$

---

[5] F. MANDL and T. H. SKYRME: *Proc. Roy. Soc.*, **215**, 497 (1952).

These values are to be compared with the values calculated from the theory under our experimental conditions: $\sigma_D = 4.52 \cdot 10^{-30}$ cm^2·sterad^{-1}.

6. – Discussion of the results.

The error attributed to this measurement can be estimated at about 20% and are principally due to the uncertainty of the corrections which are made on the experimental results. The most important correction is that due to the yield of the crystal for the detection of γ-rays.

The agreement of the two measurements with each other and with the theoretical value appears to be quite satisfactory, as is also the agreement of the experimental curves of the energy distribution with the theoretical results, considering the experimental errors which are of the order of 30% on each energy channel.

The agreement between the measurement made with targets of different thickness and the analysis of the distribution of points on the chart excludes the presence, at least to an appreciable extent, of an effect due to coincidences between a γ-ray scattered by a single Compton effect and one emitted by the bremsstrahlung effect of the electrons in the target. In fact the number of events due to a process of this type should increase proportionally to the square of the target thickness.

* * *

The authors wish to express their appreciation to Professor G. Bolla, Professor P. Caldirola, Professor B. Ferretti and Professor U. Facchini for many valuable suggestions and discussions; and to Professor E. Gatti and to C. Cottini for the study of the electronic devices.

RIASSUNTO

È stata misurata la sezione d'urto dell'effetto Compton doppio nel caso particolare di diffusione dei due quanti γ a 90° tra loro e con il quanto γ incidente. È stata pure rilevata la distribuzione energetica dei γ diffusi. I quanti γ sono rivelati per mezzo di due spettrografi a scintillazione formati da cristalli di NaI(Tl) e fotomoltiplicatori EMI, posti in coincidenza. Le coppie di impulsi corrispondenti a due γ in coincidenza vengono fotografate su di uno schermo oscillografico a quindi esaminate. I risultati sperimentali per la sezione d'urto e per lo spettro sono in buon accordo con i valori teorici calcolati da Mandl e Skyrme.

Supplementary Remark on My Previous Note "Velocity of the Dirac Electron".

Z. KOBA

Research Institute for Fundamental Physics, Kyoto University - Kyoto, Japan

(ricevuto il 30 Ottobre 1955)

In a previous note [1] concerned with the velocity eingenvalues of the Dirac electron, the mechanism was analyzed by which a Dirac wave packet representing a simultaneous eigenstate of position and velocity travels with the light velocity during a very short interval. As a supplementary remark to this note I should like to point out that two successive « ideal measurements » of the position, if performed within a time very short compared with the reciprocal Compton frequency, $t_c = \hbar/mc^2$, would indeed lead to an eigenstate of the corresponding component of the velocity operator. Thus it turns out that the procedure of the velocity measurement described in Dirac's text-book [2], is justified under the above-mentioned limitation. (As I remarked before, it appeared quite dubious at first sight, but a more detailed examination has witnessed its correctness, which is essentially due to the peculiar behaviour of a relativistic wave packet immediately after an ideal position determination.)

It is quite doubtful whether a quantum mechanical measurement of a coordinate of a relativistic particle with the accuracy $\Delta x \lesssim \hbar/mc$ can be carried out [3]. In the following, nevertheless, I shall argue as if an absolutely exact measurement of the position, $\Delta x \to 0$, were possible with the only restriction $\Delta x \cdot \Delta p \gtrsim \hbar$ being imposed. My reasoning is therefore simply meant to clarify a subtle property of the relativistic wave equation and perhaps has little to do with a real process of the position measurement.

Suppose an exact determination of the x_3-coordinate, say, of a Dirac electron has been performed. (One has to restrict oneself to one component of coordinates, since the different components of the velocity do not commute with each other.) As the result of this measurement the wave packet will shrink to a δ-function-like form at the eigenvalue x_3', say. Now this shrinked packet is in general a superposition of the two eigenfunctions of α_3 belonging to the eigenvales $+1$ and -1 respectively. Now the previous analysis holds for each of these two components and they will.

---

(1) Z. KOBA: *Nuovo Cimento*, **3**, 1 (1956).

(2) P. A. M. DIRAC: *Principles of Quantum Mechanics* (Oxford, 1947), p. 261.

(3) E.g., W. PAULI: *Handb. d. Phys.*, **24**-1 (1933), p. 91.

proceed in the opposite directions ($+x_3$ and $-x_3$ respectively) with the light velocity. (See the figure). A simple calculation shows that this behaviour lasts for a time Δt far shorter than t_c. Besides the above-mentioned two peaks there arises a smaller swelling at the point x_3' whose height is proportional to Δt. After a time $\sim t_c$ the wave packet is smeared

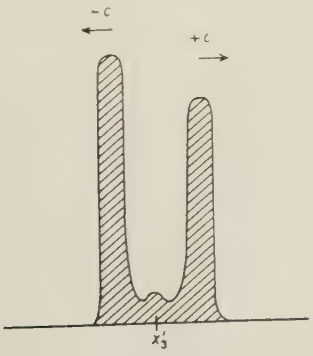

Fig. 1.

completely and its behaviour becomes somewhat similar to that of a Schrödinger packet, though its both « edges » proceed further with the light velocities c and $-c$ as is required from the hyperbolic character of the relativistic wave equation.

If one makes, however, another ideal determination of the x_3-coordinate immediately after the first, one will be almost sure to get either the value $x_3'+c\Delta t$ or $x_3'-c\Delta t$, Δt being the time interval, as is evidently seen from the figure. As the result of this second measurement, the packet will « shrink » again, leaving only one of the peaks. Since the state has thus jumped into a simultaneous eigenstate of α_3 and x_3, this is a velocity measurement in the quantum-mechanical sense of the term. This way of successive position measurements is just what Dirac describes as the velocity measurement [2], though its justification is not so simple as is originally suggested. Of course there will be a lot of possible ways for measuring the quantity represented by the operator α, but the above-mentioned procedure can be regarded as the one most favourable for the interpretation as « velocity ».

It is further inferred that a similar relation will hold in the cases of other relativistic wave equations.

* * *

In conclusion I should like to express my sincere gratitude to Prof. P. A. M. Dirac for his interest shown and remark given to my previous note, to Prof. R. P. Feynman for his interest and encouragement, and to Dr. I. Fujiwara for his discussions.

Three Examples of Complete τ-Decay.

M. Scharff

Institute for Theoretical Physics, University of Copenhagen, Denmark

G. Gjeldaker and S. O. Sørensen

Institute of Physics University of Oslo, Norway

(ricevuto il 30 Novembre 1955)

The three events described in this note were found in a stack of stripped emulsions exposed in the course of the 1953 Sardinia expedition. The stack (S_{17}) was later split in two halves, which were examined in Oslo and Copenhagen, respectively. The event τ_{O1} was found by the Oslo group when tracing stopped π-mesons backwards from the point of decay or interaction. The total number of π-tracks followed was 630. The other two events were found in Copenhagen during a special scan for heavy mesons. In 106 cm^3 of emulsion, 17 K-mesons were found to decay with emission of a single charged particle. A detailed account of these events has already been published [1].

The data concerning the τ-meson decays are set out in Table I. For each secondary track is given the angle ϑ between the opposite pair of secondary tracks and the angle φ between the plane containing the pair and the plane of the emulsion. The secondary tracks from the decay of τ_{O1} and τ_{K2} are apparently coplanar within narrow limits, but, in the case of τ_{K3}, track *a*) was too scattered to allow a reliable measurement of dip, and the angles ϑ_b and ϑ_c were therefore calculated from the projected angles on the basis of assumed coplanarity. This assumption, as well as that of the identity of the negative secondaries, is justified by the resulting momentum balance. A thickness of 600 μm for the unshrunk emulsion was used for the calculation of angles and ranges, but the results are rather unsensitive to small changes in this figure.

In each of the three events, two of the secondaries decayed to μ-mesons at the end of their range, while the third secondary showed nuclear interaction. Assuming all the secondaries to be π-mesons, the energies were calculated from the range-energy relation of Baroni *et al.* [2]. The mean Q-value is

[1] J. K. Bøggild, J. E. Hooper, W. C. G. Ortel and M. Scharff: *Dan. Mat. Fys. Medd.*, **30**, no. 3 (1955).

[2] G. Baroni, C. Castagnoli, G. Cortini, C. Franzinetti and A. Manfredini: *Bureau of Standards CERN*, Bull. no. 9 (1954).

TABLE I.

PRIMARY			SECONDARIES						
Event	Parent Star	Length mm	Track	Charge	ϑ degrees	φ degrees	Range mm	Energy MeV	$pc/\sin\vartheta$ MeV
τ_{01}	15+16p	6	*a*	—	148.0 ± 1.4	47	2.50	10.5 ± .2	104.0 ± 4.2
			b	+	116.0 ± 1.5	47	14.90	29.7 ± .5	106.3 ± 1.5
			c	+	95.8 ± 1.6	47	19.03	34.4 ± .6	104.5 ± 1.1
							$Q = 74.6 \pm .9$ MeV		
τ_{K2}	27+ 8p	49	*a*	—	155.2 ± .7	20	4.33	14.3 ± .3	154.5 ± 4.2
			b	+	155.8 ± .8	22	4.38	14.4 ± .3	158.5 ± 5.1
			c	+	48.6 ± 1.0	21	28.40	44.0 ± .7	159.0 ± 2.8
							$Q = 72.7 \pm .8$ MeV		
τ_{K3}	22+12p	13	*a*	+	165.8 ± .3	13	0.209	2.55 ± .06	109.3 ± 2.4
			b	+	115.7 ± .5	—	18.10	33.4 ± .6	113.6 ± 1.2
			c	—	78.5 ± .5	—	23.08	38.8 ± .7	113.0 ± 1.1
							$Q = 74.8 \pm .9$ MeV.		

(74.0 ± .5) MeV, corresponding to a τ-meson mass of (964 ± 1) m_e. The errors on these figures are those derived from the range straggling of the secondaries, which, being 3÷4%, is far more important than the errors of measurement. Larger systematic errors could, however, be introduced through the conversion of range to energy. For this reason, we checked the range-energy relation with μ-mesons from the decay of stopped π-mesons. 20 such μ-meson tracks in a single plate were analyzed by the regression method of FRY and

WHITE [3] (slightly modified for use in thick emulsions). As a byproduct of this analysis, the thickness of the unshrunk emulsion was found to be 590 ± 40 μm, in good agreement with the nominal value. The fluctuation of thickness between different plates was less than 2%. The mean range of the μ-mesons was (594 ± 10) μm, which deviates (0.0 ± 1.7) % from the range of 4.11 MeV μ-mesons as given by the range-energy curve.

Unfortunately, this very good fit at low energy is only relevant for the τ-secondaries if the shape of the curve is correct. That this is the case to a first approximation is demonstrated by the momentum balance of the secondaries; however, on account of the limited accuracy of the measurement of angles one cannot exclude a systematic error of $\approx 2\%$ in the energy of the fast secondaries, which corresponds to an error of $\approx 3\, m_e$ on the τ-meson mass. An analysis of the proton stopping power of different substances, measured at various energies, shows that such an error in the range-energy relation is possible, even if the curve is correct both at lower and at higher energies.

[3] W. F. FRY and G. R. WHITE: *Phys. Rev.*, **93**. 1427 (1954).

Energetics of Elimination of Adsorbed Gases from Dielectric Surfaces Under Electrodeless Discharge.

S. R. Mohanty

Physico-Chemical Laboratories, Banaras Hindu University, India

(ricevuto il 5 Dicembre 1955)

The author [1] has shown that the increase in the current i under continued A.C. electrodeless discharge through electronegative gases (and vapours) is represented accurately by the relationship

$$(1) \qquad (i_{\max} - i_t) = (i_{\max} - i^0)\, e^{-kt},$$

where i^0 is the value of i at commencement of the discharge ($t=0$), i_t that at time t, $i_{\max}$ that of the constant maximum obtained on prolonged discharge, and k a constant. This has been traced [2] to diminution in the work function φ of the (instantaneous) cathode through elimination of adsorbed gas layer(s) by desorption or/and chemical interaction [3]. Equation (1) is identical in form to that of the first order chemical reaction. This communication reports on the determination of the heat of activation ΔH_a from the Arrhenius equation

$$(2) \qquad k = A \exp\left[-\Delta H_a/RT\right]$$

for the dependence of k on the Kelvin temperature T.

All-glass Siemens' ozonizers of identical dimensions (internal diameter of the outer tube, 19.9 mm; external diameter of the inner tube, 9.4 mm; electrode separation, 5.25 mm; thickness of the glass walls, 1.0 mm; length of the discharge column, 18.0 cm), chemically cleaned and degassed, were filled with pure oxygen at 160 mm (28 °C). Each discharge tube

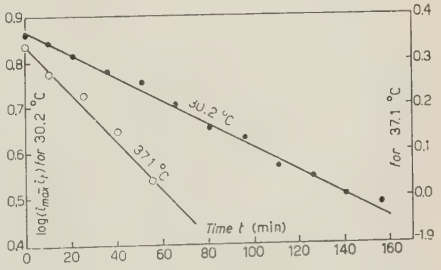

Fig. 1. – Time dependence of the current under electrodeless discharge at different temperatures.

assembly was enclosed in a glass jacket through which thermostated water of temperature (25 ÷ 40 °C) regulated to ± 0.05 °C was circulated. The ozonizers were subjected to continuous discharge

(1) S. R. Mohanty: *Nuovo Cimento* **2**, 1107 (1955).

(2) S. R. Mohanty: *J. Chim. Phys.* (Under publication).

(3) S. R. Mohanty: *J. Indian Chem. Soc.*, **28**, 487 (1951).

at 3.7 kV (rms, 50 Hz) and i was measured at intervals of t. Data for 30.2 and 37.1 °C are contained in Fig. 1.

Values of k at 30.2 and 37.1 °C calculated from the slopes of the lines are respectively 0.005889 and 0.01214 min^{-1}. The heat of activation ΔH_a over this range of T, from the integrated form of equation (2), is 19.61 kcal $mole^{-1}$. That this is of the order of activation energies characteristic of chemical reactions indicates that the agency responsible for the elimination of the adsorbed gas from the electrode surface is predominantly of chemical nature.

* * *

Grateful thanks of the author are due to Prof. S. S. Joshi for his kind interest in the work.

Un'osservazione sulla condizione supplementare dell'elettrodinamica.

P. Bocchieri e A. Loinger

Istituto di Fisica dell'Università - Pavia
Istituto Nazionale di Fisica Nucleare - Sezione di Milano

(ricevuto il 9 Dicembre 1955)

Nell'elettrodinamica classica (« in vacuo ») la condizione di Lorentz $(\partial\Phi_\mu/\partial x_\mu)=0$ è evidentemente incompatibile con la parentesi di Poisson $(\Phi_\mu(x), \Phi_\nu(x')) = \delta_{\mu\nu}D(x-x')$. Tale difficoltà è caratteristica del formalismo canonico [1]. Essa si ripresenta nell'elettrodinamica quantistica: infatti la relazione che dà il commutatore di $\Phi_\mu(x)$ e $\Phi_\nu(x')$,

$$[\Phi_\mu(x), \Phi_\nu(x')] = i\delta_{\mu\nu}D(x-x'), \tag{1}$$

è chiaramente anch'essa incompatibile con la condizione di Lorentz.

Come tutti sanno, Fermi (1929) ritenne di poter superare questa difficoltà, imponendo più debolmente, in luogo della condizione di Lorentz, che tutti i ket descriventi stati fisici del sistema soddisfino (nella descrizione di Heisenberg) alla:

$$\frac{\partial\Phi_\mu}{\partial x_\mu}\,|\rangle = 0\,. \tag{2}$$

È però noto [2] che la (2), unita alla (1), fa sì che il vettore di stato del sistema abbia una norma infinita, rendendo a rigore privo di senso il considerare valori di aspettazione; a ciò fu ovviato col metodo di Gupta e Bleuler [3].

La (2) dà però origine anche ad una difficoltà di natura assai meno riposta, anzi, a dire il vero, affatto banale e che è stranamente passata inosservata: se si deriva infatti la (1) rispetto a x_μ e si prendono i valori di aspettazione di ambo i membri, si ottiene

$$\langle|\left[\frac{\partial\Phi_\mu(x)}{\partial x_\mu},\ \Phi_\nu(x')\right]|\rangle = i\,\frac{\partial D(x-x')}{\partial x_\nu}\,.$$

[1] Nella formulazione hamiltoniana classica di Dirac essa viene aggirata assumendo la condizione di Lorentz come equazione « debole ».

[2] Vedi, per esempio, W. Pauli: *Ausgewählte Kapitel aus der Feldquantisierung* (Zürich, 1951), p. 51 e segg.

[3] K. Bleuler: *Helv. Phys. Acta*, **23**, 567 (1950).

Ma, in forza della (2), il primo membro è nullo, mentre il secondo è generalmente diverso da zero.

È facile vedere che un inconveniente di questo genere *non* si presenta nella formulazione di Gupta e Bleuler.

La condizione supplementare di Gupta e Bleuler è:

$$\frac{\partial \Phi_\mu^{(+)}}{\partial x_\mu} |\rangle = 0 \,, \tag{3}$$

da cui:

$$\left(\frac{\partial \Phi_j^{(+)}}{\partial x_j} - \frac{\partial \Phi_4^{(-)}}{\partial x_4} \right) \quad 0 \,;$$

(si ricordi che nel formalismo di Gupta e Bleuler Φ_μ è hermitiano). Derivando la (1) rispetto a x_μ e prendendo i valori di aspettazione di ambo i membri, si ha:

$$|\eta \left[\frac{\partial \Phi_\mu(x)}{\partial x_\mu} \,,\, \Phi_\nu(x') \right] |\rangle = i \frac{\partial D(x - x')}{\partial x_\nu} \langle |\eta| \rangle \,.$$

Il primo membro si può scrivere:

$$\eta \left[\frac{\partial \Phi_\mu^{(+)}(x)}{\partial x_\mu} \,,\, \Phi_\nu(x') \right] |\rangle + \langle | \eta \left[\frac{\partial \Phi_\mu^{(-)}(x)}{\partial x_\mu} \,,\, \Phi_\nu(x') \right] |\rangle \,;$$

e, tenendo conto della (3):

$$\langle | \eta \frac{\partial \Phi_\mu^{(+)}(x)}{\partial x_\mu} \Phi_\nu(x') |\rangle - \langle | \eta \Phi_\nu(x') \frac{\partial \Phi_\mu^{(-)}(x)}{\partial x_\mu} |\rangle =$$

$$= \langle |\eta| \rangle \left(i \frac{\partial D^{(+)}(x - x')}{\partial x_\nu} + i \frac{\partial D^{(-)}(x - x')}{\partial x_\nu} \right) = \langle |\eta| \rangle \, i \frac{\partial D(x - x')}{\partial x_\nu} \,; \quad \text{q. e. d.}$$

Considerazioni completamente analoghe valgono anche nel caso più generale di campi interagenti, purchè ci si metta nella descrizione d'interazione.

IL NUOVO CIMENTO Vol. III, N. 1 1° Gennaio 1956

Number of Feynman Graphs and Convergence (*).

E. R. Caianiello (+)

University of Rochester - Rochester N.Y.

(ricevuto il 15 Dicembre 1955)

Approximate estimates of the number of Feynman graphs pertaining to the n-th order term of a perturbative expansion have often been attempted, with a view to investigating questions of summability. In particular, it has been stated several times, on such premises, that expansions such as occur in electrodynamics are asymptotically convergent at best. While this may well be the case, we propose to show here that arguments of this sort are definitely inconclusive. We do so by producing a counter-example: a finite model of electrodynamics, which is amenable to the exact theory if a limiting process is performed, and exhibits in any case the same number and type of graphs as the latter; all perturbative expansions obtained from this model certainly converge within a finite radius of convergence, while an evaluation of the exact number of graphs would lead, mistakenly, to infer their divergence.

It will suffice, to this effect, to adopt, very rough majoration procedures; for the sake of simplicity, we also disregard relativistic covariance, and assume a finite volume V and time interval T of integration. Our model consists in assuming that the fermion field admits only a finite number F of free modes; this, clearly, sets also an upper limit B to the number of effective free boson modes. One finds then easily, from the definition of D_F and S_F as vacuum expectation values:

$$|[xy]_{\mu\nu}| < \frac{B}{2Vm_B}, \quad |(xy)_{\beta\alpha}| < \frac{\sqrt{2}F}{V}, \tag{1}$$

with [1]

$$[xy]_{\mu\nu} = \tfrac{1}{2}\delta_{\mu\nu}D_F(x-y),$$

$$(xy) \quad = (\gamma\partial - m_F)\Delta_F(x-y),$$

$$m_B;\ m_F = \text{boson and fermion masses.}$$

(*) This work was assisted by the AEC.

(+) On leave during summer 1955 from the University of Rome.

(1) Notation and formulae are as in *Nuovo Cimento* **11**, 492 (1954).

From the expansion [1]

$$(2) \qquad K\begin{pmatrix} x_1 \dots x_{N_0} \\ y_1 \dots y_{N_0} \end{pmatrix} = \sum_0^\infty \left(\frac{\lambda^2}{2}\right)^n \frac{1}{n!} \int \sum \gamma^{11} \dots \gamma^{2n} [\xi_1 \xi_2] \dots [\xi_{2n-1} \xi_{2n}] \begin{pmatrix} x_1 \dots x_{N_0} \ \xi_1 \dots \xi_{2n} \\ y_1 \dots y_{N_0} \ \xi_1 \dots \xi_{2n} \end{pmatrix},$$

one has then, for any values of indices and variables, if

$$(3) \qquad x = \lambda^2 4^6 B F^2 \frac{T^2}{V m_B},$$

that

$$(4) \qquad \left| K\begin{pmatrix} x_1 \dots x_{N_0} \\ y_1 \dots y_{N_0} \end{pmatrix} \right| <$$

$$< \sum_0^\infty \left(\frac{\lambda^2}{2}\right)^n \frac{1}{n!} V^{2n} T^{2n} \sum_{\mu,\alpha,\beta} |\gamma^{\mu_1}_{\alpha_1\beta_1}| \dots |\gamma^{\mu_{2n}}_{\alpha_{2n}\beta_{2n}}| \left(\frac{B}{2 V m_B}\right)^n \left(\frac{\sqrt{2}F}{V}\right)^{N_0+2n} (N_0 + 2n)^{(N_0/2)+n} =$$

$$= \left(\frac{2F}{V}\right)^{N_0} \sum_0^\infty \frac{((N_0/2) + n)^{(N_0/2)+n}}{n!} x^n,$$

which converges for any N_0 provided $x < 1/e$. (The expression for arbitrary N_0 can be connected easily to that corresponding to $N_0 = 0$, the sum of which is $1/(1+\tau)$, with $\tau e^\tau = -x$). If $m_B = 0$, then $V m_B$ in (1) must be replaced by $V^{\frac{2}{3}}$, since the wavelength cannot exceed the side of the cube (in a finite volume there can be no infrared catastrophe).

The majorant is convergent because (2) contains determinants (due to the exclusion principle for fermions), which can be treated with Hadamard's inequality. Sheer counting of the number of graphs, that is of the number of terms which arise on expanding the determinants, times the numerical coefficient of λ^{2n}, would yield instead a divergent sum (if each graph is given the same weight, as is the case in che customary discussions). (3) shows most perspicuously how divergencies arise when the limit to the actual theory is taken.

(4) is the natural counterpart, in a linear fermion-boson theory, of the classical Fredholm majorant of the one-field theory: we find here a finite radius of convergence. It is clear that this procedure becomes meaningless, because yielding divergent majorants, in other cases, as for instance that of a boson field coupled quadratically to another boson field, or of a Fermi interaction; nor is there any reason to expect holomorphy (apart from well known arguments), even in a finite theory, except when it can be proved explicitly.

The main problem, of course, is that of studying the transition from this model to the actual theory, including the effects of renormalization. A complete discussion, which requires the handling of quite critical limiting processes, will be presented elsewhere. We may notice here that we have thus proved a result which may have some interest in itself (apart from the excessive simplifications introduced, which can be adjusted without much trouble to have a covariant theory): if we think that the « true » theory of particles contains a fundamental length which sets a lower limit to Compton wavelengths; or that, in agreement with general rela-

tivity, no energy can exceed the total mass of the universe; or if we just find some good reason for believing in a cut-off: then electrodynamics, and related meson theories, certainly converge in configuration space, previous to the (finite) renormalizations, within some finite range of λ.

* * *

In conclusion, the author takes pleasure in expressing his sincerest thanks to Dr. R. E. Marshak for the kind and warm hospitality extended to him in his department, in the stimulating atmosphere of which this work was completed.

A High Energy Shower.

A. Debenedetti, C. M. Garelli, L. Tallone, M. Vigone and G. Wataghin

Istituto di Fisica dell'Università - Torino
Istituto Nazionale di Fisica Nucleare - Sezione di Torino

(ricevuto il 17 Dicembre 1955)

The analysis of the phenomena produced by electrons and photons of energy greater than 10^{11} eV is interesting in view of a possible check of the laws of quantum electrodynamics. The observed events are in some cases associated with mesons and nucleons; but in other cases it has not been possible to relate them to any nuclear interaction.

Some examples of high energy cascade showers have recently been observed ([1-6]). They seem to present the following deviations from the previsions of the cascade theory: a marked excess of high energy pairs and an anomalously high trident production.

A tentative interpretation of these phenomena will be possible only on the basis of a richer statistics. The purpose of the present work is to contribute to the collection of data with the description of a possibly anomalous event ([7]) (Fig. 1),

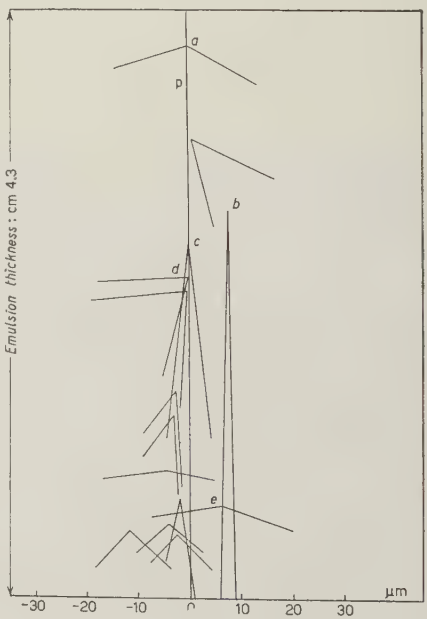

Fig. 1.

([1]) N. Schein, D. M. Haskin and M. G. Glasser: *Phys. Rev.*, **95**, 855 (1954).

([2]) A. Debenedetti, C. M. Garelli, L. Tallone, M. Vigone and G. Wataghin: *Nuovo Cimento*, **12**, 954 (1954); *Nuovo Cimento* **2**, 220 (1955).

([3]) A. Milone (Genova): comunicated at the Pisa Conference. June 1955.

([4]) M. Miesowicz W. Wolter and O. Stanisz: comunicated at the Pisa Conference. June 1955.

([5]) M. Koshiba and M. F. Kaplon: *Phys. Rev.*, **100**, 327 (1955).

([6]) E. Lohrmann (Bern): private communication.

([7]) The event has been reported by G. Wataghin at the Rochester Conference on High Energy Physics, February 1955 (see Proceedings p. 120), and at the Mexico Conference, September 1955.

that was observed in an emulsion stack of the Sardinia Expedition 1953.

A minimum track (p) enters the emulsion at an angle of 22° with the vertical; after a range of 3 mm it gives origin to a low energy trident (a) (about 50 MeV). After 16 mm at a radial distance of 7.5 μm from track p a high energy pair (b) starts, whose tracks are unresolvable for more than 5 mm. A careful measurement of the distance between pair b and track p seems to indicate that they are parallel or form an angle $\leqslant 5 \cdot 10^{-4}$ rad. Along the path of track p a shower of pairs of minimum tracks is observed, among which two are tridents originating on track p: (c) of energy of some GeV, and (d) of energy of some hundred MeV. Another low energy trident (e) is created on a track of pair b.

Some of the secondary pairs have energies of the order of $10^9 \div 10^{11}$ eV, and it is possible to establish that they are electron pairs.

Within the limits of the errors, it is not possible to decide whether pair b has been irradiated by track p or the event is due to a charged particle entering the emulsion associated to a high energy photon. If we try to interpret the phenomenon in the simplest hypothesis of an electro-photonic shower produced by track p, the number of tridents seems higher than the expected value.

To compare the number of the observed tridents with the theoretical predictions it is necessary to know the energy of the parent particles (track p and pair b). Scattering measurements on these tracks are unreliable owing to the steepness of the event. However, the energy of particle p can be evaluated from the analysis of the cascade; on the basis of Arley's calculations ([8]) it turns out to be of the order of $5 \cdot 10^{11}$ eV. As it is unreliable to derive the energy of pair b from its opening angle ([9]), we tried to get some information about its order of magnitude from the ionization method proposed by Perkins ([10]). The measurements seem to indicate an energy of about 10^{11} eV.

The 4 tridents observed are therefore produced by 3 particles of energy ranging from 10^{11} and 10^{12} eV, whose total path is about 10 cm. If from the number of apparent tridents we subtract the pseudo-tridents, according to the correction proposed by Koshiba and Kaplon ([5]), we obtain a value of 2.5 true tridents.

Following Bhabha's theory ([11]) the mean free path for trident production in emulsion by electrons of energy $10^{11} \div 10^{12}$ eV, varies from 14 to 9.6 cm; it seems 2 or 3 times greater than the observed one. Of course a definite conclusion can only arise from the comparison of all the results known up to date ([4-6]).

Anyhow, if further examples confirm the anomalous abundance of tridents in showers of the described type, this will be a first indication of the inadequacy of the present quantum electrodynamics in the high energy region.

A systematic investigation on high energy showers in a big stack is in progress in this laboratory.

([8]) M. Arley: *Proc. Roy. Soc.*, **168**, 519 (1938).

([9]) E. Lohrmann: *Nuovo Cimento*, **2**, 1029 (1955).

([10]) D. H. Perkins: *Phil. Mag.* **46**, 1146 (1955).

([11]) H. Y. Bhabha: *Proc. Roy. Soc.*, **152**, 559 (1935).

A Possible Example of Production and Annihilation of an Antiproton.

M. Teucher and H. Winzeler

Physikalisches Institut der Universität - Bern

E. Lohrmann

Hochspannungslaboratorium Hechingen

(ricevuto il 23 Dicembre 1955)

In a stack of 108 stripped emulsions 20 cm × 30 cm, 600 μm thick, flown at an altitude of 29 km in Texas on January 13th, 1955, an event was found consisting of two stars connected by a heavily ionizing particle. The primary star (A) is a «jet» of type 2+12p with a median angle of 4.5°. One of the heavy tracks ends uneventfully after 10.4 mm. The other one comes to rest after 308 μm and produces a star (B) of type 9+1. The mass of this particle is according to constant sagitta measurements

$$1\,880^{+1000}_{-650}\ m_e.$$

Its direction of flight was determined by constant cell scattering in two halfs, the ratio r between the sagittas of the two halves being $1.4 < r < \infty$. The ratio of the total number of gaps in the two halfs is 4/7. This indicates that the particle runs from A to B.

The number of δ-rays of more than 3 grains was found to be 5, while one should expect 6 for a proton of the same rest range.

The details of star B are given in Table I and Fig. 1.

The particle producing track No. 7 leaves the stack after crossing 42 emulsions. The mass and the energy were determined by variation of mean gap-length with range. The identity and energy of track 4 were determined by the ionisation-scattering-method. It undergoes an inelastic collision producing a star of type 5+1π after 4.6 mm.

The probability of a chance coincidence was calculated assuming that two stars of energy 1 GeV are lying within a distance of 600 μm and are connected by a proton track ending in a volume of 10 μm^3 around the cente of one star. It is found to be $2 \cdot 10^{-4}$, taking into account the total volume of 100 cm^3 scanned by our laboratory up to now. Even adding an estimated scanning power of all other laboratories 100 times greater than ours leaves the probability as small as 2%. It seems therefore justified to interprete this event as due to some physical process.

The total visible momentum of star B is 1500 ± 150 MeV/c. The total visible kinetic energy is 790 ± 120 MeV. If one includes the rest mass of the π-meson and the binding energies one gets an

energy of

$$990 \pm 120 \text{ MeV} .$$

Therefore star B cannot be explained by the absorption of a K^- or one of the known hyperons.

The possibility that star B is made by a hyperfragment coming to rest can be ruled out. The charge of the hyperfragment should be at least $Z=9$, because 7 protons and 1 α-particle are observed in star B. This is in complete disagreement with the total number of δ-rays and the total number of gaps observed. From all measurements, from the energy release and the unbalanced momentum in star B also the possibility that this star has been produced by a fragment or a hyperfragment in flight can be excluded.

We suggest that the whole event is due to the production and annihilation of an antiproton as was first suggested by AMALDI *et al.* (E. AMALDI, C. CASTAGNOLI, G. CORTINI, C. FRANZINETTI and A. MANFREDINI: *Nuovo Cimento*, **1**, 492 (1955)) for a similar event.

The production of antiprotons by protons of 6.3 GeV has been observed in Berkeley (O. CHAMBERLAIN, E. SEGRÈ, C. WIEGAND and TH. YPSILANTIS: *UCRL Report* 3172, 1955).

The possibility of production of a proton-antiproton pair together with the meson field was investigated assuming pure multiple production in nucleon-nucleon or in a meson-nucleon collision. This seems to be justified by the fact that star A has only one evaporation track. As the kinetic energy of the antiproton in the laboratory system (L) is only 7 MeV it must have been emitted with high energy exactly backward in the centre of mass system (C.M). There exist two possible cases:

If we first assume that the energy of the positive proton is lower the meson field has to go mainly in the forward direction in order to fulfill momentum conservation. Even if one takes a π-meson for the primary particle the energy left for the meson field in the C.M-system cannot produce the necessary momentum to account for momentum balance and the observed angular distribution in the L-system. In the second case the positive proton emitted in the forward direction has the higher energy and the meson field has to go mainly backwards. Also in this case we have to deal with

Track No.	Identity	Rest range (microns)	Energy (MeV)
1	proton	1 200	15.8
2	recoil?	5	—
3	proton	4 420	34
4	π-meson (1)	—	450 ± 100 (2)
5	proton	780	12.1
6	proton	212	5.7
7	proton (3)	—	191 ± 7
8	proton	733	11.9
9	α-particle	1 552	70
10	proton	25	1.5

(1) The mean gap-length was $11 \pm 6\%$ above plateau, the blob density $15 \pm 6\%$ below plateau.
(2) $p\beta = 550 \pm 100$ MeV.
(3) Hyperonic mass could not be excluded.

the same difficulty. It cannot be removed assuming that some of the shower particles are heavier than π-mesons.

We can therefore not deduce any reasonable value for the primary energy from the observed angular distribution of the mesons. In order to maintain the model of multiple production of all particles one has to assume that the antiproton lost an energy of 30 MeV or more in a collision inside the nucleus.

The above mentioned asymmetry of the meson field as a result of antiparticle production would perhaps account for similar difficulties in explaining other high energy cosmic-ray phenomena.

* * *

We thank Proff. F. G. HOUTERMANS, CH. PEYROU and Dr. W. THIRRING for their stimulating discussions and Mrs. B. MESMER, who found the event.

We thank Prof. CH. HAENNY, Lausanne, and his plate group for the possibility of following through track No. 7.

The Texas flight was organized by the Office of Naval Research and we are very grateful to Dr. A. ROBERTS. The financial means for the stack were granted by the Schweizer Nationalfonds. One of us (E.L.) thanks Prof. F. G. HOUTERMANS for the hospitality in his Institute, Prof. E. SCHOPPER for granting a leave of absence and the Deutsche Forschungsgemeinschaft for a maintenance grant.

Our special thanks are due to Prof. E. AMALDI and the staff of the Rome group for the possibility of discussion and comparison of our event with those found by the Rome group (loc. cit.: O. CHAMBERLAIN, W. W. CHUPP, G. GOLDHABER, E. SEGRÈ, C. WIEGAND, E. AMALDI, G. BARONI, C. CASTAGNOLI, C. FRANZINETTI and A. MANFREDINI: *Phys. Rev.*, in press and *Nuovo Cimento*, in press).

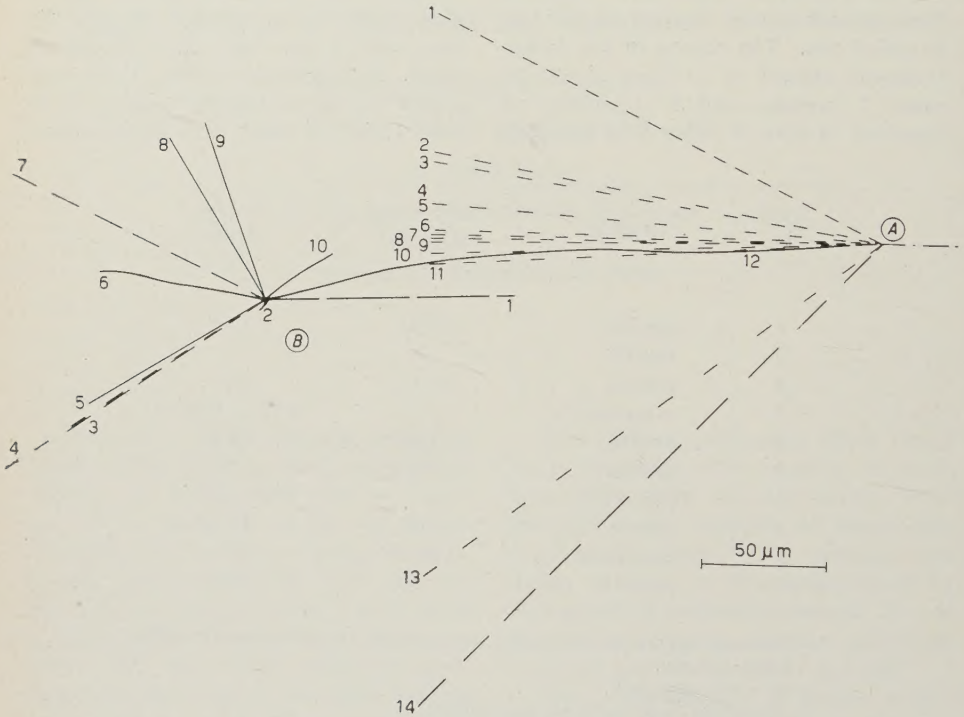

Fig. 1.

LIBRI RICEVUTI E RECENSIONI

H. Scheiber und F. Seide: *Lecher Lehrbuch der Physik für Mediziner und Biologen* - Elfte Auflage, B. G. Teubner Verlagsgesellschaft, Leipzig, 1954; volume rilegato in 383 pagine, 502 figure ed 8 tabelle.

Nella prefazione gli Autori riconoscono il diritto degli studenti di Medicina e Biologia ad una forma di insegnamento della fisica che tenga conto delle particolari finalità dei loro studi: cosa questa naturale. Solo che sembra lecito dissentire dagli Autori sul fatto che questa forma di insegnamento « particolare » sia proprio lungo la via tracciata nel volume in questione. In esso, di bella veste tipografica, corredato di ben 502 figure in generale molto chiare e curate, si parte dal tentativo di fornire allo studente una quantità sovrabbondante di nozioni con mete chiaramente pratiche, riducendo invece al minimo non solo le trattazioni a carattere matematico ma anche i concetti fondamentali strettamente fisici. L'abbondanza di descrizioni di apparati strumentali può essere senza dubbio utile, sebbene lo studente abbia generalmente occasione di incontrare nuovamente le stesse descrizioni, spesso più dettagliate, in altri corsi di studio, cui tali apparecchiature interessano. Ma quello che appare il lato più criticabile del libro è (oltre all'aver adottato il sistema C.G.S.) l'aver sacrificato la chiarezza dei concetti e delle leggi e principi fondamentali, riducendoli spesso a poche parole che non possono dare affatto un quadro sufficientemente preciso dell'ampiezza e dell'importanza dell'argomento (cfr. per es. il secondo principio della termodinamica e lo studio del campo magnetico basato sul concetto di massa magnetica e sulla legge di Coulomb).

Questo metodo di insegnamento non sembra il più adatto per lo studente medio, in quanto favorisce la tendenza ad avere conoscenze non chiare sulle leggi fisiche fondamentali, le quali viceversa rappresentano la base della cultura in qualsiasi branca di studi scientifici. Manca insomma qualche cosa di costruttivo nel campo della formazione di una mentalità scientifica, mentalità che ovviamente non deve essere estranea al medico ed al biologo.

M. Chiozzotto

W. B. Fretter – *Introduction to Experimental Physics.* Blackie and Son, London and Glasgow, 1955.

Il titolo del libro fa pensare a quei corsi di fisica generale che in Italia vanno sotto il nome di « fisica sperimentale ». Si tratta invece di un libro di tecniche sperimentali, molto diverso, peraltro, dal noto trattato dello Strong. Quest'ultimo è una specie di manuale dello sperimentatore, dove un fisico può anche trovare i dettagli che gli occorrono per il lavoro quotidiano (sebbene per molti argomenti sia largamente superato da pubblicazioni più moderne e più specializzate). W. B. Fretter vuole porre i giovani che si avviano alla ricerca, di fronte ai problemi sperimentali di attualità, perchè ne apprendano l'esistenza ma ne cerchino indipendentemente la soluzione. Il libro dà solo l'avvio, per quel tanto che permetta di pensarci su.

Esso è stato scritto sulla traccia di un corso di lezioni tenuto per la prima volta nel 1954 presso l'Università di California da persone fornite di esperienza propria nelle singole tecniche: persone, ci sembra di capire dalla lunga lista di citazioni, che hanno maturato la tecnica nel progetto e nella esecuzione di esperimenti fondamentali. Il corso era destinato a « graduate students ».

Nei trentadue capitoli, ognuno di poche pagine, si parla di misure elettriche e magnetiche, progetto di magneti, macchine acceleratrici, rivelatori di particelle (contatori di Geiger, camere a ionizzazione e a nebbia, emulsioni, scintillatori) basse temperature, tecnica del vuoto, ottica in un vasto intervallo di frequenze, tecnica dei reattori. C'è anche un capitolo dedicato ai « pericoli » del laboratorio.

Ci sono alcune disuniformità: per esempio nel capitoletto sugli oscillatori, questi vengono presentati molto qualitativamente in due pagine, mentre una pagina è dedicata a come si può ovviare ai difetti dei medesimi. Comunque, certi dettagli sproporzionati vanno piuttosto considerati come aperture sulle voragini che talora si aprono dietro uno schema di circuito o di esperienza dall'aspetto molto semplice.

L'esposizione è piacevole e colorita.

La bibliografia è scarna come si conviene ad un libro di questo tipo.

I disegni sono chiari nella loro schematicità.

In un certo senso il libro fornisce un aiuto per colmare la lacuna che intercorre fra l'insegnamento basilare e quel gruppo di nozioni che negli ultimi anni sono diventate anch'esse fondamentali senza inquadrarsi nei regolari ordini di studio universitari.

Il libro ci sembra utile, quando, naturalmente, si legga o si faccia leggere nello spirito con cui è stato scritto.

Questo spirito si può, forse, individuare nell'ultimo capitolo che si intitola « progetto di esperienze »: « non si può insegnare ad alcuno come si progetti un'esperienza. In un'esperienza si deve penetrare personalmente ». Sembra una tautologia, ma alcune volte ci si dimentica questa evidenza.

Certo non è, e non vuole essere un « handbook ». Del resto, per chi fosse interessato, si fanno sempre più frequenti, da ogni parte del mondo, le « panoramiche » annuali, o quasi, sui vari campi, per molti degli argomenti che appaiono qui.

MARIA FIDECARO

Direttore responsabile: G. POLVANI Tipografia Compositori - Bologna

Questo fascicolo è stato licenziato dai torchi il 5-I-1956